Fiber optic chemical sensors based on molecularly imprinted polymers for the detection of mycotoxins

Xuan-Anh Ton

Par **Xuan-Anh TON**

Fiber optic chemical sensors based on molecularly imprinted polymers for the detection of mycotoxins

Thèse présentée pour l'obtention du grade de Docteur de l'UTC

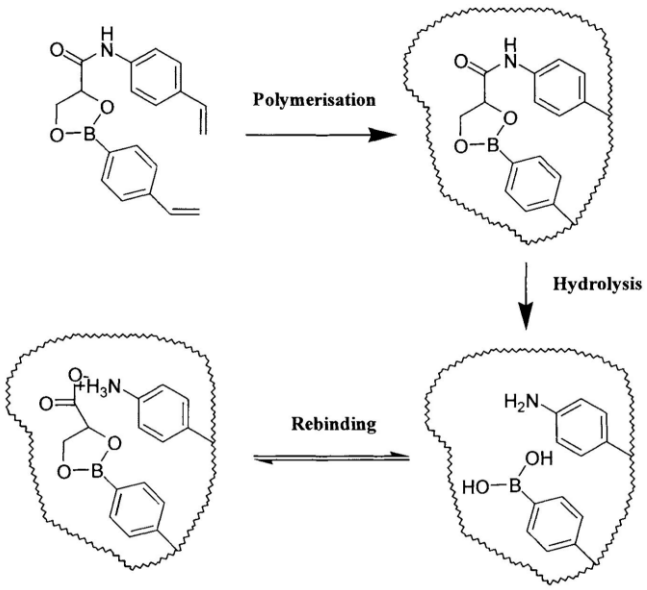

Soutenue le 25 octobre 2013
Spécialité : Biotechnologie

D2103

Ce projet est co-financé par l'Union Européenne. L'Europe s'engage en Picardie avec le Fonds européen de développement régional.

DOCTORAL THESIS

submitted for graduation as

DOCTEUR de l'Université de Technologie de Compiègne

Field: Biotechnology

by **Xuan-Anh TON**

Fiber Optic Chemical Sensors Based on Molecularly Imprinted Polymers for the Detection of Mycotoxins

Thesis supervised by Prof. Karsten HAUPT and Dr. Bernadette TSE SUM BUI

Disputation on 25th October 2013, in front of the jury composed of:

▪ Chris ALLENDER, Dr.	Cardiff University, *United Kingdom*	Reviewer
▪ Wolfgang KNOLL, Prof.	Austrian Institute of Technology, *Austria*	Reviewer
▪ Daniel THOMAS, Prof.	Université de Technologie de Compiègne, *France*	President
▪ Victor ACHA, Dr.	Institut LaSalle Beauvais, *France*	Examiner
▪ Bernadette TSE SUM BUI, Dr.	Université de Technologie de Compiègne, *France*	Supervisor
▪ Karsten HAUPT, Prof.	Université de Technologie de Compiègne, *France*	Supervisor

“ Là où est la Volonté
est le Chemin.”

Acknowledgments

First of all, I gratefully acknowledge Dr. Chris Allender and Prof. Wolfgang Knoll for giving me the honor to review this thesis, as well as Prof. Daniel Thomas and Dr. Victor Acha for being the examiners of this work.

My biggest acknowledgments go to my supervisors Prof. Karsten Haupt and Dr. Bernadette Tse Sum Bui, for their guidance during these challenging three years, their constant availability and their confidence in this project and in me.
Karsten, first, thank you for giving me the chance to work on this project. Throughout these three years, thank you for your expertise, your enthusiasm and all your creative ideas that built this thesis. Personally, warm thanks for your pleasant company, your humor and your open-mindedness. It has been a real pleasure to work and interact with you.
Bernadette, thank you for your professionalism, your constant support and your numerous advice, ideas and encouragements. Above all, thanks for sharing your experience with me; you taught me a lot about the research world. Besides work, deep thanks for your attentiveness, your kindness and your good mood.

As for our external collaborators, I am very grateful to Dr. Olivier Soppera, for kindly welcoming me in IS2M, and for his precious help and his deep interest in my work, as well as Dr. Arnaud Spangenberg and Ihab Dika for the nice collaboration. I am also thankful to Dr. Marina Resmini and Dr. Paolo Bonomi for their contribution to this project, and to Dr. Victor Acha for the coordination of this project to the Région Picardie. I gratefully thank Dr. Jean-François Masson from Montréal University for the nice collaboration. Also, thanks to Frédéric Nadaud from the Physico-Chemical Analysis Unit of UTC for his efficiency. To finish, warm thanks to C.D. Tôn, Diego Ros and Jérôme Istria for their personal implication and their very valuable contribution.

I sincerely thank all the members of the Enzyme and Cell Engineering Laboratory for their sympathy, their help, and the friendly working environment. Above all, I especially thank the "Karsten's Dream Team": the MIP group, former or present members: Aude, Pinar, Jacqueline, Serena, Amani, Selim, Zeynep, Yi, Paolo, Marcos…Thanks also to the non-imprinted people: Thierry, Jean, Sébastien, Melody… Special thanks to Sofia, Maria and Jingjing, who contributed to this work. To finish, very warm thanks to my "coffee-mates", the first generation, Yannick, Carlo and Li Bin, and the second (German) generation, Stephanie and Jan, for the very nice company and the numerous exchanges (scientific or not). For all of you, thank you for making my life in Compiègne so enjoyable and lively!

I will conclude these acknowledgements for my dearest relatives. First, warm thanks to Nelly and Gérard for the nice company. Among my close friends, I especially thank Diane and Marion for their lovely friendship. Very special thanks to you, Jarek, for being here during these (difficult) last months. To finish, the most important thanks go to my family, my grand-mother and my aunts Thanh, Mai and Yen for their constant and kind support, and finally my father for his unique guidance, and my mother, my sister Anh-Chi and my brother Anh-Kiet, for their unconditional love, support and patience.

Abstract in English: Fiber optic chemical sensors based on molecularly imprinted polymers for the detection of mycotoxins

Keywords: molecularly imprinted polymer, synthetic receptor, biomimetic sensor, optical fiber, fluorescence, photostructuring.

This thesis describes the development of highly selective fiber optic sensors using molecularly imprinted polymers (MIPs) as recognition elements associated with fluorescence for detection. Additionally, we extended the study to the development of other MIP-based optical sensors and sensing methods.

MIPs are synthetic biomimetic receptors possessing specific cavities designed for a target molecule. Produced by a templating process at the molecular level, MIPs are capable of recognizing and binding target molecules with selectivities and affinities comparable to those of natural receptors. Compared to biological recognition elements, MIPs are more stable, cheaper and easier to integrate into standard industrial fabrication processes. Hence, MIPs have become interesting alternatives to biomolecules as recognition elements for biosensing.

In the first part of this thesis (*Chapter 2*), MIPs were synthesized by *in-situ* laser-induced photopolymerization in only a few seconds, as a micrometer-sized tip at the extremity of a telecommunication optical fiber. Photonic and physico-chemical parameters were optimized to tailor the properties of the polymer micro-objects. Gold nanoparticles were incorporated into the MIP microtip for signal enhancement. To prove the efficiency of the sensor, initial studies were performed with a MIP templated with N-carbobenzyloxy-L-phenylalanine (Z-L-Phe) and the fluorescent amino acid derivative dansyl-L-phenylalanine as analyte. The fluorescence was collected either externally at the tip level by an optical fiber connected to a spectrofluorimeter or by collection of the fluorescent signal re-emitted into the fiber through the second arm of a Y-shaped bifurcated fiber. The fluorescent analyte could be detected in the low nM concentrations. In order to monitor non-fluorescent analytes, a naphthalimide-based fluorescent monomer was incorporated into the MIP during its synthesis; fluorescence enhancement was observed when analyte binding occurs. Using this system, the sensor containing a MIP specific for the herbicide 2,4-dichlorophenoxyacetic acid (2,4-D), could detect and quantify this analyte at concentrations as low as 2.5 nM. The signaling MIP-based sensor was also applied to analytes of interest for food safety and biomedical applications, such as the mycotoxin citrinin and the sphingolipid, D-*erythro*-sphingosine-1-phosphate.

In the second part of the thesis (*Chapter 3*), a different type of fiber optic sensor: cheap, fast and made for “single-use”, was developed by using 4-cm long disposable polystyrene evanescent wave optical fiber waveguides. The coating of the MIP was either performed *ex-situ*, by dip-coating the fiber in a suspension of MIP particles synthesized beforehand, or *in-situ* by evanescent-wave photopolymerization directly on the fiber. The resulting fiber optic sensor could detect 2,4-D in the low nM range and demonstrated specific and selective recognition of the herbicide over its structural analogues and other non-related carboxyl-containing analytes. Additionally, we demonstrated the versatility of the system by applying the evanescent wave fiber optic sensor to detect citrinin, a mycotoxin, by simply coating the waveguide with a MIP specific for citrinin. This type of technology could possibly be extended to detect other carboxyl-containing analytes, as long as a specific MIP for the concerned analyte is available. In parallel, the technique of evanescent-wave photopolymerization was used for the synthesis of signaling MIP microdots on continuous and nanostructured gold films. This study lays the foundations for future development of plasmonic MIP nanosensors and microchips.

In the last part of the thesis (*Chapter 4*), an innovative sensing method, based on the use of MIPs and analysis by fluorescence polarization, was developed in order to allow the fast and direct quantification of analytes in food and environmental samples This technique was successfully applied to detect fluoroquinolone antibiotics in tap water and milk, below their maximum residue limits.

We can conclude from these studies that we have opened a new era towards the development of a new generation of miniaturized portable MIP-based optical sensors, suitable for on-site measurements and real-time monitoring of environmental and biological analytes in complex media.

Résumé en Français: Capteurs chimiques à fibres optiques utilisant les polymères à empreintes moléculaires pour la détection de mycotoxines

Mots-clés: polymère à empreinte moléculaire, récepteur synthétique, capteur biomimétique, fibre optique, fluorescence, photostructuration.

Cette thèse décrit le développement de capteurs à fibre optique hautement sélectifs, utilisant des polymères à empreintes moléculaires (MIPs, de l'anglais *molecularly imprinted polymers*) comme éléments de reconnaissance, et se basant sur la fluorescence pour la détection. Nous avons étendu l'étude à d'autres types de capteurs et de méthodes de détection optiques, toujours basés sur les MIPs.

Les MIPs sont des récepteurs synthétiques biomimétiques possédant des cavités spécifiques pour une molécule cible. Produits par un processus de moulage à l'échelle moléculaire, les MIPs sont capables de reconnaître et de se lier à leurs molécules cibles, avec des spécificités et affinités comparables aux récepteurs naturels. De plus, comparé aux récepteurs biologiques, les MIPs sont plus stables, moins chers et plus faciles à intégrer dans les procédés standard industriels de fabrication. Ainsi, les MIPs apparaissent comme une alternative intéressante aux biomolécules en tant qu'éléments de reconnaissance dans les biocapteurs.

Dans la première partie de la thèse (*Chapitre 2*), les MIPs ont été synthétisés en tant que micropointe à l'extrémité d'une fibre optique, par polymérisation *in-situ* induite par un laser en seulement quelques secondes. Les paramètres photoniques et physico-chimiques ont été optimisés pour moduler les propriétés des micro-objets de polymères. Des nanoparticules d'or ont été incorporées dans la micropointe de MIP afin d'induire une exaltation du signal. Afin de prouver l'efficacité de notre capteur, les études initiales ont été réalisées avec un MIP synthétisé avec le N-carbobenzyloxy-L-phenylalanine (Z-L-Phe) comme template et le dérivé d'acide aminé fluorescent dansyl-L-phenylalanine, comme analyte. La fluorescence a été collectée de l'extérieur au niveau de la micropointe par une fibre optique connectée à un spectrofluorimètre, ou par collection du signal fluorescent ré-émis dans l'un des bras d'une fibre bifurquée en Y. L'analyte fluorescent a pu être détecté à des concentrations de l'ordre du nM. Afin de quantifier les analytes non fluorescents, un monomère fluorescent, possédant un groupe naphthalimide, a été incorporé dans le MIP ; celui-çi déployant une augmentation de la fluorescence quand l'analyte se lie. Utilisant ce système avec un MIP spécifique pour l'herbicide 2,4-D (acide 2,4-dichlorophénoxyacétique), des concentrations aussi basses que 2,5 nM en 2,4-D ont pu être mesurées. Le capteur MIP a également été appliqué à des analytes d'intérêt pour la sécurité alimentaire et le domaine biomédical, comme la mycotoxine citrinine et le sphingolipide, D-*erythro*-sphingosine-1-phosphate.

Dans la seconde partie (*Chapitre 3*), un autre type de capteur à fibre optique, en polystyrène, peu cher, rapide et "à usage unique", a été développé en utilisant des guides d'ondes à ondes évanescentes. Le dépôt du MIP, contenant un monomère rapporteur de fluorescence, est réalisé soit *ex-situ*, en plongeant la fibre optique dans une suspension de particules de MIPs synthétisées préalablement, ou *in-situ* par photopolymérisation par onde évanescente directement sur la fibre. Le capteur a été appliqué pour la détection du 2,4-D et de la citrinine. En parallèle, la technique de photopolymérisation par ondes évanescentes a été utilisée pour la synthèse de microdots de MIPs rapporteurs de fluorescence, sur des films d'or et des surfaces d'or nanostructurées. Cette étude pose les bases pour le développement futur de nanocapteurs et de micropuces de MIPs plasmoniques.

Dans la dernière partie (*Chapitre 4*), une méthode d'analyse novatrice, basée sur l'utilisation des MIPs et l'analyse par polarisation de fluorescence, a été développée en vue de permettre la quantification directe et rapide d'analytes dans des échantillons alimentaires et environnementaux. Cette technique a été appliquée avec succès pour détecter des antibiotiques fluoroquinolones dans l'eau du robinet et le lait, en-dessous de leur limite maximale de résidus.

En conclusion, nous pouvons dire que ce travail ouvre la voie vers l'application d'une nouvelle génération de capteurs optiques portables, robustes et miniaturisables basés sur les MIPs, pour des mesures «sur-site » et la quantification en temps réel d'analytes biologiques et environnementaux dans des milieux complexes.

Table of Contents

List of Abbreviations

ABDV	azo-bis-dimethylvaleronitrile
ACN	acetonitrile
AcOH	acetic acid
AFM	atomic force microscopy
AIBN	azo-bis-isobutyronitrile
AMP	adenosine-5'-monophosphate
AMPI	ampicillin
CCD	charge-coupled device
CIPRO	ciprofloxacin
CMMC	7-carboxymethoxy-4-methylcoumarin
CP	control polymer
2,4-D	2,4-dichlorophenoxyacetic acid
DANO	danofloxacin
Dansyl-Phe	dansyl-phenylalanine
DVB	divinyl benzene
2,4-D-OMe	2,4-dichlorophenoxyacetic acid methyl ester
EDMA	ethylene glycol dimethacrylate
EDS	energy dispersive X-ray spectroscopy
ELISA	enzyme-linked immunosorbent assay
ENRO	enrofloxacin
EtOH	ethanol
FB_1	fumonisin B_1
FIM	« fluorescent monomer »
FLU	flumequine
FQ	fluoroquinolone
FPIA	fluorescence polarization immunoassay
FRET	Förster resonance energy transfer
GlcA	β-D-glucuronic acid
GlcN-6S	D-glucosamine-6-sulfate
GC	gas chromatography
HEMA	2-hydroxyethyl methacrylate
HEPES	2-[4-(2-hydroxyethyl)piperazin-1-yl]ethanesulfonic acid
HPLC	high-performance liquid chromatography
IF	imprinting factor
KANA	kanamycin
LOD	limit of detection
LSP	localized surface plasmon
LSPR	localized surface plasmon resonance
MAA	methacrylic acid
MMA	methyl methacrylate
MeOH	methanol
MIP	molecularly imprinted polymer
MRL	maximum residue limit
MS	mass spectrometry
NIP	non-imprinted polymer
NOR	norfloxacin
NPs	nanoparticles
PET	photoinduced electron transfer
PETIA	pentaerythritol triacrylate
PMT	photomultiplier tube
POAc	phenoxyacetic acid
PVA	poly(vinyl alcohol)
QD	quantum dot
RAFT	reversible addition-fragmentation chain transfer
SEM	scanning electron microscopy
SERS	surface-enhanced Raman spectroscopy
SPE	solid phase extraction
SPR	surface plasmon resonance
STRE	streptomycin
TEM	transmission electron microscopy
Tetraglyme	tetraethylene glycol dimethyl ether
TRIM	trimethylolpropane trimethacrylate
UV	ultra-violet
4-VPY	4-vinyl pyridine
Z-L-Phe	*N*-(carbobenzyloxy)-L-phenylalanine

General Introduction

The research project CBI-PEM presented in this thesis was funded by the Regional Council of Picardy in France and co-funded by the European Union (FEDER). The work was performed from October 2010 to September 2013, in the UTC/CNRS Laboratory of Enzyme and Cell Engineering – Molecular Recognition and Catalysis, headed by Prof. Karsten Haupt at the Université de Technologie de Compiègne (UTC). This thesis was conducted under the supervision of Prof. Karsten Haupt and Dr. Bernadette Tse Sum Bui (UTC), and was coordinated to the Regional Council of Picardy by Dr. Victor Acha (Institut LaSalle Beauvais).

The project CBI-PEM was initiated due to a pressing need for efficient food and environmental analysis and control. Everyday, we are confronted to various potentially toxic and endocrine disrupting compounds such as antibiotic residues, hormones, pesticides, bacterial and fungal toxins. In this project, we have specially focused on mycotoxins, toxins produced by fungi in a large variety of food (fruits, cereals, vegetables…). Mycotoxins are very resistant to biological, chemical and physical treatments, and can even remain in food after the disappearance of the fungi when cooking at high temperatures. Very toxic for humans and animals, most of them are mutagenic, teratogenic and/or carcinogenic such that nowadays mycotoxins have become a major concern for public health. Current methods used to detect mycotoxins are mostly chromatography coupled to mass spectrometry (HPLC, GC, LC/MS-MS, GC/MS-MS). Although these techniques are very sensitive, they are unfortunately time-consuming, expensive, and laborious, often necessitating specialized laboratory staff. Alternative methods employ biosensors (with immobilized antibodies) and ELISA (Enzyme-Linked Immunosorbent Assay). These methods are sensitive and much faster; however, serious problems of reproducibility and stability are encountered.

In this context has emerged a real need for a new kind of sensor, which would be sensitive, fast, robust, stable, reliable but also portable and easy to handle, even for non-specialized people, thus making possible on-site monitoring. Hence, biomimetic sensors based on the use of molecularly imprinted polymers (MIPs) that are tailor-made synthetic receptors, constitute a very promising alternative to the existing sensing methods. The project CBI-PEM aimed to develop an innovative technology based on optical fibers and MIPs for the sensitive and rapid detection of mycotoxins, and more generally, for the detection and quantification of any biological analyte of interest. Fiber optic sensors are of particular interest as they allow the design of cheap and portable devices, whereas MIPs combine high specificity and selectivity with superior stability and robustness compared to biological recognition elements such as antibodies. In this thesis, we designed a new generation of MIP-based optical sensors that could be industrialized in the near future, and ready to use for sensing in the “real world”, for food safety, environmental and biomedical control, and even for household use. This project was performed for some specific parts with external collaborators: Dr. Olivier Soppera (Institut de Sciences des Matériaux de Mulhouse, France) for the optimization of MIP photostructuring on optical fibers, Dr. Paolo Bonomi and Dr. Marina Resmini (Queen Mary University

of London, UK) for the synthesis of the naphthalimide-based monomer, and Dr. Jean-François Masson (Université de Montréal, Canada), for the gold films and the micro- and nanostructured gold arrays.

The thesis is organized in four chapters: one bibliographic chapter and three results chapters.

Chapter 1 provides a literature overview of molecularly imprinted polymers (history, development, synthesis, applications), with an outline on their applications as recognition elements in optical chemical sensors.

Chapter 2 presents the development of intrinsic fluorescence fiber optic sensors carrying *in-situ* polymerized MIP microstructures as recognition elements. Initially, dansyl-L-phenylalanine was used as fluorescent model target, for the optimization of the material photostructuring, to get the best sensitivity of the sensor. Composite gold nanoparticle-MIP tips were synthesized in order to use the effect of noble metal signal enhancement to increase the sensitivity of the sensor. Finally we generated intrinsic fluorescent MIPs by using a naphthalimide-based signaling monomer, whose fluorescence increases upon binding with analyte. The sensor was applied for the detection of low concentrations of non-fluorescent analytes such as the herbicide 2,4-D, the mycotoxin citrinin and the sphingolipid D-*erythro*-sphingosine-1-phosphate.

Chapter 3 reports the use of evanescent waves for the synthesis of molecularly imprinted polymers and for fiber optic sensing. A disposable, cheap and versatile evanescent wave fiber optic sensor was developed by coating a signaling fluorescent MIP on a 4-cm long polystyrene optical waveguide. The sensor could be applied for the detection of the herbicide 2,4-D and the mycotoxin citrinin. In parallel, the technique of evanescent-wave photopolymerization was used for the synthesis of signaling MIP microdots on gold films and gold nanostructured surfaces. This study will enable the future development of plasmonic MIP nanosensors.

Chapter 4 describes the development of a rapid, sensitive and economic sensing method for the direct detection of UV-excited fluorescent analytes in food and environmental samples. This sensing method is based on a fluorescence polarization assay using molecularly imprinted polymer nanoparticles. The technique was successfully applied for the detection of fluoroquinolone antibiotic residues in water and milk samples below their maximum residue limit.

Chapter 1

Molecularly Imprinted Polymers and Their Applications in Optical Sensing

A Literature Review

Chapter 1: Molecularly Imprinted Polymers and Their Applications in Optical Sensing – *A Literature Review*

I. Molecular imprinting

I.1. The origin of molecular imprinting

The first "molecular imprinting" effect, that is, a molecule leaving an imprint in a synthetic material, was observed in 1931 by the Russian chemist Polyakov, while he was studying porous silica matrices as new materials for chromatographic applications (Polyakov and Khim, 1931). In his study, polymerization of sodium silicate was performed with ammonium carbonate as gelating agent, and just before the drying step, an additive (benzene, toluene or xylene) was added in the medium. After drying of the silica gel, the additive was removed by washing with hot water. Subsequent adsorption studies revealed that the additive that had been added to the gel during the polymerization step showed higher adsorption on the silica gel, at least for benzene (Table 1.1). The adsorption was even higher over the two other additives in the case of benzene, as if the silica gel has demonstrated some sort of "molecular memory". A few years later, this effect was explained by the structural changes induced by the additive in the silica matrix.

Table 1.1. *Rebinding on silica gels of different additives used during the preparation of the respective gels. Reproduced from Sellergren, 2000.*

	Adsorption on the silica gel (%)		
Gel prepared with	Benzene	Toluene	Xylene
Benzene	**87.5**	80.6	80.1
Toluene	88.5	**87.2**	86.7
Xylene	75.1	79	**68.3**

Later, Linus Pauling proposed an interesting, although proven wrong, theory about the formation of antibodies (Pauling, 1940). He suggested that all antibodies had the same primary structure as normal globulin, and that the functional antibody was formed using the antigen as a template for the folding of the antibody's polypeptide chain, resulting in a chain configuration that is complementary to the antigen. This template-induced conformation could then explain the high selectivity of antibodies. He was even able to prove his theory: he precipitated globulins under denaturing conditions in the presence of an 'antigen', and then slowly removed the denaturing agent, leading to redissolution of the globulins. He then observed that the globulins exhibited selective binding of the antigen. Even though we know today that this theory about the formation of antibodies is wrong, this is the first example of 'bio-imprinting'. Similarly to the experiments carried out by Polyakov, Pauling applied this theory to an inorganic system, silica, and the results were reported by his student Dickey (Dickey, 1949). In this study, polymerization of sodium silicate was performed in the presence of methyl orange (and other alkyl orange dyes) used as the template. Subsequent adsorptions studies showed that the silica gel demonstrated selectivity for the dye that was present in the system during the polymerization, over other dyes. Furthermore, adsorption of the dye was also much higher on the corresponding "dye-imprinted" silica than on a "non-imprinted" silica gel (polymerized in absence of dye) (Table 1.2).

To explain this result, Morrison and co-workers proposed an "association mechanism" instead of the "footprint" or "imprint mechanism" (Morrison et al., 1959). In the "association mechanism", the trapped dyes that remained after washing acted as "nucleation sites", inducing the formation of complexes, which can explain the selectivity of the gel. Waksmundzki and co-workers performed extensive studies on the sorption of template to imprinted silicas combined with thermodynamic studies that led to the conclusion that the templates were adsorbed as multilayers to the silica. These results support the association mechanism proposed by the group of Morrison. However, later, Beckett and Youssef challenged the association mechanism theory with a study on quinine-selective silica (Beckett and Youssef, 1963). They showed that the selectivity of silica was suppressed when steam was forced through silica, or after treatment with dry organic solvents that did not remove the trapped molecules. These changes in selectivity are more likely to result from changes in the "footprint" structure, than from changes in the attractive forces of the trapped molecules. At the moment, most of the literature data seem to support the "footprint" mechanism, even if there is not enough evidence to refute definitely the association mechanism (Alexander, 2006). It also seems that the possibility of the two mechanisms both taking place has not been considered (Sellergren, 2000).

Table 1.2. *Relative adsorption of different dyes on silica gels: the amount adsorbed on the "imprinted" silica related to a "non-imprinted" silica gel. Reproduced from Sellergren, 2000.*

	Relative adsorption power			
Gel prepared with	Methyl orange	Ethyl orange	Propyl orange	Butyl orange
Methyl orange	**3.5**	1.6	1.1	1.1
Ethyl orange	2.5	**9**	2.1	2.2
Propyl orange	2.3	5	**20**	6
Butyl orange	1.5	2.8	5	**15**

During two decades, intensive research was done on molecular imprinting in silica, but it was only in 1972 that molecular imprinting in organic polymers appeared, thanks to the independent contributions of Klotz (Takagishi and Klotz, 1972) and Wulff (Wulff and Sarhan, 1972).

Takagishi and Klotz reported the synthesis of a molecularly imprinted polymer consisting in a polyethyleneimine polymer bearing –SH groups for cross-linking via the formation of disulfide bridges from thiobutyrolactone monomers, and using methyl orange as the template. As a result, as expected, they observed that the MIP demonstrated higher adsorption capacity towards the methyl orange dye than the non-imprinted control polymer.

In his work, Wulff introduced for the first time the notion of enantiospecificity induced by a 'molecular memory' of chemical interactions. He co-polymerized a template molecule functionalized with polymerizable vinyl groups with divinylbenzene (DVB), in a solvent so as to form a non-swellable macroporous polymer. To illustrate his idea, he chose as a model template the 2,3-*O*-*p*-vinylphenylboronic ester of D-glyceric acid *p*-vinylanilide that was co-polymerized with DVB in acetonitrile. After polymerization, he could remove at most 50% of the D-glyceric acid by hydrolysis, leaving binding cavities with asymmetrically arranged functional groups, due to the chirality of the template (Figure 1.1). The polymer had the capacity to rebind the quantity of D-glyceric acid that was removed, and when reacted with D,L-glyceric acid, it showed selectivity for the D-enantiomer over the L-enantiomer, thus demonstrating enantiospecificity. Wulff observed finally that the polymer lost its binding properties when swollen, underlining the importance of the shape of the binding cavities in the molecular recognition process.

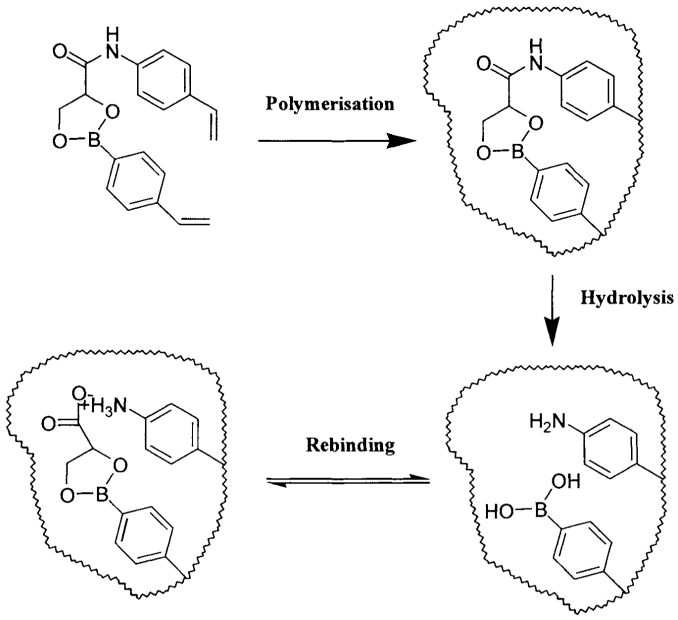

Figure 1.1. *Principle of molecular imprinting via covalent interactions, as shown by Wulff et al. 1972. Reproduced from Andersson and Nicholls, 2000.*

In the 1980s, Mosbach and co-workers proposed a new "template approach" that revolutionized the area of molecular imprinting. In his work, he synthesized highly cross-linked polymers containing monomers with chemical functional groups that were likely to interact with a template molecule via non-covalent bonds (i.e. ionic, hydrogen bonds), or the hydrophobic effect. The high cross-linking degree of the polymer enabled the formation of stable tri-dimensional binding sites complementary to the template. After removal of the template by washing with a solvent, the MIP was able to recognize and bind specifically the template, compared to a (though chemically identical) non-imprinted polymer (NIP) (Arshady and Mosbach, 1981). A few years later, similarly to the work of Wulff, Mosbach and co-workers imprinted the polymer with the D- or L-enantiomer of phenylalanine ethyl ester, and observed that, when incubated with a racemic mixture, the MIP showed selective binding of the enantiomer that had been used for imprinting. The synthesis of the phenylalanine ethyl ester-imprinted polymer was performed with p-vinylbenzoic acid as the functional monomer and DVB as the cross-linker. The molecular recognition process was based on ionic interactions between the template and the functional monomer (Andersson et al., 1984).

During the early days, the great potential of MIPs as separation materials was demonstrated. However, in 1993 the group of Mosbach opened a new perspective for these materials, by showing that MIPs could also be used as antibody mimics. In a paper published in Nature (Vlatakis et al., 1993), they showed that a theophylline-imprinted polymer and a diazepam-imprinted polymer could bind respectively theophylline and diazepam in human serum with specificities and selectivities comparable to those of antibodies.

This work provoked a significant raise of interest in the technique of molecular imprinting, as it opened a whole new range of applications and research perspectives for MIPs, which subsequently were termed 'plastic antibodies'.

I.2. Fundamentals of molecularly imprinted polymers

I.2.1. The covalent approach

As mentioned previously, the covalent approach for molecular imprinting in organic polymers was first introduced by Wulff in 1972, and later developed by Shea (Shea and Thompson, 1978). In this approach, the template molecule is covalently bonded by chemical reaction with functional monomers, followed by co-polymerization with an excess of cross-linking monomers. After polymerization, the template is removed by chemical cleavage (such as by hydrolysis), resulting in cavities in the polymer matrix that are complementary to the template molecule in terms of shape and chemical functionalities. Rebinding of the template takes place via the same covalent interactions. As demonstrated by Wulff and by Shea, the resulting MIP was able to distinguish between enantiomers when a chiral template was used, due to the local asymmetry of the binding sites.

The advantage of this covalent approach is that the template/monomer complex is stoichiometric, avoiding non-specific binding by randomly distributed binding groups. Furthermore the bonds between template and monomers are very stable, resulting in a high yield in binding sites. The resulting MIP therefore shows high specificity and selectivity towards the analyte. However, this approach is not very versatile as not all imprinting targets can be derivatized so as to carry polymerizable moieties. Moreover, as the rebinding occurs via covalent bonding, the kinetics of this binding process may be slow.

I.2.2. The non-covalent approach based on self-assembly

As mentioned before, the non-covalent approach to molecular imprinting was for the first time described by Mosbach and co-workers in 1981, who aimed to apply the “biochemist’s” point of view to the “template-polymerization” introduced by Wulff. They called it the “host-guest polymerization”, and in this approach, the interactions between the template and the functional monomers are only based on non-covalent interactions, such as hydrogen bonds, ionic, hydrophobic or π–π stacking interactions, van der Waals forces, etc. The complex between template and functional monomers is formed by self-assembly, and the polymerization is carried out with an excess of cross-linkers, in order to give rigidity to the polymer matrix and preserve the shape of the binding cavities formed (Figure 1.2). Similarly to the covalent approach, rebinding of the analyte occurs via the same interactions.

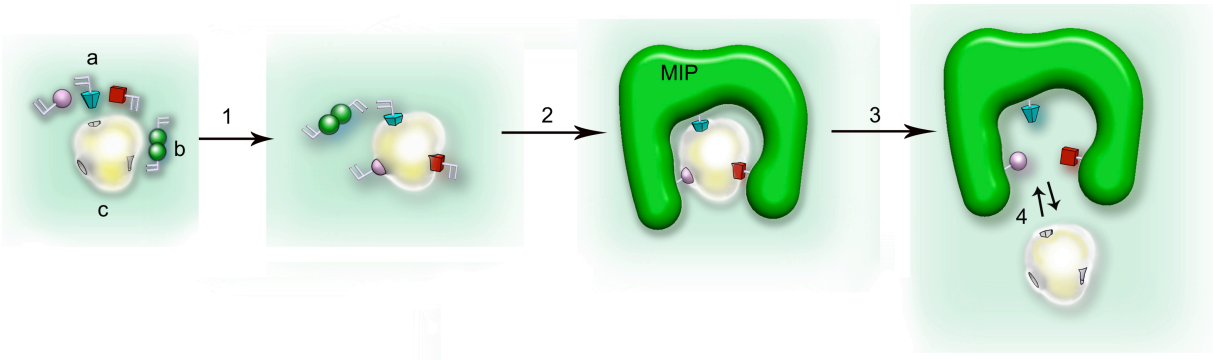

Figure 1.2. *Schematic representation of the molecular imprinting principle by self-assembly approach. a: functional monomers, b: cross-linkers; c: template; 1: assembly of the pre-polymerization complex template/functional monomers, 2: polymerization, 3: extraction of the template, 4: rebinding of the analyte.*

The advantage of this approach is that it can make use of a large choice of functional monomers, and be applied to a vast range of target analytes. Moreover, the synthesis is quite straightforward, even for non-chemists, as the protocol simply consists in mixing template, functional and cross-linking monomers, a polymerization initiator and a solvent. After polymerization, the template is removed by solvent extraction. Given the relative simplicity of this protocol, the range of applications of these MIPs is quite vast, as they can be synthesized in various formats. Thus this approach is more versatile than the covalent approach. However, it is based on the equilibrium of the pre-polymerization complex, whose stability depends on the affinity constants between the template and the functional monomers. Moreover, in most cases, the functional monomers have to be used in excess with respect to the template (typically 4 times the amount of template or more), in order to shift the equilibrium towards the formation of the complex. Consequently, some functional groups are distributed randomly in the polymer, thus creating low-affinity binding sites that are source of non-specific binding. The highest affinity sites define the specific binding of the MIP. As a result, the population of binding sites is often heterogeneous (Figure 1.3).

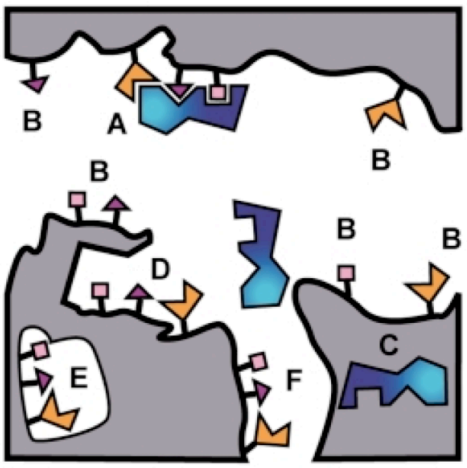

Figure 1.3. *Schematic representation of the heterogeneity of the population of binding sites in a MIP: high affinity site in (A) macropore and (F) micropore, (B) lower affinity site in macropore, (C) trapped template, (D) highest affinity site with shape selectivity for the template, (E) embedded site. Reproduced from Zimmerman and Lemcoff, 2004.*

However, despite these disadvantages, the non-covalent approach has been the most popular one, because of its flexibility and versatility. Moreover, the binding properties of a non-covalent MIP, can be optimized if one takes into account the complexity of the system, which is composed of numerous reactants (the template, the functional monomers, the cross-linker, the initiator, the solvent) and influenced by a number other external parameters (the temperature, the pressure, the reaction time, etc.). In the following sections, we will consider more in detail how to choose the suitable monomers, and we will also discuss the “stoichiometric” functional monomers first introduced by Wulff (Wulff and Knorr, 2002) that allow binding with the analyte at a 1:1 molar ratio.

I.2.2.1. The functional monomers

Molecular imprinting by self-assembly is based on the non-covalent interactions that occur between the template and the functional monomers. Thus the choice of the functional monomers is of great importance. The functional monomer should carry a chemical group that can interact with the chemical

groups of the template, and the interactions should be as strong as possible. For example, acidic functional monomers are generally chosen to interact with basic templates, and vice-versa.

Among the acid monomers, the most popular one is methacrylic acid (MAA), as its carboxylic acid group is able to establish ionic interactions with basic chemical groups, such as amino groups, and hydrogen bonds as a donor or as an acceptor. MAA was used for example to imprint theophylline (Vlatakis et al., 1993) (Figure 1.4), and a great variety of other targets. Some examples are reported in Table 3.

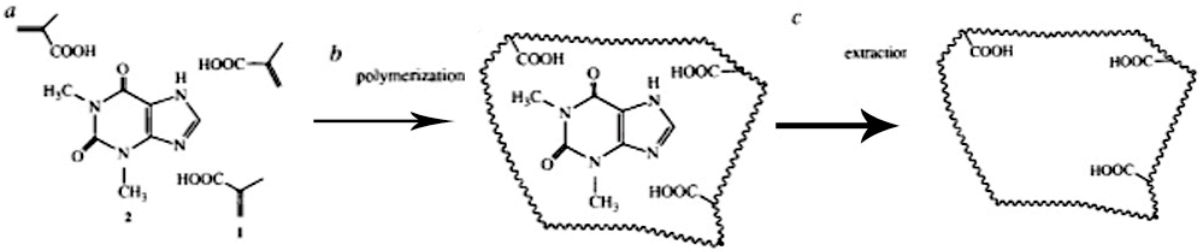

Figure 1.4. *Schematic representation of the synthesis of the theophylline-imprinted polymer. (a) Complex formation between the functional monomer MAA and the template theophylline in a solvent; (b) Polymerization in the presence of the cross-linker; (c) Extraction of the template, leaving the specific binding sites in the MIP matrix. Adapted from (Vlatakis et al., 1993).*

Apart from MAA, some other acidic functional monomers have been used in the literature, including acrylic acid, 2-acrylamido-2-methyl-1-propanesulfonic acid, itaconic acid, vinylbenzoic acid, etc. (Table 1.3).

Among the basic monomers, 4-vinylpyridine (4-VPY) is the most commonly used. In particular, 4-VPY interacts strongly with carboxylic acids by ionic interactions, but also with with compounds that possess an aromatic ring, since in this case, π–π stacking can occur (Haupt et al., 1998a). Some other basic functional monomers with examples of templates are also reported in Table 1.3.

In some cases, a combination of acidic and basic monomers can give rise to an enhanced selectivity, such as the combination MAA/4-VPY used for a MIP against N-protected L-phenylalanine derivatives (Ramstroem et al., 1993). Indeed L-phenylalanine possesses a carboxylic acid function that interacts with 4-VPY and hydrogen bond moieties that interact with MAA.

Finally neutral functional monomers can be used, sometimes in addition, if certain specific properties of the material are required. For example, the functional monomer 2-hydroxyethyl methacrylate (HEMA) is hydrophilic and is often used in order to render the MIP less hydrophobic, in particular as a co-functional monomer in combination with MAA (Dirion et al., 2003). Among the other examples that can be found in the literature, we can cite styrene, which is hydrophobic and can interact with hydrophobic compounds or form π–π interactions with aromatic rings; another example is acrylamide, which is hydrophilic, and hydrogen bonding and can interact for example with carboxylic acids as well as amide groups. (Haupt, 2003b).

Table 1.3. *Examples of the most popular functional monomers used in the non-covalent approach, with some associated templates. Adapted from Alexander et al., 2006 and Sellergren, 2000.*

Nature of monomers	Functional monomers	Templates	References
Acidic	Methacrylic acid	Proton acceptors, H-bond donors and acceptors (theophylline, steroids, nucleotide bases, peptides…)	Vlatakis *et al.*, 1993; Rachkov *et al.*, 1998; Tse Sum Bui *et al.*, 2010; Spivak and Shea, 1998; Kempe, 1996
	Acrylic acid	Amino acids	Sellergren *et al.*, 1985
	4-Vinyl benzoic acid	Amino acids	Andersson *et al.*, 1984
	2-Acrylamido-2-methyl-1-propanesulfonic acid	Tricyclic aromatics	Dunkin *et al.*, 1993
	2-(Trifluoromethyl)acrylic acid	Nicotine	Matsui *et al.*, 1997
	Itaconic acid	Drugs	Fischer *et al.*, 1991
Basic	4-Vinylpyridine	Carboxylic acids (amino acids, 2,4-D…)	Kempe *et al.*, 1993; Haupt, Dzgoev, *et al.*, 1998
	N,N-Diethylaminoethyl methacrylate	Alcohols and polar templates (estrogenic compounds, chloramphenicol, fumonisin B1…)	Levi *et al.*, 1997; Tarbin and Sharman, 1999; De Smet *et al.*, 2009
	Allylamine	Sialic acid	Piletsky *et al.*, 1996
Neutral	Acrylamide	Carboxylic acids and amides (N-protected amino acids)	Yu and Mosbach, 1998
	2-Hydroxyethyl methacrylate	Hydrophilic templates (cAMP, salicylic acid, enrofloxacin…)	Turkewitsch *et al.*, 1998; Sreenivasan, 1997; Qiao and Sun, 2010
	Styrene	Hydrophobic or aromatic templates (tamoxifen)	Claude *et al.*, 2008

With the above-mentioned weakly interacting monomers, in order to shift the equilibrium towards the formation of the pre-polymerization complex, an excess of functional monomers is used, typically a ratio of template:functional monomers of 1:4 or higher. However, this can result in high non-specific binding and has to be modulated depending on the template. There should be at least the same number of functional monomers than chemical functionalities in the template. In order to eliminate this drawback, Wulff and co-workers developed for the first time monomers that formed stoichiometric non-covalent complexes with the template, thanks to association constants of $K_a > 10^3$ M^{-1}. In this case no non-specific binding is produced since no excess of monomer is required (Wulff

and Knorr, 2002). For comparison, the association constants of hydrogen bonds and electrostatic interactions between carboxylic acids and basic nitrogen, and with additional hydrogen bonds are respectively K_a = 1.7, 3.3 and 30 M^{-1}, in acetonitrile.

In their work, Wulff and co-workers synthesized a series of monomers containing an amidine group, which can interact strongly with carboxylic acids by a combination of electrostatic and bidendate hydrogen bonds. An example of monomer is *N,N'*-diethyl-4-vinyl-benzamidine that can interact strongly with carboxylates, phosphonates and phosphates, with an association constant of 5.10^3 M^{-1} < K_a < 10^6 M^{-1} (Figure 1.5).

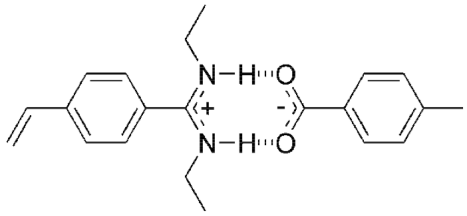

Figure 1.5. *Complex formed between the monomer N,N'-diethyl-4-vinyl-benzamidine and the carboxyl group of the template. Adapted from Wulff and Knorr, 2002.*

Later, Hall and co-workers developed a series of urea-based vinyl monomers for the stoichiometric recognition of oxyanions (they chose as first model templates *Z*-D or L-glutamic acid) (Hall et al., 2005). In particular, the urea-based monomer 1-(4-vinylphenyl)-3-(3,5-bis(trifluoromethyl)phenyl)urea was employed stoichiometrically with penicillin G (Urraca et al., 2006; Urraca et al., 2007) (Figure 1.6) and the fluoroquinolone enrofloxacin (Benito-Peña et al., 2008), to extract them from aqueous samples. Besides carboxylates, the urea-monomer was also able to bind tyrosine phosphorylated peptides (Emgenbroich et al., 2008) and sulfated protein fragments in aqueous media (Shinde et al., 2012).

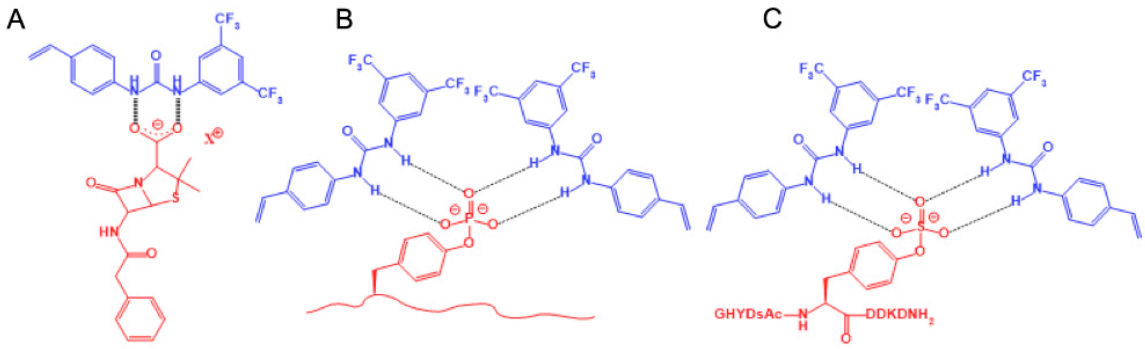

Figure 1.6. *Stoichiometric electrostatic interactions between the monomer 1-(4-vinylphenyl)-3-(3,5-bis(trifluoromethyl)phenyl)urea and (A) penicillin G (Urraca et al., 2006; 2007), (B) tyrosine phosphorylated peptides (Emgenbroich et al., 2008) and (C) sulfated protein fragments in aqueous media (Shinde et al., 2012).*

I.2.2.2. The cross-linker

The nature and the ratio of the cross-linker are of special importance, as in molecular imprinting, the polymer network should be rigid enough to maintain the tri-dimensional conformation of the specific binding sites (Wulff, 1995). However, at the same time, the binding sites should be easily accessible to

the analyte, and for this reason, the cross-linking degree should not be too high (Wulff, 2002). Usually, the cross-linking degree of a MIP ranges from 70% to 90%.

The most commonly used cross-linkers are DVB (divinylbenzene) and EDMA (ethylene glycol dimethacrylate), which are bifunctional (they contain two polymerizable groups). They are generally used in organic media because of their hydrophobicity (Sellergren, 2000). EDMA is particularly popular in molecular imprinting as it combines a flexible chain structure with the rigidity and the prochiral character of the methacrylate groups (Wulff et al., 1987; Alexander et al., 2006). Other cross-linkers possessing three polymerizable groups are also often used in MIPs, such as TRIM (trimethylolpropane trimethacrylate) and PETIA (pentaerythritol triacrylate), which were shown to convey better properties to the MIP in some cases, for example as chiral stationary phases in HPLC (Kempe, 1996).

Even if interactions are to take place only between the template and the functional monomers, it has been reported that the cross-linker can interact with the template as well (Wulff et al., 1987; Olsson et al., 2012). A very interesting approach was introduced by Spivak and co-workers, who developed MIP containing a single cross-linking monomer, *N,O*-bismethacrylolyl ethanolamine (NOBE) (Figure 1.7). These MIPs were called "OMNiMIPs" (one monomer molecularly imprinted polymer) (Sibrian-Vasquez and Spivak, 2004). The advantage of this approach is to simplify the formulation of the MIP. NOBE possess an amide group that can interact with alcohols and carboxylic acid groups (but not with amines). The OMNiMIPs were compared with traditional MAA/EDMA MIPs as separation materials in HPLC. As a result, the OMNiMIPs showed improved results in terms of enantioselective recognition in organic media, and similar results in aqueous media, compared to the MAA/EDMA MIPs. The incorporation of another functional monomer into the NOBE cross-linked MIP interfered with the good recognition process between the analyte and NOBE, resulting in lower selectivity.

Apart from that, choosing the right cross-linker can render the MIP more compatible with a certain environment. For example, PETIA is a hydrophilic monomer and is often used to impart water compatibility to the MIP (Manesiotis et al., 2009; Ambrosini et al., 2012). Amide-based cross-linkers, such as N,N'-methylene-bis-acrylamide, provide a more polar environment, and are thus interesting for the imprinting of polar templates that show poor solubility in organic solvents (Sellergren, 2000).

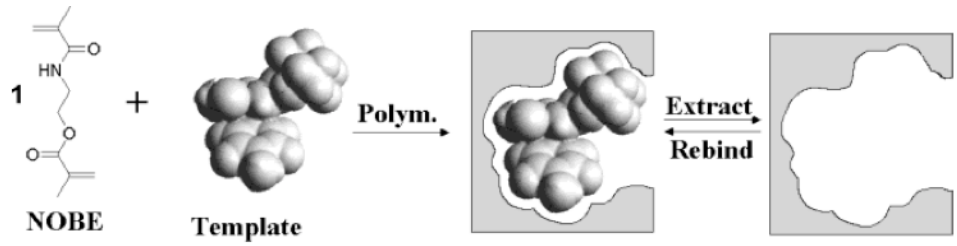

Figure 1.7. *Synthesis of an OMNiMIP, with NOBE,* **1** *as single cross-linking monomer. Reproduced from Sibrian-Vasquez and Spivak, 2004.*

I.2.2.3. The solvent

The role of the solvent is to dissolve the reactants of the pre-polymerization mixture, but also to induce porosity in the polymer, so that the inner binding sites are accessible to the analyte. If a bad solvent (for the polymer chains) is used, macroporosity is created in the MIP during the polymerization through phase separation between the growing polymer chains and the solvent. In a good solvent, the chains

remain solvated and a microporous gel-like material is obtained. A solvent is good for the polymer chains if their solubility parameters are close or identical (Sellergren, 2000).

Generally, MIPs show the best recognition properties in the solvent in which they are synthesized (Andersson, 1996). Indeed, in this case the MIP is solvated in the same manner (no swelling or shrinking of the polymer with respect to the situation after synthesis), and the accessibility and the geometry of the binding sites are preserved.

Considering that the molecular recognition process is based on weak non-covalents bonds (mostly hydrogen bonds), an apolar and aprotic solvent is often the most suitable, such as toluene or chloroform (Vlatakis et al., 1993). Acetonitrile, which is aprotic and moderately polar, is also popular for the synthesis of MIPs (Spivak and Shea, 1998). However, for some MIP formulations, it is also possible to use polar and protic solvents such as methanol (Turkewitsch et al., 1998), or even a mixture of methanol/water (Haupt et al., 1998a). In the latter case, the 2,4-D MIP even showed good rebinding of 2,4-D in pure buffer, due to the combination of ionic and π–π interactions that occurred between the template 2,4-D and the functional monomer 4-VPY.

However, for some applications, solvents with specific properties are required. For example, in the case of MIP films obtained by spin-coating (Schmidt et al., 2004; 2005), the use of pure solvents (toluene, chloroform) resulted in MIPs with no porosity and very low binding properties, probably because solvent evaporation occurred before the phase separation between the polymer chains and the solvent. The use of a solvent with lower vapor pressure, diethylene glycol dimethyl ether (diglyme) only led to moderately improved MIP properties. The best binding properties and the highest porosity were finally obtained with the MIP prepared with a mixture diglyme/poly(vinyl acetate) (PVAc). The presence of the linear polymer PVAc was expected to accelerate the process of phase separation through spinodal decomposition (rather than nucleation and growth). Another example is the use of triethylene glycol dimethyl ether (triglyme) at only 33% of the volume of the monomers, for the fabrication of holographic MIPs (Fuchs et al., 2013). In this case, a compromise had to be made because porosity is necessary to promote access of the analyte to the binding sites, while in diffractive structures, porosity leads to light scattering and loss of efficiency.

Nonetheless, it is also possible to obtain MIPs with good binding properties without any solvent in the precursors solution. For example, Byrne and co-workers synthesized MIPs hydrogels as soft contact lenses for uses in ophthalmic drug delivery. The MIP formulations consisted of 5 mole% of cross-linking monomer and 95 mole% of functional monomers (92 mole% of HEMA and 3 mole% of a combination of other functional monomers) (Venkatesh et al., 2007; Tieppo et al., 2012). Thus no solvent was incorporated into the MIP formulation during the polymerization, and yet, the MIP contact lenses could be successfully applied for drug loading and *in-vivo* controlled release (Tieppo et al., 2012).

I.2.3. The 'semi-covalent' approach

The semi-covalent approach was first introduced by Sellergren and Andersson (Sellergren and Andersson, 1990) and allows combining the advantages of covalent and non-covalent imprinting. In this approach, the template is covalently bound to the functional monomers, resulting, after extraction of the template by chemical cleavage, in a homogeneous population of binding sites. However, the rebinding of the template takes place via non-covalent interactions, resulting in fast binding kinetics.

In the approach proposed by Sellergren and Andersson, the template is directly coupled to the monomer. As illustrated in Figure 1.8, the "monomer-template" M^2-propionyl-O^1-acryl-oyl-L-2-amino-3-(O^4-acrylol-4-hydroxyphenyl)-1-propanol was synthesized from L-2-amino-3-(4-hydroxyphenyl)-1-propanol, and co-polymerized with the cross-linker DVB. Hydrolysis of the template moiety left binding sites with carboxylic acid groups as functional groups. The MIP was then incubated with *p*-amino-L-phenylalanine ethyl ester, resulting in binding of the amino acid to the functional groups of the MIP, via hydrogen bonds and electrostatic interactions. However, the problem of this approach is that non-covalent interactions occur at a longer distance than covalent interactions, which can result in a possible distortion of the binding site geometry.

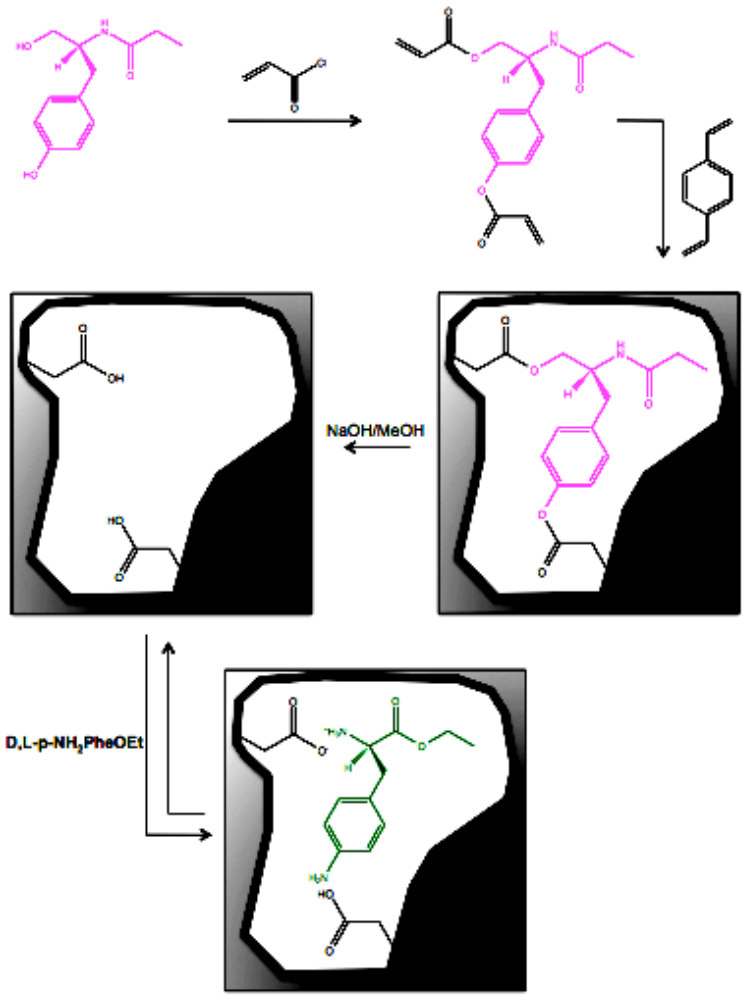

Figure 1.8. *Synthetic route of the semi-covalent approach proposed by Sellergren and Andersson. Adapted from Sellergren and Andersson, 1990.*

In order to circumvent this drawback, Whitcombe and co-workers introduced the semi-covalent imprinting with the use of a sacrificial spacer (Whitcombe et al., 1995). As shown in Figure 1.9, they applied their approach to imprint cholesterol, through the use of the "monomer-template" cholesteryl(4-vinyl)-phenyl carbonate. The "monomer-template" was obtained by attaching cholesterol with 4-vinylphenol via a carbonyl spacer. After co-polymerization with the cross-linker EDMA, the cholesterol template was removed by hydrolysis, and the spacer was also extracted as CO_2. Rebinding of cholesterol could now take place via hydrogen bonding between its hydroxyl group and the phenolic group in the binding site.

However, this strategy can be applied only when hydroxyl groups are involved. The big drawback of the semi-covalent approach, as with the covalent approach, is the limited number of templates to which it can be applied.

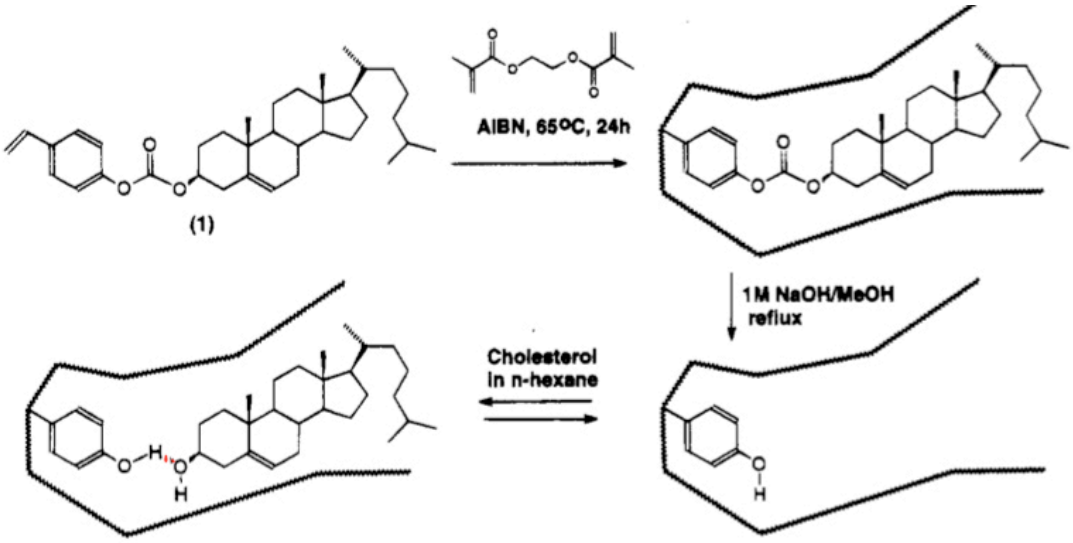

Figure 1.9. *Synthetic route of the semi-covalent approach using a sacrificial spacer for the imprinting of cholesterol through the use of cholesteryl(4-vinyl)phenyl carbonate* **(1)***. Reproduced from Whitcombe et al., 1995.*

I.2.4. Polymerization procedures for MIPs

MIPs are generally prepared by free-radical polymerization, which is a versatile method to synthesize MIPs under various physical formats, such as bulk, nanoparticles, dispersion, or films. In the following sections, we will have an overview over bulk and precipitation polymerization techniques, which were used in this thesis to prepare MIPs. The other methods will be presented briefly, but will not be discussed in detail, as they were not used in this work.

I.2.4.1. Bulk polymerization

Bulk polymerization is the traditional way to obtain polymers. Monomers are polymerized in the presence of an initiator or a catalyst, and no dispersing media or additional reactants are required. In this case, the probability of undesired chain transfer reactions is minimized. Bulk polymerization is often used for achieving step-growth polymerizations, such as polycondensations and polyadditions. However it is not used in industry for chain-growth polymerization, because of the Trommsdorff (Trommsdorff et al., 1948) or Norrish-Smith effect (Norrish and Smith, 1942) (also called the “auto-acceleration” effect). Briefly, bulk polymerization induces a local increase in the viscosity of the polymerizing system that slow the Brownian motion of the growing polymer chains and the termination reactions. However, small monomers can still diffuse through the polymerizing system, thus increasing the propagation rate, and also the reaction heat, which can result in an alteration of the polymer properties. For industrial applications, the need for heat dissipation is a drawback for using bulk polymerization for chain-growth reactions.

In the case of MIPs, the presence of solvent is required in order to generate porosity in the polymer. Thus bulk polymerization of MIPs refers to a system where the volume of solvent generally constitutes 50% of the volume of the pre-polymerization mixture. After polymerization, the resulting

bulk monolith is ground and sieved to obtain irregularly shaped particles of appropriate size (typically 5-50 μm), which can be used for various applications such as separation materials in chromatography or solid-phase extraction. Until now, bulk polymerization still remains the most used procedure for MIP synthesis (Alexander et al., 2006).

However, bulk polymerization possesses several drawbacks: the procedure is time-consuming and causes loss of material, and as mentioned before, it is not suitable for industrial applications (Poma et al., 2010). Moreover, some applications require specific formats of MIPs, such as nanoparticles, core-shell beads, thin layers, membranes... For these other physical formats of MIPs, other polymerization procedures are specially adapted (Haupt, 2003b).

I.2.4.2. Precipitation polymerization

Precipitation polymerization was first introduced by Ye and co-workers (Ye et al., 1999), to synthesize MIP nanoparticles for the recognition of estradiol and theophylline. The nanoparticles had an average diameter of 200 nm for the theophylline-MIP, and of 300 nm for the estradiol-MIP (Figure 1.10). This method is now widely used in the MIP field in order to synthesize nanoparticles as it is quite easy and straightforward, and does not require stabilizers or other additives.

The approach is based on the use of a solvent, where the monomers are soluble but the resulting polymer is not. The solvent generally constitutes at least 90% of the volume of the pre-polymerization mixture. Contrary to bulk polymerization, the final material is not obtained by coagulation of the polymer chains, but is formed when the polymer chains grow until being insoluble, thus forming a precipitate.

Compared to bulk materials, MIP beads prepared by precipitation polymerization can show better molecular recognition properties (Jiang and Tong, 2004; Lai et al., 2007). Indeed they have higher surface-to-volume ratios, resulting in higher binding capacities and kinetics, and better accessibility to the binding sites (Poma et al., 2010). Due to their enhanced properties, their small size and their spherical shape, these MIP particles have found numerous applications, such as immunoassays (Surugiu et al., 2000), capillary electrochromatography (Schweitz et al., 2000), fluorescence polarization assays (Hunt et al., 2006), chemiluminescence imaging (Surugiu et al., 2001a,b), or sensing materials (Reimhult et al., 2008).

However, the drawback of this approach is the high dilution of monomers (a few percent, w/w) required in order to obtain small beads, which can affect the strength of the interactions between template and monomers. This problem can be overcome by choosing a couple of templates and functional monomers that interact strongly enough to form a stable complex under these conditions. Moreover, the size, shape and binding properties of the MIP nanoparticles obtained with this technique are not always well controlled, as it depends on several parameters, such as the reactants, the initiation, the temperature, the reaction time, and most importantly, the properties of the solvent with respect to the polymer.

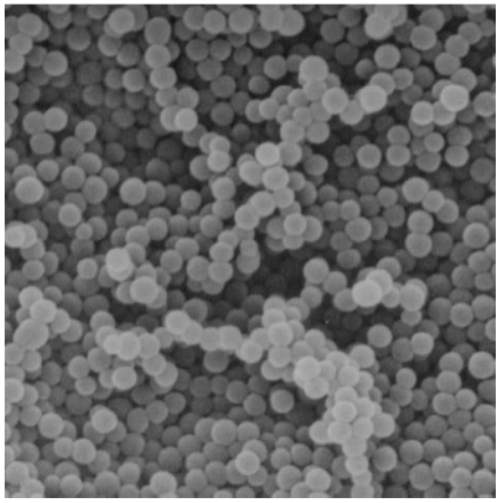

Figure 1.10. *Scanning electron micrograph of estradiol-imprinted polymer particles obtained by precipitation polymerization, of an average size of 300 nm. Reproduced from Ye et al., 1999.*

I.2.4.3. Heterogeneous synthesis procedures of MIPs

Heterogeneous procedures are used to synthesize MIPs and allow controlling the heat of the reaction, the viscosity of the medium, but also the size of the polymer beads. Contrary to bulk and precipitation polymerizations, heterogeneous polymerizations take place in two-phase systems where the starting monomers and/or the resulting polymer are in the form of a fine dispersion in an immiscible liquid. In addition to the monomers, the solvent and the initiator, some additives are added to the pre-polymerization mixture to emulsify the monomers, and/or stabilize the monomer droplets and the resulting polymer. These polymerization procedures allow the synthesis of spherical polymer particles with typical sizes ranging from about 50 nm to 1-2 mm or larger (Arshady, 1992). Below, the techniques of suspension and emulsion polymerizations will be described briefly.

Suspension polymerization

In this approach, the monomers are mechanically dispersed in the form of small droplets in a non-compatible liquid, usually water, and are polymerized using a monomer-soluble initiator (Odian, 2004). The monomers are kept in suspension by continuous agitation and the addition of non-ionic stabilizers, such as poly(vinyl) alcohol or methyl cellulose, which can prevent droplet coalescence. The polymerization is confined into monomer droplets, where the mechanism and kinetics of polymerization are equivalent to bulk polymerization. The parameters that can be used to control the particle size are the stirring rate, the ratio of reactants, stabilizers, and temperature. If required a porogen can be added to the monomer droplets in order to make the resulting particles porous. This approach can be used to synthesize particles of any size, but is most suitable for synthesizing particles of size ranging from 20 to 2000 μm. However the size polydispersity obtained with this method is high.

Several examples of MIPs beads obtained by suspension polymerization in aqueous phases can be found in the literature (Flores et al., 2000). However, given that water can affect the interactions between the template and the functional monomers, water has been replaced as the continuous phase by other media such as perfluorocarbons (Mayes and Mosbach, 1996), liquid paraffine (Kempe and Kempe, 2004) or silicone oil (Wang et al., 1996).

Emulsion polymerization

In this approach, the monomers are also mechanically dispersed in the form of small droplets in a non-compatible liquid, but unlike suspension polymerization, the initiator is soluble in the continuous phase and not in the monomer, and monomers are emulsified in the medium by the aid of surfactants. In these conditions, the monomer is present in the medium partly as monomer droplets (1-100 μm) and partly as surfactant-coated micelles (2-10 nm); the ratio and dimensions of which depending on the concentration and the nature of the emulsifying agent, and on the reaction conditions. Usually, the particles obtained with emulsion polymerization are quite monodisperse. The radical species are generated in the continuous phase and diffuse as oligoradicals into the micelles, where the propagation step takes place. As a result, the particle size increases as new monomers migrate from the droplets to the micelles.

There are two methods of emulsion polymerizations: *mini-emulsion* and *micro-emulsion*, which can be obtained depending on the amount of emulsifying agent.

In the case of *mini-emulsion* are used a high dispersing shear rate and a surfactant concentration below the critical micelle concentration (CMC). This system consists then in a kinetically stable emulsion containing very small monomer droplets (50-500 nm) with surfactants adsorbed on their surface, and very few micelles. The polymerization takes place in the droplets, and as a result, particles of 50-500 nm are obtained.

In the case of *micro-emulsion* are used a high dispersing shear rate and a surfactant concentration above the critical micelle concentration (CMC). All the monomers are then included in the micelles, and as a result, particles of 10-100 nm are obtained.

The drawbacks of this method are the presence of surfactants and other stabilizers and the need for water as continuous phase, which can both disturb the molecular recognition process. There are also some examples of MIPs that were synthesized in inverse water-in-oil systems, which means that a hydrophilic phase is polymerized in a hydrophobic phase. Water-in-oil emulsions were used for the imprinting of water-soluble substrates, and most notably metal ions (Kido et al., 1992). A very interesting study was performed by the group of Shea, who used inverse microemulsion polymerization to synthesize MIP nanoparticles with surface binding sites for hydrophilic peptides (Zeng et al., 2010). In order to ensure that the hydrophilic peptide will remain at the interface water-oil during polymerization, the peptide template was coupled with fatty acids at the N-terminus. As a result, MIP nanoparticles with nM affinity for the target peptide were obtained.

I.3. Some applications of MIPs

I.3.1. Separation

As mentioned previously, MIPs were first applied as separation materials, and more precisely as chiral stationary phases for the separation of racemic mixtures. Other applications concern capillary electrochromatography (CEC), principally for chiral separations, and solid-phase extraction (SPE). MIP-based CEC is a promising technique as it achieves better resolution and separation factors than MIP-HPLC (> 100 000 plates.m^{-1} for CEC compared to 2000-5000 plates.m^{-1} for HPLC) (Haupt, 2001).

MIPs as sorbents for SPE (in abbreviation MISPE) are very interesting when compared to their 'biological counterpart', the immunoadsorbents, due to their lower price, their high adsorption capacity

and their stability in different environments, especially organic solvents. At the same time they are much more selective than the common C18-based adsorbents. MIPs have been used to extract and pre-concentrate analytes from a great variety of matrices, such as biofluids (urine, plasma, serum, milk), environmental waters, tissue samples, food, soil samples and plants. For MISPE, extraction from aqueous environments such as biofluids or environmental waters is challenging because water is not compatible with the molecular recognition process. To overcome this problem, a solvent switch can be included into the procedure, that is, the first adsorption step is in water where a number of different molecules are non-specifically retained, followed by drying the polymer prior to washing with an organic solvent more compatible with the MIP, to establish the specific interactions of only the target analyte with the binding sites, followed by elution and analysis with a general method such as, LC-MS/MS.

The other problem concerning the use of MIPs in SPE is template leakage, as it is sometimes impossible to remove 100% of the template during the washing steps, except using harsh conditions that may affect the binding properties of the MIP. This can lead to false positive results especially in trace analysis. The best solution remains the use of a template analogue during the imprinting step rather than the target analyte itself, which can be easily distinguished from each other in LC-MS/MS.

For use as separation materials, MIPs should be in bulk form, in the 25-50 μm size range, but to overcome the drawbacks of bulk MIPs, some examples of MIPs synthesized *in-situ* in the columns can be found in the literature (Tse Sum Bui and Haupt, 2010).

I.3.2. Binding assays

MIPs can be applied as “artificial antibodies” in immunoassays, as they possess the feature to bind selectively a target analyte. This was shown for the first time by Mosbach and co-workers (Vlatakis et al., 1993) who developed MIP-based pseudo-immunoassays for theophylline and diazepam using radiolabels, which showed good correlation with antibody-based enzyme immunoassays. The cross-reactivities of the MIPs were also similar to those of the antibodies. Since then, MIPs have been widely used in radioimmunoassays for the detection of several analytes such as drugs (Andersson, 1996), herbicides (Haupt et al., 1998a) or corticosteroids (Ramström et al., 1996). Later, MIP-based assays were developed using fluorescence (Haupt et al., 1998b), optical absorption (Piletsky et al., 2000) or chemiluminescence (Surugiu et al., 2000) for detection. An exciting use of MIP as artificial antibody was performed by Shea and co-workers, who developed MIP nanoparticles that could capture the cytotoxic peptide melittin in the bloodstream of living mice. This is the first demonstration of biocompatible MIPs for *in-vivo* applications (Hoshino et al., 2010). Similarly, in our group, water-compatible MIP microgels were used as specific enzymes inhibitors (Cutivet et al., 2009), which shows the strong potential of MIPs as drug candidates.

MIPs can also be used in automated and high-throughput assays of chemical and biological combinatorial libraries, which is interesting for industrial applications or drug screening. For example, a high-performance MIP-based assay for 2,4-D using chemiluminescence imaging was reported by Haupt and co-workers (Surugiu et al., 2001a). Microtiters plates (96 or 384 wells) were coated with MIP microspheres using poly(vinyl alcohol) as glue, and the analyte 2,4-D-peroxidase conjugate was detected using luminol as the chemiluminescent substrate. Light emission was then quantified with a CCD camera imaging system.

More recently, we reported a MIP-based assay using fluorescence polarization, for the detection of fluoroquinolone antibiotics in water and milk samples (Ton et al., 2012).

I.3.3. Drug delivery

MIPs have been recently applied for drug delivery, as the specific interactions between the therapeutic drug and the MIP and the possibility to tune the MIP composition can be used to control drug loading and release (Wang et al., 2011). The first MIP that was applied for drug delivery was a theophylline-imprinted polymer. Theophylline is a drug for the treatment of asthma, and is of interest for controlled release studies, as it possesses a narrow therapeutic index and shows toxic effects at high concentrations. Norell and co-workers (Norell et al., 1998) synthesized the same theophylline-imprinted polymer as Mosbach and coworkers (Vlatakis et al., 1993) and loaded it with different concentrations of theophylline. The release profile of the MIP in phosphate buffer (pH 7) was determined by UV spectroscopy and scintillation counting. As a result, for low concentrations of theophylline (< 2 mg theophylline/g polymer), the release was somewhat linear; however for high concentrations of theophylline, the release profile was that of a non-imprinted system. This was probably due to the fact that for high concentrations of template, the interactions are mostly non-specific. An interesting study was performed by Suedee and co-workers, who used a classic MAA-EDMA-based system to study the controlled delivery of β-blockers, especially S-propanolol. In particular, they showed that MIPs beads obtained by suspension polymerization or granules obtained by bulk polymerization could be used for the selective delivery of one enantiomer from a racemic mixture (Suedee et al., 2000; 2002).

A challenge in the application of MIPs in drug delivery can be their use in aqueous environments, as generally the highly polar and hydrogen-bonding molecules of water disturb the interactions between the template and the functional monomers. Depending on the applications, this would not be a problem, since the MIP can be synthesized in an organic solvent, and be used afterwards in an aqueous solvent for the release of the analyte. However, the low water-compatibility of the MIP could be a limitation for the drug uptake in water, and for the control of the drug release rate in water. Several approaches exist to make MIPs more water-compatible. For example, Allender and co-workers proposed to embed the MIP and drug within a secondary polymer matrix of commercially available non-polar transdermal adhesive (Allender et al., 2000). As a result, the release of theophylline and propranolol was slower in the case of MIPs, compared to non-imprinted systems.

An interesting application of MIP concerns the treatment of ocular diseases. MIPs were synthesized in the form of hydrogel-based contact lenses capable of controlled drug delivery. For example, molecularly imprinted hydrogels were prepared as soft contact lenses for the controlled delivery of timolol, a drug commonly used for glaucoma therapy (Hiratani and Alvarez-Lorenzo, 2002).

I.3.4. Sensors

MIPs are interesting alternatives to biological elements as recognition elements in chemical and biosensors, because of their superior stability combined to their molecular recognition properties. In particular, the quartz crystal microbalance, a mass-sensitive acoustic transducer, has become very popular in combination with MIPs, probably because of its low price, robustness and ease of use (Haupt et al., 1999). Applications of MIPs in optical sensors will be developed in the next section.

II. Application of MIPs in opto-chemical sensors

II.1. Chemical sensors: definition and classification

A sensor is a device that can deliver, in response to a physical or chemical stimulus, a measurable signal. In nature, sensors are widely used by living organisms, the most obvious ones being the five organs (eye, ear, tongue, nose, skin) that give the commonly called "five senses". The "five senses" are, by definition, physiological capacities that provide data for perception to the human being (but also numerous other living organisms). Each sensor responds to an external stimulus by converting it into an electrical signal that is sent to the brain through the nerves. These "five senses" are:

- Sight or more formally, ophtalmoception. The sensor is the eye; the photoreceptors located on the retina convert light, which is the external stimulus, into an electrical signal that is interpreted by the visual cortex of the brain.
- Hearing or audioception. The sensor is the ear; the mechanoreceptors located in the inner ear respond to the mechanical pressure that constitutes the sound.
- Taste or gustaoception. The sensor is the tongue; the chemical substance (which is the food dissolved in saliva) reacts chemically with the taste receptors located in the taste buds of the tongue. Sweetness and bitterness are perceived upon binding of the corresponding molecules to the G protein-coupled receptors of the taste buds, whereas saltiness and sourness perceptions are produced by the presence of alkali metal (mostly sodium) or hydrogen ions in the taste buds.
- Smell or olfacoception. The sensor is the nose; the odorant molecules bind to the olfactory receptors, and this binding event provokes a complex signal transduction cascade (induced by protein structural changes) that is finally converted into an electrical signal conducted to the brain.
- Touch or tactioception. The sensor is mostly the skin (but for this perception, it can be also the tongue, mucosa…); the pressure receptors located in the skin and some other areas respond to variations in pressure.

Apart from these five "traditional" sensors, the human body possesses a great variety of other sensors. We can cite for illustration again the skin that is also a temperature sensor and possesses receptors for heat and cold. At the cellular level, we can find for example sensors sensitive to glucose or oxygen level. Examples of biological sensors are innumerous.

During the 20th century, the wide development of industry has led to the broad development of sensor technology. Nowadays, sensors have become an integral part of our daily life and are encountered in so many fields and used for so numerous applications, that it would be too long to describe all of them in this chapter. For example, sensors are used in the automotive industry, in environmental or food analysis, in clinical diagnostics, or for the detection of illicit drugs. Concerning these "artificial" sensors, they can be divided into two types: physical sensors and chemical sensors. Physical sensors provide information about a physical property of the system. Chemical sensors respond to specific chemical substances (molecules or ions) by delivering a measurable physical or chemical signal. For chemical sensors, a recognition element is required in order to respond to the presence of analyte. The recognition element can be of three natures:

- *Physical*: No chemical reaction takes place. Typical measurements are based on change of absorbance, refractive index, conductivity, temperature or mass.
- *Chemical*: A chemical reaction involving the analyte and the recognition element induces the analytical signal.
- *Biological*: A sub-class of the chemical sensors; here the chemical reaction occurs between the analyte and a biological recognition element, which can be an enzyme, an antibody, a cell membrane, a cell, etc.

However, in some cases, it is difficult, or even impossible, to clearly distinguish between physical and chemical transduction modes, especially when the sensing device is a multiplexed device and is composed of several sensors or transducers.

Two functional units constitute the chemical sensor: the *receptor* or *recognition element*, and the *transducer* (Figure 1.11). As mentioned above, the receptor transforms the chemical information given by the presence of a specific analyte into a form of energy that can be measured by the transducer. Then the transducer transforms this energy into a useful measurable signal that can be analyzed by an observer.

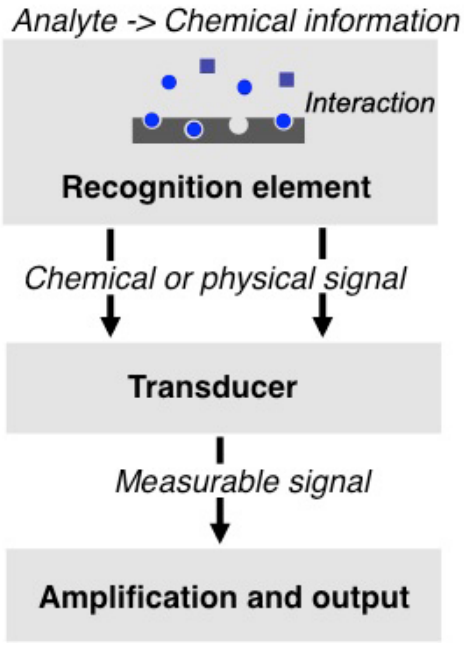

Figure 1.11. *Schematic representation of a chemical sensor.*

In 1991, the International Union of Pure and Applied Chemistry (IUPAC) has set a definition for a chemical sensor as "*a device that transforms chemical information, ranging from the concentration of a specific sample component to total composition analysis, into an analytical useful signal. The chemical information may originate from a chemical reaction of the analyte or a physical property of the system investigated.*" A more restrictive definition of chemical sensors was set in 2008 that define chemical sensors as "*miniaturized analytical devices than can deliver real-time and online information on the presence of specific compounds or ions in complex samples.*" (McDonagh et al., 2008). In general, characteristics of good chemical sensors are the following: specificity of the response towards the measured analyte only (which means that the sensor should not respond to other molecules that can be encountered), sensitivity, and fast response time.

Chemical sensors can be divided into four main groups depending on the working principle of their transducers, which are: optical sensors, electrochemical sensors, mass sensitive sensors and calorimetric sensors. These groups can again be divided into subgroups depending on the type of measurements (Table 1.4).

Table 1.4. *General classification of chemical sensors, based on the classification made by IUPAC.*

Chemical sensor (type)	Working principle of the transducer	Sensing mode	Comments
Optical	Transform changes in optical parameters resulting from the interaction between the analyte and the recognition element	**Absorbance**	Measured in a transparent medium
		Reflectance	Measured in a non-transparent medium
		Luminescence	Based on the measurement of light intensity emitted by a chemical reaction
		Fluorescence	Positive emission caused by irradiation (includes also quenching)
		Refractive index	Result of change in composition (includes surface plasmon resonance)
Electrochemical	Transforms the effect of the electrochemical reaction between the analyte and the electrode into a measurable signal	**Voltammetric**	Measurement of the current
		Potentiometric	Measurement of the potential of the indicator electrode (against a reference electrode)
Mass sensitive	The device transforms a mass change into a change in a property of the support	**Piezoelectric**	Measurement of the frequency change of the quartz oscillating plate induced by mass absorption of the analyte
		Surface acoustic wave	Based on the change of the propagation velocity of an acoustic wave induced by mass absorption of the analyte
Calorimetric	Heat effects induced by a chemical reaction or after absorption of the analyte	**Heat**	Measurement of the molar enthalpy changes in enzymatic reactions

This table summarizes the general way to classify sensors. There are, of course, other possible classifications, for example, depending on their applications and the analyte detected (pH sensors, metal ions sensors, gas sensors, etc). In the next section of this chapter, we will focus exclusively on the description of MIP opto-chemical sensors, which were the purpose of this work.

II.2. Surface Plasmon Resonance

Surface plasmons can be defined as coherent electron oscillations that occur at, for example, a metal-dielelectric interface. A surface plasmon resonance (SPR) measurement is based on a difference of refractive index of two transparent media separated by a thin metal film. An incident polarized light hits the interface between the lower refractive index medium and the higher refractive medium at an angle above the "critical angle", so that total internal reflection occurs. However, given that the surface of the higher refractive index medium is coated with a thin film of noble metal (gold, silver, platinium), the reflection is not total because some of the energy is lost in the metallic layer in the form of the evanescent wave. At the surface of the thin metal film, interaction of the wave with the oscillating mobile electrons (surface plasmons) occurs, leading to a loss of energy and to a simultaneous and sharp decrease in the intensity of the reflected light under resonance conditions. In an SPR measurement, the reflectivity is measured, which represents the ratio between the reflected and incident light intensities as a function of the incident angle θ. The SPR angle is the angle at which the loss of energy is maximal, and thus the reflectivity is minimal. Adsorption of an analyte on the metallic interface induces changes in its refractive index, resulting in a shift of the SPR angle ($\Delta\theta_r$) as well as a change in reflectivity (ΔR) measured at a fixed incident angle. The angle of the incident light is dependent on the characterics of the metal layer, which means that the resonance angle will be sensitive to analyte adsorption on the metal layer (Figure 1.12).

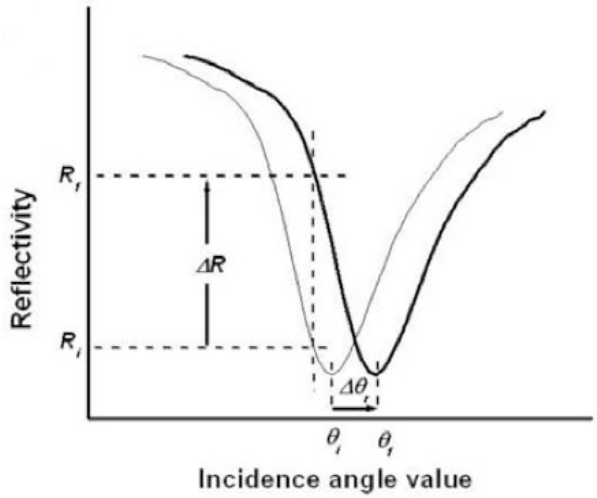

Figure 1.12. *Variation of the SPR signal intensity, namely the reflectivity as a function of the incidence angle value. Reproduced from Lépinay et al., 2012.*

Promising work combining MIPs with SPR can be found in the literature. Takeuchi and co-workers directly synthesized a MIP against sialic acid on the SPR chip. As a result the MIP-based SPR sensor chip showed selective response to the ganglioside GM_1 in the range 0.1-1.0 mg/mL, and worked in aqueous media. However no change in refractive index could be detected upon binding of sialic acid (Kugimiya and Takeuchi, 2001). Indeed, the major drawback of using MIPs with SPR is the low sensitivity of the evanescent field that could not detect small changes in refractive index induced by the adsorption of small molecules. In other examples, ultra-thin MIP films were prepared by methods such as electropolymerization or surface grafting (Lépinay et al., 2012). For example, electropolymerized MIP films were combined with a SPR transducer for the detection of the mycotoxin zearalenone with a limit of detection (LOD) of 0.3 ng/g corn, which is comparable to the LOD obtained

with the enzyme-linked immunosorbent assay (ELISA) (Choi et al., 2009). An example of surface grafting was demonstrated by Lotierzo et al., 2004, where a MIP film was synthesized by direct photografting of a MIP film on a gold chip surface. The grafting consisted of surface functionalization with a self-assembled monolayer followed by covalent attachment of the photoinitiator, and finally polymerization of the MIP. Another approach is to use spin-coating to fabricate thin MIP films on gold-coated glass plates, as reported by Yoshikawa et al., 2008. More recently, protein-imprinted polymers were synthesized on SPR sensors chips by photolithographic patterning, resulting in binding with the template protein avidin with dissociation constants in the submicromolar range (125 nM) (Lautner et al., 2011).

To improve the sensitivity of the detection of small molecules, an original approach was developed by Matsui and co-workers, who prepared a MIP gel with embedded gold nanoparticles on a gold-coated SPR chip (Figure 1.13) (Matsui et al., 2005). Binding of the analyte (dopamine) induced swelling of the gel, resulting in a greater distance between the gold chip and the gold nanoparticles embedded in the MIP and shifting the dip of the SPR curve to higher angles. Moreover, the authors showed that the presence of gold nanoparticles in the MIP matrix resulted in an enhancement of the signal intensity (i.e. the change of the SPR angle) in comparison with the sensor chip with no gold nanoparticles.

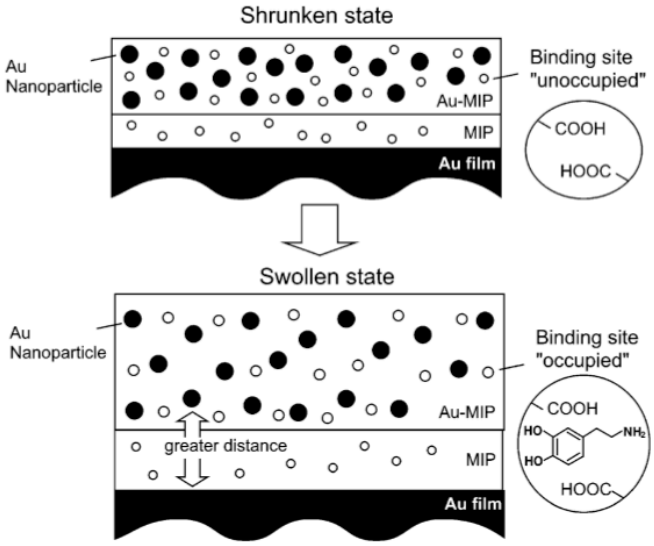

Figure 1.13. *Schematic representation of the MIP with embedded Au nanoparticles coated on the MIP-gold-coated SPR sensor chip. Reproduced from Matsui et al., 2005.*

The localized surface plasmon resonance (LSPR) effect is defined as the charge density oscillation confined around metal nanoislands or nanoparticles (Figure 1.14). Since the work of Matsui in 2005, gold nanoparticles have been used in other works for the enhancement of the SPR signal. For example, ultra-thin MIP films containing gold nanoparticles were synthesized on gold nanoislands deposited on a glass substrate, for the detection of cholesterol using enhanced transmission SPR spectroscopy (Tokareva et al., 2006). As a result, the LSP band shifted from 654 nm to 598 nm after rebinding of the MIP sensor with 1 mM cholesterol.

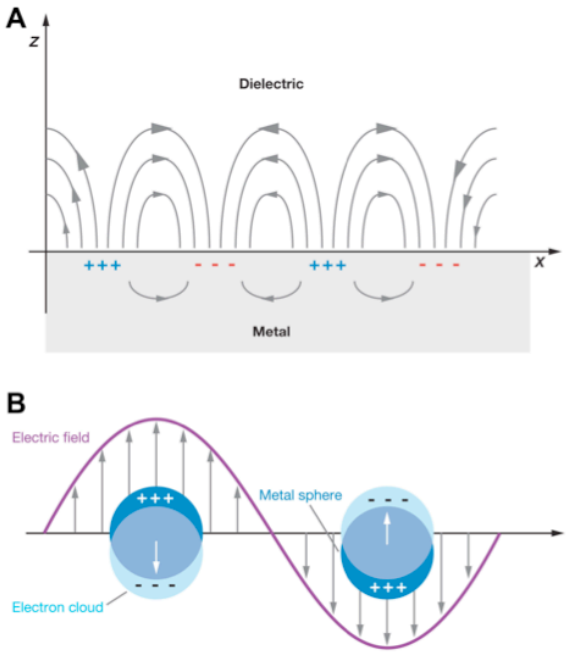

Figure 1.14. *Schematic representation of (A) a propagating surface plasmon and (B) a localized surface plasmon. Reproduced from Willets and Van Duyne, 2007.*

Very recently, a MIP-based fiber optic sensor using SPR for detection was described in the literature for the detection of trinitrotoluene (TNT) (Cennamo et al., 2013). The sensor was fabricated as follows: the cladding of an optical fiber was removed along half of the circumference, then a thin gold film was coated on it, followed by deposition of a TNT-imprinted polymer layer. Detection of TNT was performed by SPR, with a LOD of 50 μM, which is still quite high.

II.2. Surface Enhanced Raman Scattering

Surface enhanced Raman scattering (SERS) is a technique defined as the enhancement of the Raman scattering (the inelastic scattering of a photon) by molecules adsorbed on a metal surface or on metallic nanostructures. The enhancement of the Raman scattering can be explained as a combination of electromagnetic enhancement (LSPR effect) and chemical enhancement (formation of charge-transfer complexes between the molecule and the metal surface). However the major contribution is the electromagnetic enhancement (Willets and Van Duyne, 2007). This technique is highly sensitive as it may allow the detection of single molecules (Nie and Emory, 1997). Moreover, it is also very selective as the vibrational spectra given by this technique are characteristic for the adsorbed substance and are less affected by cross-selectivity compared to other techniques such as SPR. However the main difficulty is to combine the recognition layer with a SERS-active surface.

Wulff and co-workers were the first to report a MIP-based SERS sensor (Kostrewa et al., 2003). They generated by spin-coating thin MIP films of 500-750 nm of thickness on gold or silver surfaces. They could follow with the SERS bands the release and uptake of tartaric acid or aspartic acid under physiological conditions (aqueous buffer, ambient temperature). In their work, gold layers were preferred as sharper and stronger bands were obtained, with a better signal-to-noise ratio. However the stability of the polymer layers had to be improved.

Later, MIP droplets were deposited on a SERS-active surface by a nanofountain pen, to directly follow by SERS the uptake and release of the template, the drug S-propanolol (Kantarovich et

al., 2009). The enhancement by the SERS-active surface was demonstrated by comparing the Raman spectra of the MIP droplets deposited on a smooth gold surface and on a SERS-active gold coated patterned Klarite surface. As a result, the Raman signal was enhanced with the Klarite substrate and the SERS bands could be attributed to the template S-propanolol. More recently, a pattern of MIP droplets were deposited on the Klarite substrate using the nanofountain pen, in order to create a miniaturized MIP biochip for SERS measurements (Figure 1.15). Such an analytical platform could be useful for the simultaneous detection of multiple targets (Kantarovich et al., 2012).

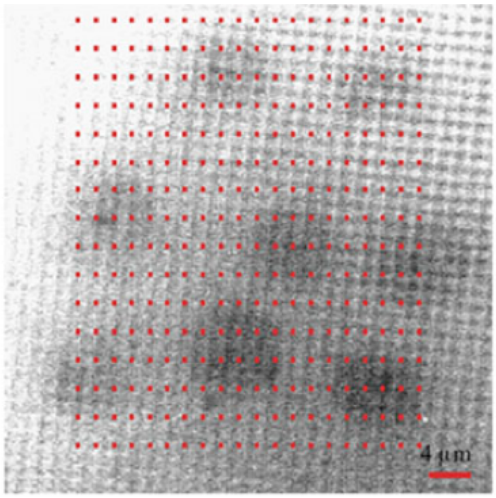

Figure 1.15. *Scanning electron micrograph of a MIP array on a Klarite patterned surface, where the droplets were printed by a nanopipette (around 600 nm diameter). The red spots mark the points of measurements of the SERS spectra. Reproduced from Kantarovich et al., 2012.*

A new approach was reported by our group, with the design of core-shell composite MIP nanoparticles for SERS measurements (Bompart et al., 2010). The core-shell nanoparticles consisted in a polymeric core of 400 nm diameter covered by a thin MIP shell of around 17 nm diameter, with gold colloids located between the core and the MIP shell (Figure 1.16).

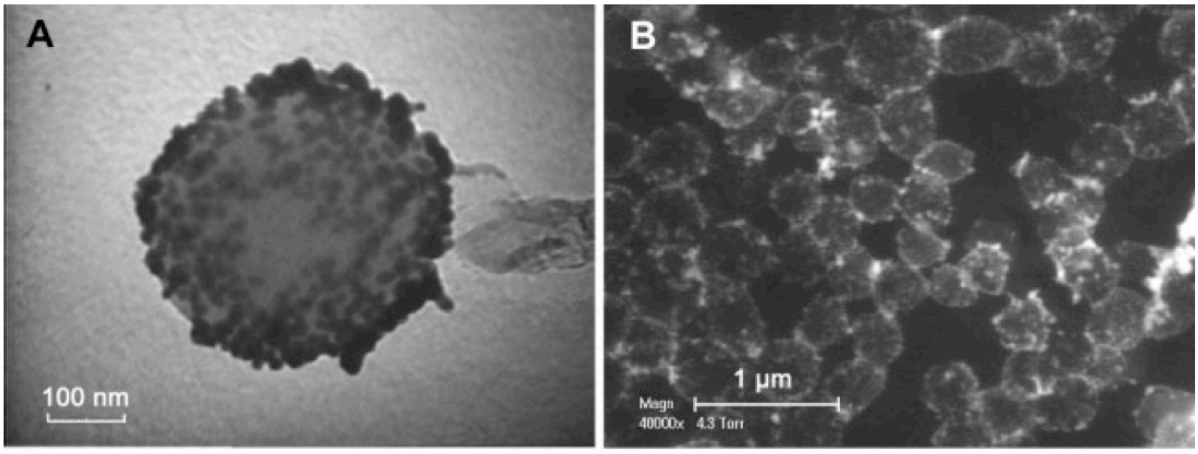

Figure 1.16. *(A) Transmission electron microscopy image of a core-shell composite MIP nanoparticle. (B) Scanning electron micrograph of the core-shell composite MIP nanoparticles. Reproduced from Bompart et al., 2010.*

As a result, specific binding of the template S-propanolol could be measured by SERS, with a LOD of 10^{-7} M, which was three orders of magnitude better than conventional Raman measurements performed on plain MIP particles (Bompart et al., 2009), and two orders of magnitude better than NIP particles (Figure 1.17). Moreover, SERS spectra were taken from single MIP or NIP nanoparticles, and measurements could be done even in diluted equine serum with a LOD of 10^{-6} M, which is a promising result for the direct use of MIPs as nanosensors in biological samples.

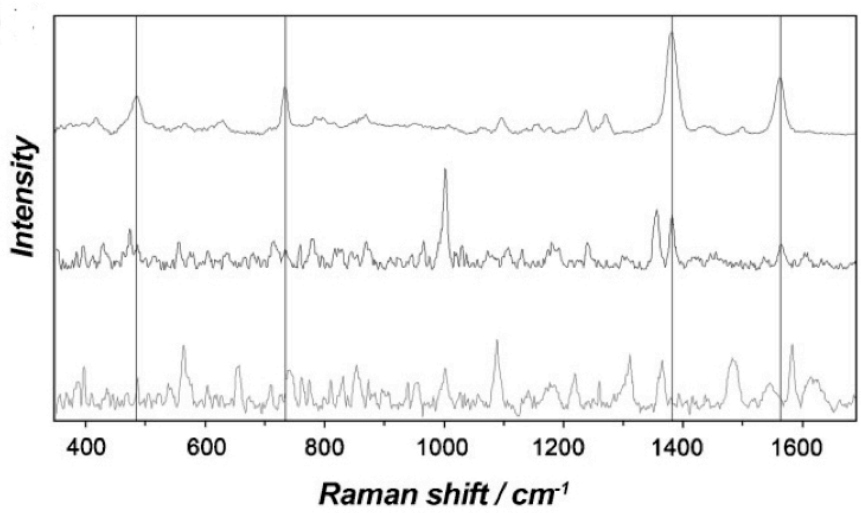

Figure 1.17. *SERS spectrum of 10^{-5} propranolol on aggregated gold colloids (top); SERS spectrum of a single composite MIP nanoparticle incubated in 10^{-7} M propranolol (middle), and SERS spectrum of a single composite NIP nanoparticle incubated in 10^{-6} M propranolol (bottom). The vertical lines represent the SERS bands at 785 nm of S-propanolol at 483, 733, 1380 and 1563 cm^{-1}. Reproduced from Bompart et al., 2010.*

II.3. Fluorescence-based MIP optical sensors

II.3.1. Introduction on fluorescence-based molecular sensors

Fluorescence can be defined as the emission of an electromagnetic radiation by a molecule that was excited by the absorption of an incident light. The fluorescence signal is emitted when the molecule relaxes from the excited state to its initial ground state, during a time called “fluorescence lifetime”. The fluorescent signal is emitted a longer wavelength than the excitation signal, due to the loss of energy between the absorption of the photons and the emission. This phenomenon is called the Stokes shift. Due to its high sensitivity and the intrinsic selectivity of communication between the excitation and the emission wavelengths, fluorescence has become a powerful tool for signaling and sensing purposes.

In the following sections, we will focus on fluorescence-based sensors using MIPs as the recognition element. Three strategies can be employed for monitoring the binding event (Haupt and Mosbach, 2000): (i) the analyte is fluorescent, (ii) the analyte is not fluorescent and the binding is monitored by a competitive or displacement assay with a fluorescent analogue of the template, or (iii) a fluorescent monomer is incorporated into the MIP, the fluorescence of which is changing upon binding.

II.3.2. Fluorescent analytes

If the analyte is fluorescent, the recognition event can be measured directly by steady-state fluorescence spectroscopy. The first MIP-based fluorescence sensor was developed by Mosbach and co-workers (Kriz et al., 1995). The device consisted in a layer of MIP held in front of a quartz window; an excitation light from an optical fiber was used to excite the fluorescent analyte retained by the MIP. The emitted light was collected and guided through an optofiber bundle to the detector. The model analyte used here was the fluorescent amino acid derivative dansyl-L-phenylalanine (dansyl-L-Phe). As a result the authors could follow the recognition process of dansyl-L-Phe, as the emitted fluorescence signal was function of the analyte concentration. Moroever, they could also demonstrate the specificity of the MIP using the opposite enantiomer dansyl-D-phenylalanine. These results were very promising for the use of MIPs in fluorescence-based sensing devices.

Later, Dickert and co-workers developed imprinted polyurethane layers for the fluorescence detection of polycyclic aromatic hydrocarbons (PAHs) in water (Dickert et al., 1998). These layers could be integrated into a flow cell system in order to constitute a fluorescence or mass-sensitive sensing device (Dickert et al., 1999). The interactions that occur between the analyte and the MIP layer are $\pi-\pi$ interactions. More recently, the group found out that using double templating of PAHs could increase the sensitivity of the MIP sensor. Indeed using a mixture naphthalene:pyrene (1:4, w/w) as template resulted in an increase in the sensitivity of one order of magnitude, and a low limit of detection of 10 ng/L was achieved for fluorescence measurements of the rebinding of pyrene (Lieberzeit et al., 2008). Other MIP-based flow-through fluorosensors have been described in the literature, such as for the detection of digoxin in serum, with a LOD of 17 ng/mL achieved (Gonzalez et al., 2008), or the detection of monoamine naphtalenes in drinking water in the ng/mL range (Valero-Navarro et al., 2009).

Apart from flow-through fluorosensors, some examples of MIP-based fiber optic sensors using fluorescence for detection have been reported in the literature, but these examples will be developed in detail in the next chapter about fiber optic chemical sensors.

The major drawback of using fluorescent templates is that the MIP usually exhibits residual fluorescence due to the entrapped template molecules. To overcome this, one possibility is to use a non-fluorescent analogue of a fluorescent template, such as N-carbobenzyloxy-L-phenylalanine and dansyl-L-phenylalanine as the fluorescent probe (Fuchs et al., 2011).

An interesting approach was very recently proposed by the group of Moreno-Bondi, in collaboration with our group (Zdunek et al., 2013). In this work, the MIP was imprinted with the fluoroquinolone antibiotic enrofloxacin (ENRO), which is fluorescent (excitation λ_{EX}= 292 nm and emission λ_{EM}=447 nm), and for the detection, ENRO was coupled with the lanthanide ion europium(III) in order to generate a europium(III)-ENRO complex (Figure 1.18). Thus the detection was based on the luminescence of europium(III), with λ_{EX}= 340 nm and λ_{EM}=612 nm. Lanthanides complexes possess several advantages: their narrow excitation and emission spectra allow for sensitive and selective analyses, they possess long emission lifetimes and a large Stokes shift, and exhibit an intense luminescence when complexed by appropriate ligands. Moreover, they emit in the red/near-infrared region, avoiding the fluorescence background of the polymer matrix or sample components. Thus this approach is interesting for all UV-excited analytes. In this work, the LOD was 580 nM. The method was sensitive, even though the LOD was above the maximum residue limit of 280 nM (100 ng/g) established by the Council Regulation No 37/2010 of the European Union for ENRO in milk, muscle and fat.

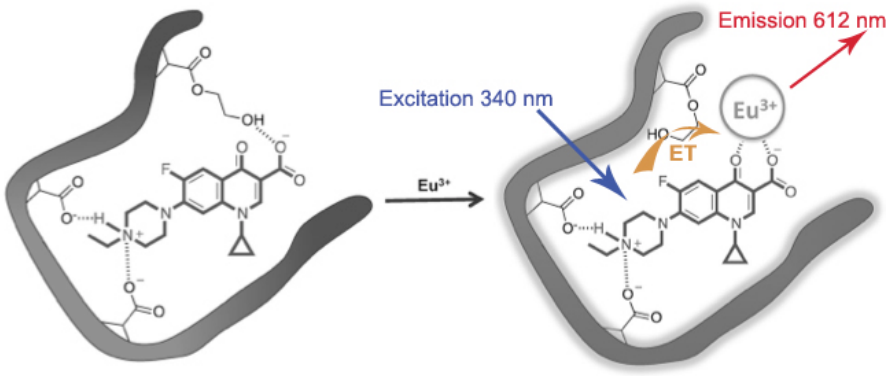

Figure 1.18. *Schematic representation of the sensing method based on the formation of the complex ENRO-europium(III) in the MAA-HEMA-based-MIP. ET:energy transfer. Adapted from Zdunek et al., 2013.*

The other noticeable aspect of this work was the nanostructuring of the MIP, which as prepared by nanomolding under the format of surface-imprinted nanofilaments. These nanofilaments should be very useful for applications in sensors, as they display a greater area/volume ratio and a good site accessibility leading to a fast response time. The nanofilament-based MIPs were for the first time developed in our group using S-propanolol, fluorescein and the protein myoglobin as model analytes (Figure 1.19) (Vandevelde et al., 2007 ; Linares et al., 2009).

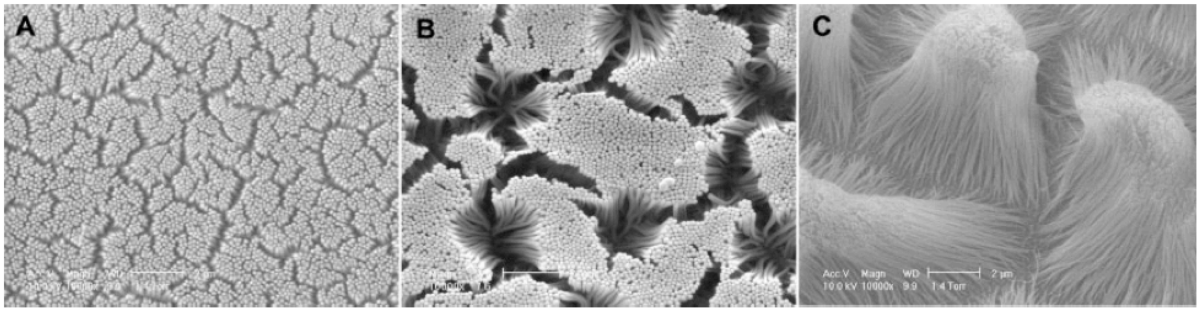

Figure 1.19. *Scanning electron microscopy (SEM) images of polymer nanofilaments obtained under different experimental conditions: electro-oxidation/phosphoric acid treatment durations of: (A) 1 min/70 min; (B) 4 min/70 min; (C) 4 min/15 min. The scale bar corresponds to 2 μm. Reproduced from Linares et al., 2009.*

Another interesting approach is the work performed by Takeuchi and co-workers, who developed a MIP that showed fluorescence shift upon binding (Matsui et al., 2000a). The MIP was prepared with 2-(trifluoromethyl)acrylic acid (TFMAA) for the recognition of cinchonidine. The process of fluorescence shift was explained by the authors as follows: TFMAA is a strong proton donor and protonates the template cinchonidine when it binds to the MIP. The protonated species may show a distinct fluorescence, which explains the red shift with increasing concentrations of cinchonidine. A similar study was performed earlier by the authors, but with a metalloporphyrin-based MIP that showed a shift in its maximum of absorption upon binding of the template. A visible shift appeared for 10^{-5} M of the analyte 9-ethyladenine (Matsui et al., 1998).

II.3.3. Competitive and displacement assays

If the template is not fluorescent and cannot be easily labeled, one possibility is to perform competitive or displacement assays with a fluorescent nonrelated probe that shows structural similarities to the target analyte. Either the fluorescent probe competes with the analyte for the binding sites of the MIP, or the fluorescent derivative is allowed to bind first and is subsequently displaced from the binding sites by the analyte (Haupt and Mosbach, 2000). For example, Piletsky and co-workers developed a displacement assay from a MIP chromatographic stationary phase, for the monitoring of the non-fluorescent analyte L-phenylalaninamide (Piletsky et al., 1999). For the detection, a mobile phase containing a fluorescent non-related probe rhodamine B was used, and subsequent injection of L-phenylalaninamide resulted in displacement of rhodamine B.

Previously, a similar displacement assay from a MIP chromatographic stationary phase was developed using the labeled chloramphenicol-methyl red for the detection of the template chloramphenicol. In this work, UV-absorbance measurements were performed (Levi et al., 1997). More recently, another fluorescent displacement assay for sensing of the mycotoxin zearalenone was reported (Navarro-Villoslada et al., 2007). Similarly to the previous work mentioned above, a HPLC column was filled with a MIP imprinted with cyclododecyl-2,4-dihydroxybenzoate (a synthetic mimic of zearalenone), which was used as stationary phase. Three fluorescent analogues of zearalenone were designed and synthesized for this work, and the best one was selected for the displacement assay, upon binding of zearalenone. However, the LOD was 25 μM in acetonitrile, which is high compared to the maximum residue levels for zearalenone that range from 20 to 400 μg/kg depending on the food matrix (i.e. 63 nM – 1.3 μM), according to the Commission Regulation (EC) No. 1881/2006 of the European Union.

Haupt and co-workers reported competitive and displacement assays for the detection of the herbicide 2,4-dichlorophenoxyacetic acid (2,4-D), using a fluorescent non-related probe 7-carboxymethoxy-4-methylcoumarin (CMMC) (Haupt et al., 1998b). The LOD was around 100 nM. Later, the same couple 2,4-D/CMMC was used for the first MIP-based fluorescence polarization immunoassay described with a MIP (Hunt et al., 2006). The amount of bound 2,4-D could be directly quantified by measuring the anisotropy of the CMMC in the MIP microgel suspension.

Very recently, a competitive assay for the detection of the antibiotic ENRO was developed, based on the principle of Förster resonance energy transfer (FRET) (Descalzo et al., 2013). FRET is a process of energy transfer between two chromophores: an energy donor (D) and an acceptor (A). The electronic energy transfer occurs from the photoexcited state of D to the ground state of A, and its efficiency is inversely proportional to the sixth power of the distance between D and A. Thus FRET occurs if the two species D and A are close enough (<10 nm), if there is a significant overlap between the emission spectrum of D and the absorption spectrum of A and if the orientations of the dipole moments of D and A are favorable. In the work of Descalzo et al., the FRET process occurred between the donor D Ru-$(phen)_3^{2+}$ complex (phen:1,10-phenantroline) and the acceptor A cyanine-labeled ENRO (NIR-ENR) (Figure 1.20). The FRET donor D was incorporated into the silica core, which was covered by a thin ENRO-MIP shell with a thickness of 4 nm, corresponding to the calculated Förster distance. Competitive assays were performed by incubating the MIP nanoparticles with NIR-ENR and increasing amounts of the target ENRO. Changes in the FRET signal were used to determine the binding of ENRO to the MIP. As a result, the quenching of the donor Ru-$(phen)_3^{2+}$ emission was reduced with increasing concentrations of ENRO. The LOD was 2 μM, which is quite

high. Moreover it would also have been interesting to see the data on the changes of the emission spectrum of the acceptor NIR-ENRO upon binding to ENRO. The advantage of this method is that the FRET signal change occurred immediately after addition of NIR-ENR.

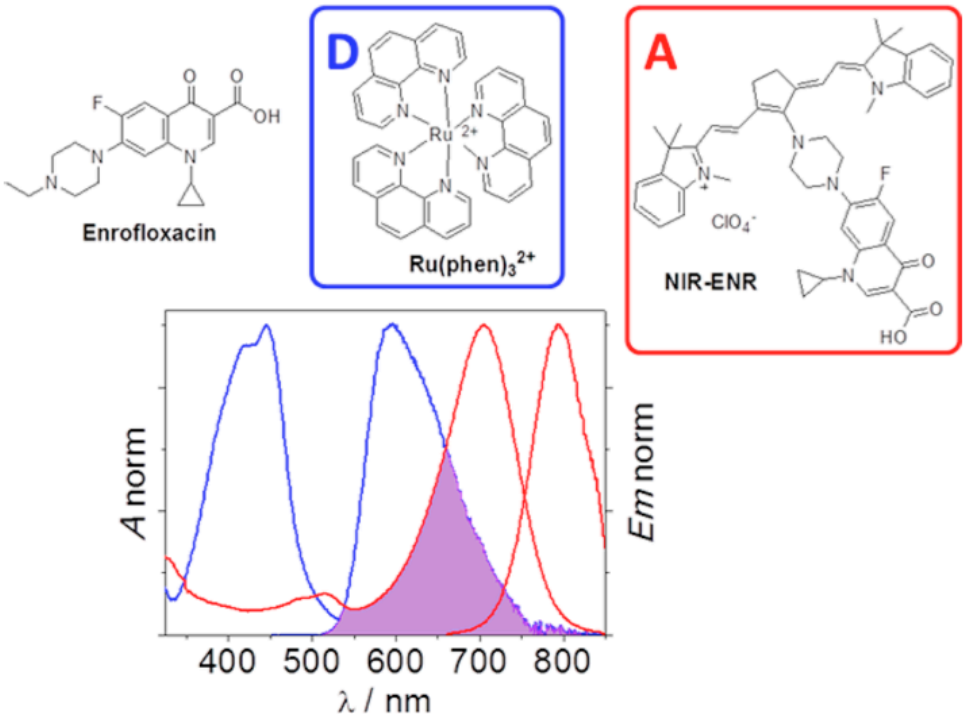

Figure 1.20. *Chemical structures of the target analyte, enrofloxacin, and the FRET donor (D) $Ru(phen)_3^{2+}$ and acceptor (A) cyanine-labeled enrofloxacin. Absorption and emission spectra of D (blue) and A (red) in ethanol. The violet region shows the spectral overlap.*

II.3.4. Fluorescence generated by the polymer

An attractive approach for the design of fluorescence MIP-based sensors is to incorporate fluorescent probes in the MIP matrix, the fluorescence of which changes upon binding, which can be quenching, enhancement or appearance of the fluorescence. This section describes the efforts that have been made to develop signaling MIPs with good sensing properties, with the perspectives of using them as recognition elements of optical sensors.

The first one was described by Turkewitsch and co-workers, who incorporated a fluorescent dye (trans-4-[p-N,N-dimethylamino)styryl]-N-vinylbenzylpyridinium chloride) as functional monomer for the recognition of cyclic adenosine-3',5'- monophosphate (cAMP) (Turkewitsch et al., 1998). As a result, binding of cAMP to the MIP resulted in quenching of the MIP with a LOD of 100 nM, whereas no effect was observed with the structural analogue guanosine-3',5'-cyclic monophosphate. Later, time-resolved fluorescence spectroscopy was used to characterize the fluorescent cAMP-MIPs. They could observe that the fluorescence lifetime of the MIP changed simultaneously with the quenching process (Wandelt et al., 2002; 2003)

Leung and co-workers described for the first time a signaling MIP based on fluorescence enhancement upon binding of the analyte (Leung et al., 2001). Generally, fluorescence enhancement is more interesting for sensing purposes than quenching, as it is a more specific phenomenon. They synthesized a fluorescent organosilane, and the sensing mode was based on the suppression of the

photoinduced electron transfer (PET) quenching when binding with an analyte occurs, i.e. when the tertiary amino moiety is protonated (Figure 1.21). The suppression of the PET quenching effect results then in a fluorescence enhancement. They applied it for a sol-gel MIP imprinted with 2,4-D, and could show that the fluorescence enhancement was dependent on the concentrations of 2,4-D, with a LOD of 45 μM.

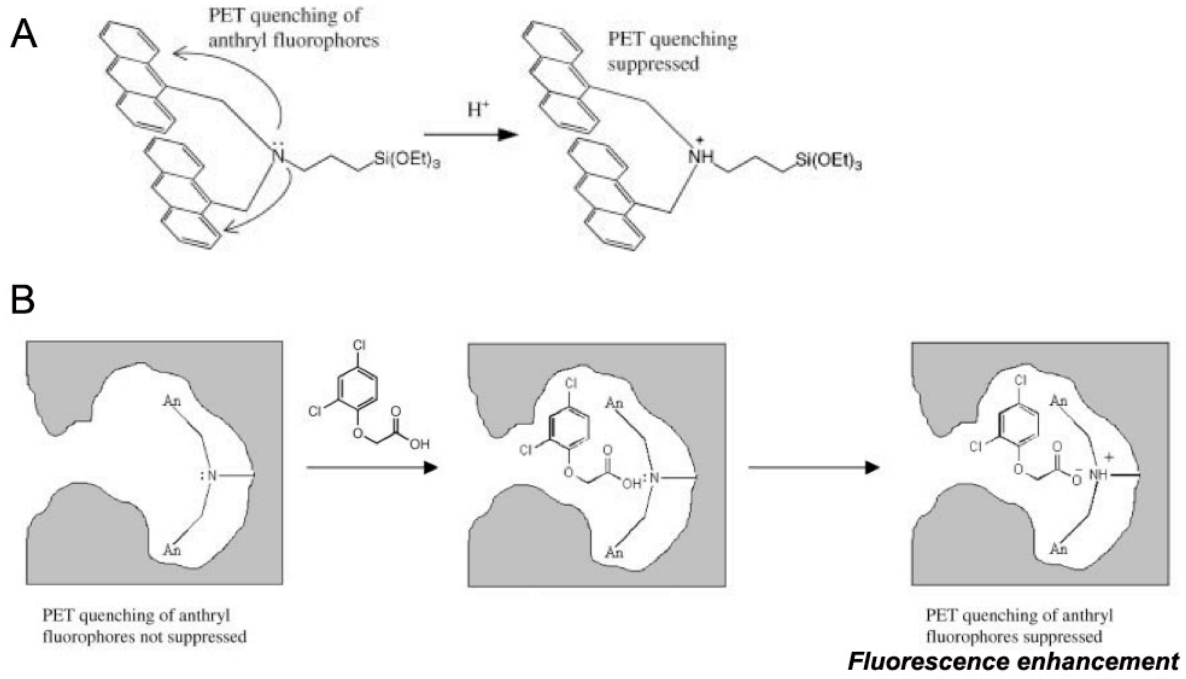

Figure 1.21. *(A) Suppression of the PET quenching effect upon protonation of the tertiary amine. (B) Interactions of 2,4-D in the binding sites of the sol-gel MIP leading to the suppression of the PET quenching effect and thus to fluorescence enhancement. Adapted from Leung et al., 2001.*

Takeuchi and co-workers have also extensively worked on signaling MIPs for the detection of non-fluorescent analytes. They prepared a cyclobarbital-imprinted polymer using the fluorescent functional monomer 2,6-bis(acrylamido)pyridine (Kubo et al., 2003), and later the fluorescent monomer 2-acrylamidoquinoline (Kubo et al., 2005), which both showed fluorescence enhancement upon binding of cyclobarbital. The authors explained the mechanism of enhancement of the second monomer as follows: the formation of the hydrogen bond between cyclobarbital and the quinoline nitrogen is similar to its protonation, which yields fluorescence enhancement (De Silva et al., 1997). For both monomers, no or little fluorescence enhancement was observed upon binding of structurally related analytes, showing the specific aspect of the enhancement process. Signaling metalloporphyrin-based imprinted polymers were also designed, such as a MIP containing a functional monomer with a zinc(II)-porphyrin (Zn-Por) moiety in which fluorescence intensity is quenched upon coordination of an axial ligand (Matsui et al., 2000b). They applied it for the detection of the template 9-ethyladenine (9EA) (Figure 1.22), and quenching of the MIP was observed when binding occurred. A signaling Zn-Por-based MIP was also synthesized for the recognition of cinchonidine. However, the fluorescent metalloporphyrins are limited to zinc(II) and magnesium(II).

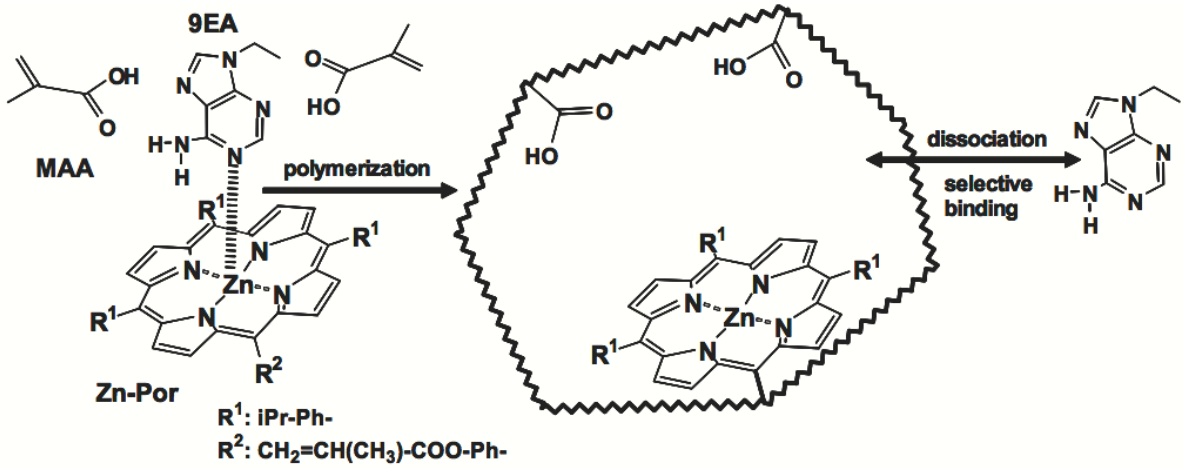

Figure 1.22. *Schematic representation of the preparation of the 9EA-imprinted polymer using [5,10,15-tris(4-isopropylphenyl)-20-(4-methacryloyloxy)porphyrinato]zinc(II) (Zn-Por) and MAA as functional monomers. Reproduced from Takeuchi et al., 2005.*

Later on, Takeuchi and co-workers designed fluorescent monomers for protein-imprinted polymers. In their first paper on this subject, they prepare lysozyme-imprinted polymers thin films on initiator-immobilized glass substrates. For the detection, they synthesized a non-fluorescent functional monomer that was coupled to a fluorescent dye, fluorescein isothiocyanate (FITC) after synthesis of the MIP (Figure 1.23). In this way, high fluorescent background could be avoided. Binding of lysozyme resulted in fluorescence enhancement, and the relationship between these two events was confirmed by SPR. Detection was performed in the low μM range (Sunayama et al., 2010). More recently, a similar work was performed but with dansyl ethylenediamine-conjugated *O*-acryloyl-L-hydroxyproline, as fluorescent functional monomer, for the detection of human serum albumin as model protein (Inoue et al., 2013). The MIP showed fluorescence enhancement upon binding, which was explained by the fact that the dansyl moiety is oriented towards the hydrophobic part of the protein, resulting in fluorescence enhancement and blue shift of the emission. The spatial orientation of the protein template in the binding cavity explained the specificity and the selectivity of the fluorescence enhancement process. Again, the relationship between the binding event and fluorescence enhancement was confirmed by SPR. Detection was performed in the μM range.

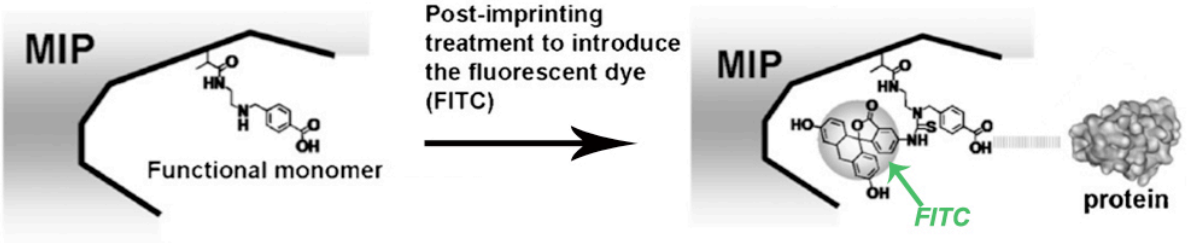

Figure 1.23. *Schematic representation of the preparation of the fluorescent imprinting cavity by post-imprinting coupling between the functional monomer and the FITC dye. Adapted from Sunayama et al., 2010.*

A fluorescent functional monomer containing fluorescein *o*-acrylate and boric acid moieties was incorporated in a MIP for the detection of glucose in aqueous media. The binding event of glucose was followed by quenching of the fluorescence, which was attributed to a change in the

polymer chains conformations upon binding. The presence of glucose could be monitored by quenching even in synthetic tear fluid, and in presence of other sugars. The LOD of the MIP film was 10 μg/mL (Manju et al., 2010).

An original approach was performed by Piletsky and co-workers who synthesized cubic core-shell MIP nanoparticles, in which the fluorophore (dansyl chloride) was located at the interface between the dendrimer core and the MIP shell (Ivanova-Mitseva et al., 2012). Binding of the template induced changes in the solvation of the fluorophore and in the conformation of the MIP shell, resulting in fluorescence enhancement. This enhancement was shown to be specific and selective, as only small effect was observed with other molecules. The response time was 10 minutes, and measurements were performed in the 10^{-8} M range. Since then, Sellergren and co-workers have also developed two fluorescent functional monomers that possess a urea binding site to respond to carboxylate analytes. In both cases, the MIP was imprinted with N-carbobenzyloxy-L-phenylalanine (Z-L-Phe) as model analyte. In the first work, the monomer contained a fluorescent naphthalimide moiety that responded to binding by quenching (Wagner et al., 2013). The quenching phenomenon was demonstrated to be specific and selective, and detection was performed in the mM range. In the second paper, the fluorophore was a nitrobenzoxadiazole group, and MIP nanoparticles were synthesized under a shell format on a silica core by RAFT polymerization Binding led to red shift of the emission peak as well as fluorescence enhancement. Detection was performed in the μM range (Wan et al., 2013).

Extensive work has been performed on the development of fluorescent signaling MIPs, which is promising for the design of fluorescence-based MIP optical sensors. However, only a few examples of signaling MIPs have been effectively integrated into optical sensors, which mostly concern fiber optic sensors.

An interesting approach was performed by the group of Murray, who used lanthanide luminescence combined with a MIP-based fiber optic sensor to selectively measure the hydrolysis product of the nerve agent Soman in water (Jenkins et al., 1999). MIPs containing coordinately bound europium ions (Eu^{3+}) were coated on the distal end of an optical fiber, and rebinding was characterized by the appearance of the narrow luminescence band in the 610-nm region characteristic of Eu^{3+}, which results from the coordination between the analyte and the copolymer. The influence of pH and thickness of polymer coating on the response time of the sensor was studied. The shortest response time (80% of maximum) was 8 minutes. The LOD was 660 ppq for the benchtop version, and 7 ppt and for the portable version (with an Ocean Optics spectrometer). Moreover, the sensor was shown to be highly selective as none of the other pesticides tested produced a luminescence band in the 610-nm region. However, the drawbacks of this set-up were the big size of the argon laser, used for excitation, but also the multi-step time-consuming protocol needed for the preparation of the fiber and the MIP coating.

In a recent paper, Nguyen and co-workers described a fiber optic sensor for the detection of cocaine, using a signaling MIP as recognition element (Nguyen et al., 2012). The MIP was covalently attached on the distal end of a bifurcated fiber, and contained acrylamidofluorescein as fluorescent functional monomer. Upon binding of cocaine, the carboxylate group of acrylamidofluorescein was deprotonated, resulting in a fluorescence enhancement of the MIP that was dependent on the concentration of cocaine. The enhancement was shown to be specific and selective, as a smaller enhancement was observed respectively for the NIP, and for the MIP with other drugs such as ketamine, codeine or amphetamine sulfate. The response time was dependent on the concentration of

cocaine, and was of 15 minutes for 250 μM cocaine. However, 70% of the total signal change was observed in 5 minutes. Detection was performed in the μM range, with a LOD of 2 μM, which can still be improved according to the authors.

II.3.5. Quantum dot photoluminescence

Besides fluorescent analytes and signaling polymers, the incorporation of semi-conductor nanocrystals or quantum dots (QDs) in a MIP leads to a sensory material, in which binding event can be monitored by a change in the photoluminescence response of the QD. QDs are of great interest in optical sensing as they possess several advantages over fluorescent labels. For example, they are highly photostable and their excitation and emission properties can be tuned by controlling their size.

Nickel and co-workers coated ammonia-imprinted poly(acrylic acid) films on cadmium selenide QDs. As a result, bare CdSe QDs could not discriminate between triethylamine and ammonia whereas the MIP-coated CdSe QD showed a selective photoluminescence response to ammonia (signal enhancement of around 20%), and no response to triethylamine. Moreover, a non-imprinted poly(acrylic acid)-coated CdSe QDs did not show any response to triethylamine or ammonia, demonstrating that imprinting is necessary for analyte access to the CdSe QD surface (Nickel et al., 2001). Another study was performed with CdSe QDs coated with guanosine-imprinted nanoshells for DNA recognition (Diltemiz et al., 2008). Methacryloyamidohistidine-platinium was used as a new metal-chelating monomer and binding of guanosine occurred via chelation to the Pt(II) metal ion. The selective fluorescence enhancement upon binding was attributed to the high complexation geometric affinity between guanosine molecules and the binding cavities.

Some studies used fluorescence quenching of QDs to characterize the binding process. For example, Lin and co-workers reported the synthesis of MAA-EDMA-based MIP shells on CdSe/ZnS QDs functionalized with 4-vinylpyridine (Figure 1.24) (Lin et al., 2004). Template rebinding resulted in quenching of the photoluminescence emission of the QDs, for several analytes such as caffeine, uric acid, L-cysteine or estriol. Non-imprinted systems showed no response to analyte, for all analytes. The quenching phenomenon was explained by the authors as a FRET process occuring between CdSe/ZnS QDs and bound analytes.

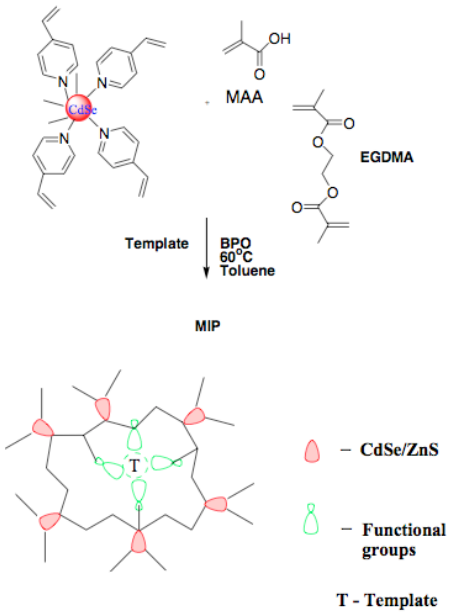

Figure 1.24. *Preparation of the CdSe/ZnS QDs incorporated MIP. Reproduced from Lin et al., 2004.*

However, until now, MIPs combined with QDs have not proved yet that they could be applied for sensing of analytes in the "real world". The first problem to overcome is the rather complicated procedure to obtain MIP-based QDs. Then, in most of the papers describing MIP-based QDs, some data are missing, such as the response time, the LOD or the dynamic range of detection.

II.4. Molecularly imprinted photonic polymers

Photonic crystals are optical nanostructures that show a periodicity in their dielectric constant in some particular dimensions (one, two or three dimensions). Photons propagate through photonic crystals depending on their wavelength. Photonic crystals were for the first time combined with MIPs by the group of Guangtao Li, in order to generate a readable optical signal upon binding of the analyte without any labeling (Hu et al., 2006). Weakly cross-linked hydrogels were used. Binding events were characterized by a change in the diffraction properties of the ordered macroporous array due to the volume change of the hydrogel. If the shift is large enough, it can result in a color change perceptible with the naked eye (Hu et al., 2006; 2008). The strategy of fabrication of the photonic MIP film is described in Figure 1.25. Briefly, a highly 3D ordered macroporous imprinted hydrogel was obtained by silica colloidal crystal templating. The template used here was L-3,4-dihydroxyphenylalanine (L-dopa). Rebinding of L-dopa to the photonic MIP film resulted in a concentration-dependent blue shift of the Bragg diffraction signal, with a LOD of 10 nM. In comparaison, the Bragg signal remained unshifted in presence of the opposite enantiomer D-dopa, which showed the selectivity of the rebinding process. It can be noticed that the rebinding process took place in pure aqueous medium, which is promising for environmental or biomedical applications. Later on, this approach was extended for the detection of other small analytes, such as theophylline, ephedrine (Hu et al., 2008) and vanillin (Peng et al., 2012).

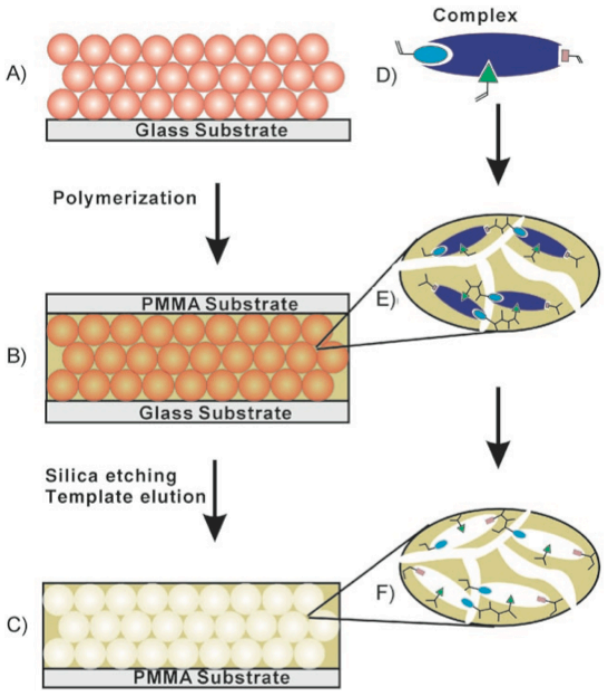

Figure 1.25. *Scheme of the protocol for the preparation of photonic MIP films: (A) SiO_2 colloidal crystals on glass substrate; (B) Infiltration of complex solution into colloidal template followed by photopolymerization; (C) Photonic MIP film after the removal of SiO_2 nanoparticles and dopa template molecules; (D) Complex of*

monomer and template molecule; (E) Imprinted molecules within the polymer matrix; (F) Imprinted specific cavities. Reproduced from Hu et al., 2006.

In order to avoid the use of hydrofluoric acid for the removal of silica colloidal crystals after polymerization, some research groups investigated the fabrication of molecularly imprinted photonic hydrogels using organic colloidal crystals. An example is the synthesis of imprinted photonic hydrogels templated with polystyrene colloidal crystals, for the recognition of 3-pyridine-carboxamide (Yuan et al., 2012).

Recently, a new approach for the preparation of imprinted photonic hydrogels has been introduced: the novelty is that the photonic MIP contained a 2D defect layer, and the protocol of synthesis combined the Langmuir-Blodgett technique with the photonic crystal template method. The MIP was imprinted with bisphenol A (Griffete et al., 2011). Multilayers colloidal assemblies of silica particles were fabricated by the Langmuir-Blodgett technique. In order to prove the influence of the defect layer on the sensing properties of the photonic MIP, two samples were fabricated: the first one consisting in a defect-free colloidal crystal, made from 10 layers of silica particles of 280 nm diameter; and the second one that is a colloidal crystal containing a defect layer, which consists in a layer of larger silica particles (390 nm diameter) embedded between two opals of 5 layers of silica particles of 240 nm (Figure 1.26). Both samples showed the same thickness of around 2.8 μm. The reflection spectrum of the MIP containing the defect showed that the defect layer of larger macropores behaves like an optical cavity, which appears as a pronounced dip inside the original stop band of the defect-free MIP. After rebinding of both MIP samples with bisphenol A, a bigger shift was observed for the MIP with the defect layer, allowing to conclude that the presence of the defect layer enhances the sensitivity of the photonic MIP.

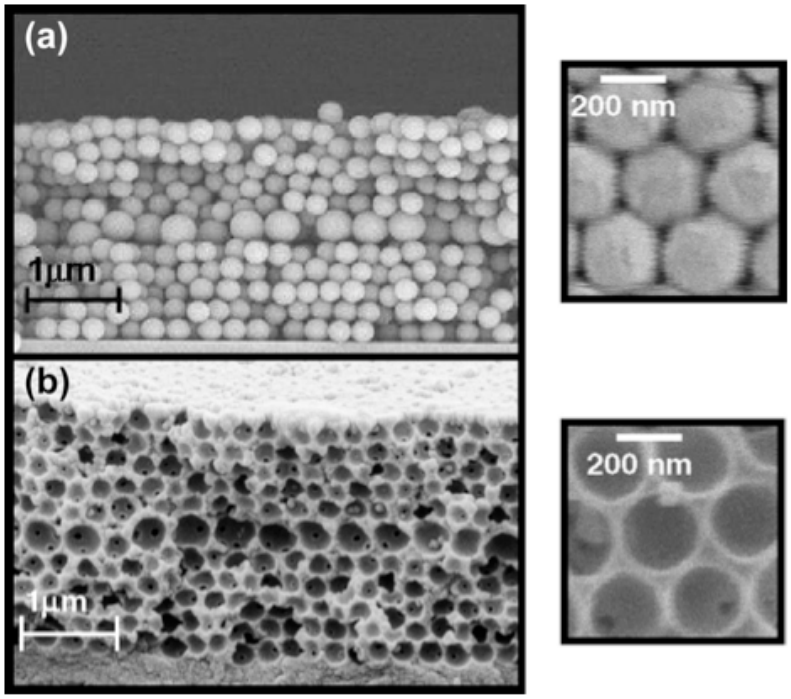

Figure 1.26. *SEM images of (a) the colloidal crystal template with an embedded defect layer and (b) the resulting photonic MIP film. Reproduced from Griffete et al., 2011.*

Very recently, a fiber optic sensor using a photonic hydrogel imprinted with vitamin B_3 as recognition element and SPR for detection was described in the literature (Verma and Gupta, 2013).

The sensing probe was prepared in three steps: first, the silver coated optical fiber probe was fabricated; then, colloidal crystal templates were prepared on it, followed by polymerization of the imprinted hydrogel. The whole probe was fixed in a flow cell and a Tungsten halogen lamp was used as light source for the detection (Figure 1.27). Control experiments were performed to outline the role of the colloidal crystal templating and the imprinting effect. As a result, the photonic imprinted hydrogel showed the best performance, with the largest shift of 16.651 nm in the resonance wavelength. The concentration of analyte studied ranged from 0.5 mg/mL to 10 mg/mL, which is the range of interest for pharmaceutical applications.

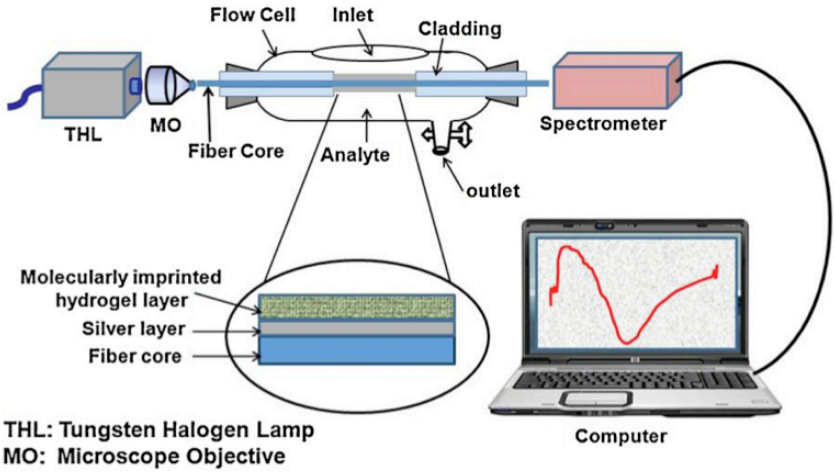

Figure 1.27. *Experimental set-up for the characterization of the fiber optic sensor. Reproduced from Verma and Gupta, 2013.*

II.5. Other MIP-based optical sensors

Besides the techniques described previously in this chapter, several other optical transduction methods have been combined with MIPs for sensing purposes. Several examples will be described in this section. However, the list is not exhaustive.

Concerning **light diffraction-based MIP sensors** other than photonic MIPs, the group of Moreno-Bondi reported the fabrication of a MIP 2D diffraction grafting for label-free optical sensing (Barrios et al., 2011). The MIP 2D diffraction grafting was obtained by a microtransfer molding using SiO_2/Si molds (Figure 1.28). The MIP was applied for the detection of the antibiotic enrofloxacin in the μM range. Even though the proof of concept was demonstrated, the LOD (18 μM enrofloxacin) and the response time (a few hours) still need to be improved, for example by improving the instrument set-up (i.e. smaller cell volume than 17 mL), as suggested by the authors, or by an optimization of the MIP formulation and format.

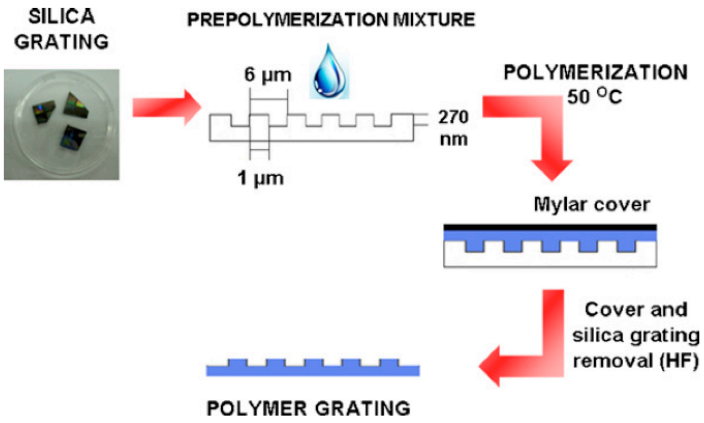

Figure 1.28. *Micropatterning of MIP films using SiO_2/Si grafting molds. Reproduced from Barrios et al., 2011.*

Our group recently reported the first example of transmission holographic MIP films obtained by interference photolithography (holography) (Fuchs et al., 2013). For the synthesis, coherent laser beams were combined in order to create a stable pattern of light intensity trough interference. Polymerization occurred only in the bright zones, resulting in a MIP hologram, with controlled surface fringes. The template used here was testosterone (Figure 1.29). Binding of analyte resulted in a change in the refractive index of the MIP film. As a result, a specific change in the refractive index was measured after incubation of the MIP with 100 µM testosterone, and the change was three times lower when the MIP was incubated with 100 µM 5α-androstane, a structural analogue, and when the NIP was incubated with 100 µM testosterone. These results confirm the specificity and the selectivity of the holographic MIP. The LOD was 1 µM testosterone. This work is very promising for the use of MIPs for label-free chemical sensing; and for the perspectives, the LOD and the response time can still be improved, for example by an optimization of the hologram format.

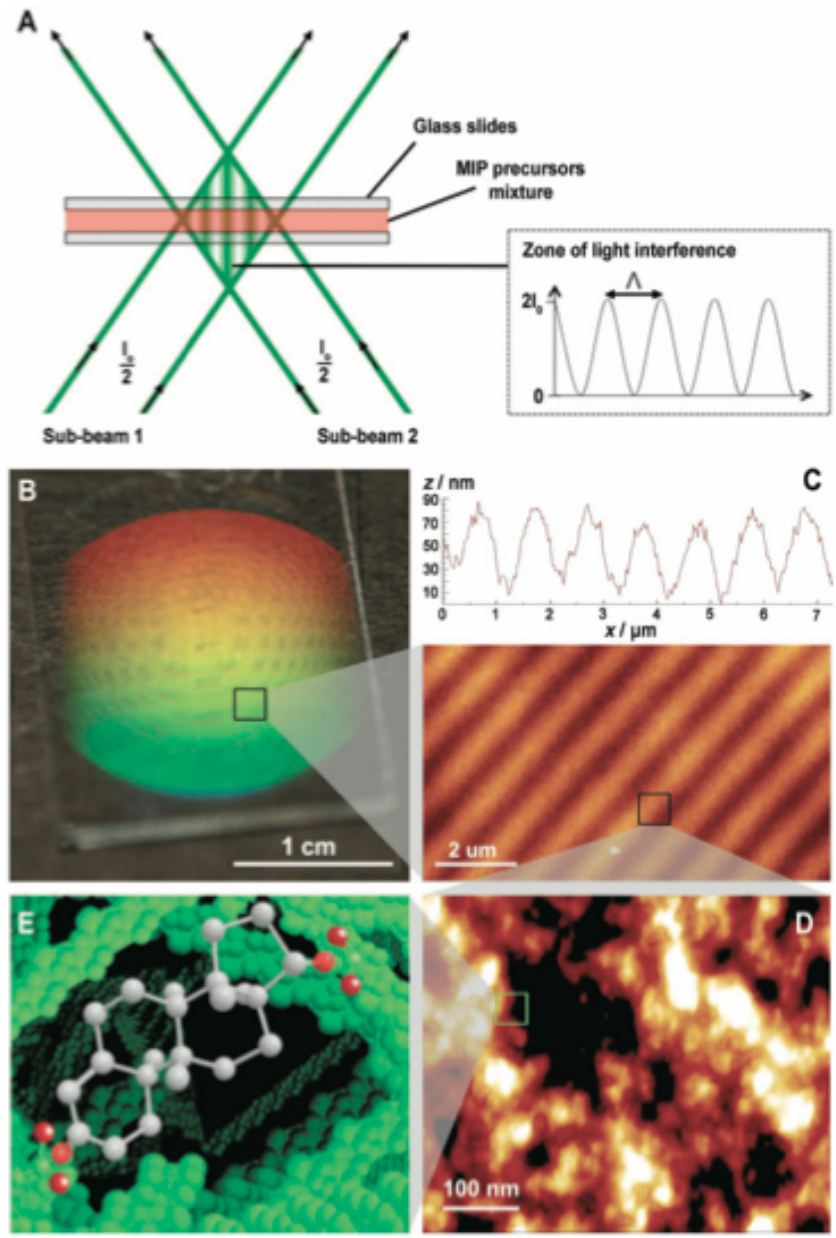

Figure 1.29. *(A) Scheme showing the in-situ MIP microstructuring process by photopolymerization with two interfering laser beams at 532 nm. (B) Holographic MIP film supported on a glass slide. (C) Atomic force microscopy (AFM) image of the surface topography of the holographic MIP film (10 µm x 10 µm). (D) Porosity of the holographic MIP film (0.7 µm x 0.7 µm) imaged by AFM. (E) Illustration of an imprinted cavity specific for testosterone. Reproduced from Fuchs et al., 2013.*

UV/vis spectroscopy has also gained interested for the rapid and sensitive detection of analytes (Henry et al., 2005). For example, UV/vis spectrocospy was used for rapid screening of MIP formulations. Piletsky and co-workers grafted a thin epinephrine-imprinted polymer layer at the surface of polystyrene microplates (Piletsky et al., 2000). The binding properties were determined in an ELISA assay by competition between free ligand and a conjugate of horseradish peroxidase and norepinephrine. The MIP assay exhibited sensitivity in the range 1-100 µM.

Another ELISA assay using MIP as artificial receptor was also reported by Haupt and co-workers (Surugiu et al., 2001a). In their work, **chemiluminescence** was used for detection. Microtiters

plates (96 or 384 wells) were coated with MIP microspheres using poly(vinyl alcohol) as glue, and the analyte 2,4-D-peroxidase conjugate was detected using luminol as the chemiluminescent substrate. Light emission was then quantified with a CCD camera imaging system. A calibration curve ranging from 0.01 to 100 μg/mL could be obtained. Then, using the same principle (same MIP with chemiluminescence detection), a flow injection competitive assay was developed by covalently attaching the MIP to the inner wall of a glass capillary that was mounted in a flow system (Surugiu et al., 2001b). Chemiluminescence was detected with a CCD camera or a photomultiplier tube (PMT), which was more sensitive. In this study, a commercial luminescent substrate, Pierce, was used instead of luminol, in order to increase the sensitivity and the exposure time. When using the PMT for detection, a very high sensitivity in the pM range was obtained, and the dynamic range was 5 pg/mL – 100 ng/mL 2,4-D (i.e. 22.5 pM – 450 nM), which was of several orders of magnitude better than the CCD camera. However, using the CCD camera for detection would allow the simultaneous monitoring of several capillaries, and the fabrication of a multi-sensor for multiple analytes.

Another label-free approach was developed in our group in collaboration with Gauglitz' group, combining **reflectometric interference spectroscopy** with MIPs (Belmont et al., 2007). An atrazine-imprinted polymer film was coated on a glass substrate by spin-coating, either as a continuous film or as a film of MIP nanoparticles, and a white beam was directed on the glass transducer so as to obtain characteristic interference patterns. Binding of analyte resulted in a shift of these interference patterns, which corresponds to the change of optical thickness (product of physical thickness and refractive index) of the layer. As a result, atrazine could be detected at concentrations as low as 1.7 ppm.

A **Fabry-Pérot interferometer** was used to monitor microcystin-LR in water, using an optical fiber coated with a sol-gel MIP (Queirós et al., 2011). In this fiber Fabry-Pérot interferometer, two or more light waves were combined between the partially reflecting end face surface of the fiber and an external mirror, resulting in interferences. Binding of the analyte resulted in a wavelength shift in the optical power, which was dependent on the concentration of analyte (Figure 1.30). The shift was smaller for the corresponding NIP, which showed the specificity of the process. The detection of microcystin-LR was not disturbed when ions were added into the medium, which shows that this sensor could be used in environmental waters. The sensor also showed a response time of 2 minutes and a LOD of 0.3 μg/L, which is below the maximum value of 1 μg/L of microcystin-LR in water recommended by the World Health Organization.

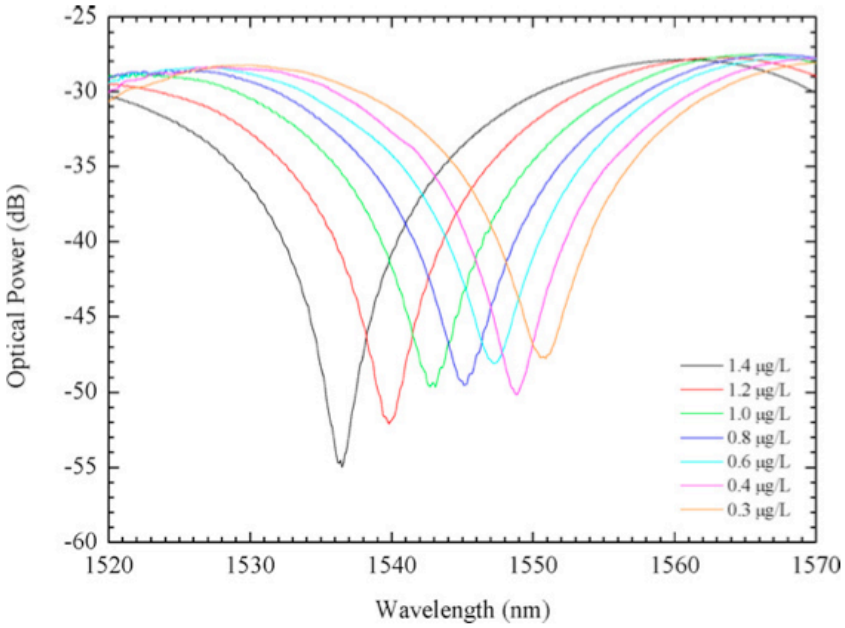

Figure 1.30. *Optical power and wavelength shift variation according to the concentration of microcystin-LR using the fiber Fabry-Pérot interferometer with the MIP sol-gel membrane. Reproduced from Queirós et al., 2011.*

III. Conclusions

In this chapter, the history, concept and applications of molecularly imprinted polymers have been presented. In particular, their role as recognition elements in opto-chemical sensors has been outlined, with a focus on fluorescence-based MIP sensors, which is also the purpose of this thesis. The great variety of MIP devices presented in this chapter (SPR, SERS, fluorescence-based and photonic MIPs, etc.) shows that the technique of molecular imprinting is continuously improving and that MIPs are promising candidates as recognition elements for optical sensing, as they are relatively easy to prepare and to functionalize, but also stable and quite cheap. Continuous efforts are being made to improve the properties of MIP-based optical sensors, such as the limit of detection, the dynamic range, the response time, etc. Undoubtedly, MIP-based sensors will find in the near future their applications in the “real world”, next to biosensors.

The next chapters of this thesis describe the development of fluorescence-based optical sensors using MIPs as the specific recognition element. In particular, optical fibers were developed. Our first aim was to develop a fiber optic sensor based on *in-situ* polymerized MIP microstructures, described in Chapter 2. We then focused in Chapter 3 on the use of evanescent-wave spectroscopy for the synthesis of MIP-coated sensing elements, and for detection. In the last chapter (Chapter 4), we evaluated direct fluorimetric sensing of UV-excited analytes with a method based on the use of MIP nanoparticles and fluorescence polarization.

In these experimental chapters, we aimed to develop a new generation of MIP-based optical sensing platforms by using innovative combinations of well-known principles, i.e. MIPs and fiber optic, or more generally, fluorescence-based detection principles.

IV. References

Alexander, C.; Andersson, H. S.; Andersson, L. I.; Ansell, R. J.; Kirsch, N.; Nicholls, I. A.; O'Mahony, J.; Whitcombe, M. J. Molecular imprinting science and technology: a survey of the literature for the years up to and including 2003. *Journal of Molecular Recognition* **2006**, *19*, 106.

Allender, C.; Richardson, C.; Woodhouse, B.; Heard, C.; Brain, K. Pharmaceutical applications for molecularly imprinted polymers. *International Journal of Pharmaceutics* **2000**, *195*, 39.

Ambrosini, S.; Shinde, S.; De Lorenzi, E.; Sellergren, B. Glucuronide directed molecularly imprinted solid-phase extraction: isolation of testosterone glucuronide from its parent drug in urine. *Analyst* **2012**, *137*, 249.

Andersson, H. S.; Nicholls, I. A. A historical perspective of the development of molecular imprinting. *Techniques and Instrumentation in Analytical Chemistry* **2000**, *23*, 1.

Andersson, L.; Sellergren, B.; Mosbach, K. Imprinting of amino acid derivatives in macroporous polymers. *Tetrahedron letters* **1984**, *25*, 5211.

Andersson, L. I. Application of molecular imprinting to the development of aqueous buffer and organic solvent based radioligand binding assays for (S)-propranolol. *Analytical Chemistry* **1996**, *68*, 111.

Arshady, R.; Mosbach, K. Synthesis of substrate selective polymers by host guest polymerization. *Makromolekulare Chemie* **1981**, *182*, 687.

Arshady, R. Suspension, emulsion, and dispersion polymerization: A methodological survey. *Colloid & Polymer Science* **1992**, *270*, 717.

Barrios, C. A.; Zhenhe, C.; Navarro-Villoslada, F.; Lopez-Romero, D.; Moreno-Bondi, M. C. Molecularly imprinted polymer diffraction grating as label-free optical bio (mimetic) sensor. *Biosensors and Bioelectronics* **2011**, *26*, 2801.

Beckett, A.; Youssef, H. Active sites in stereoselective adsorbents as models of drug receptors and enzyme active sites. *Journal of Pharmacy and Pharmacology* **1963**, *15*, 253T.

Belmont, A. S.; Jaeger, S.; Knopp, D.; Niessner, R.; Gauglitz, G.; Haupt, K. Molecularly imprinted polymer films for reflectometric interference spectroscopic sensors. *Biosensors and Bioelectronics* **2007**, *22*, 3267.

Benito-Peña, E.; Urraca, J. L.; Sellergren, B.; Moreno-Bondi, M. C. Solid-phase extraction of fluoroquinolones from aqueous samples using a water-compatible stochiometrically imprinted polymer. *Journal of Chromatography A* **2008**, *1208*, 62.

Bompart, M.; Gheber, L. A.; De Wilde, Y.; Haupt, K. Direct detection of analyte binding to single molecularly imprinted polymer particles by confocal Raman spectroscopy. *Biosensors and Bioelectronics* **2009**, *25*, 568.

Bompart, M.; De Wilde, Y.; Haupt, K. Chemical Nanosensors Based on Composite Molecularly Imprinted Polymer Particles and Surface Enhanced Raman Scattering. *Advanced Materials* **2010**, *22*, 2343.

Breton, F.; Delépée, R.; Agrofoglio, L. A. Molecular imprinting of AMP by an ionic-noncovalent dual approach. *Journal of separation science* **2009**, *32*, 3285.

Cennamo, N.; D'Agostino, G.; Galatus, R.; Bibbò, L.; Pesavento, M.; Zeni, L. Sensors based on Surface Plasmon Resonance in a plastic optical fiber for the detection of trinitrotoluene. *Sensors and Actuators B: Chemical* **2013**, *188*, 221.

Choi, S.-W.; Chang, H.-J.; Lee, N.; Kim, J.-H.; Chun, H. S. Detection of mycoestrogen zearalenone by a molecularly imprinted polypyrrole-based surface plasmon resonance (SPR) sensor. *Journal of Agricultural and Food Chemistry* **2009**, *57*, 1113.

Claude, B.; Morin, P.; Bayoudh, S.; de Ceaurriz, J. Interest of molecularly imprinted polymers in the fight against doping: Extraction of tamoxifen and its main metabolite from urine followed by high-performance liquid chromatography with UV detection. *Journal of Chromatography A* **2008**, *1196*, 81.

Cutivet, A.; Schembri, C.; Kovensky, J.; Haupt, K. Molecularly imprinted microgels as enzyme inhibitors. *Journal of the American Chemical Society* **2009**, *131*, 14699.

De Silva, A. P.; Gunaratne, H. Q. N.; Gunnlaugsson, T.; Huxley, A. J. M.; McCoy, C. P.; Rademacher, J. T.; Rice, T. E. Signaling recognition events with fluorescent sensors and switches. *Chemical Reviews* **1997**, *28*, 1515.

De Smet, D.; Dubruel, P.; Van Peteghem, C.; Schacht, E.; De Saeger, S. Molecularly imprinted solid-phase extraction of fumonisin B analogues in bell pepper, rice and corn flakes. *Food Additives and Contaminants* **2009**, *26*, 874.

Descalzo, A. B.; Somoza, C.; Moreno-Bondi, M. C.; Orellana, G. Luminescent Core–Shell Imprinted Nanoparticles Engineered for Targeted Förster Resonance Energy Transfer-Based Sensing. *Analytical Chemistry* **2013**.

Dickert, F. L.; Besenböck, H.; Tortschanoff, M. Molecular imprinting through van der Waals interactions: fluorescence detection of PAHs in water. *Advanced Materials* **1998**, *10*, 149.

Dickert, F. L.; Tortschanoff, M.; Bulst, W. E.; Fischerauer, G. Molecularly imprinted sensor layers for the detection of polycyclic aromatic hydrocarbons in water. *Analytical Chemistry* **1999**, *71*, 4559.

Dickey, F. H. The preparation of specific adsorbents. *Proceedings of the National Academy of Sciences of the United States of America* **1949**, *35*, 227.

Diltemiz, S. E.; Say, R.; Büyüktiryaki, S.; Hür, D.; Denizli, A.; Ersöz, A. Quantum dot nanocrystals having guanosine imprinted nanoshell for DNA recognition. *Talanta* **2008**, *75*, 890.

Dirion, B.; Cobb, Z.; Schillinger, E.; Andersson, L. I.; Sellergren, B. Water-compatible molecularly imprinted polymers obtained via high-throughput synthesis and experimental design. *Journal of the American Chemical Society* **2003**, *125*, 15101.

Dunkin, I.; Lenfeld, J.; Sherrington, D. Molecular imprinting of flat polycondensed aromatic molecules in macroporous polymers. *Polymer* **1993**, *34*, 77.

Emgenbroich, M.; Borrelli, C.; Shinde, S.; Lazraq, I.; Vilela, F.; Hall, A. J.; Oxelbark, J.; De Lorenzi, E.; Courtois, J.; Simanova, A.; Verhage, J.; Irgum, K.; Karim, K.; Sellergren, B. A Phosphotyrosine-Imprinted Polymer Receptor for the Recognition of Tyrosine Phosphorylated Peptides. *Chemistry-A European Journal* **2008**, *14*, 9516.

Fischer, L.; Mueller, R.; Ekberg, B.; Mosbach, K. Direct enantioseparation of. beta.-adrenergic blockers using a chiral stationary phase prepared by molecular imprinting. *Journal of the American Chemical Society* **1991**, *113*, 9358.

Flores, A.; Cunliffe, D.; Whitcombe, M. J.; Vulfson, E. N. Imprinted polymers prepared by aqueous suspension polymerization. *Journal of Applied Polymer Science* **2000**, *77*, 1841.

Fuchs, Y.; Linares, A. V.; Mayes, A. G.; Haupt, K.; Soppera, O. Ultrathin Selective Molecularly Imprinted Polymer Microdots Obtained by Evanescent Wave Photopolymerization. *Chemistry of Materials* **2011**, *23*, 3645

Fuchs, Y.; Soppera, O.; Mayes, A. G.; Haupt, K. Holographic Molecularly Imprinted Polymers for Label-Free Chemical Sensing. *Advanced Materials* **2013**, *25*, 566.

Gonzalez, G. P.; Hernando, P. F.; Durand Alegria, J. Determination of digoxin in serum samples using a flow-through fluorosensor based on a molecularly imprinted polymer. *Biosensors and Bioelectronics* **2008**, *23*, 1754.

Griffete, N.; Frederich, H.; Maitre, A.; Schwob, C.; Ravaine, S.; Carbonnier, B.; Chehimi, M. M.; Mangeney, C. Introduction of a planar defect in a molecularly imprinted photonic crystal sensor for the detection of bisphenol A. *Journal of colloid and interface science* **2011**, *364*, 18.

Hall, A. J.; Manesiotis, P.; Emgenbroich, M.; Quaglia, M.; De Lorenzi, E.; Sellergren, B. Urea Host Monomers for Stoichiometric Molecular Imprinting of Oxyanions §. *The Journal of Organic Chemistry* **2005**, *70*, 1732.

Haupt, K.; Dzgoev, A.; Mosbach, K. Assay system for the herbicide 2, 4-dichlorophenoxyacetic acid using a molecularly imprinted polymer as an artificial recognition element. *Analytical Chemistry* **1998**a, *70*, 628.

Haupt, K.; Mayes, A. G.; Mosbach, K. Herbicide assay using an imprinted polymer-based system analogous to competitive fluoroimmunoassays. *Analytical Chemistry* **1998**b, *70*, 3936.

Haupt, K.; Noworyta, K.; Kutner, W. Imprinted polymer-based enantioselective acoustic sensor using a quartz crystal microbalance. *Anal. Commun.* **1999**, *36*, 391.

Haupt, K.; Mosbach, K. Molecularly imprinted polymers and their use in biomimetic sensors. *Chem. Rev* **2000**, *100*, 2495.

Haupt, K. Molecularly imprinted polymers in analytical chemistry. *Analyst* **2001**, *126*, 747.

Haupt, K. Peer Reviewed: Molecularly Imprinted Polymers: The Next Generation. *Analytical Chemistry* **2003**a, *75*, 376.

Haupt, K. Imprinted polymers - Tailor-made mimics of antibodies and receptors. *Chemical Communications* **2003**b, *2003*, 171.

Hiratani, H.; Alvarez-Lorenzo, C. Timolol uptake and release by imprinted soft contact lenses made of *N,N*-diethylacrylamide and methacrylic acid. *Journal of Controlled Release* **2002**, *83*, 223.

Hoshino, Y.; Koide, H.; Urakami, T.; Kanazawa, H.; Kodama, T.; Oku, N.; Shea, K. J. Recognition, neutralization, and clearance of target peptides in the bloodstream of living mice by molecularly imprinted polymer nanoparticles: a plastic antibody. *Journal of the American Chemical Society* **2010**, *132*, 6644.

Hu, X.; An, Q.; Li, G.; Tao, S.; Liu, J. Imprinted photonic polymers for chiral recognition. *Angewandte Chemie International Edition* **2006**, *45*, 8145.

Hu, X.; Li, G.; Huang, J.; Zhang, D.; Qiu, Y. Construction of Self-Reporting Specific Chemical Sensors with High Sensitivity. *Advanced Materials* **2007**, *19*, 4327.

Hu, X.; Li, G.; Li, M.; Huang, J.; Li, Y.; Gao, Y.; Zhang, Y. Ultrasensitive specific stimulant assay based on molecularly imprinted photonic hydrogels. *Advanced Functional Materials* **2008**, *18*, 575.

Hunt, C. E.; Pasetto, P.; Ansell, R. J.; Haupt, K. A fluorescence polarisation molecular imprint sorbent assay for 2, 4-D: a non-separation pseudo-immunoassay. *Chemical Communications* **2006**, 1754.

Inoue, Y.; Kuwahara, A.; Ohmori, K.; Sunayama, H.; Ooya, T.; Takeuchi, T. Fluorescent Molecularly Imprinted Polymer Thin Films for Specific Protein Detection Prepared with Dansyl Ethylenediamine-Conjugated O-Acryloyl L-Hydroxyproline. *Biosensors and Bioelectronics* **2013**.

Ivanova-Mitseva, P. K.; Guerreiro, A.; Piletska, E. V.; Whitcombe, M.; Zhou, Z.; Mitsev, P. A.; Davis, F.; Piletsky, S. A. Cubic Molecularly Imprinted Polymer Nanoparticles with a Fluorescent Core. *Angewandte Chemie International Edition* **2012**, *51*, 5196.

Jiang, Y.; Tong, A. J. Synthesis of molecularly imprinted microspheres for recognition of trans-aconitic acid. *Journal of Applied Polymer Science* **2004**, *94*, 542.

Jenkins, A. L.; Uy, O. M.; Murray, G. M. Polymer-based lanthanide luminescent sensor for detection of the hydrolysis product of the nerve agent soman in water. *Analytical Chemistry* **1999**, *71*, 373.

Kantarovich, K.; Tsarfati, I.; Gheber, L. A.; Haupt, K.; Bar, I. Writing droplets of molecularly imprinted polymers by nano fountain pen and detecting their molecular interactions by surface-enhanced raman scattering. *Analytical Chemistry* **2009**, *81*, 5686.

Kantarovich, K.; Tsarfati-BarAd, I.; Gheber, L. A.; Haupt, K.; Bar, I. Reading Biochips by Raman and Surface-Enhanced Raman Spectroscopies. *Plasmonics* **2012**, 1.

Kempe, H.; Kempe, M. Novel method for the synthesis of molecularly imprinted polymer bead libraries. *Macromolecular Rapid Communications* **2004**, *25*, 315.

Kempe, M.; Mosbach, K.; Fischer, L. Chiral separation using molecularly imprinted heteroaromatic polymers. *Journal of Molecular Recognition* **1993**, *6*, 25.

Kempe, M. Antibody-mimicking polymers as chiral stationary phases in HPLC. *Analytical Chemistry* **1996**, *68*, 1948.

Kido, H.; Miyajila, T.; Kazuhiko, T.; Maeda, M.; Takagi, M. Metal-Ion Complexation Behavior of Resins Prepared by a Novel Template Polymerization Technique. *Analytical sciences* **1992**, *8*, 749.

Kostrewa, S.; Emgenbroich, M.; Klockow, D.; Wulff, G. Surface-Enhanced Raman Scattering on Molecularly Imprinted Polymers in Water. *Macromolecular Chemistry and Physics* **2003**, *204*, 481.

Kriz, D.; Ramstroem, O.; Svensson, A.; Mosbach, K. A biomimetic sensor based on a molecularly imprinted polymer as a recognition element combined with fiber-optic detection. *Analytical Chemistry* **1995**, *67*, 2142.

Kubo, H.; Nariai, H.; Takeuchi, T. Multiple hydrogen bonding-based fluorescent imprinted polymers for cyclobarbital prepared with 2, 6-bis (acrylamido) pyridine. *Chemical Communications* **2003**, 2792.

Kubo, H.; Yoshioka, N.; Takeuchi, T. Fluorescent imprinted polymers prepared with 2-acrylamidoquinoline as a signaling monomer. *Organic Letters* **2005**, *7*, 359.

Kugimiya, A.; Takeuchi, T. Surface plasmon resonance sensor using molecularly imprinted polymer for detection of sialic acid. *Biosensors and Bioelectronics* **2001**, *16*, 1059.

Lai, J.-P.; Yang, M.-L.; Niessner, R.; Knopp, D. Molecularly imprinted microspheres and nanospheres for di (2-ethylhexyl) phthalate prepared by precipitation polymerization. *Analytical and Bioanalytical Chemistry* **2007**, *389*, 405.

Lautner, G.; Kaev, J.; Reut, J.; Oepik, A.; Rappich, J.; Syritski, V.; Gyurcsanyi, R. E. Selective Artificial Receptors Based on Micropatterned Surface Imprinted Polymers for Label Free Detection of Proteins by SPR Imaging. *Advanced Functional Materials* **2011**, *21*, 591.

Lépinay, S.; Kham, K.; Millot, M. C.; Carbonnier, B. In-situ polymerized molecularly imprinted polymeric thin films used as sensing layers in surface plasmon resonance sensors: Mini-review focused on 2010-2011. *Chemical Papers* **2012**, *65*, 340.

Leung, M. K.-P.; Chow, C.-F.; Lam, M. H.-W. A sol–gel derived molecular imprinted luminescent PET sensing material for 2, 4-dichlorophenoxyacetic acid. *J. Mater. Chem.* **2001**, *11*, 2985.

Levi, R.; McNiven, S.; Piletsky, S. A.; Cheong, S. H.; Yano, K.; Karube, I. Optical detection of chloramphenicol using molecularly imprinted polymers. *Analytical Chemistry* **1997**, *69*, 2017.

Lieberzeit, P. A.; Halikias, K.; Afzal, A.; Dickert, F. L. Polymers imprinted with PAH mixtures - Comparing fluorescence and QCM sensors. *Analytical and Bioanalytical Chemistry* **2008**, *392*, 1405.

Linares, A. V.; Vandevelde, F.; Pantigny, J.; Falcimaigne Cordin, A.; Haupt, K. Polymer Films Composed of Surface Bound Nanofilaments with a High Aspect Ratio, Molecularly Imprinted with Small Molecules and Proteins. *Advanced Functional Materials* **2009**, *19*, 1299.

Lotierzo, M.; Henry, O.; Piletsky, S.; Tothill, I.; Cullen, D.; Kania, M.; Hock, B.; Turner, A. P. F. Surface plasmon resonance sensor for domoic acid based on grafted imprinted polymer. *Biosensors and Bioelectronics* **2004**, *20*, 145.

Manesiotis, P.; Borrelli, C.; Aureliano, C. S.; Svensson, C.; Sellergren, B. Water-compatible imprinted polymers for selective depletion of riboflavine from beverages. *Journal of Materials Chemistry* **2009**, *19*, 6185.

Manju, S.; Hari, P.; Sreenivasan, K. Fluorescent molecularly imprinted polymer film binds glucose with a concomitant changes in fluorescence. *Biosensors and Bioelectronics* **2010**, *26*, 894.

Matsui, J.; Doblhoff-Dier, O.; Takeuchi, T. 2-(Trifluoromethyl) acrylic acid: a novel functional monomer in non-covalent molecular imprinting. *Analytica chimica acta* **1997**, *343*, 1.

Matsui, J.; Tachibana, Y.; Takeuchi, T. Molecularly imprinted receptor having metalloporphyrin-based signaling binding site. *Analytical Communications* **1998**, *35*, 225.

Matsui, J.; Kubo, H.; Takeuchi, T. Molecularly imprinted fluorescent-shift receptors prepared with 2-(trifluoromethyl) acrylic acid. *Analytical Chemistry* **2000**a, *72*, 3286.

Matsui, J.; Higashi, M.; Takeuchi, T. Molecularly imprinted polymer as 9-ethyladenine receptor having a porphyrin-based recognition center. *Journal of the American Chemical Society* **2000**b, *122*, 5218.

Matsui, J.; Akamatsu, K.; Hara, N.; Miyoshi, D.; Nawafune, H.; Tamaki, K.; Sugimoto, N. SPR sensor chip for detection of small molecules using molecularly imprinted polymer with embedded gold nanoparticles. *Anal. Chem* **2005**, *77*, 4282.

Mayes, A. G.; Mosbach, K. Molecularly imprinted polymer beads: suspension polymerization using a liquid perfluorocarbon as the dispersing phase. *Analytical Chemistry* **1996**, *68*, 3769.

McDonagh, C.; Burke, C. S.; MacCraith, B. D. Optical chemical sensors. *Chemical Reviews* **2008**, *108*, 400.

Morrison, J. L.; Worsley, M.; Shaw, D.; Hodgson, G. The nature of the specificity of adsorption of alkyl orange dyes on silica gel. *Canadian Journal of Chemistry* **1959**, *37*, 1986.

Navarro-Villoslada, F.; Urraca, J. L.; Moreno-Bondi, M. C.; Orellana, G. Zearalenone sensing with molecularly imprinted polymers and tailored fluorescent probes. *Sensors and Actuators B: Chemical* **2007**, *121*, 67.

Nguyen, T. H.; Hardwick, S. A.; Sun, T.; Grattan, K. T. V. Intrinsic Fluorescence-Based Optical Fiber Sensor for Cocaine Using a Molecularly Imprinted Polymer as the Recognition Element. *IEEE Sensors Journal* **2012**, *12*, 255.

Nickel, A. M. L.; Seker, F.; Ziemer, B. P.; Ellis, A. B. Imprinted poly (acrylic acid) films on cadmium selenide. A composite sensor structure that couples selective amine binding with semiconductor substrate photoluminescence. *Chemistry of Materials* **2001**, *13*, 1391.

Nie, S.; Emory, S. R. Probing single molecules and single nanoparticles by surface-enhanced Raman scattering. *Science* **1997**, *275*, 1102.

Norell, M. C.; Andersson, H. S.; Nicholls, I. A. Theophylline molecularly imprinted polymer dissociation kinetics: a novel sustained release drug dosage mechanism. *Journal of Molecular Recognition* **1998**, *11*, 98.

Norrish, R.; Smith, R. Catalyzed polymerization of methyl methacrylate in the liquid phase. *Nature* **1942**, *150*, 336.

Odian, G. G.: Radical Chain Polymerization. In *Principles of polymerization - Fourth edition*; Odian, G. G., Ed.; John Wiley and Sons, 2004; pp 198.

Olsson, G. D.; Karlsson, B. C.; Shoravi, S.; Wiklander, J. G.; Nicholls, I. A. Mechanisms underlying molecularly imprinted polymer molecular memory and the role of crosslinker: resolving debate on the nature of template recognition in phenylalanine anilide imprinted polymers. *Journal of Molecular Recognition* **2012**, *25*, 69.

Pauling, L. A Theory of the Structure and Process of Formation of Antibodies. *Journal of the American Chemical Society* **1940**, *62*, 2643.

Peng, H.; Wang, S.; Zhang, Z.; Xiong, H.; Li, J.; Chen, L.; Li, Y. Molecularly Imprinted Photonic Hydrogels as Colorimetric Sensor for Rapid and Label-Free Detection of Vanillin. *Journal of Agricultural and Food Chemistry* **2012**, *60*, 1921.

Piletsky, S.; Piletskaya, E.; Yano, K.; Kugimiya, A.; Elgersma, A.; Levi, R.; Kahlow, U.; Takeuchi, T.; Karube, I.; Panasyuk, T. A biomimetic receptor system for sialic acid based on molecular imprinting. *Analytical Letters* **1996**, *29*, 157.

Piletsky, S. A.; Terpetschnig, E.; Andersson, H. S.; Nicholls, I. A.; Wolfbeis, O. S. Application of non-specific fluorescent dyes for monitoring enantio-selective ligand binding to molecularly imprinted polymers. *Fresenius' journal of analytical chemistry* **1999**, *364*, 512.

Piletsky, S. A.; Piletska, E. V.; Chen, B.; Karim, K.; Weston, D.; Barrett, G.; Lowe, P.; Turner, A. P. F. Chemical grafting of molecularly imprinted homopolymers to the surface of microplates. Application of artificial adrenergic receptor in enzyme-linked assay for B-agonists determination. *Analytical Chemistry* **2000**, *72*, 4381.

Polyakov, M.; Khim, Z. Adsorption properties of silica gel and its structure. *Zh. Fiz. Khim., Ser. B* **1931**, *2*, 799.

Poma, A.; Turner, A. P. F.; Piletsky, S. A. Advances in the manufacture of MIP nanoparticles. *Trends in biotechnology* **2010**, *28*, 629.

Qiao, F.; Sun, H. Simultaneous extraction of enrofloxacin and ciprofloxacin from chicken tissue by molecularly imprinted matrix solid-phase dispersion. *Journal of pharmaceutical and biomedical analysis* **2010**, *53*, 795.

Queirós, R. B.; Silva, S.; Noronha, J.; Frazão, O.; Jorge, P.; Aguilar, G.; Marques, P.; Sales, M. Microcystin-LR detection in water by the Fabry–Pérot interferometer using an optical fibre coated with a sol–gel imprinted sensing membrane. *Biosensors and Bioelectronics* **2011**, *26*, 3932.

Rachkov, A. E.; Cheong, S. H.; Elískaya, A. V.; Yano, K.; Karube, I. Molecularly imprinted polymers as artificial steroid receptors. *Polymers for Advanced Technologies* **1998**, *9*, 511.

Ramstroem, O.; Andersson, L.; Mosbach, K. Recognition sites incorporating both pyridinyl and carboxy functionalities prepared by molecular imprinting. *The Journal of Organic Chemistry* **1993**, *58*, 7562.

Ramström, O.; Ye, L.; Mosbach, K. Artificial antibodies to corticosteroids prepared by molecular imprinting. *Chemistry & Biology* **1996**, *3*, 471.

Reimhult, K.; Yoshimatsu, K.; Risveden, K.; Chen, S.; Ye, L.; Krozer, A. Characterization of QCM sensor surfaces coated with molecularly imprinted nanoparticles. *Biosensors and Bioelectronics* **2008**, *23*, 1908.

Schmidt, R. H.; Mosbach, K.; Haupt, K. A Simple Method for Spin Coating Molecularly Imprinted Polymer Films of Controlled Thickness and Porosity. *Advanced Materials* **2004**, *16*, 719.

Schmidt, R. H.; Belmont, A.-S.; Haupt, K. Porogen formulations for obtaining molecularly imprinted polymers with optimized binding properties. *Analytica chimica acta* **2005**, *542*, 118.

Schweitz, L.; Spégel, P.; Nilsson, S. Molecularly imprinted microparticles for capillary electrochromatographic enantiomer separation of propranolol. *Analyst* **2000**, *125*, 1899.

Sellergren, B.; Ekberg, B.; Mosbach, K. Molecular imprinting of amino acid derivatives in macroporous polymers:: Demonstration of substrate-and enantio-selectivity by chromatographic resolution of racemic mixtures of amino acid derivatives. *Journal of Chromatography A* **1985**, *347*, 1.

Sellergren, B.; Andersson, L. Molecular recognition in macroporous polymers prepared by a substrate analog imprinting strategy. *J. Org. Chem.* **1990**, *55*, 3381.

Sellergren, B.: *Molecularly imprinted polymers: man-made mimics of antibodies and their application in analytical chemistry*; Techniques and Instrumentation in Analytical Chemistry ed.; Elsevier Science: Amsterdam, 2000; Vol. 23.

Shea, K. J.; Thompson, E. Template synthesis of macromolecules. Selective functionalization of an organic polymer. *The Journal of Organic Chemistry* **1978**, *43*, 4253.

Shinde, S.; Bunschoten, A.; Kruijtzer, J. A.; Liskamp, R. M.; Sellergren, B. Imprinted Polymers Displaying High Affinity for Sulfated Protein Fragments. *Angewandte Chemie International Edition* **2012**, *51*, 8326.

Sibrian-Vazquez, M.; Spivak, D. A. Molecular imprinting made easy. *Journal of the American Chemical Society* **2004**, *126*, 7827.

Spivak, D. A.; Shea, K. J. Binding of nucleotide bases by imprinted polymers. *Macromolecules* **1998**, *31*, 2160.

Sreenivasan, K. On the feasibility of using molecularly imprinted poly (Hema) as a sensor component. *Talanta* **1997**, *44*, 1137.

Suedee, R.; Srichana, T.; Martin, G. P. Evaluation of matrices containing molecularly imprinted polymers in the enantioselective-controlled delivery of β-blockers. *Journal of controlled release* **2000**, *66*, 135.

Suedee, R.; Srichana, T.; Rattananont, T. Enantioselective release of controlled delivery granules based on molecularly imprinted polymers. *Drug Delivery* **2002**, *9*, 19.

Sunayama, H.; Ooya, T.; Takeuchi, T. Fluorescent protein recognition polymer thin films capable of selective signal transduction of target binding events prepared by molecular imprinting with a post-imprinting treatment. *Biosensors and Bioelectronics* **2010**, *26*, 458.

Surugiu, I.; Ye, L.; Yilmaz, E.; Dzgoev, A.; Danielsson, B.; Mosbach, K.; Haupt, K. An enzyme-linked molecularly imprinted sorbent assay. *Analyst* **2000**, *125*, 13.

Surugiu, I.; Danielsson, B.; Ye, L.; Mosbach, K.; Haupt, K. Chemiluminescence imaging ELISA using an imprinted polymer as the recognition element instead of an antibody. *Analytical Chemistry* **2001**a, *73*, 487.

Surugiu, I.; Svitel, J.; Ye, L.; Haupt, K.; Danielsson, B. Development of a flow injection capillary chemiluminescent ELISA using an imprinted polymer instead of the antibody. *Analytical Chemistry* **2001**b, *73*, 4388.

Takagishi, T.; Klotz, I. M. Macromolecule-small molecule interactions; introduction of additional binding sites in polyethyleneimine by disulfide cross-linkages. *Biopolymers* **1972**, *11*, 483.

Takeuchi, T.; Mukawa, T.; Shinmori, H. Signaling molecularly imprinted polymers: molecular recognition-based sensing materials. *The Chemical Record* **2005**, *5*, 263.

Tarbin, J. A.; Sharman, M. Synthesis and preliminary evaluation of a molecularly imprinted polymer selective for artificial phenolic estrogenic compounds. *Anal. Commun.* **1999**, *36*, 105.

Tieppo, A.; White, C.; Paine, A.; Voyles, M.; McBride, M.; Byrne, M. Sustained in vivo release from imprinted therapeutic contact lenses. *Journal of Controlled Release* **2012**, *157*, 391.

Tokareva, I.; Tokarev, I.; Minko, S.; Hutter, E.; Fendler, J. H. Ultrathin molecularly imprinted polymer sensors employing enhanced transmission surface plasmon resonance spectroscopy. *Chemical Communications* **2006**, 3343.

Ton, X.-A.; Acha, V.; Haupt, K.; Tse Sum Bui, B. Direct fluorimetric sensing of UV-excited analytes in biological and environmental samples using molecularly imprinted polymer nanoparticles and fluorescence polarization. *Biosensors and Bioelectronics* **2012**, *36*, 22.

Trommsdorff, E.; Kohle, H.; Lagally, P. Polymerization of methyl methacrylates. *Makromol Chem* **1948**, *1*, 169.

Tse Sum Bui, B.; Haupt, K. Molecularly imprinted polymers: synthetic receptors in bioanalysis. *Analytical and Bioanalytical Chemistry* **2010**, *398*, 2481.

Tse Sum Bui, B.; Merlier, F.; Haupt, K. Toward the Use of a Molecularly Imprinted Polymer in Doping Analysis: Selective Preconcentration and Analysis of Testosterone and Epitestosterone in Human Urine. *Analytical Chemistry* **2010**, *82*, 4420.

Turkewitsch, P.; Wandelt, B.; Darling, G. D.; Powell, W. S. Fluorescent functional recognition sites through molecular imprinting. A polymer-based fluorescent chemosensor for aqueous cAMP. *Analytical Chemistry* **1998**, *70*, 2025.

Urraca, J. L.; Hall, A. J.; Moreno-Bondi, M. C.; Sellergren, B. A Stoichiometric Molecularly Imprinted Polymer for the Class-Selective Recognition of Antibiotics in Aqueous Media. *Angewandte Chemie* **2006**, *118*, 5282.

Urraca, J. L.; Moreno-Bondi, M. C.; Hall, A. J.; Sellergren, B. Direct extraction of penicillin G and derivatives from aqueous samples using a stoichiometrically imprinted polymer. *Analytical Chemistry* **2007**, *79*, 695.

Valero-Navarro, A.; Salinas-Castillo, A.; Fernandez-Sanchez, J. F.; Segura-Carretero, A.; Mallavia, R.; Fernandez-Gutierrez, A. The development of a MIP-optosensor for the detection of monoamine naphthalenes in drinking water. *Biosensors and Bioelectronics* **2009**, *24*, 2305.

Vandevelde, F.; Belmont, A. S.; Pantigny, J.; Haupt, K. Hierarchically nanostructured polymer films based on molecularly imprinted surface-bound nanofilaments. *Advanced Materials* **2007**, *19*, 3717.

Venkatesh, S.; Sizemore, S. P.; Byrne, M. E. Biomimetic hydrogels for enhanced loading and extended release of ocular therapeutics. *Biomaterials* **2007**, *28*, 717.

Verma, R.; Gupta, B. D. Fiber optic SPR sensor for the detection of 3-pyridinecarboxamide (vitamin B_3) using molecularly imprinted hydrogel. *Sensors and Actuators B: Chemical* **2013**, *177*, 279.

Vlatakis, G.; Andersson, L. I.; Müller, R.; Mosbach, K. Drug assay using antibody mimics made by molecular imprinting. *Nature* **1993**, *361*, 645.

Wagner, R.; Wan, W.; Biyikal, M.; Benito-Peña, E.; Moreno-Bondi, M. a. C.; Lazraq, I.; Rurack, K.; Sellergren, B. r. Synthesis, Spectroscopic, and Analyte-Responsive Behavior of a Polymerizable Naphthalimide-Based Carboxylate Probe and Molecularly Imprinted Polymers Prepared Thereof. *The Journal of Organic Chemistry* **2013**, *78*, 1377.

Wan, W.; Biyikal, M.; Wagner, R.; Sellergren, B.; Rurack, K. Fluorescent Sensory Microparticles that "Light-up" Consisting of a Silica Core and a Molecularly Imprinted Polymer (MIP) Shell. *Angewandte Chemie International Edition* **2013**, *52*, 7023.

Wandelt, B.; Turkewitsch, P.; Wysocki, S.; Darling, G. D. Fluorescent molecularly imprinted polymer studied by time-resolved fluorescence spectroscopy. *Polymer* **2002**, *43*, 2777.

Wandelt, B.; Mielniczak, A.; Turkewitsch, P.; Wysocki, S. Steady-state and time-resolved fluorescence studies of fluorescent imprinted polymers. *Journal of luminescence* **2003**, *102*, 774.

Wang, H. Y.; Kobayashi, T.; Fujii, N. Molecular imprint membranes prepared by the phase inversion precipitation technique. *Langmuir* **1996**, *12*, 4850.

Wang, N. X.; von Recum, H. A. Affinity Based Drug Delivery. *Macromolecular Bioscience* **2011**, *11*, 321.

Whitcombe, M. J.; Rodriguez, M. E.; Villar, P.; Vulfson, E. N. A new method for the introduction of recognition site functionality into polymers prepared by molecular imprinting: synthesis and

characterization of polymeric receptors for cholesterol. *Journal of the American Chemical Society* **1995**, *117*, 7105.

Willets, K. A.; Van Duyne, R. P. Localized surface plasmon resonance spectroscopy and sensing. *Annu. Rev. Phys. Chem.* **2007**, *58*, 267.

Wu, Z.; Tao, C.; Lin, C.; Shen, D.; Li, G. Label Free Colorimetric Detection of Trace Atrazine in Aqueous Solution by Using Molecularly Imprinted Photonic Polymers. *Chemistry A European Journal* **2008**, *14*, 11358.

Wulff, G.; Sarhan, A. The use of polymers with enzyme-analogous structures for the resolution of racemates. *Angewandte Chemie International Edition* **1972**, *11*, 341.

Wulff, G.; Vietmeier, J.; Poll, H. Enzyme analogue built polymers, 22. Influence of the nature of the crosslinking agent on the performance of imprinted polymers in racemic resolution. *Die Makromolekulare Chemie* **1987**, *188*, 731.

Wulff, G. Molecular imprinting in cross linked materials with the aid of molecular templates - A way towards Artificial Antibodies. *Angewandte Chemie International Edition* **1995**, *34*, 1812.

Wulff, G. Enzyme-like catalysis by molecularly imprinted polymers. *Chemical Reviews* **2002**, *102*, 1.

Wulff, G.; Knorr, K. Stoichiometric noncovalent interaction in molecular imprinting. *Bioseparation* **2002**, *10*, 257.

Ye, L.; Cormack, P. A. G.; Mosbach, K. Molecularly imprinted monodisperse microspheres for competitive radioassay. *Anal. Commun.* **1999**, *36*, 35.

Yoshikawa, M.; Guiver, M. D.; Robertson, G. P. Surface plasmon resonance studies on molecularly imprinted films. *Journal of Applied Polymer Science* **2008**, *110*, 2826.

Yu, C.; Mosbach, K. Insights into the origins of binding and the recognition properties of molecularly imprinted polymers prepared using an amide as the hydrogen-bonding functional group. *Journal of Molecular Recognition* **1998**, *11*, 69.

Yuan, Y.; Li, Z.; Liu, Y.; Gao, J.; Pan, Z. Hydrogel Photonic Sensor for the Detection of 3-Pyridinecarboxamide. *Chemistry-A European Journal* **2012**, *18*, 303.

Zdunek, J.; Benito-Peña, E.; Linares, A.; Falcimaigne-Cordin, A.; Orellana, G.; Haupt, K.; Moreno-Bondi, M. C. Surface-Imprinted Nanofilaments for Europium-Amplified Luminescent Detection of Fluoroquinolone Antibiotics. *Chemistry-A European Journal* **2013**, 19, 10209.

Zeng, Z.; Hoshino, Y.; Rodriguez, A.; Yoo, H.; Shea, K. J. Synthetic polymer nanoparticles with antibody-like affinity for a hydrophilic peptide. *ACS Nano* **2010**, *4*, 199.

Zimmerman, S. C.; Lemcoff, N. G. Synthetic hosts via molecular imprinting—are universal synthetic antibodies realistically possible? *Chemical Communications* **2004**, *2004*, 5.

Commission Regulation (EC) No. 1881/2006 of 19 December 2006 of the European Union, setting maximum levels for certain contaminants in foodstuffs. http://eur-lex.europa.eu/LexUriServ/LexUriServ.do?uri=OJ:L:2006:364:0005:0024:EN:PDF

Commission Regulation (EU) No. 37/2010 of 22 December 2009 of the European Union, on pharmacologically active substances and their classification regarding maximum residue limits in foodstuffs of animal origin. http://ec.europa.eu/health/files/eudralex/vol-5/reg_2010_37/reg_2010_37_en.pdf

Chapter 2

A fluorescence fiber optic sensor based on *in-situ* polymerized molecularly imprinted microstructures

Chapter 2: A fluorescence fiber optic sensor based on *in-situ* polymerized molecularly imprinted microstructures

I. Introduction

The molecular recognition properties of molecularly imprinted polymers (MIPs) combined with their high stability, robustness and easy engineering make them extremely attractive as sensing materials (Wulff, 1995; Haupt and Mosbach, 2000). Therefore they are considered as interesting alternatives to biological recognition elements in biosensors. In this context, MIPs have been widely applied over the last years in optical sensors, in particular by using fluorescence for detection. Indeed, good sensing properties (sensitivity or time response) and an easy miniaturization can be achieved with MIP-based optical sensors. However, some challenges remain, such as an improvement of the MIP specificity and sensitivity in some cases, or a better integration of the MIP with the transducer (Al-Kindy et al., 2000; Henry et al., 2005).

In this work, we have focused on the utilization of optical fibers as sensing platforms. Optical fibers are composed of a plastic or glass core surrounded by a cladding material of lower refractive index. As a result, light propagates through the fiber core with minimal attenuation, as light is totally reflected at the core-cladding interface. There are two types of optical fibers:

- *single-mode fibers* (SMF), which carry only one single ray of light (called mode). A typical single-mode fiber consists of a core of 8-10 μm diameter, surrounded by a cladding of 125 μm diameter. They are typically used for communications over long distances (telecommunications). In this chapter, we use single-mode fibers in the first part of our study, to establish the "proof of concept". However, these fibers are single-mode for wavelengths > 1280 nm, whereas at the wavelength used in our study (375 nm), the fiber is in fact multimode. However, this was not a problem for our application, and these fibers are economical and convenient to use.
- *multimode fibers*, which carry several rays of lights (several modes). Multimode fibers possess a larger core than the single-mode fibers, varying from dozens to hundreds of μm. They are mostly used for communications over short distances, for example within a building. In this chapter, we use a multimode fiber for the development of a sensitive fiber optic sensor based on a fiber in Y-configuration.

Optical fibers are of interest as they offer many advantages such as ease of miniaturization and integration, low cost, limited loss of light and possibilities of measurement over long distances (Epstein and Walt, 2003). Simple polymer-based fiber optical sensors have been extensively reported in the literature (Wang and Wolfbeis, 2012). For instance, Walt and co-workers developed polymer-based fiber optic sensors that can be divided in two types (Epstein and Walt, 2003):

- *polymer-coated single core optical fibers*: These were used for pH, ion or O_2 sensing (Munkholm et al., 1986; Healey and Walt, 1997). For instance, the group of Walt has prepared a fiber optic pH sensor based on fluorescence enhancement (Munkholm et al., 1986). A fluorescent pH-dependent dye, fluoresceinamine, was incorporated into an acrylamide-methylenebis(acrylamide) copolymer that was covalently bound to a surface-modified glass fiber. As a result the fluorescence signal of the sensor increased with increasing pH (upon deprotonation) in the range 4.0-8.0, and the sensor gave reversible and instantaneous responses (less than 9 seconds).

- *"artificial noses"*: These are fiber bundles consisting of several (19 or more) individual fibers, each coated at its end with a different recognition element. For example, polymer microspheres were attached to the ends of the individual fibers for vapor sensing. Each fiber responds to an analyte vapor in a cross-reactive manner. Correlating all the responses allowed for the identification of the gas analyte (White et al., 1996; Walt et al., 1998).

In the same category falls another optical fiber bundle that was described for the simultaneous monitoring of pH, CO_2 and O_2 (Ferguson et al., 1997). The different analyte-selective sensing elements were fabricated in distinct regions of the polymer matrix located at the distal end of the fiber. For detection, different fluorescent indicators were covalently bound to the polymer matrix via photopolymerization. The pH-sensitive polymer was fabricated by immobilizing a fluorescent pH indicator, acryloylfluorescein, in a poly(hydroxyethylmethacrylate) polymer. This polymer showed fluorescence enhancement when pH increases, in the range 5.5-7.5. For the formation of the CO_2-sensitive polymer, the pH-sensitive polymer was saturated with a CO_2-sensitive buffer, and then covered by a gas-permeable siloxane membrane. When CO_2 crosses the membrane, the microenvironmental pH of the polymer decreases, resulting in a decrease in the fluorescence intensity. Finally, the presence of O_2 results in quenching of ruthenium tris(diphenyl phenanthroline) entrapped in a gas-permeable siloxane membrane. This triple-analyte-sensor was used for the simultaneous monitoring of pH, CO_2 and O_2 during beer fermentation.

A few examples of fiber optic sensors using MIPs as recognition elements have been reported. Two categories of MIP-based optical fiber sensors can be found in the literature:

- *extrinsic sensors*, in which the optical fiber is used to transmit light to and from a MIP, itself separated from the fiber. This has been first exemplified by the work of the group of Mosbach (Kriz et al., 1995) who described a device consisting of a layer of MIP held in front of a quartz window; an excitation light from an optical fiber was used to excite the fluorescent analyte, dansyl-L-phenylalanine, retained by the MIP. The emitted light was collected and guided through an optical fiber bundle to the detector. The measured fluorescence signal was dependent on the concentration of analyte, and the sensor could distinguish between the L- and D-enantiomers of dansyl-phenylalanine. Later, other examples based on the same principle have been described, for example for ion recognition (Ng and Narayanaswamy, 2006; Medina-Castillo et al., 2010).
- *intrinsic sensors*, in which the MIP is an integrated element of the optical fiber, i.e. the MIP is physically or chemically attached to the optical fiber. Very few examples have been described in the literature: a fiber optic sensor for the luminescence detection of nerve agents was described by the group of Murray. It consists of a bifurcated fiber with its extremity coated with a MIP (Jenkins et al., 1999). Prior to polymerization, the fiber was subjected to various conditionings: the cladding of the fiber was removed and its distal end polished or tapered fibers created by heating in an air/acetylene flame were employed. The sensor was then prepared by dip-coating the end in the pre-polymerization solution and polymerization was initiated by an external UV lamp. The bifurcated fiber carried the excitation light to the MIP and the luminescence produced due to the binding of the analyte to the MIP, was redirected by the fiber to a detector. The binding was monitored with the luminescence band in the 610-nm region produced by the europium(III) ions covalently bound to the MIP. The sensor showed good sensitivity (660 ppq for the benchtop version and 7 ppt for the portable version with an Ocean Optics mini-spectrometer) and a fast response (8 minutes).

More recently, a MIP-based fiber optical interferometer for the detection of cyanotoxins (Queirós et al., 2011), was developed at the tip of a fiber by dip-coating into a sensing sol-gel matrix.

Then binding of analyte (microcystin-LR) was monitored by a wavelength shift of the optical power, because the interaction of the analyte with the sol-gel MIP had a strong effect on the phase of the fiber Fabry-Pérot interferometer. The sensor showed specificity, good selectivity, a low LOD (0.3 μg/mL) and a fast response (2 minutes).

A fluorescence-based optical fiber MIP sensor for the detection of cocaine was reported very recently (Nguyen et al., 2012). Here, the end of the fiber was subjected to a succession of polishing and surface activation treatments before being silanized to attach acrylate groups, thus allowing for covalent attachment of a cocaine-MIP by copolymerization. For detection, a fluorescein-based functional monomer was incorporated into the MIP, which showed fluorescence enhancement upon binding of cocaine. The sensor demonstrated good specificity and selectivity. However, the sensitivity in the μM range and the response time could still be improved.

A SPR fiber optic sensor combining colloidal crystal and molecularly imprinted hydrogel has also been reported recently for the detection of vitamin B_3 (Verma and Gupta, 2013). The sensing probe was prepared in three steps: first, a silver coated optical fiber probe was fabricated; then, colloidal crystal templates were prepared on it, followed by polymerization of the imprinted polymer during 24 hours. The authors demonstrated that the colloidal crystal templating and the imprinting effect resulted in an improved detection of the analyte.

In these examples, the coating of the polymer on the fiber was by a complex procedure, requiring time-consuming multi-step protocols like pre-treatment of the fiber (polishing, surface activation, silanization) before the polymer can be covalently attached.

In this chapter we describe a new type of fluorimetric sensor based on an optical fiber that carries at one end an in-situ photopolymerized micrometer-sized MIP tip (Ton et al., 2013). In our system, we use a laser beam emerging from the fiber core to synthesize a polymer microtip at the extremity of the fiber that appears as an extension of the fiber core, an approach that had been developed earlier by our collaborators, mainly in order to connect optical fibers to each other (Soppera et al., 2008). Our optical fibers were employed as such after cleavage, without any additional treatment.

Two different set-ups were used to demonstrate our concept. In the first set-up (Figure 2.1A), the sensor tip is illuminated through the fiber using a diode laser, the fluorescence response of the MIP is detected at the tip level, by external collection using a fiber optic mini-spectrofluorimeter or by fluorescence microscopy. This set-up can be used, for example, to integrate the sensor into a microfluidic chip. In the second set-up (Figure 2.1B), a Y-shaped bifurcated fiber is used; the sensor tip at the common end is illuminated through one arm of the fiber using a diode laser, and the fluorescent light emitted from the MIP tip is collected and guided through the other arm of the optical fiber for detection by a spectrofluorimeter. This set-up is particularly useful for sensing at long distances and in setups where the light collection cannot be done externally.

Standard telecommunication optical fibers (single-mode for > 1280 nm) with an 8 μm core were first used for both set-ups. Later, we moved to a customized bifurcated 2 x 1 Y fiber made of three multimode UV/visible optical fibers with a 400 μm core. One arm of this bifurcated fiber was directly connected to an Ocean Optics mini-spectrometer for readout of the fluorescence signal.

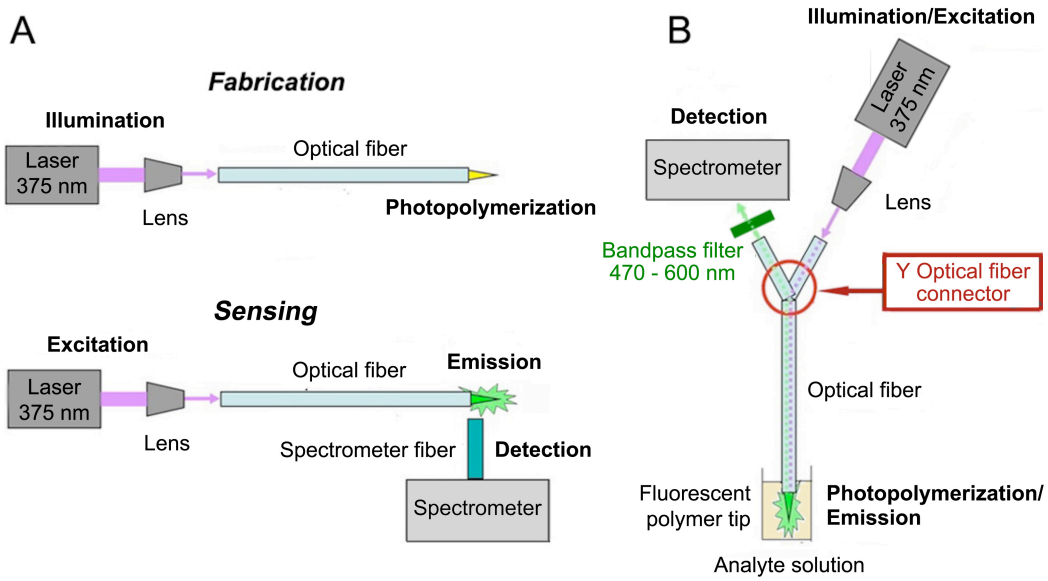

Figure 2.1. *MIP microtip fabrication, and sensing by spectrofluorimetry with (A) a simple fiber or (B) with a bifurcated fiber.*

The novelty of our approach is to use the emerging light from the optical fiber to photopolymerize a MIP at the extremity of the fiber. In addition, in order to develop a versatile sensor system, we have used three approaches as described below: (i) a core-shell format of the sensing tip for a faster response, (ii) enhancement of the optical signal by incorporating gold nanoparticles into the MIP, and (iii) fluorescent reporter groups were incorporated into the MIP as functional monomers, for the detection of non-fluorescent analytes.

II. Materials and methods

II.1. Reagents and materials

Table 2.1 shows the structures of some of the chemicals used in this work. All chemicals and solvents were of analytical grade and purchased from Sigma-Aldrich (St-Quentin Fallavier, France), unless otherwise stated. 2,2'-azobis(2,4-dimethylvaleronitrile) (ABDV) was obtained from DuPont Chemicals (Wilmington, USA). Dansyl-D-phenylalanine (dansyl-D-Phe) was obtained from Biosynthan GmbH (Germany) and the initiator, bis(2,4,6-trimethylbenzoyl)-phenylphosphineoxide (Irgacure 819) was generously provided by Ciba Specialty Chemicals (Saint Fons, France). D-*erythro*-sphingosine-1-phosphate (S-1-P) was purchased from Biovalley (Marne-la-Vallée, France).
4-Vinylpyridine (4-VPY) was vacuum-distilled before use. The other monomers, methacrylic acid (MAA), methyl methacrylate (MMA), ethylene glycol dimethacrylate EDMA and pentaerythritol triacrylate (PETIA) and trimethylolpropane trimethacrylate (TRIM) were employed without further purification. PETIA and 4-VPY contain respectively 300-400 ppm and 100 ppm of polymerization inhibitors. Water was purified using a Milli-Q system (Millipore, Molsheim, France).
The gold nanoparticles used in this study were octanethiol-functionalized gold nanoparticles (2% (w/v) in toluene) and were purchased from Sigma-Aldrich. The silver nanoparticles (0.02 mg/mL in aqueous buffer, 40 nm diameter (TEM)) were also purchased from Sigma-Aldrich.
The single-mode optical fiber SMF-28e® was purchased from Sedi Fibres Optiques (Courcouronnes, France) and the bifurcated telecom fiber SMF-28e® was generously provided by Idil Fibres Optiques (Lannion, France). The bifurcated multimode fiber was custom-made by Idil Fibres Optiques using three FT400UMT UV/visible multimode optical fibers (400 μm core and numerical aperture of 0.39) that were purchased from Thorlabs (Maisons-Laffite, France). One arm of the bifurcated fiber possesses a SMA connector at its end, to be inserted into a HR2000+ Ocean Optics spectrometer (Ocean Optics, Dunedin, USA) for detection.
The laser used in this study was a 375 nm LaserBoxx laser diode (max. 70 mW, adjustable) and was purchased from Oxxius (Lannion, France).

Table 2.1. *Chemical structures of compounds used in this study.*

Reagents (abbreviation)	Role	Molecular structure
Dansyl-L-phenylalanine (Dansyl-L-Phe)	Target	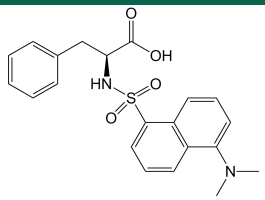
***N*-carbobenzyloxy-L-phenylalanine (Z-L-Phe)**	Template	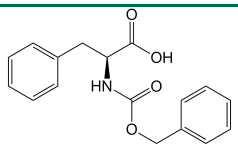
2,4-dichlorophenoxyacetic acid (2,4-D)	Template & target	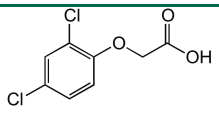

Citrinin	Template & target	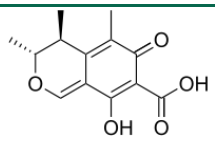
D-*erythro*-sphingosine-1-phosphate (S-1-P)	Template & target	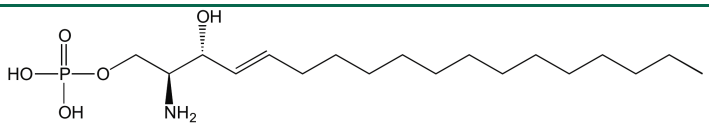
2,4-dichlorophenoxyacetic acid methyl ester (2,4-D-OMe)	Template analogue, competitor	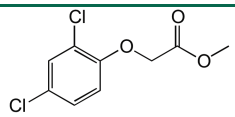
Phenoxyacetic acid (POAc)	Template analogue, competitor	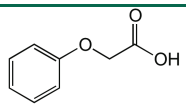
Adenosine monophosphate (AMP)	Competitor	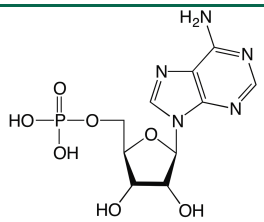
β-D-glucuronic acid (GlcA)	Competitor	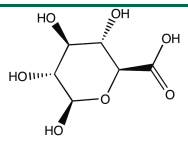
N-2-(6-(4-methylpiperazin-1-yl)-1,3-dioxo-1H-benzo[de]iso-quinolin-2(3H)-yl-ethyl)acrylamide (FIM for "fluorescent monomer")	Functional monomer	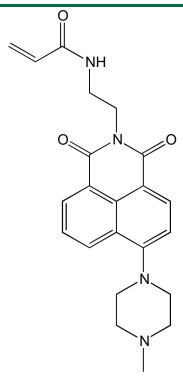
Methacrylic acid (MAA)	Functional monomer	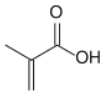
4-vinylpyridine (4-VPY)	Functional monomer	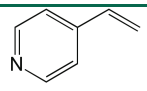
Methyl methacrylate (MMA)	Functional monomer	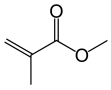
Acrylamide (AAm)	Functional monomer	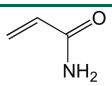
Ethylene glycol dimethacrylate (EDMA)	Cross-linker	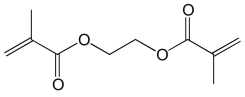

Pentaerythritol triacrylate (PETIA)	Cross-linker	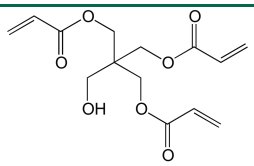
Trimethylolpropane trimethacrylate (TRIM)	Cross-linker	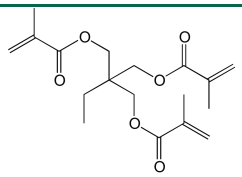
Bis(2,4,6-trimethylbenzoyl)phenyl phosphine oxide (Irgacure® 819)	Photoinitiator	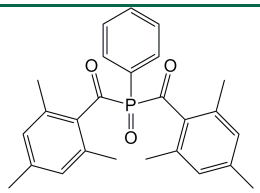
2,2'-azo-bis-(2,4-dimethylvaleronitrile) (ABDV, Vazo® 52)	Initiator	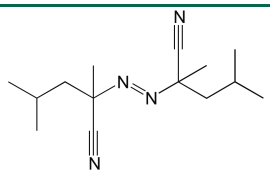
Acetonitrile (ACN)	Solvent	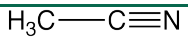
Tetraethylene glycol dimethyl ether (tetraglyme)	Solvent	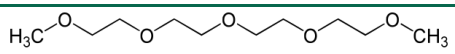

II.2. MIP microtip fabrication process

The compositions of MIP precursors solutions are described in Table 2.2. A 375 nm laser diode (max. 70 mW, adjustable), used as actinic light source was coupled into a single-mode optical fiber (outer diameter: 125 µm, core: 8 µm), in a simple (Figure 2.1A) or bifurcated (Figure 2.1B) configuration. The set-up for the simple fiber is illustrated in Scheme 2.1. The optical fiber was first cleaved to obtain a flat extremity. The laser power at the end of the fiber was adjusted to 100 µW using a real time single-channel power meter (Coherent Power Max USB-PS19Q). The extremity of the optical fiber was put in contact with the surface of the MIP precursors solution for a few seconds, which produced a precursor drop at the end of the fiber. The actinic light emerging from the fiber core induced polymerization in the drop, and the irradiation time was 10 seconds. For the "core-shell" format of the polymer **P1**, a tip of poly(PETIA) was first fabricated by 5 seconds of laser irradiation through a drop of PETIA containing 1 mol% Irgacure 819. After rinsing with ethanol, the tip was immersed into the MIP **P1** precursors solution and the laser was switched on for 3 seconds, resulting in the formation of the MIP layer.

The "core-shell" polymers **P2, P4** and **P5** were fabricated in the same way, except that for the formation of the MIP layer on the poly(PETIA) tip, the laser was switched on for 10 seconds on the single-mode fiber, and 25 seconds on the multimode bifurcated fiber. Images of the microtips were taken using an optical microscope (2 Mpixel CCD Camera mounted on a 12 X Navitar ultra-zoom). After polymerization, the template was extracted by placing the microtip in ethanol:acetic acid (4:1), 3 times for 1 hour each. The microtips were then rinsed 3 times with methanol and left to dry, prior to incubation with the analyte.

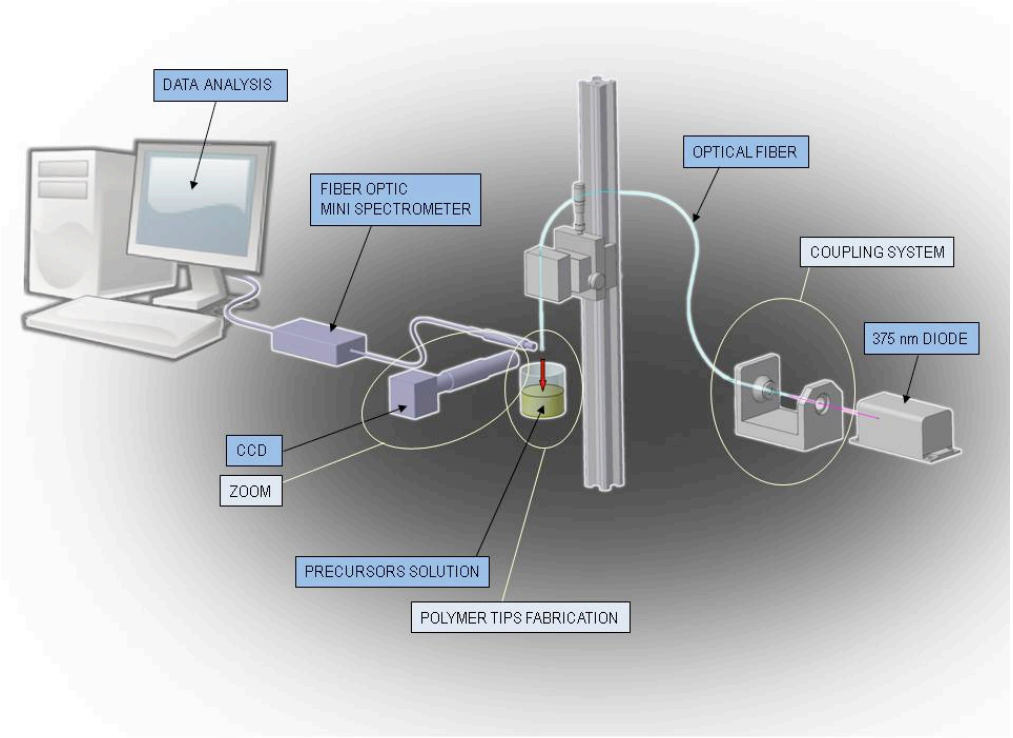

Scheme 2.1. *Scheme in 3D of the simple fiber set-up.*

II.3. Formulations of MIPs

Table 2.2. *Formulations of MIP precursors solutions used in this study.*

Polymer	Format of the MIP	Template	Functional monomers	Cross-linker	Initiator	Solvent	Metal NPs (only)
P1	Plain tip	Z-L-Phe (0.05 mmol)	MAA/4-VPY (0.2/0.2 mmol)	EDMA/PETIA (1.3/0.7 mmol)	Irgacure 819 (0.025 mmol)	Tetraglyme (230 µL)	-
P1-Au	Plain tip	Z-L-Phe (0.05 mmol)	MAA/4-VPY (0.2/0.2 mmol)	EDMA/PETIA (1.3/0.7 mmol)	Irgacure 819 (0.025 mmol)	Tetraglyme (230 µL)	0.6 mg
Phe2	Plain tip	Z-L-Phe (0.05 mmol)	MAA/4-VPY (0.2/0.2 mmol)	TRIM (2 mmol)	Irgacure 819 (0.032 mmol)	Tetraglyme (230 µL)	-
P2	Core-shell tip	2,4-D (0.02 mmol)	FIM/4-VPY (0.04/0.04 mmol)	EDMA (0.4 mmol)	Irgacure 819 (0.008 mmol)	Methanol/water (4/1) (1 mL)	-
P2-Au	Core-shell tip	2,4-D (0.02 mmol)	FIM/4-VPY (0.04/0.04 mmol)	EDMA (0.4 mmol)	Irgacure 819 (0.008 mmol)	Methanol/water (4/1) (1 mL)	3.6 mg
P3	Particles by precipitation	2,4-D (0.025 mmol)	FIM/4-VPY (0.05/0.05 mmol)	EDMA (0.5 mmol)	ABDV (0.016 mmol)	Methanol/water (4/1) (3 mL)	-
P4	Core-shell tip	Citrinin (0.02 mmol)	FIM/4-VPY (0.04/0.04 mmol)	EDMA (0.4 mmol)	Irgacure 819 (0.008 mmol)	Methanol (1.2 mL)	-
P5	Core-shell tip	S-1-P (2.6 µmol)	FIM/MMA (5.3/5.3 µmol)	EDMA (52 µmol)	Irgacure 819 (1.1 µmol)	Methanol (1 mL)	-
P6	Core-shell tip	S-1-P (2.6 µmol)	FIM/MMA/AAm (5.3/5.3/5.3 µmol)	EDMA (52 µmol)	Irgacure 819 (1.1 µmol)	Methanol (1 mL)	-
P7	Core-shell tip	S-1-P (2.6 µmol)	FIM/MMA/AAm (5.3/5.3/5.3 µmol)	EDMA (52 µmol)	Irgacure 819 (1.1 µmol)	Methanol/water (5/1) (1.2 mL)	-
P7-Au/Ag	Core-shell tip	S-1-P (2.6 µmol)	FIM/MMA/AAm (5.3/5.3/5.3 µmol)	EDMA (52 µmol)	Irgacure 819 (1.1 µmol)	Methanol/water (5/1) (1.2 mL)	$2.5.10^{8}$ NPs

II.4. Preparation of bulk polymers

The polymer precursors solutions **P1** and **Phe2** (Table 2.2) were dissolved in 500 µL of the solvent tetraglyme in a four-milliliter glass vial fitted with an airtight septum, and the mixture was purged with nitrogen for 2 minutes. Polymerization was carried out with a daylight lamp equipped with a 18W standard tube. After 15 minutes of irradiation, the polymers were recovered by breaking the glass vials. The monoliths were manually crushed in a mortar and then transferred to microcentrifuge tubes, suspended in methanol and finely ground with 2.8 mm-diameter ceramic beads in a Precellys 24 homogenizer (Bertin Technologies, Montigny le Bretonneux, France). The polymers were then transferred to 50 mL centrifuge tubes and washed on a tube rotator (SB2, Stuart Scientific) with 3 rounds of ethanol-acetic acid (4:1), and then rinsed three times with methanol. The polymer particles were finally dried overnight under vacuum and stored at 4°C. A control non-imprinted polymer (NIP) was prepared using the same protocol except for the omission of the template.

For the fluorescence lifetime measurements (paragraph II.5.), the precursors solution **P1** and **P1 Au**, but with dansyl-L-Phe as template, were synthesized by bulk polymerization with the exact same protocol than the one described above.

II.5. Fluorescence emission decay measurements

Fluorescence lifetime measurements were performed with a Horiba Jobin-Yvon Fluorolog fluorescence spectrophotometer (Kyoto, Japan), by right-angle illumination of the samples: a solution of 10 µM dansyl-L-Phe in ACN, and suspensions of bulk dansyl-L-Phe MIPs **P1** and **P1 Au** (0.02 mg/mL and 0.05 mg/mL in ACN). The excitation light source used was a pulsed diode Horiba NanoLED (model N-340) with a peak wavelength at 341 nm and a pulse duration of <1 ns. The fluorescence emission wavelength was set at 520 nm, and excitation and emission bandpass were set at 3 nm. The data were collected using DataStation software, to 10 000 counts in the peak and the time calibration was 0.0549 ns per channel. The data were then analyzed using DAS6 software, from channel 440 to channel 1500, and fitted by a first-exponential model.

II.6. Preparation of the MIP P3 by precipitation polymerization

0.025 mmol 2,4-D, 0.05 mmol FIM, 0.05 mmol 4-VPY, 0.5 mmol EDMA and 0.016 mmol ABDV were dissolved in 3 mL of methanol/water (4/1) (Table 2) at 50°C, in a glass vial fitted with an airtight septum. The mixture was then sonicated at room temperature for 5 minutes and purged with nitrogen for 2 minutes on ice. Polymerization was done overnight at 50°C in a water-bath. The polymers were then washed with 3 rounds of methanol/acetic acid (7/3) and rinsed 3 times with methanol, before drying overnight under vacuum. The non-imprinted polymer (NIP) was prepared with the same protocol but in the absence of the template 2,4-D.

II.7. Binding studies of polymer microtips with the simple fiber

II.7.1. Plain microtip – analyte: dansyl-L-Phe

The microtips (**P1, P1-Au, Phe2**) were incubated for 10 or 45 minutes with dansyl-L-Phe. After incubation, the microtips were rinsed by immersion for a few seconds in ethanol and dried prior to fluorescence measurements. The excitation light (375 nm) was switched on and the fluorescence of

the tip was externally recorded with a HR2000+ fiber optic spectrometer. The fluorescence signals of tips incubated with dansyl-D-Phe were corrected using a multiplicative factor of 1.3 determined by fluorescence spectroscopy measurements of several dansyl-L-Phe and dansyl-D-Phe solutions in ACN of exactly the same concentrations.

II.7.2. Core-shell microtip P2 – Analyte: 2,4-D

The microtip **P2** was incubated 5 minutes with 2,4-D. After incubation, the microtip was rinsed by immersion for a few seconds in ethanol and dried prior to fluorescence measurements. The excitation light (375 nm) was switched on and the tip fluorescence was externally recorded with a HR2000+ fiber optic spectrometer. The fluorescence enhancement (%) was defined as [(F-F0)/F0]*100, with F and F0 the fluorescence intensities of the polymer, respectively in presence and in absence of 2,4-D. Fluorescence microscope images were recorded using a Leica DMI6000 B fluorescence microscope, equipped with 360 nm excitation/470 nm emission and 470 nm excitation/527 nm emission filter cubes.

II.8. Binding studies of polymer microtips on the bifurcated fibers

Measurements were done with the tip remaining immersed in the analyte solution. Two types of bifurcated fibers were used: (i) a single-mode telecom fiber (core diameter: 8 μm), initially used for the “proof-of-concept” of the bifurcated fiber set-up (determination of the binding properties of the MIP, time response, limit of detection, etc) and (ii) a multimode fiber (core diameter: 400 μm) used to increase the sensitivity of the MIP-based fiber sensor.

II.8.1. The bifurcated single-mode fiber

The laser (375 nm) was coupled into one arm of the Y-shaped fiber and the tip fluorescence was recorded with the spectrometer of a Witec alpha 300 SR microscopy system equipped with a DV970N-BV Electron Multiplying CCD camera (Ulm, Germany), by focusing onto the end of the other arm of the fiber. The fluorescence intensity values were obtained after subtraction of the fluorescent background measured as 300 counts.

II.8.2. The multimode bifurcated fiber

The laser (375 nm) was coupled into one arm of the Y-shaped fiber and the other arm was inserted into a HR2000+ Ocean Optics spectrometer with a SMA connector, for detection and readout of the fluorescence signal.

II.9. Batch binding studies with MIP particles P3

A stock solution of 500 nM of 2,4-D in methanol was prepared and stored in the dark at -20°C; and the polymer particles were suspended by sonication in methanol/water (4/1) at 0.5 mg/mL. From this stock suspension, a polymer concentration of 5 μg/mL was pipetted in 1.5 mL polypropylene microcentrifuge tubes and a volume ranging from 5 μL to 200 μL of 2,4-D solution was added so as to obtain final 2,4-D concentrations ranging from 2.5 nM to 100 nM. The final volume was adjusted to 1 mL with solvent. The tubes were incubated in the dark for 1 hour at ambient temperature on a tube

rotator. The suspensions were then put into a quartz cell for recording of their fluorescence emission spectra with a Horiba Jobin-Yvon Fluorolog fluorescence spectrophotometer (Horiba, Kyoto, Japan). Excitation was set at 390 nm. Fluorescence enhancement was calculated as follows: [(F-F0)/F0)*100, with F and F0 the emitted fluorescence intensity of MIP respectively in presence and in absence of the analyte.

II.10. Synthesis and characterization of the fluorescent monomer "FIM" N-(2-(6-(4-methylpiperazin-1-yl)-1,3-dioxo-1H-benzo[de]isoquinolin-2(3H)-yl-ethyl)acrylamide

Instrumental: Proton (^{1}H NMR) and carbon (^{13}C NMR) were recorded at 400 MHz on a Bruker Avance III 400 spectrometer. Chemical shifts (d) are given in part per million (ppm), and coupling constants (J) are given in Hertz (Hz). The mass spectrum (*m/z*) was recorded using a LC-MS/MS Q-TOF Agilent Technologies 6538 spectrometer.

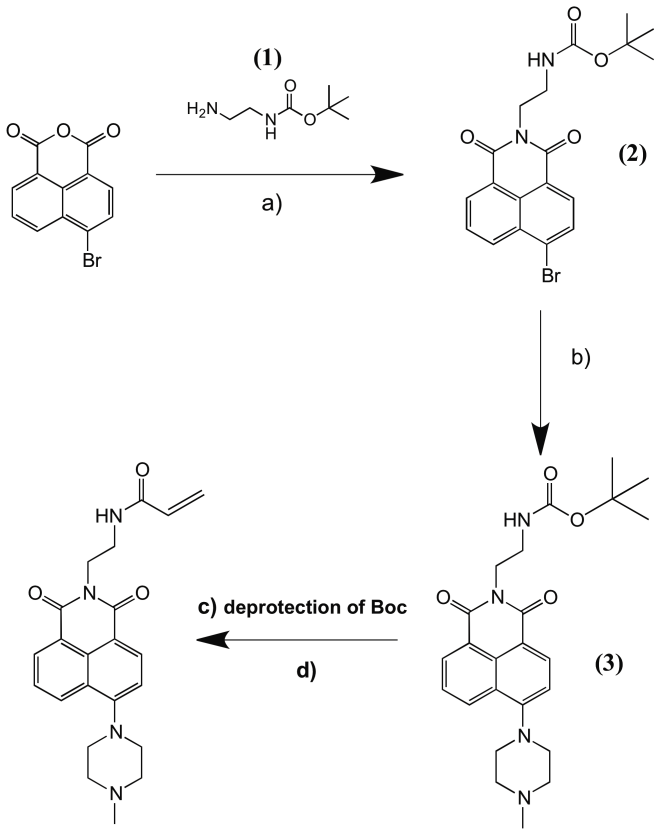

a) N-Boc-1,2-diaminoethane (1), 1,4-dioxane, reflux, 4h
b) 1-methylpiperazine, methoxyethanol, reflux, 16h
c) HCl 4M in THF, r.t., 4h; d) acryloyl chloride, DCM, TEA, under N_2, r.t.

Scheme 2.2*. Synthetis of the functional monomer "FIM".*

***N-tert*-butyloxycarbonyl-1,2-diaminoethane (1).** A solution of di-*tert*-butyldicarbonate (8.74 g, 40 mmol) in $CHCl_3$ (200 mL) was added dropwise at 0°C over a period of 3 h to a solution of 1,2-diaminoethane (28 mL, 400 mmol) in $CHCl_3$ (400 mL). After stirring at ambient temperature for 16 h, the mixture was washed with brine (6x100 mL) and water (1x100 mL), dried over $MgSO_4$ and concentrated in vacuum to afford 6.40 g (quantitative yield) of *N*-Boc-1,2-diaminoethane as a colorless oil. ^{1}H NMR (400 MHz, $CDCl_3$): d 4.82 (br. s, 1H), 3.15 (app q, J=5.7 Hz, 2H), 2.78 (t, J=5.9 Hz, 2H), 1.44 (s, 9H), 1.22 (s, 2H).

a) *tert*-butyl 2-(6-bromo-1,3-dioxo-1H-benzo[de]isoquinolin-2(3H)-yl)ethylcarbamate (2): 1,298 g (8.1 mmol) of (**1**) were added to a suspension of 4-bromo-1,8-naphtalic anhydride (1.5 g, 5.41 mmol) in 60 mL of 1,4-dioxane. The suspension was heated at 105°C for 16 h to give a dark red solution. After cooling down at room temperature the addition of 200 mL of brine to the reaction solution allowed the formation of a yellow precipitate that was filtered off and dried under vacuum. The yellow solid was purified by flash chromatography using 30% of ethyl acetate in hexane to afford a pure yellow solid in a 80% yield. ^{1}H NMR (400 MHz, $CDCl_3$): d 8.63 (d, 1H), 8.53 (d, 1H), 8.35 (d, 1H), 8.01 (d, 1H), 7.69 (t, J=7.9 Hz, 1H), 4.96 (br, 1H), 4.34 (m, 2H), 3.53 (m, 2H), 1.27 (s, 9H). ^{13}C NMR (400 MHz, $CDCl_3$): d 164.06, 164.04, 156.2, 133.48, 132.32, 131.49, 131.22, 130.7, 130.5, 129.16, 128.20, 123.04, 122.17, 79.29, 40.17, 39.64, 28.34. IR: n_{max} / cm^{-1}: 3365, 2990, 1650, 1586, 1365, 1141.

***b)* *tert*-butyl-2-(6-(4-methylpiperazin-1-yl)-1,3-dioxo-1H-benzo[de]isoquinolin-2(3H)yl)ethylcarbamate (3):** 840 mg of (**2**) (2 mmol) were dissolved in 12 mL of methoxyethanol at 105°C. 1.1 mL (10 mmol) of 1-methylpiperazine was added and the solution was left overnight under stirring. After cooling at room temperature, 100 mL of brine were added to the solution to precipitate the compound as a brown orange solid. After filtration and purification by flash chromatography using 40% of ethyl acetate in hexane, 0,6 grams (1.37 mmol) of pure compound were obtained as a yellow solid in a 68.5% yield. ^{1}H NMR (400 MHz, $CDCl_3$): d 8.55 (d, 1H), 8.48 (d, 1H), 8.37 (d, 1H), 7.66 (t, J=7.8 Hz, 1H), 7.19 (d, 1H), 5.05 (br, 1H), 4.33 (m, 2H), 3.5 (m, 2H), 3.29 (m, 4H), 2.74 (m, 4H), 2,43 (s, 3H), 1,27 (s, 9H). ^{13}C NMR (400 MHz, $CDCl_3$): d 164.92, 164.44, 156.18, 132.89, 131.32, 131.39, 130.51, 130.09, 126.23, 125.72, 123.17, 116.58, 115.08, 79.11, 55.25, 53.06, 46.22, 40.05, 39.73, 28.38. IR: n_{max} / cm^{-1}: 3249, 3000, 2799, 1645, 1592, 1551, 1288, 1234, 1044, 1140, 736.

c) 2-(2-aminoethyl)-6-(4-methylpiperazin-1-yl)-1H-benzo[de]isoquinoline-1,3(2H)-dione hydrochloride (3) (deprotection): 0.44 g (1.00 mmol) were added to 4 mL of a 4M solution of HCl in tetrahydrofurane (THF) and left under stirring for 4 h at room temperature. The reaction was monitored by thin layer chromatography (TLC) (20% methanol (MeOH) in dichloromethane (DCM)) and after complete consumption of starting material the reaction was diluted with 100 mL of THF and kept at 0°C for 1 hr. After filtration 220 mg of a pure yellow solid were obtained with a 53 % yield. ^{1}H NMR (400 MHz, DMSO-*d*6): d 11.70 (br, 1H), 8.51 (app d, 2H), 8.44 (d, 1H), 8.06 (br, 3H), 7.87 (t, J=7.9 Hz, 1H), 7.46 (d, 1H), 4.33 (m, 2H), 3.7-3.4 (m, 8H), 3.11 (m, 2H), 2.87 (d, 3H), ^{13}C NMR (400 MHz, CD_3OD): d 166.74, 166.21, 156.7, 134.13, 132.81, 132.21, 130.93, 127.58, 127.21, 123.52, 117.60, 116.93, 55.13, 52.00, 44.72, 39.83, 38.91. IR: n_{max} / cm^{-1}: 3382, 2676, 1651, 1587, 1235, 1192.

d) N-(2-(6-(4-methylpiperazin-1-yl)-1,3-dioxo-1H-benzo[de]isoquinolin-2(3H)-yl)ethyl)acrylamide (4): 0.42 g (1.02 mmol) of amine were solubilised at room temperature in 40 mL of dry DCM in the presence of 2 equivalents of triethylamine (TEA). 91 mL (1.12 mmol) of acryloyl chloride were added dropwise to the solution over 10 minutes and the reaction was monitored by TLC (0.5% of MeOH in DCM). After 4 h the solvent was removed under *vacuum* and the raw product was purified by flash chromatography with the same eluent as for TLC. 250 mg (0.637 mmol) of a pure yellow solid were obtained in a 62.5% yield. ^{1}H NMR (400 MHz, $CDCl_3$): d 8.58 (dd, 1H), 8.52 (d, 1H), 8.42 (dd, 1H), 7.69 (app.t, J=7.5Hz, 1H), 7.22 (d, 1H), 6.50 (br, 1H), 6.17 (dd, J=17.1Hz, J=1.5Hz, 1H), 6.06 (dd, J=17.1Hz, J=10.1Hz, 1H), 5.55 (dd, J=10.1 Hz, J=1.5 Hz, 1H), 4.44 (m, 2H), 3.73 (m, 2H), 3.33 (m, 4H), 2.76 (m, 4H), 2.45 (s, 3H). ^{13}C NMR (400 MHz, $CDCl_3$): d 166.74,

165.34, 164.93, 156.55, 133.16, 131.61, 131.29, 130.89, 130.19, 126.31, 125.88, 125.80, 123.02, 116.28, 115.17, 55.27, 53.14, 46.25, 40.29, 39.31. IR: n_{max} / cm^{-1}: 3277, 2924, 2849, 2793, 1692, 1646, 1591, 1287, 1234.

Mass spectrum (*m/z*): $[M+H]^+$ = 393.1922, $[M+Na]^+$ = 415.1742.

II.11. Synthesis and characterization of the Au_{core}-Ag_{shell} bimetallic nanoparticles

The protocol of synthesis of the core-shell gold-silver nanoparticles was from Pande et al., 2007. The synthetic strategy is illustrated in Scheme 2.3.

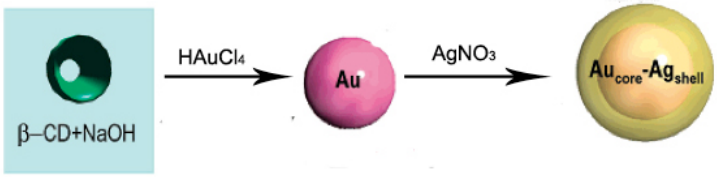

Scheme 2.3. *Schematic representation of the formation of the core-shell gold-silver bimetallic NPs. Adapted from Pande et al., 2007.*

II.11.1. Synthesis of the monometallic gold nanoparticles

A solution of 8 mg/mL (7 mM) of β-cyclodextrin (β-CD) was prepared by dissolving 160 mg of β-CD in 20 mL of water. 80 µL of 10 mM $HAuCl_4$ (0.8 µmol) was added to 19.72 mL of the solution of β-CD (138 µmol) under agitation. After 2 minutes, 0.2 mL of 1 M NaOH (0.2 µmol) was added to the solution. Then, the reaction mixture was heated in a water-bath during 20 minutes. The solution finally turned pink, indicating the formation of the gold colloids. After this, the solutions were cooled down in ice and stored at 4°C.

II.11.2. Synthesis of the silver shell on the gold core

80 µL of 10 mM $AgNO_3$ (0.8 µmol) were added dropwise to 10 mL of the gold colloidal solution. The solution was heated in a water-bath for 30 minutes, and the pink solution gradually turned yellow, indicating the formation of the Ag shell on the Au nanoparticles, i.e. the formation of the Au_{core}-Ag_{shell} nanoparticles. The solution was finally cooled down on ice and stored at 4°C.

II.11.3. Characterization of the Au_{core}-Ag_{shell} nanoparticles

The bimetallic NPs were characterized by UV-visible spectroscopy, dynamic light scattering (DLS), nanoparticle tracking analysis and transmission electron microscopy (TEM).

The nanoparticle tracking analysis allowed us to determine the concentration of bimetallic NPs, which was of $2.5.10^9$ particles/mL.

As shown in Figure 2.2, the gold NPs showed a maximum of absorption at 520 nm and the bimetallic Au_{core}-Ag_{shell} NPs showed one plasmon resonance band at 410 nm. The plasmon

resonance of the core-shell NPs can be attributed to the plasmon resonance of the Ag shell, which indicates that the core is completely covered by the shell, as the plasmon resonance of the Au core is not visible in the spectra. In order to confirm this, the absorption spectrum of Ag nanoparticles was recorded, which showed a maximum of absorption at 400 nm. The Ag NPs were synthesized following the exact same procedure than for the synthesis of Au NPs, except that a solution of $AgNO_3$ was used instead of $HAuCl_4$.

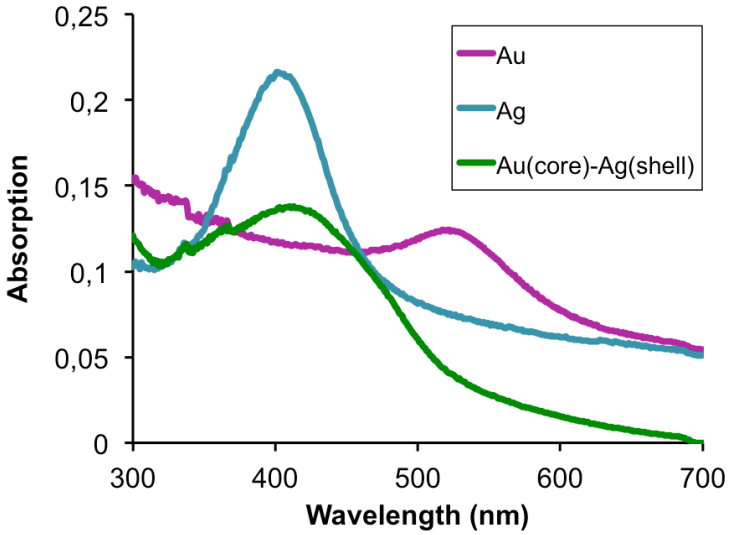

***Figure 2.2**. Absorption spectra of Au, Ag and Au_{core}-Ag_{shell} NPs in water.*

DLS measurements were performed in order to determine the size of the noble metal NPs. Measurements by intensity (Figure 2.3) reveal two populations for all NPs, one population at around 15-20 nm, and a population of bigger size varying from around 100 nm to around 600 nm. We suspect the population of bigger size to be aggregates of NPs. Measurements by number (Figure 2.4) revealed that all NPs have a size of around 13 nm.

Au

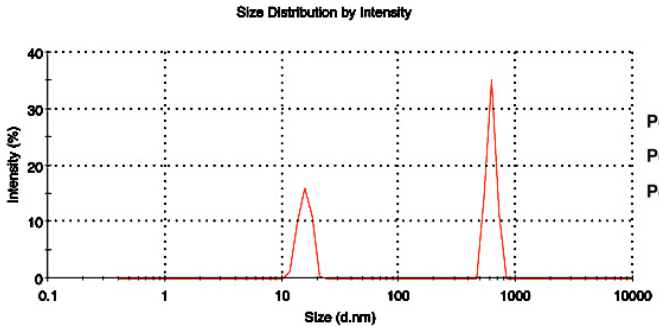

	Diam. (nm)	% Intensity	Width (nm)
Peak 1:	613,4	61,4	58,80
Peak 2:	15,76	38,6	1,932
Peak 3:	0,000	0,0	0,000

Au_{core}-Ag_{shell}

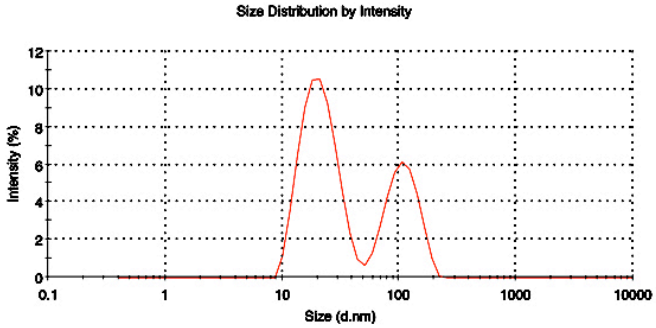

	Diam. (nm)	% Intensity	Width (nm)
Peak 1:	21,70	65,7	7,752
Peak 2:	109,1	34,3	32,91
Peak 3:	0,000	0,0	0,000

Figure 2.3. *DLS measurements by intensity of solutions of Au and Au_{core}-Ag_{shell} NPs in water.*

Au

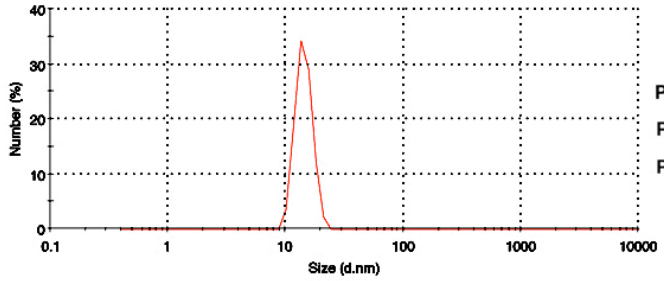

	Diam. (nm)	% Number	Width (nm)
Peak 1:	14,43	100,0	2,349
Peak 2:	0,000	0,0	0,000
Peak 3:	0,000	0,0	0,000

Au_{core}-Ag_{shell}

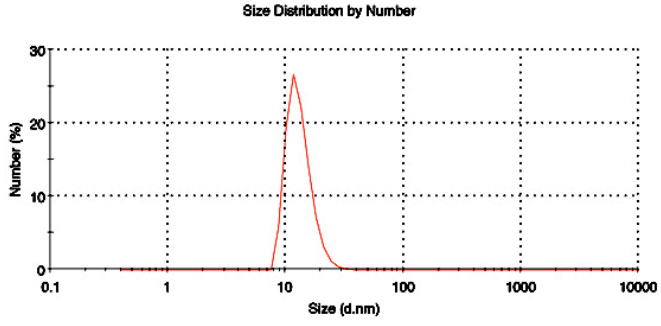

	Diam. (nm)	% Number	Width (nm)
Peak 1:	13,19	100,0	3,394
Peak 2:	0,000	0,0	0,000
Peak 3:	0,000	0,0	0,000

Figure 2.4. *DLS measurements by number of solutions of Au and Au_{core}-Ag_{shell} NPs in water.*

TEM images were recorded for the Au NPs and the Au_{core}-Ag_{shell} NPs, to measure the size of the NPs and to investigate the core-shell structure of the Au_{core}-Ag_{shell} NPs. As shown in Figure 2.5, the Au NPs were about 10 nm, which was consistent with the DLS measurements. Concerning the Au_{core}-Ag_{shell} NPs, the Au core was about 10 nm (± 2 nm), and the less dense Ag shell could be visualized around the Au core, with a thickness of around 5 nm.

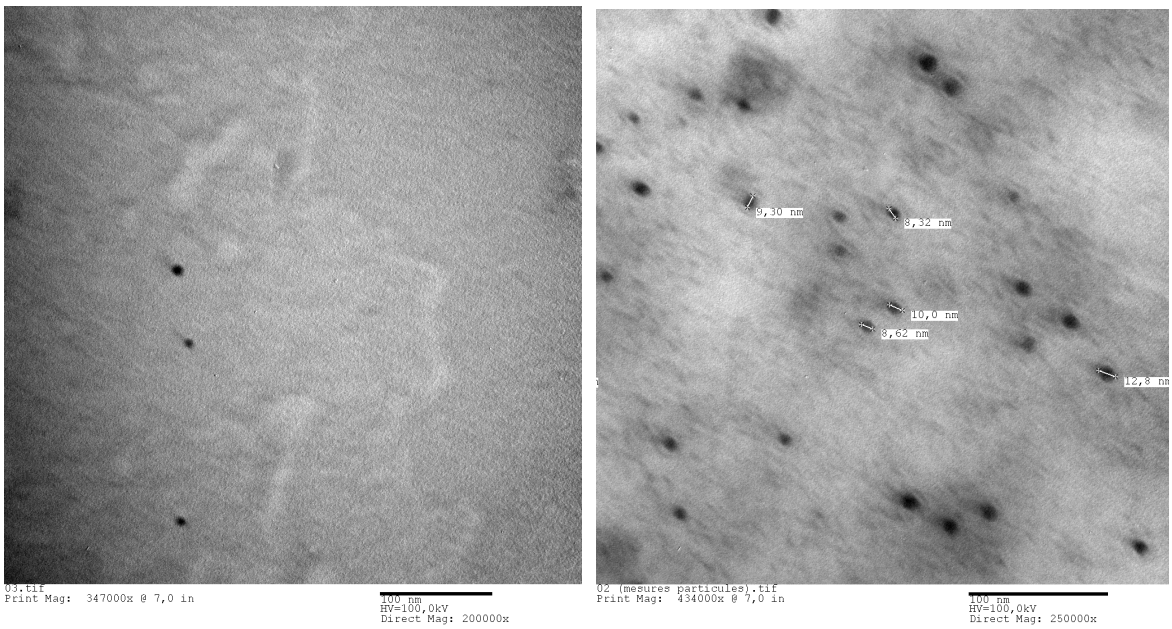

Figure 2.5. *Transmission electron micrographs of gold colloids (left, scale bar 100 nm) and Au_{core}-Ag_{shell} nanoparticles (right, scale bar 100 nm).*

III. Results and discussion

We use a laser beam emerging from the core of an optical fiber to synthesize a polymer microtip at the extremity of the fiber that appears as an extension of the fiber core. This microtip is later used for opto-chemical sensing purposes. Three configurations were used at the different stages of our study:

(i) The **simple SMF** (single-mode fiber; 8 μm core diameter) set-up (Figure 2.1A; Scheme 2.1) was initially used to establish the concept of our sensor. The optimization of the MIP formulation and photostructuring of the microtip was performed with the simple fiber. For the binding studies, we first chose the amino acid derivative Z-L-Phe as model template, and the fluorescent analyte dansyl-L-Phe was used to monitor the binding. In a second time, we developed a naphthalimide-based signaling MIP that shows fluorescence enhancement upon analyte binding. The MIP was imprinted with the herbicide 2,4-D.

(ii) The **bifurcated SMF** set-up (Figure 1B) was subsequently developed because this set-up allows real-time measurements over long distances.

(iii) The **bifurcated multimode fiber** (core diameter 400 μm) set-up was used in order to increase the sensitivity of the bifurcated fiber-based sensor. The naphthalimide-based signaling monomer was incorporated into the MIP. In order to demonstrate the versatility of our approach, the MIP-based sensor was applied to several analytes of interest: the herbicide 2,4-D, the mycotoxin citrinin and the sphingolipid D-*erythro*-sphingosine-1-phosphate.

III.1. Studies with the simple single-mode fiber (SMF) set-up

III.1.1. Optimization of the MIP formulation and tailoring of the tip geometry

Our first aim was to obtain a MIP formulation compatible with three-dimensional photostructuring, without compromising the molecular recognition properties of the MIP. Z-L-Phe was used as model template and its fluorescent analogue dansyl-L-Phe was used to monitor the binding.

MIPs with specific recognition towards the amino acid derivatives Z-L-Phe and the fluorescent dansyl-L-Phe in acetonitrile (ACN), have already been reported in the literature (Ramstroem et al., 1993; Fuchs et al., 2011; Piperno et al., 2011). The template, the functional monomers MAA / 4-VPY and the cross-linker EDMA were employed in a molar ratio 1:4/4:40 respectively. As we used laser light at 375 nm for polymerization, the photoinitiator Irgacure 819 (Fuchs et al., 2011), instead of azo-bis-dimethylvaleronitrile (Ramstroem et al., 1993; Piperno et al., 2011) was selected for our studies, because it absorbs strongly in the range 300-450 nm and is very reactive towards methacrylates and acrylates (Szablan et al., 2007).

It has been shown earlier that the geometry of an end-of-fiber poly(PETIA) microtip was governed by the physico-chemical parameters of the formulation and by the photonic parameters (Jradi et al., 2009; Soppera et al., 2008). Images of the different steps of a successful MIP tip fabrication are shown in Figure 2.6. The influence of the above-mentioned parameters on the photostructuring process of the MIP was therefore investigated by varying the formulation of the polymer (amount and type cross-linker) and the photonic conditions (laser power and time of irradiation). As a general rule, the MIP precursor solution has to be highly viscous, as high viscosity prevents the random diffusion of polymer chains, thus favoring spatially limited photopolymerization in the drop of precursor solution at the end of the fiber.. The solvent tetraethylene glycol dimethyl ether (tetraglyme) was selected, as it is quite viscous (4.1 cP at 20°C), solubilizes the template Z-L-

Phe and does not possess hydrogen-bonding donor groups that might interfere with the template-monomers interactions. From a MIP point of view, the use of solvent is necessary to generate a porous material and the degree of cross-linking should be high enough so as to maintain the structure of the binding sites (Wulff, 1995). However, a too rigid polymer network can result in low binding due to a difficult access of the analyte to the binding sites (Wulff, 2002).

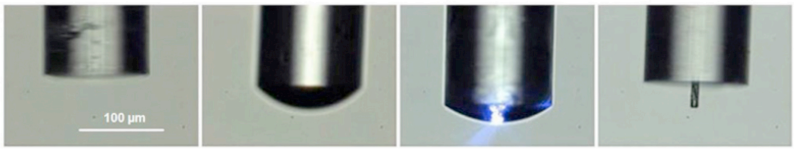

Figure 2.6. *Procedure of MIP tip preparation (Bright field microscope images).*

In the search for the best MIP formulation compatible with photostructuring, several cross-linkers were tested: EDMA, a dimethacrylate monomer that was used previously for the formulation of a MIP for dansyl-L-Phe (Ramstroem et al., 1993; Fuchs et al., 2011), TRIM, a trimethacrylate monomer that generates a higher cross-linked MIP, and a mixture of EDMA/PETIA (2/1), which is used in our group to fabricate microstructured holographic MIP films. Formulations containing EDMA alone did not give stiff polymer tips; EDMA apparently generated too low cross-linked polymers that were not studied further. Formulations based on a mixture EDMA/PETIA (2/1) (polymer P1) or TRIM (polymer Phe2) as cross-linkers (Table 2.3) yielded stiff microtips and were therefore more promising, thus MIPs were prepared using this formulation with Z-L-Phe as the template.

Table 2.3. *Formulations of Z-L-Phe MIP microtips.*

Polymer	Template	Functional monomers	Cross-linker	Initiator	Solvent
P1	Z-L-Phe (0.05 mmol)	MAA/4-VPY (0.2/0.2 mmol)	EDMA/PETIA (1.3/0.7 mmol)	Irgacure 819 (0.025 mmol)	Tetraglyme (230 µL)
Phe2	Z-L-Phe (0.05 mmol)	MAA/4-VPY (0.2/0.2 mmol)	TRIM (2 mmol)	Irgacure 819 (0.032 mmol)	Tetraglyme (230 µL)

Figure 2.7 shows the set of polymer tips fabricated with the two formulations, at two different laser powers P=100 µW and P=10 µW, and for various irradiation times. The precursors solutions were all highly photosensitive and therefore the polymerization process was extremely fast, and was completed in less than ten seconds for all formulations. The final shapes of the tips were reached for a time of irradiation varying from 1 to 5 seconds depending on the formulation. The final shape is attained when the length of the tip corresponds to the radius of the precursor drop. Subsequently, a slight enlargement of the polymer tip is observed. This is because the fiber used here is multimode at 375 nm so the beam emerging from the fiber does not have a gaussian shape but a multimodal diverging profile. The length of the tip was ca. 35-40 µm, and its diameter was measured to be 15 µm for P=100 µW. A lower incident power of 10 µW produced thinner tips of 7-8 µm diameter, but apart from that, the tendencies observed were the same as with 100 µW.

Differences of shapes and kinetics of growth appeared between the two formulations. Comparing the cross-linkers (TRIM and mixture EDMA/PETIA), we noticed that TRIM allowed a faster polymerization and a better photostructuring. The formulation **P1** (EDMA/PETIA) gave distorted tips for short irradiation times (< 2.5sec), probably due to a too low cross-linking degree

(Soppera et al., 2008). These results seem logical, as TRIM is a trifunctional cross-linking monomer and thus should give a better cross-linked and more rigid polymer; whereas the mixture EDMA/PETIA is composed of 2/3 of a difunctional monomer and 1/3 of a trifunctional monomer.

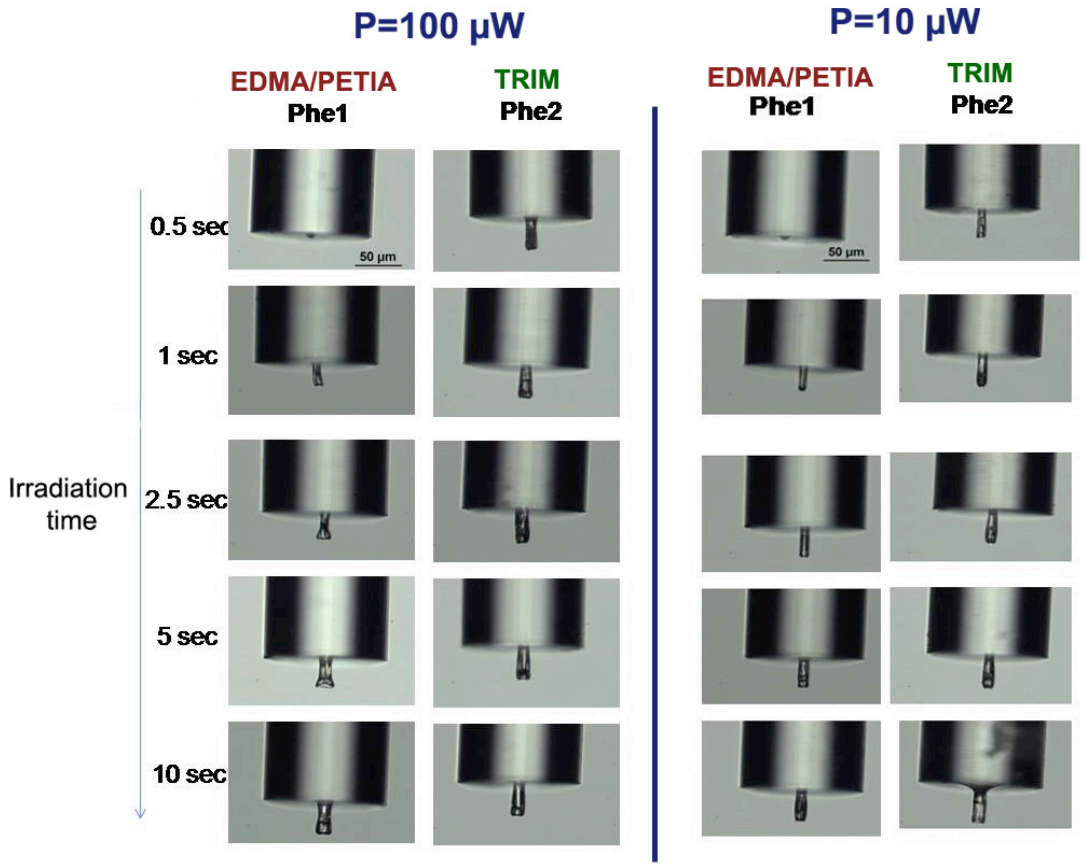

Figure 2.7. *Influence of the formulation and the time of irradiation on the shape of the tip (time of irradiation mentioned on each picture). The scale bar on the first picture corresponds to 50 µm. 375 nm laser power set at P=100 µW and P=10 µW.*

The same experiments were performed with the corresponding NIPs, and no difference of shape or kinetics of polymerization was observed when compared with the MIPs. Thus the presence of molecular template did not affect the photopolymerization process of the polymer tip.

Based on the photostructuring pictures (Figure 2.7), TRIM (**Phe2**) produced the stiffest tips and therefore would be the most appropriate cross-linker. However, this does not automatically mean that this mixture is also the optimum one from a molecular imprinting point of view. The influence of the cross-linker on the molecular recognition properties of the MIP was therefore investigated using bulk polymers, as outlined in the next section.

III.1.2. Molecular recognition properties of the imprinted bulk polymers

Binding experiments were performed in order to determine whether the formulations suitable for photostructuring were compatible with molecular imprinting. Two bulk imprinted polymers of the same formulations as described previously: EDMA/PETIA-based MIP and TRIM-based MIP were evaluated in tetraglyme, the solvent of synthesis, and in anhydrous ACN. Both polymers were

incubated with 10 µM dansyl-L-Phe, a fluorescent derivative of the template Z-L-Phe, and the binding was measured by fluorescence spectroscopy.

When incubated in tetraglyme, for both formulations, a low binding (<15%) was observed for both MIP and NIP (not illustrated). In ACN (Figure 2.8), the EDMA/PETIA-based MIP showed a better binding than the TRIM-based MIP. Indeed, the former bound up to 75% of dansyl-L-Phe, which was 5 times more than the TRIM-based MIP, which attained only ca 15% of binding. Consequently, the photostructuring of the polymers corresponding to formulation **P1** was analyzed in more detail.

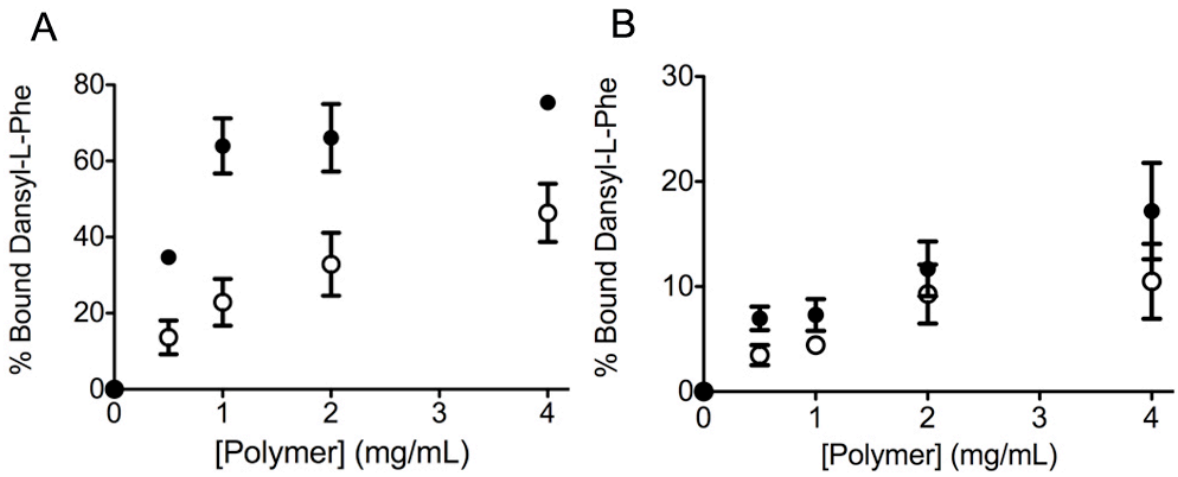

Figure 2.8. *Equilibrium binding isotherms in ACN of dansyl-L-Phe adsorption to the MIP (full circles) and NIP (empty circles) synthesized with the bulk formulation (A) EDMA/PETIA and (B) TRIM. Data are means of triplicate experiments. The error bars represent standard deviations.*

III.1.3. Effect of photonic parameters on the morphology of polymer microtips

Scanning electron micrographs of MIP and NIP tips of formulation **P1** were performed, in order to study the influence of the laser power on the morphology of the polymer. The time of irradiation was fixed to 10 seconds, so as to obtain well-structured tips, and the laser power P was set at 10 µW or 100 µW. Pictures are shown in Figure 2.9.

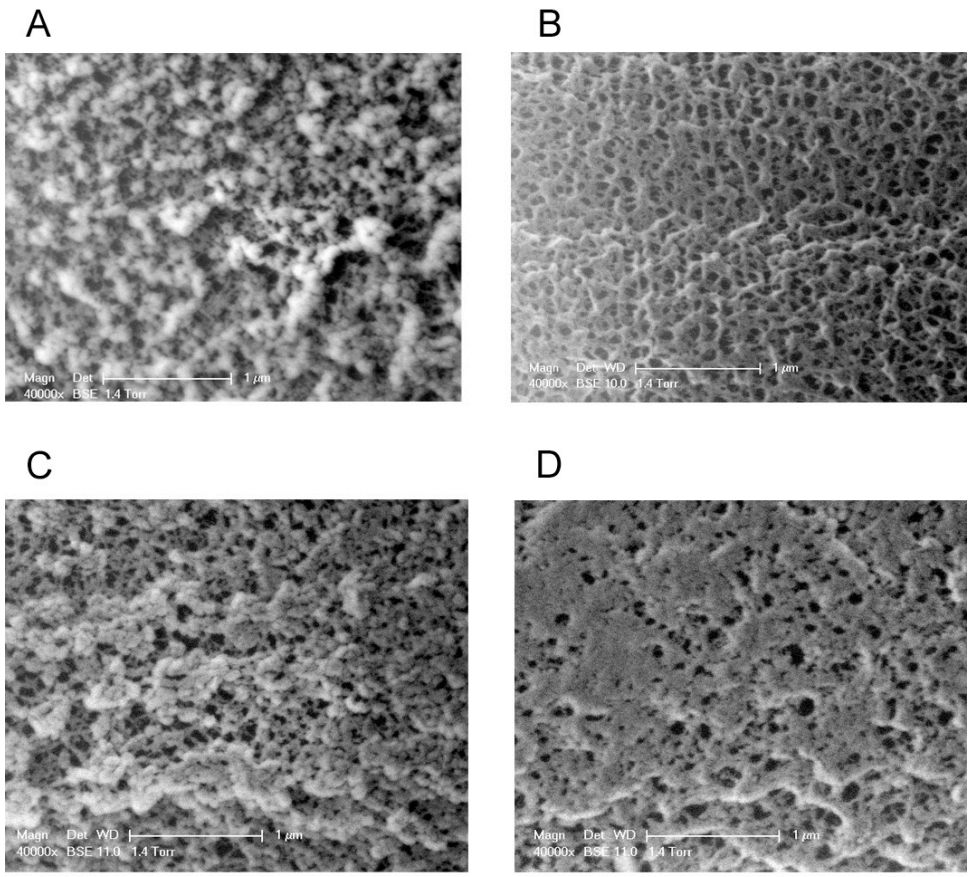

Figure 2.9. *Scanning electron micrographs of (A) MIP; P=100 µW (B) MIP; P=10 µW; (C) NIP; P=100 µW; (D) NIP; P=10 µW. The scale bar corresponds to 1 µm.*

A difference can be seen between the surface morphology of MIPs, depending on the laser power (10 or 100 µW), but most importantly, both structures were porous. With P=100 µW, agglomerates of polymer can be observed, whereas the surface looks less dense and more porous using P=10 µW. This can be explained by the fact that the polymerization was faster when a higher light intensity was used leading to less efficient phase separation between the solvent and the growing polymer (required for the formation of a porous morphology). A similar observation can be made when comparing the NIP polymerized at P=100 µW and the NIP polymerized at P=10 µW.

When comparing MIP and NIP for P=10 µW, it can be observed that the structure seems less porous and denser in the case of the NIP. Indeed the presence of template generally causes changes in the morphology of the polymer (pore size and shape, surface area, etc) (Kempe and Kempe, 2010) and the interactions between the template and the functional monomers can affect the growth of the polymer. In our case, the absence of template can favor dimerization of MAA molecules, which may explain the denser structure (Yoshimatsu et al., 2007). However, in the case of P=100 µW, the surface morphology of MIP and NIP were quite similar. Indeed using a higher light intensity led to a faster polymerization, and the presence of template has less impact on the polymer growth.

For sensor tip fabrication on the simple fiber, we selected the photonic conditions P=100 µW and $t_{irradiation}$=10 seconds because these conditions lead to polymers tips with large diameters that should potentially generate a high fluorescence signal. Furthermore, the structure of the tip seems

porous enough to perform efficient washing and to allow access to binding sites. This was verified by fluorescence measurements on a dansyl-L-Phe MIP tip using a mini-spectrometer (Figure 2.10).

III.1.4. Molecular recognition properties of the MIP microtip

The molecular recognition properties and the selectivity of the end-of-fiber MIP microtip were evaluated both by fluorescence microscopy and spectrofluorimetry using a high-resolution fiber optic spectrometer. Before validating the binding performance of the MIP microtip, two important features were checked beforehand. First, the efficiency of the washing was verified by measuring with the fiber-optic mini- spectrofluorimeter, the fluorescence signal of a tip of MIP dansyl-L-Phe after each washing step (i.e. 1 hour incubation in EtOH/AcOH (4/1)). We observed that the fluorescence intensity decreased considerably after the first and second step of washing (Figure 2.10). Three steps of washing were sufficient to elute a maximum of analyte, as the fluorescence signal did not decrease anymore after the third washing. However there was still some residual fluorescence due to entrapped dansyl-L-Phe that was impossible to remove. For this reason, the non-fluorescent template Z-L-Phe was preferred for imprinting, and dansyl-L-Phe was employed as a fluorescent analogue to study the binding behavior of the polymers.

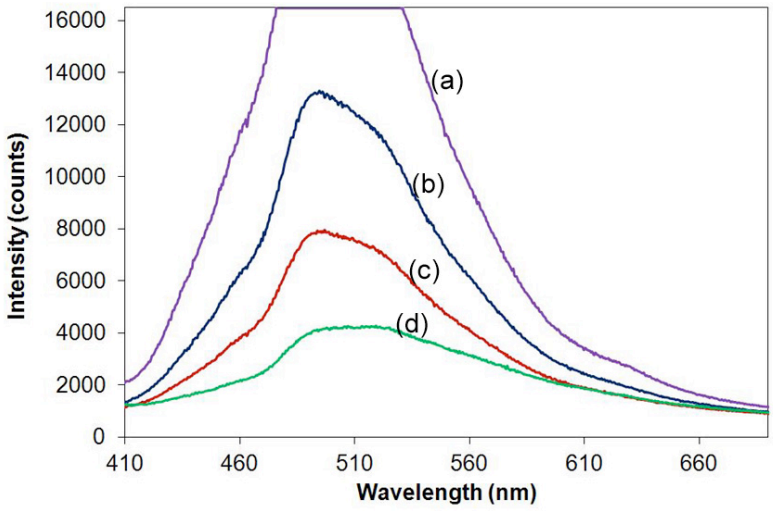

Figure 2.10. *Fluorescence intensity emitted by the MIP tip (formulation P1 with dansyl-L-Phe as template), measured with an Ocean Optics spectrometer (a) before washing (saturation of signal), and after (b) one washing step; (c) 2 washing steps and (d) 3 washing steps. One washing step corresponds to 1 hour incubation in a solution of EtOH/AcOH (4/1).*

Secondly, we checked with the fiber optic spectrometer that, after template removal, the MIP tip exhibited a linear fluorescence response when incubated with increasing concentrations of dansyl-L-Phe, in the range 1-10 µM in ACN, which is indeed the case (Figure 2.11). The limit of detection (LOD) was found to be 1 µM.

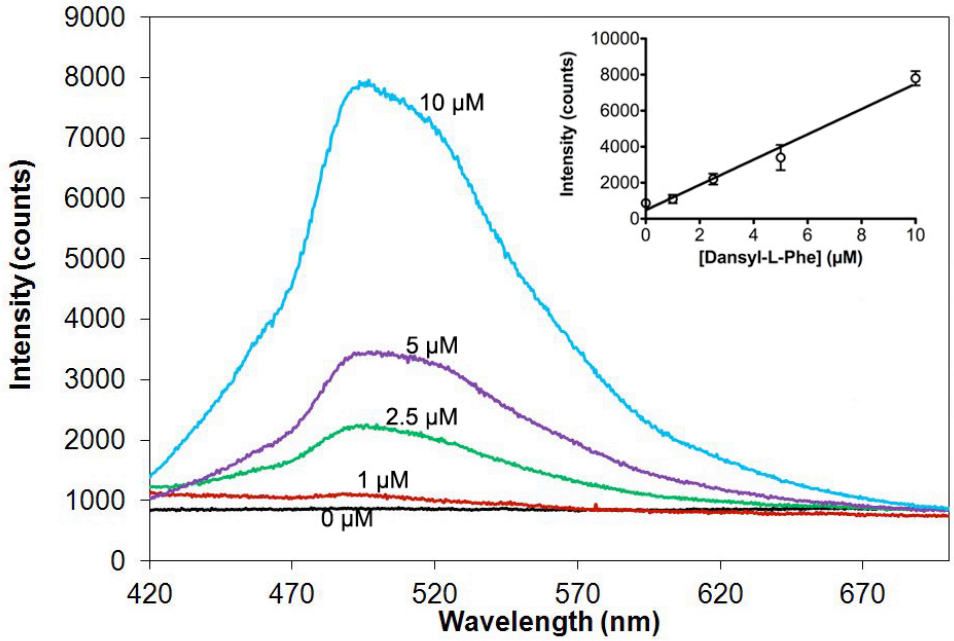

Figure 2.11. *Linearity of the fluorescence response of the MIP tip in the simple fiber setting, incubated with increasing concentrations of dansyl-L-Phe in the range 1-10 µM in anhydrous ACN, measured with an Ocean Optics spectrometer. Emission intensity measured at 495 nm.*

These verifications done, both MIP and NIP tips were incubated for 45 minutes in a solution of 10 µM dansyl-L-Phe in ACN. After rinsing with ethanol and drying, the fluorescence signal emitted from the tip was measured both by fluorescence microscopy (Figure 2.12A) and by spectrofluorimetry (Figure 2.12B). The MIP microtip bound more dansyl-L-Phe than the NIP, which confirms the specific binding (Figure 2.12B, curves (a) and (e), the imprinting factor being ca 3.5). This confirms the results from the bulk measurements in Figure 2.8.

In order to determine the selectivity of the MIP, the microtip was incubated in a solution of 10 µM of the enantiomer dansyl-D-Phe in ACN (Figure 2.12A and Figure 2.12B, curve (b)). Fluorescence microscopy and spectrometric measurements showed that the MIP bound the D-form ca 2.5 times less than the L-form, which demonstrates the enantiospecificity and thus the selectivity of the MIP. In addition, competitive binding experiments between the fluorescent probe dansyl-L-Phe and the imprinting template Z-L-Phe or its opposite enantiomer Z-D-Phe were performed in order to demonstrate that the sensor can detect the non-fluorescent target analyte. The sensor was incubated in a mixture of 10 µM Z-L-Phe and 10 µM dansyl-L-Phe (Figure 2.12A and Figure 2.12B, curve (c)). As expected, in the presence of Z-L-Phe, the MIP bound less dansyl-L-Phe than in its absence, which proves the validity of the competitive format. If 10 µM of the opposite enantiomer Z-D-Phe was used instead, the observed competition was less strong by a factor of 1.5 (Figure 2.12B, curve (d)), which reflects the selectivity of the MIP for the L-enantiomer, the original template.

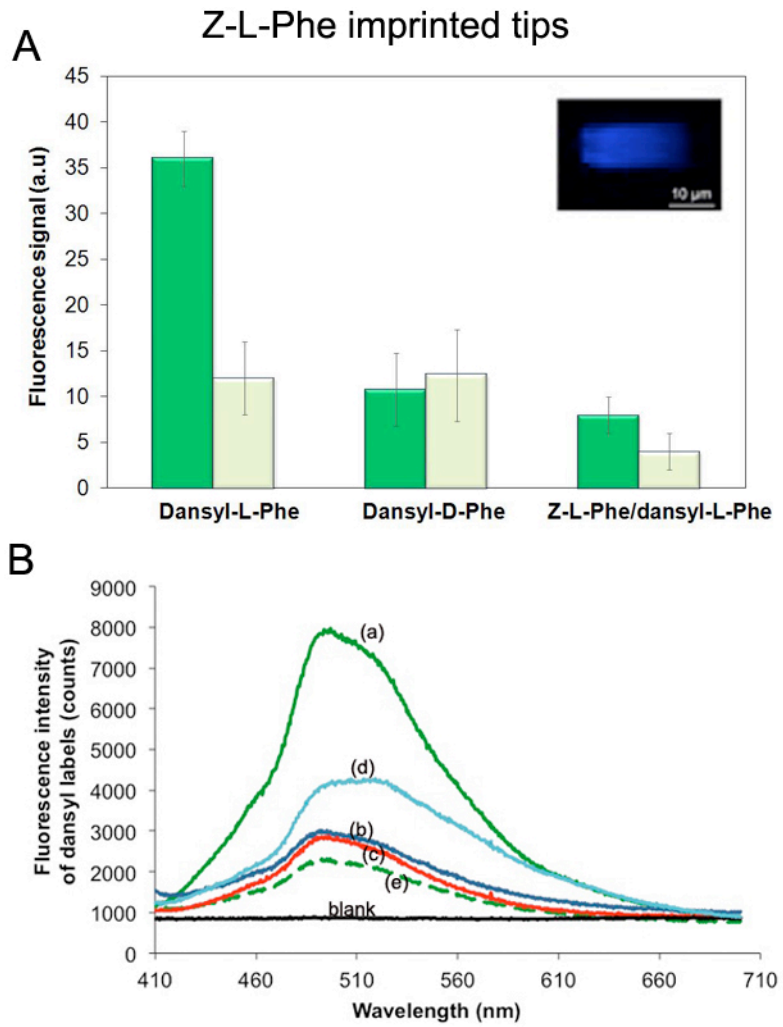

Figure 2.12. *(A) Normalized fluorescence signal of MIP (green bars) and NIP (white bars) microtips measured by fluorescence microscopy after incubation in 10 µM dansyl-L-Phe, 10 µM dansyl-D-Phe and a mixture of 10 µM dansyl-L-Phe and 10 µM Z-L-Phe, in ACN. Data are means of triplicate experiments. Inset: fluorescence microscopy image of the MIP microtip after incubation with dansyl-L-Phe (λ_{EX} = 360 nm; λ_{EM} = 470 nm).*
(B) Fluorescence spectra of Z-L-Phe-MIP microtips after incubation with (a) 10 µM dansyl-L-Phe, (b) 10 µM dansyl-D-Phe, (c) a mixture of 10 µM dansyl-L-Phe and 10 µM Z-L-Phe, (d) a mixture of 10 µM dansyl-L-Phe and 10 µM Z-D-Phe, in acetonitrile (ACN). (e) Fluorescence spectrum of the NIP microtip after incubation with 10 µM dansyl-L-Phe in ACN. Blank line: Z-L-Phe MIP microtip before incubation.

Additionally, binding experiments were performed in tetraglyme, the solvent of synthesis. Both MIP and NIP microtips were incubated with 10 µM dansyl-L-Phe in tetraglyme, and the resulting fluorescence signal was measured both by spectrometry and by fluorescence microscopy. Figure 2.13 shows that very little binding was observed compared to binding in ACN, which is consistent with the binding results obtained in tetraglyme with the bulk polymers. The high viscosity of tetraglyme probably affects the kinetics of the molecular recognition process. Given that polymerization was carried out on a lamp that probably heated the sample, it would be interesting to measure the temperature of the sample and perform the binding assays at the same temperature, in order to check if the results are better in this case. Indeed the binding assays were performed at room temperature (i.e. around 20°C), and the difference of temperature may have an influence on the molecular recognition process, as the viscosity of tetraglyme is dependent on the temperature.

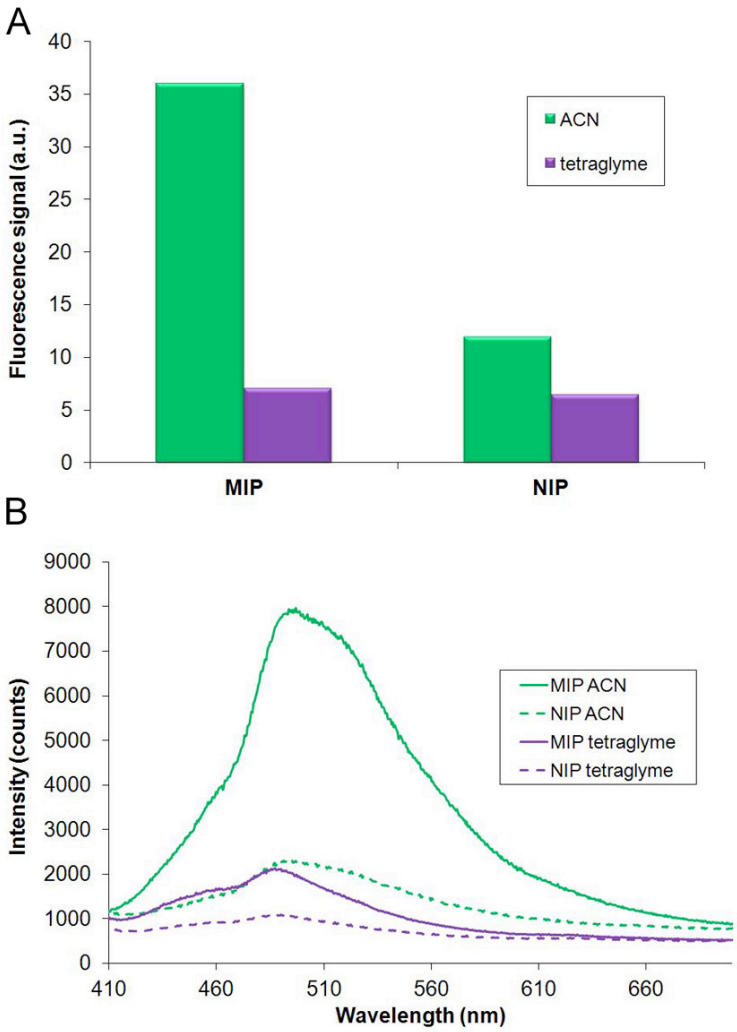

Figure 2.13. *(A) Normalized fluorescence signal of MIP and NIP microtips measured by fluorescence microscopy after incubation in 10 µM dansyl-L-Phe, in ACN (green bars) and in tetraglyme (violet bars) (B) Normalized fluorescence intensity measured by the Ocean Optics spectrofluorimeter of MIP (full lines) and NIP (dotted lines) microtips after incubation in 10 µM dansyl-L-Phe in ACN (green curves) and in tetraglyme (violet curves).*

III.1.5. Composite gold nanoparticle-MIP microtip for enhanced sensitivity

As mentioned above, the concentration-dependence of the MIP fluorescence signal was tested and the limit of detection (LOD) was found to be 1 µM (Figure 2.11). In order to lower the LOD, we attempted to use the plasmonic enhancement properties of noble metal nanoparticles in order to increase the fluorescence signal (Toma et al., 2011). Thus we incorporated commercial octanethiol-stabilized gold nanoparticles (10 nm diameter, dynamic light scattering, Figure 2.14) into the MIP precursors solution, resulting in a composite gold nanoparticle-MIP microtip (for formulation see Table 2.4).

			Diam. (nm)	% Intensity	Width (nm)
Z-Average (d.nm):	10,96	Peak 1:	12,36	97,3	4,996
PdI:	0,192	Peak 2:	4048	2,7	1065
Intercept:	0,744	Peak 3:	0,000	0,0	0,000
Result quality	Good				

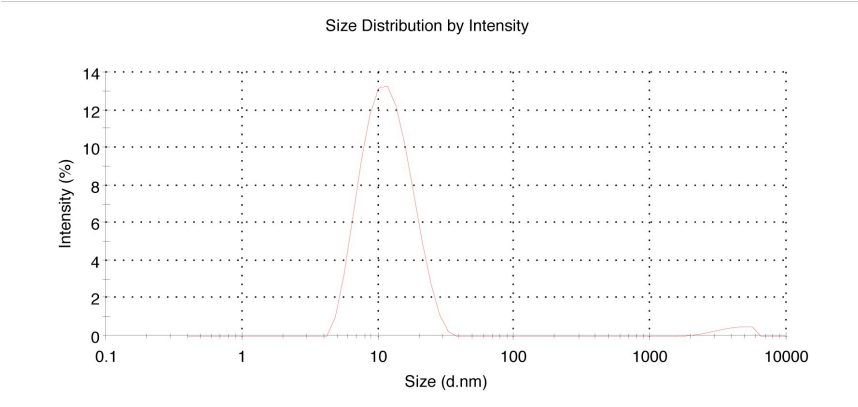

Figure 2.14. *Dynamic light scattering measurement of the solution of octanethiol-functionalized gold nanoparticles in toluene. Peak analyzes by intensity, volume and number all showed single, symmetrical peaks with a narrow distribution*

Table 2.4. *Formulations of the composite gold-MIP microtip* ***P1 Au****.*

Polymer	Template	Functional monomers	Cross-linker	Initiator	Solvent	Au NPs
P1 Au	Z-L-Phe (0.05 mmol)	MAA/4-VPY (0.2/0.2 mmol)	EDMA/PETIA (1.3/0.7 mmol)	Irgacure 819 (0.025 mmol)	Tetraglyme (230 μL)	0.6 mg

The effective incorporation of Au into the MIP was verified by energy dispersive X-ray spectroscopy (EDS), scanning electron microscopy (SEM) and transmission electron microscopy (TEM) (Figures 2.15, 2.16 and 2.17).

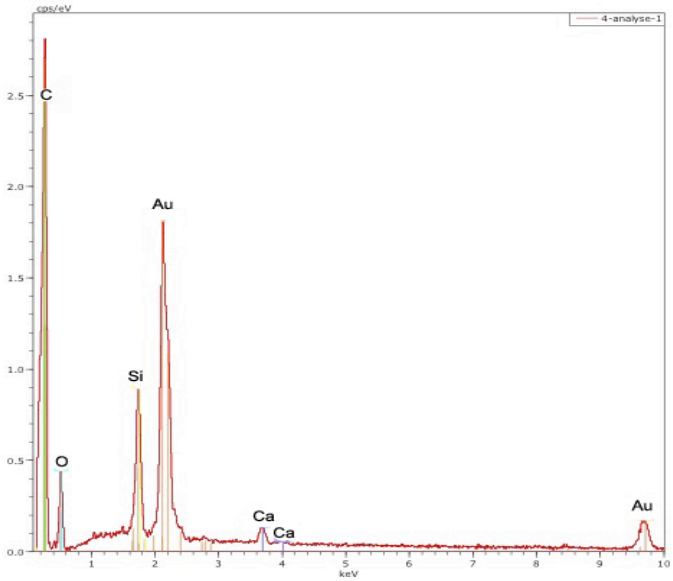

Figure 2.15*. Elemental analysis by Energy Dispersive X-ray Spectroscopy of the surface of the composite gold nanoparticle-MIP microtip.*

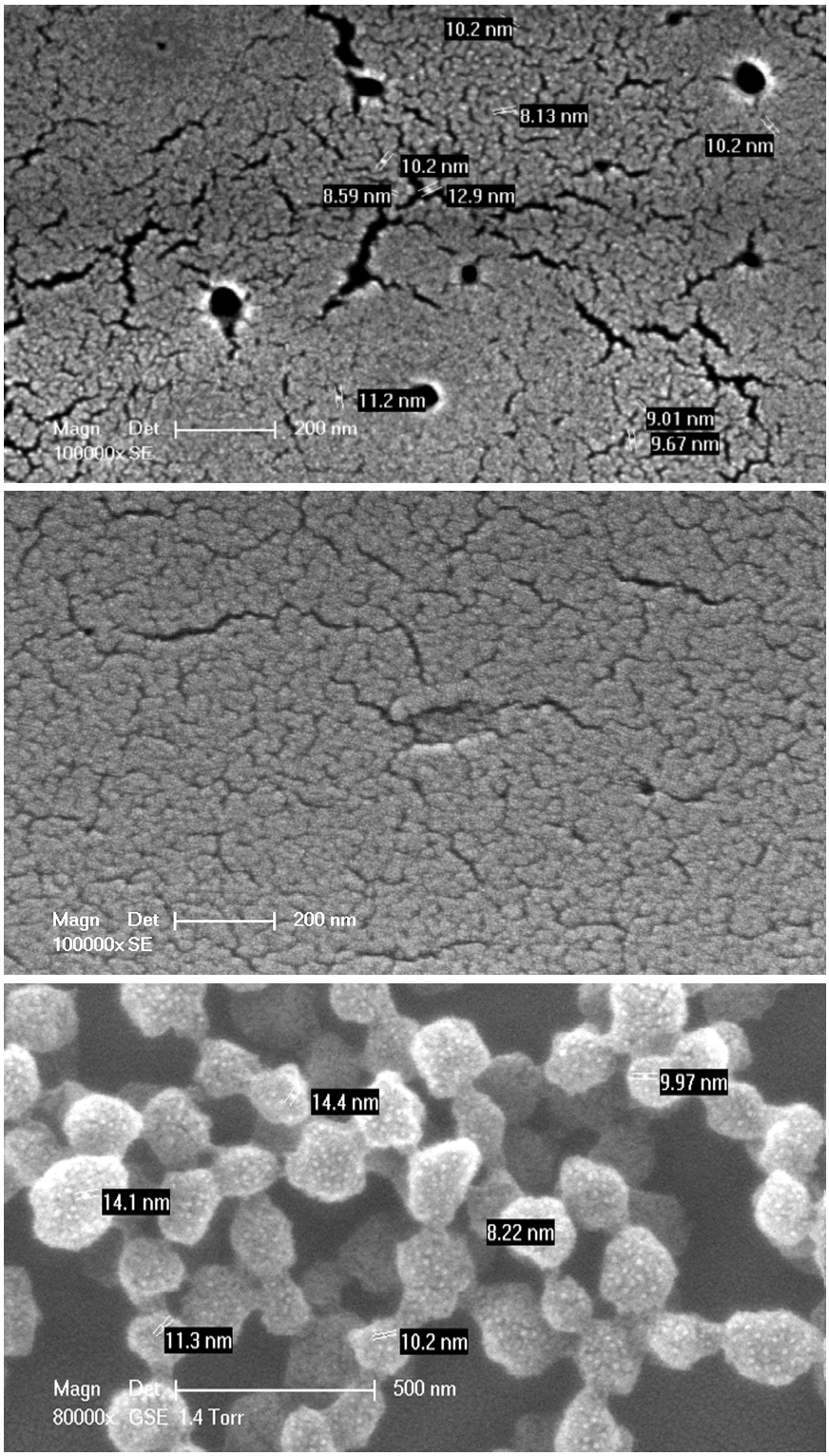

Figure 2.16. *Scanning electron micrographs of the surface of the composite gold nanoparticle-MIP (top), a MIP without gold particles (middle). Bottom image: To better visualize the incorporated gold nanoparticles, a MIP of the same composition as in the top image was synthesized by precipitation polymerization using a higher dilution of monomers.*

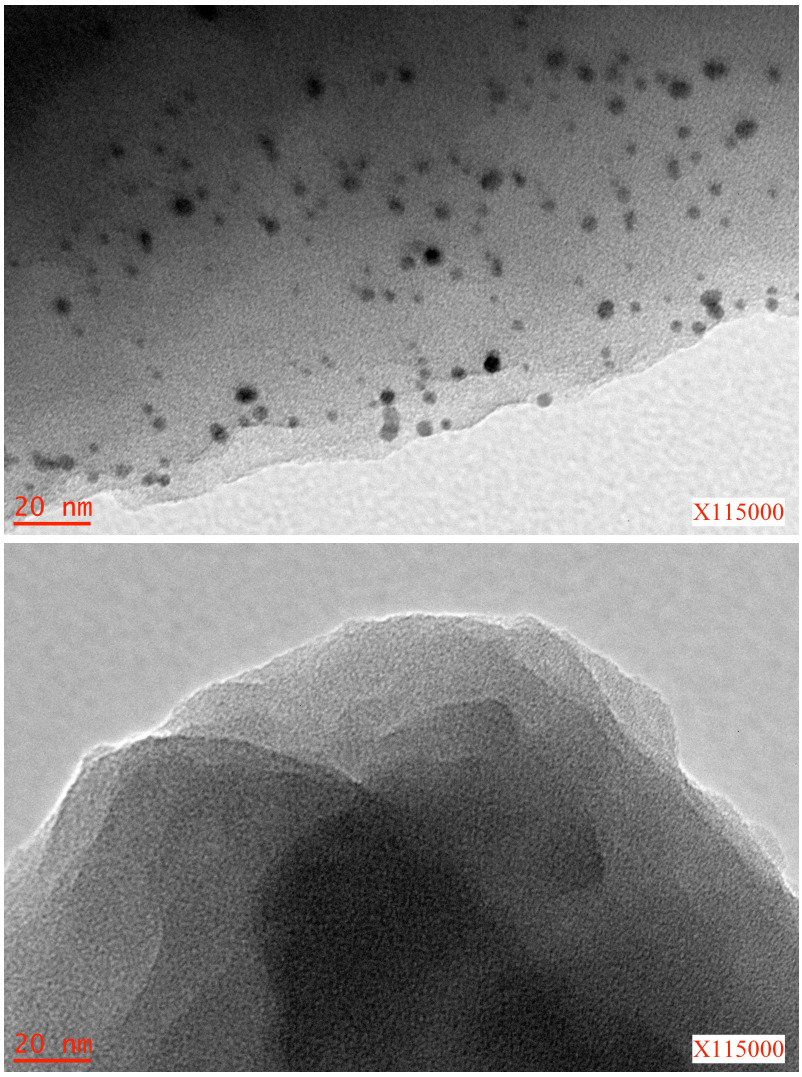

Figure 2.17. *Transmission electron micrographs of a composite gold-nanoparticle-MIP (top) and a MIP without gold particles (bottom). To better visualize the incorporated gold nanoparticles, MIPs of exactly the same composition as the microtips were synthesized as films of a few µm thickness by sandwiching between two glass plates. The surfaces of the films were slightly scraped with a micro-scalpel before imaging. Gold nanoparticles more or less deeply buried in the film can be distinguished in the top image.*

The presence of gold nanoparticles effectively led to an enhancement of the optical signal, increasing the sensitivity by a factor of 9 (slope of the calibration curve) and lowering the LOD by a factor of 20, from 1 µM to 50 nM (Figure 2.18). Note that gold nanoparticles alone do not contribute to any fluorescence signal. However in the presence of gold nanoparticles, a blue shift of 6 nm was observed in the emission peak of dansyl-L-Phe (Figure 2.18B). This may be explained by the fact that the presence of octanethiol-functionalized Au nanoparticles renders the polymer more hydrophobic, resulting in a blue shift of the fluorescence signal (Hill et al., 1996).

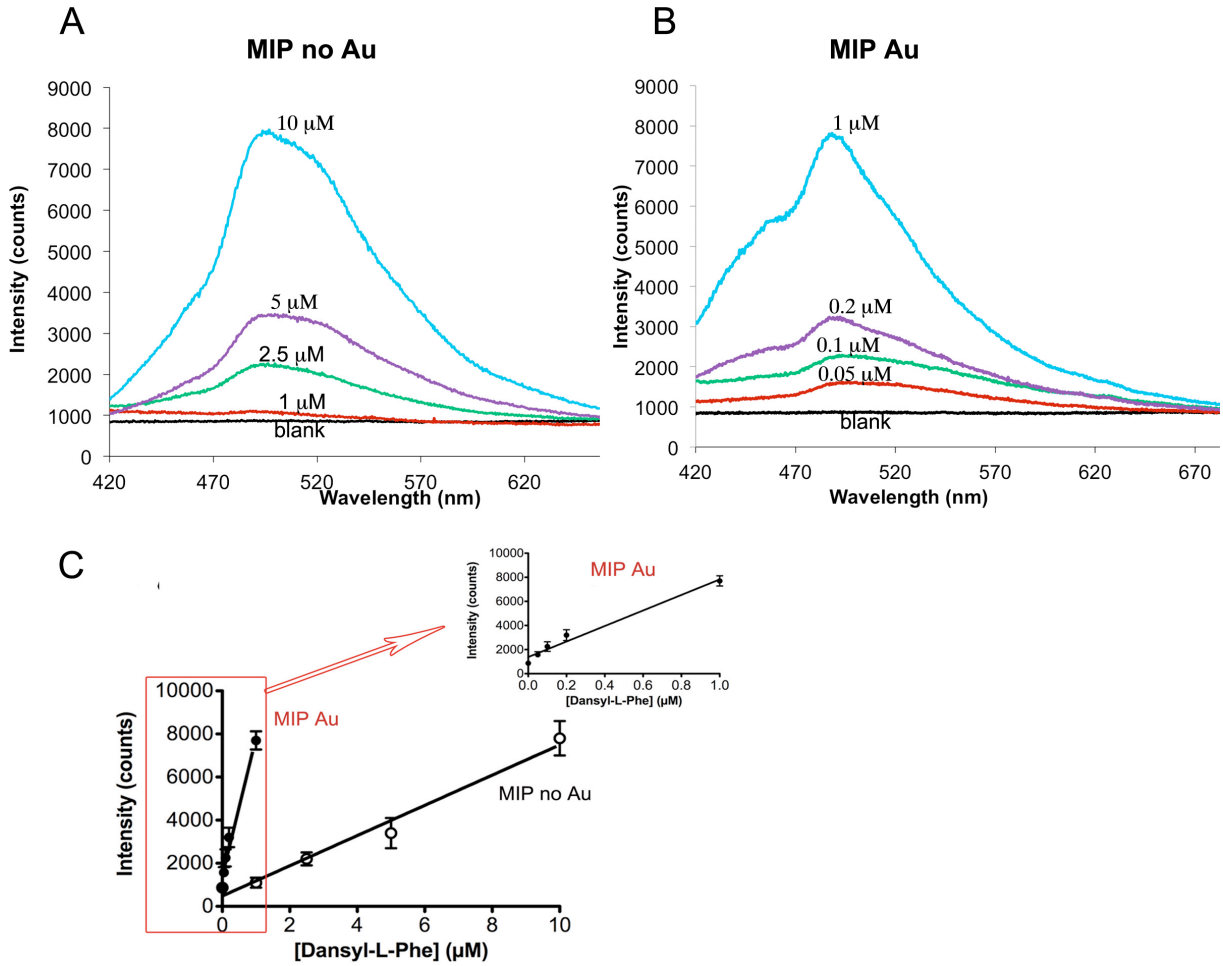

Figure 2.18. *Fluorescence responses of (A) the Z-L-Phe MIP tip* ***P1*** *without Au and (B) the composite gold nanoparticle-MIP tip, in the simple fiber setting, incubated with increasing concentrations of dansyl-L-Phe in the range (A) 1-10 µM or (B) 0.05 – 1 µM in ACN. The "blank" line corresponds to the Z-L-Phe MIP tip before incubation. Emission signal measured with an Ocean Optics spectrometer. (C) Calibration curves of the fluorescence responses of the Z-L-Phe MIP tip without gold ("MIP no Au",* λ_{EM}*=495 nm) and the composite gold-MIP tip ("MIP Au",* λ_{EM}*=489 nm) after incubation with increasing concentrations of dansyl-L-Phe in ACN. Integration time: 100 ms.*

We wanted to investigate more about the mechanism of fluorescence enhancement and in particular, to clarify if if plasmonic enhancement is effectively taking place. The process of plasmonic fluorescence enhancement can be explained as follows (Lakowicz, 2001; Stranik et al., 2005): the interaction of the incident light with metallic NPs results in an increased electromagnetic field around the metal NPs, which act as antenna. Therefore, the fluorescence properties of a fluorophore in proximity of the metal NPs are modified, and can result in an enhancement of the fluorescence emission. There are two mechanisms for the enhancement effect:

- the excitation of the fluorophore is increased, resulting in an increase of the emission intensity. The maximum enhancement of this type is achieved if the wavelength of resonance of the metal NPs λ_{RES} equals the excitation wavelength λ_{EX} of the fluorophore.
- a new radiative channel is formed, which means that there is a supplementary radiative decay rate (which is related to the process of photon emission when the excited electron goes back to its ground state). Therefore the fluorescence lifetime is shorter while the emission intensity is higher.

The maximum enhancement of this type is achieved if λ_{RES} equals the peak emission wavelength λ_{EM} of the fluorophore.

In our case, the Au NPs we use absorb at 530 nm and the fluorophore dansyl-L-Phe is excited at 375 nm and emits at around 500 nm, so if plasmonic enhancement is taking place, the second mechanism should be involved. Therefore two bulk MIPs of the exact same composition of **P1** (without Au) and **P1 Au** (with Au), but with dansyl-L-Phe as template, were synthesized, and their fluorescence lifetimes were measured (Table 2.5). For reference, the fluorescence lifetime of dansyl-L-Phe (10 μM in ACN) was measured to be τ=12.41 ns (χ^2=1.06). For all measurements, the fluorescence lifetime of the bulk MIP-Au was always lower (average 12.39 ns) compared to the bulk MIP without Au (average 12.55 ns), which means that when Au NPs were incorporated into the MIP, the average lifetime was shortened by 0.16 ns (Table 2.6). Even if this difference in lifetime is very small, this result may indicate a plasmonic fluorescence enhancement. For example, in comparison, the group of Lakowicz has studied silver-gold nanocomposite substrates for metal-enhanced fluorescence, and has observed that on the silver-gold nanocomposite substrate, the fluorescence lifetime of their fluorophore was shortened by 0.34 ns (from 0.5 ns on glass to 0.16 ns on the bimetallic substrate). Therefore the authors concluded to a fluorophore-plasmon coupling effect (Dutta Choudhury et al., 2012). In our case, the difference is less significant compared to the initial fluorescence lifetime of 12.55 ns, even if in presence of Au NPs, the fluorescence lifetime is always shorter (Table 2.5). It is possible that the reduction of lifetime is very small because in the composite bulk gold nanoparticle-MIP, the relative amount of dansyl-L-Phe that is in contact with gold is very small compared to the amount of dansyl-L-Phe that is not.

Table 2.5. *Fluorescence lifetimes and least-squares fitting of the fluorescence decays using a one-exponential decay law of the dansyl-L-Phe bulk MIPs **P1** and **P1 Au** (0.2 mg/mL and 0.5 mg/mL in ACN). One line corresponds to one set of measurement performed at the same time.*

[MIP] (mg/mL)	P1 (no Au) τ (ns)	P1 (no Au) χ^2	P1 Au τ (ns)	P1 Au χ^2
0.5 – mes. 1	**12.64**	1.04	**12.26**	1.21
0.5 – mes. 2	**12.51**	1.18	**12.35**	1.12
0.5 – mes. 3	**12.53**	1.06	**12.43**	1.17
0.2 – mes. 1	**12.53**	1.09	**12.42**	1.14
0.2 – mes. 2	**12.53**	1.06	**12.43**	1.17
0.2 – mes. 3	**12.56**	1.11	**12.45**	1.15

Table 2.6. *Average lifetimes and standard deviations of dansyl-L-Phe bulk MIPs **P1** and **P1 Au**, calculated from the lifetimes values presented in Table 5.*

	P1 (no Au)	P1 Au
Mean τ (ns)	12.55	12.39
Standard deviation (ns)	0.05	0.07

To summarize, the lifetime measurements seem to indicate that plasmonic enhancement is effectively taking place, even if we cannot say it with certainty, so this hypothesis need further investigation. Nonetheless, this is to the best of our knowledge the first description of MIP sensors using metal-enhanced fluorescence intensity measurements. We cannot exclude, though, that a more efficient collection of fluorescent light due to scattering by the gold nanoparticles back into the fiber contributes to the observed effect.

III.1.6. A core-shell format of the MIP microtip for a better response time

Another important feature for a sensor is the response time. The response time of this sensor was 45 minutes, which is due to analyte diffusion into the tip. The response time could be shortened by using a core-shell format of the tip that results in shorter diffusion distances. We synthesized a non-porous core tip of poly(PETIA) covered by a 0.7 μm layer of Z-L-Phe MIP through re-initiation with the MIP precursors. The fluorescence image (Figure 2.19, inset) is very different from that of a plain tip (Figure 2.12A, inset) and clearly shows the core-shell structure. Kinetics data of the response of the "core-shell" MIP tip incubated with 10 μM dansyl-L-Phe in ACN is shown in Figure 2.19. As a result, binding of dansyl-L-Phe could be detected after only 2 minutes, and around 80% of the total signal response occurred within 4 minutes. The core-shell MIP tip took around 10 minutes to reach equilibrium (>95%). Hence, by reducing the MIP thickness, the response time was successfully lowered from 45 minutes to 10 minutes. The reversibility of the sensor response was also demonstrated by measuring successively different concentrations of dansyl-L-Phe (Figure 2.19), which indicates that fluorescent analytes could be measured in close to real-time and without intermittent regeneration (although this is not possible in the competitive format).

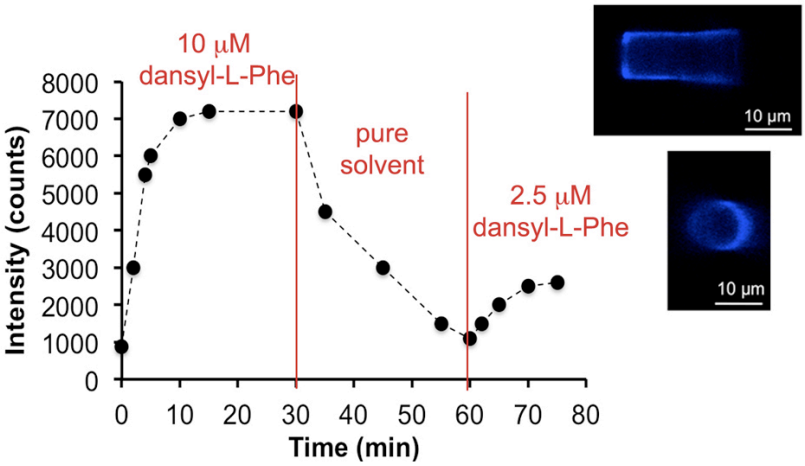

Figure 2.19. *Kinetics of the fluorescence response of the core-shell Z-L-Phe MIP tip incubated with dansyl-L-Phe. Inset: confocal fluorescence images of the core-shell MIP tip after incubation.*

III.1.7. An intrinsically fluorescent MIP fiber optic probe based on a fluorescent monomer

In order to avoid the addition of a fluorescent probe as in the competitive format and to broaden the sensor's applicability, we incorporated fluorescent reporter groups into the MIP, a concept that has been developed by Takeuchi (Matsui et al., 1998; Kubo et al., 2003; Takeuchi et al., 2005). Our objective here was to apply our sensor to non-fluorescent analytes of interests. In this part of our work, we chose as target analytes the herbicide 2,4-D and the mycotoxin citrinin. In the whole study involving the fluorescent signaling monomer, the MIP microtip was synthesized in the **core-shell** format (i.e. a non-porous poly(PETIA) core covered by a thin layer of MIP). The core-shell format has the advantage that it allows the use of any MIP formulation, even with a very low viscosity. A viscous MIP formulation was required for the photostructuring of a rigid microtip; and in the case of the core-shell microtip, this condition is already met by the poly(PETIA) core. For the deposition of the layer of

MIP on the polymer core, a less viscous formulation can be used, which is convenient as it broadens the choice of solvents and cross-linkers.

III.1.7.1. Sensing of the herbicide 2,4-D

The herbicide 2,4-D, our model analyte, is widely used and represents a threat for health due to its endocrine disruption properties. For imprinting and detecting 2,4-D, a fluorescent functional monomer based on a piperazinyl naphthalimide derivative was synthesized (FIM). FIM exhibits fluorescence amplification due to the protonation of the piperazinyl residue upon interaction with carboxyl groups (Niu et al., 2004), here 2,4-D (pK_a = 5.09, methanol/water=4/1), which was verified through fluorescence titration experiments (Figure 2.20). The mechanism of enhancement can be explained as follows: the protonation of the methyl-substituted nitrogen atom on the piperazine ring suppresses the intramolecular photoinduced electron transfer *quenching* effect, resulting in a revival of the fluorescence of the naphthalimide moiety. As a result, the fluorescence enhancement of FIM was observed to be concentration-dependent and increased with increasing concentrations of 2,4-D, confirming that FIM could be used as a functional monomer to imprint 2,4-D. The maximum excitation wavelength of FIM was found to be 390 nm, and its emission wavelength 515 nm, which is perfectly suitable for our optical sensing applications. Indeed, the Stokes shift is large and at these wavelengths, the fluorescence background is reduced.

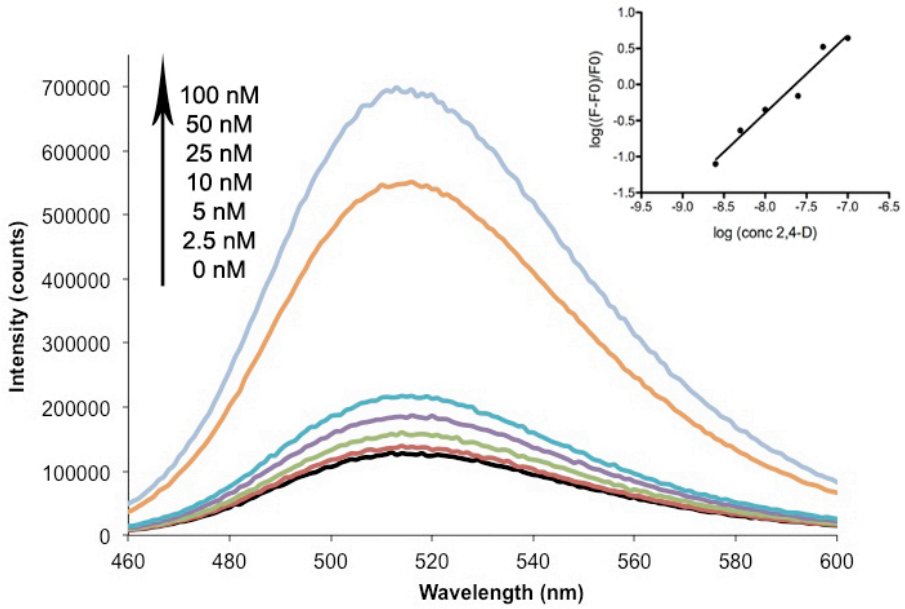

Figure 2.20. *Fluorescence titration studies of the fluorescent monomer FIM (50 μM) with increasing concentrations of 2,4-D (2.5-100 nM) in methanol/water (4/1) (λ_{EX}=390 nm). Fluorescence spectra were recorded using a Jobin-Yvon Horiba Fluorolog fluorescence spectrophotometer.*

We should add that very recently, a MIP containing a naphthalimide for sensing purposes has been reported by others. The naphthalimide monomer was different, though, as it was a urea derivative, and used fluorescence quenching for detection, resulting in sensitivity in the mM range (Wagner et al., 2013). Another fluorescent MIP that showed fluorescence enhancement upon binding was also developed very recently. The fluorescent monomer was a urea derivative that could bind carboxylates, and contained a nitrobenzoxadiazole fluorophore moiety. The MIP was synthesized

under the format of core-shell microparticles, consisting in a silica core and a MIP shell, and was applied for the detection of Z-L-Phe, resuting in sensitivity in the μM range (Wan et al., 2013).

FIM was then incorporated into a 2,4-D MIP formulation, adapted from Haupt et al., 1998, where it replaces partially the monomer 4-vinylpyridine. The MIP was first synthesized as micro- and nanoparticles by precipitation polymerization (formulation **P3**, Table 2.7). Similarly, the binding properties of the MIP were evaluated with spectrofluorimetric titrations of the MIP with 2,4-D, confirming the molecular recognition properties of the fluorescent 2,4-D imprinted polymer (Figure 2.21).

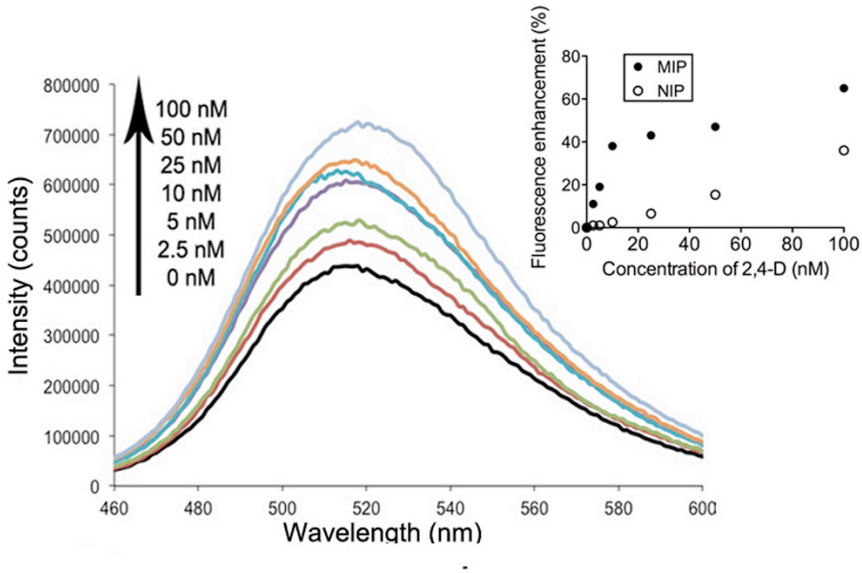

Figure 2.21. *Fluorescence spectral responses of the MIP **P3** (5 μg/mL) with increasing concentrations of 2,4-D (2.5-100 nM) in methanol/water (4/1) (λ_{EXC}=390 nm). Inset: Fluorescence signals of MIP and NIP **P3** in response to 2,4-D. Fluorescence spectra were recorded using a Jobin-Yvon Horiba Fluorolog fluorescence spectrophotometer.*

After we verified the process of fluorescence enhancement upon binding with the batch of MIP particles, the MIP was synthesized at the end of an optical fiber, using the core-shell format (**P2**, Table 2.7). The specific recognition properties were demonstrated by incubating both MIP and NIP microtips with increasing concentrations of 2,4-D. The fluorescence response of the MIP was concentration-dependent, with again a LOD of 2.5 nM, and the MIP yielded a higher signal than the NIP (Figure 2.22A). For instance, when incubated with 2.5 nM 2,4-D, the MIP tip increased in fluorescence by around 20%, while the NIP intensity increased by only 5% (Figure 2.22B).

Table 2.7. *Formulations of the fluorescent MIPs for the recognition of 2,4-D.*

Polymer	Template	Functional monomers	Cross-linker	Initiator	Solvent
P2	2,4-D (0.02 mmol)	FIM/4-VPY (0.04/0.04 mmol)	EDMA (0.4 mmol)	Irgacure 819 (0.008 mmol)	Methanol/water (4/1) (1 mL)
P3	2,4-D (0.025 mmol)	FIM/4-VPY (0.05/0.05 mmol)	EDMA (0.5 mmol)	ABDV (0.016 mmol)	Methanol/water (4/1) (3 mL)

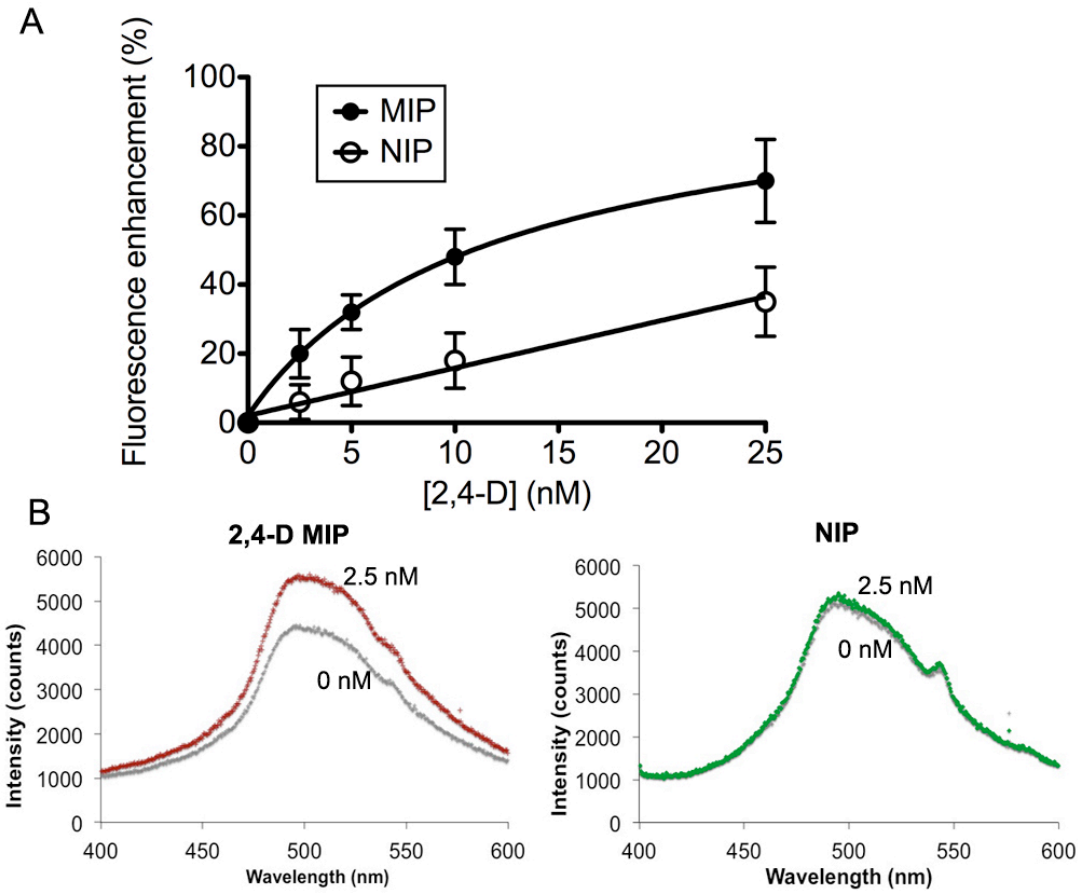

Figure 2.22. *(A) Fluorescence responses of MIP and NIP microtips* ***P2*** *after incubation with increasing concentrations of 2,4-D in methanol/water (4/1). Spectrometer integration time: 600 ms. (B) Fluorescence spectra of MIP and NIP microtips* ***P2*** *before incubation (0 nM) and after incubation with 2.5 nM 2,4-D in methanol/water (4/1). Spectrometer integration time: 600 ms.*

The 2,4-D MIP tip **P2** attained a stable response within 5 minutes of incubation. The dynamic response and reversibility of the MIP-based sensor were also demonstrated by consecutively measuring various concentrations of 2,4-D (Figure 2.23).

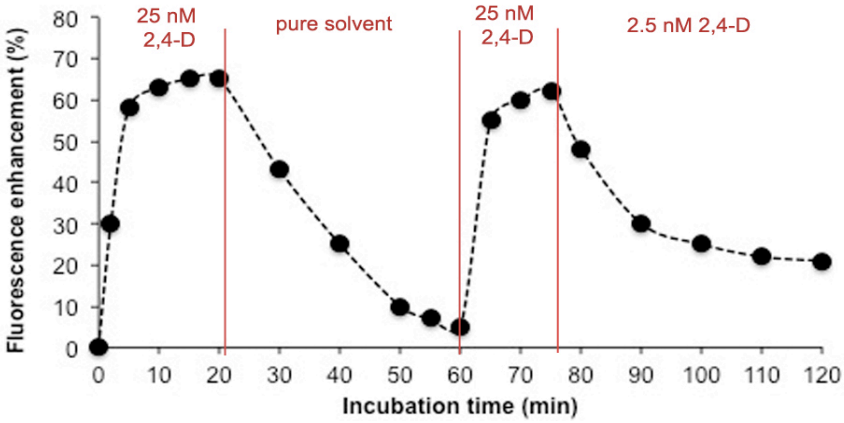

Figure 2.23. *Dynamic fluorescence response of the 2,4-D MIP tip* ***P2*** *when incubated consecutively with various concentrations of solutions of 2,4-D in methanol/water (4/1).*

The MIP's selectivity was evaluated by measuring the responses to two structurally related compounds, 2,4-dichlorophenoxyacetic acid methyl ester (2,4-D-OMe), the carboxyl group of which is blocked, and phenoxyacetic acid (POAc, pK_a=5.17, methanol/water 4/1), lacking the ring chlorines (see Table 2.1 for the structures of 2,4-D-OMe and POAc). As a result, a smaller fluorescence enhancement for POAc and no enhancement for 2,4-D-OMe were observed, hence confirming the selectivity of the MIP for 2,4-D (Figure 2.24).

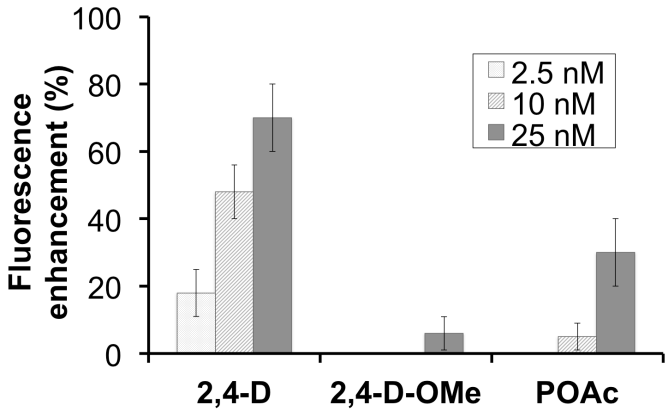

Figure 2.24. *Fluorescence signal of the 2,4-D MIP microtip* ***P2*** *after incubation with 2,4-D or the analogues 2,4-D-OMe or POAc in methanol/water (4/1).*

To further increase the sensitivity of our sensor, we again incorporated gold nanoparticles into the MIP formulation (**P2-Au**, Table 2.8), which led to a stronger fluorescence enhancement upon binding, lowering the LOD to 0.25 nM (Figure 2.25). This is lower than the more restrictive limit concentration for pesticides in drinking water set by the European Union (0.1 μg/L, i.e. 0.45 nM). In fact, the sensitivity of our sensor is comparable to that obtained with liquid chromatography/mass spectrometry for 2,4-D detection.

Table 2.8. *Formulation of the composite gold-2,4-D MIP microtip.*

Polymer	Template	Functional monomers	Cross-linker	Initiator	Solvent	Au NPs
P2-Au	2,4-D (0.02 mmol)	FIM/4-VPY (0.04/0.04 mmol)	EDMA (0.4 mmol)	Irgacure 819 (0.008 mmol)	Methanol/water (4/1) (1 mL)	3.6 mg

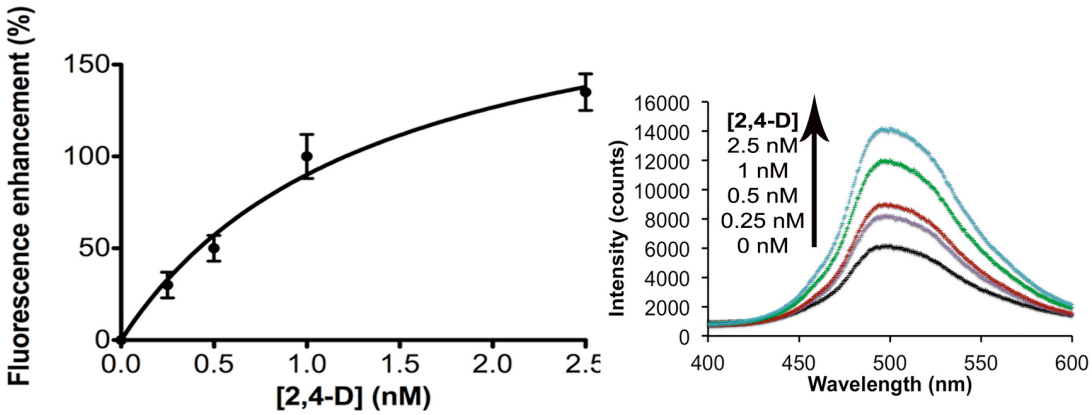

Figure 2.25*. Fluorescence signal of the composite gold-MIP* ***P2-Au*** *microtip after incubation with increasing concentrations of 2,4-D in methanol/water (4/1). Integration time: 50 ms. Experiments were*

performed in triplicate, errors bars represent standard deviations. The blank signal (tip before incubation) was recorded before each set of experiments.

III.1.7.2. Sensing of the mycotoxin citrinin

We then fabricated a MIP-based sensor for the monitoring of citrinin, an equally important analyte. Citrinin is a nephrotoxic mycotoxin produced by the fungi *Penicillium citrinum* that can be found in crops (especially red rice), vegetables and fruits. As red mold rice is widely used in Asia as natural food colorant or flavor, a maximum residue limit (MRL) for citrinin was set in China at 50 μg/kg in dry functional red kojic rice.

The formulation of the citrinin-imprinted polymer **P4** is detailed in Table 2.9. As with the 2,4-D imprinted fluorescent polymer, we used both the fluorescent monomer FIM and 4-VPY as co-functional monomers that are expected to interact with the carboxyl group of citrinin.

Table 2.9. *Formulation of the citrinin-imprinted polymer microtip.*

Polymer	Template	Functional monomers	Cross-linker	Initiator	Solvent
P4	Citrinin (0.02 mmol)	FIM/4-VPY (0.04/0.04 mmol)	EDMA (0.4 mmol)	Irgacure 819 (0.008 mmol)	Methanol (1.2 mL)

The specificity of the fluorescence enhancement process was first verified by incubating 15 minutes both MIP and NIP microtips in a solution of 10 ng/mL citrinin in methanol. Citrinin is a fluorescent compound (λ_{EX}=330 nm; λ_{EM}=500 nm); however we checked that at the concentrations we use (in the order of magnitude of the ng/mL), no fluorescence from citrinin could be detected. Indeed methanol and water have a quenching effect on the fluorescence of citrinin (Zhou et al., 2012). Thus the measured fluorescence signal was exclusively emitted by the monomer FIM. As a result, the MIP demonstrated 70% of fluorescence enhancement while the NIP showed 13% of fluorescence enhancement in response to 10 ng/mL citrinin, which confirms the specificity of our sensor (Figure 2.26).

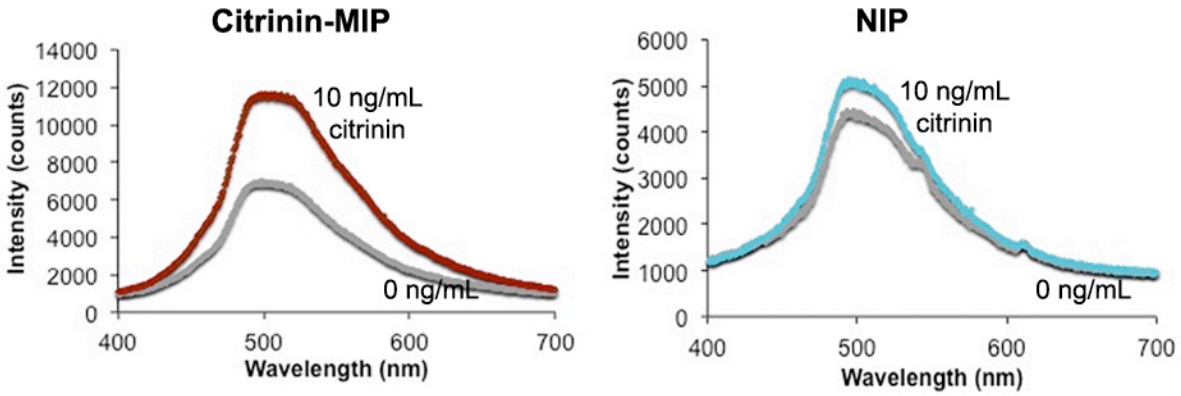

Figure 2.26. *Fluorescence spectra of MIP (left) and NIP (right) microtips before and after incubation with 10 ng/mL citrinin in MeOH (λ_{EX}=375 nm).*

The calibration of our sensor was performed by measuring the concentration-dependence of the fluorescence response of the citrinin-imprinted polymer (Figure 2.27).

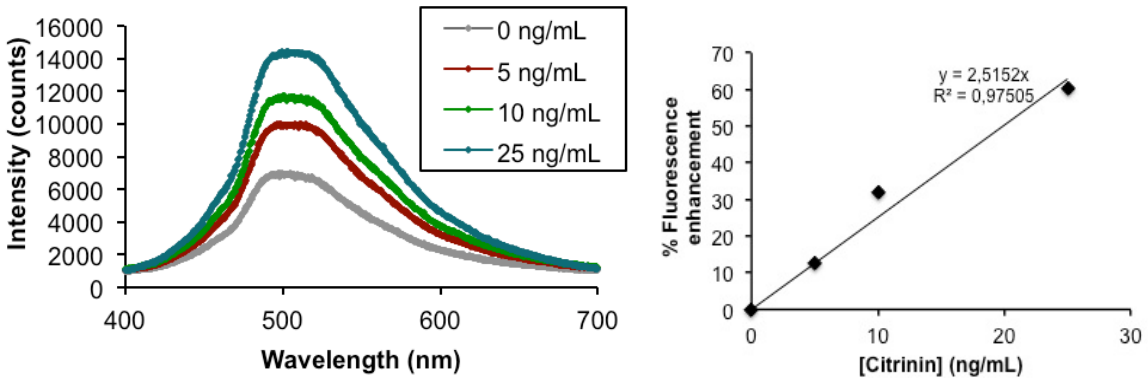

Figure 2.27. *(Left) Fluorescence spectra changes and (right) the corresponding calibration curve of the fluorescence response of the citrinin MIP microtip after incubation with 5 – 10 – 25 ng/mL citrinin in MeOH (λ_{EX}=375 nm).*

In order to confirm the specific character of the fluorescence enhancement, the MIP microtip was also incubated with 10 ng/mL 2,4-D (i.e. ≈ 45 nM) and 10 ng/mL Z-L-Phe (i.e. ≈ 33 nM), compared to 10 ng/mL citrinin (≈ 40 nM). These two compounds also possess carboxylic acid groups but present a very different structure from citrinin. As a result (Figure 2.28), no fluorescence enhancement was observed, which confirms the selectivity of our MIP.

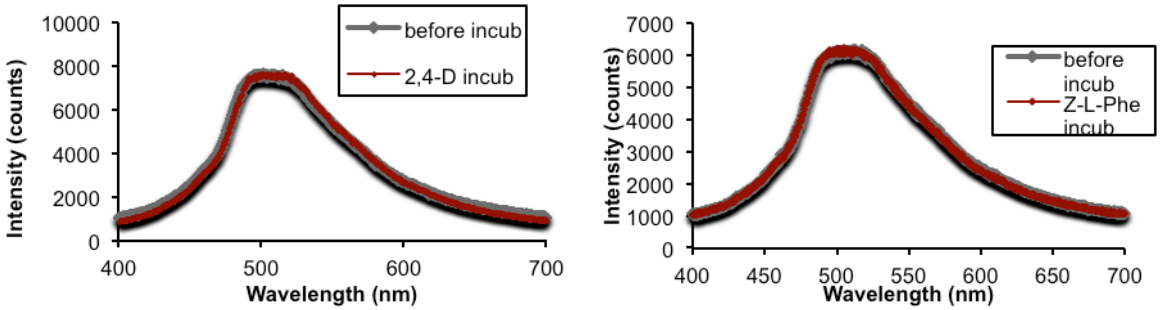

Figure 2.28*. Fluorescence emission spectra of the citrinin-imprinted microtip before and after incubation with 10 ng/mL 2,4-D (left) and 10 ng/mL Z-L-Phe (right) in MeOH (λ_{EX}=375 nm).*

III.1.8. Conclusions

We have developed a fluorescence-based optical fiber sensor using *in-situ* polymerized MIP microstructures as the recognition element. To establish the proof of concept we have initially used a simple single-mode optical fiber, which is the easiest to set-up. Photonic and physico-chemical parameters were optimized in order to tailor the photostructuring and molecular recognition properties of the MIP microtips. MIP tips imprinted with Z-L-Phe demonstrated specific binding towards the fluorescent derivative dansyl-L-Phe, as well as selectivity between the L- and D- forms of the fluorescent analogue dansyl-phenylalanine. The sensitivity of the sensors was then improved by using gold nanoparticles embedded in the MIP, to enhance the fluorescence signal. The LOD was successfully lowered from the μM to the nM range. By using a core-shell format of the microtip, we obtained a faster response time. Finally, our sensor was applied for the detection of analytes of interest, namely, the herbicide 2,4-D and the mycotoxin citrinin, which do not need to be fluorescent thanks to the incorporation of a fluorescent signaling functional monomer into the MIP. To conclude, the concept of the MIP-based fiber-optic sensor with fluorescence detection was successfully

demonstrated with the simple fiber sensor. This set-up can for example be integrated in a microfluidic sensor chip. However, it would also be interesting to be able to read the signal at a long distance from the point of measurements, which is not possible with the simple fiber set-up. For this reason, we developed another set-up based on a Y-shaped bifurcated fiber, which allows long-distance and real-time monitoring.

III.2. The bifurcated SMF set-up (telecom fiber)

III.2.1. Molecular recognition properties of the MIP microtip

In the previous set-up, the binding properties of the MIP were evaluated by collecting externally the emitted fluorescence signal from the tip. Using a bifurcated fiber would allow to measure a signal based on fluorescent light emitted back into the optical fiber, thus making possible long-distance measurements coupled to real-time detection (Figure 2.1B). An additional benefit of this configuration is that measurements in solution are now easier, since unlike in the simple fiber configuration, the emitted light does not travel through the sample on its way to the detector. For this configuration, the previous fluorescent detection system was replaced by a more sensitive spectrometer (Witec alpha 300 SR microscopy system) because the signal collected by the optical fiber was low due to the small diameter of the fiber and isotropic fluorescence light emission.

This time, the light intensity at the extremity of the common part of the fiber was fixed at 10 µW, for the synthesis of MIP microtips. Indeed, P=10 µW irradiation gave rise to a highly porous structure favoring the access to binding sites. In this set-up, during sensing experiments the measured response corresponds to the emitted light passing through the other arm of the fiber. One should note that in the previous configuration, we chose 100 µW as a large tip diameter was needed in order to collect externally the signal.

We again used the model template Z-L-Phe for optimization. Just as with the simple fiber, we checked that the MIP fluorescence signal was linear in response to incubation with dansyl-L-Phe in ACN. The specificity of the molecular recognition was also investigated by incubating both MIP and NIP microtips in a solution of dansyl-L-Phe in ACN. As can be seen in Figure 2.29 (left), the MIP bound around 2.5 to 3 times more dansyl-L-Phe than the NIP, which confirms the specific binding. During the fluorimetric measurements, the MIP tip remained into the analyte solution. No difference of signal was observed when the solution was removed, which shows that the measured signal corresponds to the analyte specifically bound to the MIP. The possibility of leaving the tip in the analyte solution is a strong advantage for further potential use in sensing applications, as it opens the possibility for real-time measurements in complex media. However, the LOD with this set-up was of 5 µM dansyl-L-Phe, which is higher than the LOD of the simple fiber set-up (1 µM). The sensitivity of the sensor was decreased, which is due to the fact that we collect only the small portion of light that is re-emitted through the fiber. To determine the MIP's selectivity, the tip was incubated with the enantiomer dansyl-D-Phe. As shown in Figure 2.29 (right), the MIP tip was able to discriminate between the enantiomers dansyl-L-Phe and dansyl-D-Phe, as it bound the L-form nearly twice as much as the D-form.

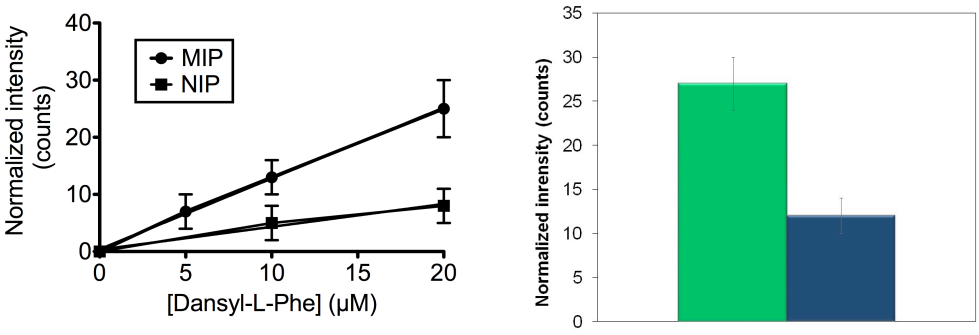

Figure 2.29. *(Left) Fluorescence response of the MIP (circles) and NIP (squares) microtips in the bifurcated fiber, incubated with increasing concentrations of dansyl-L-Phe in the range 5-20 µM in anhydrous ACN. Emission intensity measured at 495 nm. Intensity values obtained after subtraction of the fluorescent background measured as 300 counts. (Right) Normalized fluorescence signal of the MIP microtip in the bifurcated fiber, measured after incubation in 10 µM dansyl-L-Phe (green bar) and 10 µM dansyl-D-Phe (blue bar), in ACN. Emission intensity measured at 495 nm. Intensity values obtained after subtraction of the fluorescent background measured as 300 counts.*

III.2.2. Composite gold nanoparticle-MIP microtip for an enhanced sensitivity

We again aimed at enhancing the sensitivity of the sensor by incorporating gold nanoparticle into the MIP shell. In addition, we tested other noble metal NPs, which might yield better signal enhancement than the gold NPs we used previously. We screened several types of noble metal nanoparticles, and added different amounts to the MIP precursors solutions, in order to study the influence on the fluorescence signal. For this study, the bifurcated fiber set-up was used, and the detection was performed with an Ocean Optics mini-spectrometer. The fluorescence signal of an unwashed plain tip of dansyl-L-Phe MIP was recorded (formulation used described in Table 2.10). Three types of noble metal nanoparticles were studied:

- **Au:** Commercial octanethiol-functionalized gold nanoparticles (diameter: 10 nm, dynamic light scattering (DLS), Figure 2.30A; 2% (w/v) in toluene)
- **Au2:** Citrate-functionalized gold nanoparticles synthesized according to Yong et al., 2006 (diameter: 20 nm, DLS, Figure 2.30B; water)
- **Ag:** Commercial silver nanoparticles (diameter: 40 nm (TEM by Sigma-aldrich; 0.02 mg/mL in aqueous buffer, contains sodium citrate as stabilizer)

Table 2.10. *Formulation of composite noble metal-MIP microtips*

Template	Functional monomers	Cross-linker	Initiator	Solvent	Noble metal nanoparticles
Dansyl-L-Phe (0.05 mmol)	MAA/4-VPY (0.2/0.2 mmol)	EDMA/PETIA (1.3/0.7 mmol)	Irgacure 819 (0.077 mmol)	Tetraglyme (230 µL)	*Addition of Au or Au2 or Ag*

A

		Diam. (nm)	% Intensity	Width (nm)
Z-Average (d.nm): 10,96	Peak 1:	12,36	97,3	4,996
PdI: 0,192	Peak 2:	4048	2,7	1065
Intercept: 0,744	Peak 3:	0,000	0,0	0,000
Result quality Good				

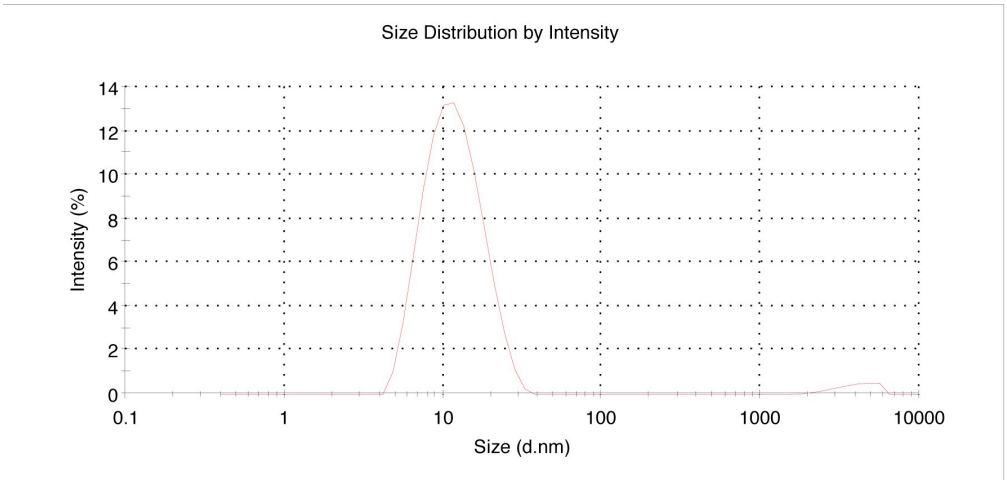

B

Results

		Diam. (nm)	% Intensity	Width (nm)
Z-Average (d.nm): 20,39	Peak 1:	19,60	89,9	6,769
PdI: 0,358	Peak 2:	226,3	8,4	64,84
Intercept: 0,865	Peak 3:	5370	1,7	328,3
Result quality Good				

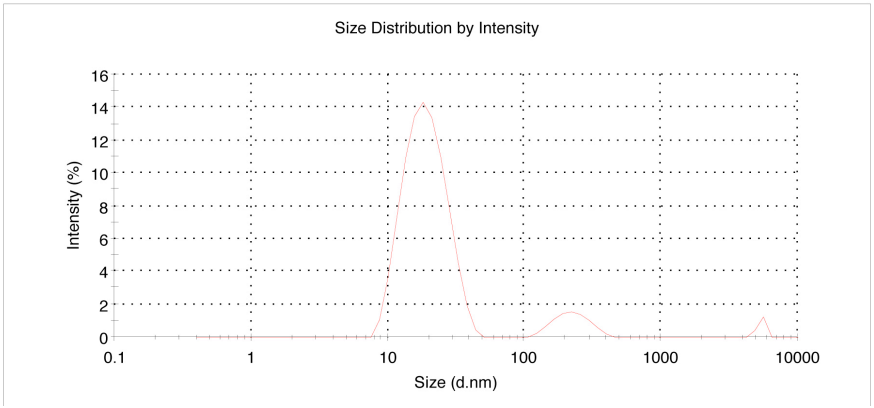

Figure 2.30. *Dynamic light scattering measurement of (A) the solution of octanethiol-functionalized gold nanoparticles in toluene and (B) citrate-functionalized gold nanoparticles in water. Peak analyzes by intensity, volume and number all showed single, symmetrical peaks with a narrow distribution.*

Different amounts of Au, Au2 and Ag NPs were added to the dansyl-L-Phe MIP precursors mixture, and the fluorescence signal of the unwashed composite dansyl-L-Phe MIP tip was recorded. As can be seen in Figure 2.31A, concerning the Au NPs, the fluorescence signal of dansyl-L-Phe increased with increasing amount of Au NPs, until an enhancement of 4 times the initial signal, obtained with 1.22 mg Au NPs/mL MIP precursors. With 1.60 mg Au NPs/mL MIP precursors and

1.96 mg Au NPs/mL MIP precursors, the signal of dansyl-L-Phe was still enhanced, but less than with 1.22 mg Au NPs/mL. The shape of the tips can explain this result. Indeed with 20 µL of added solution and more (i.e. 1.60 mg/mL and 1.96 mg Au NPs/mL MIP precursors), the precursors solution is not viscous enough to form long and thin tips. As a result, shorter tips were obtained, which produced lower signals. Then, as can be seen in Figure 2.31B, concerning the Au2 NPs, an enhancement of around x 2.5 of the signal was obtained with 5 µL of added solution. With 10 µL, a very short tip was obtained, which may explain the decrease of the signal. The same experiments were performed with the Ag NPs, as illustrated in Figure 2.31C. As a result, the best enhancement (around x3.5) of the fluorescence signal was observed when 0.83 µg Ag NPs/mL precursors solution were added to the MIP formulation. The best results were obtained with the Au NPs used previously with the simple fiber sensor,-so these Au NPs were kept for further studies related to fluorescence enhancement.

A

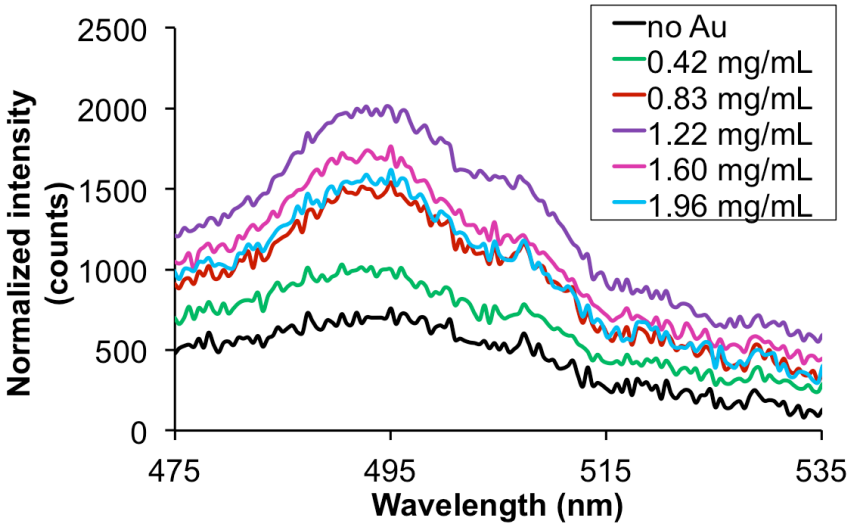

B

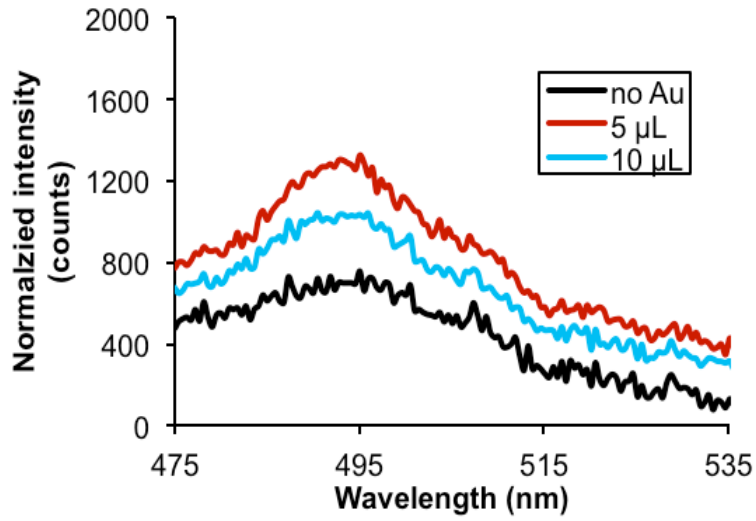

C

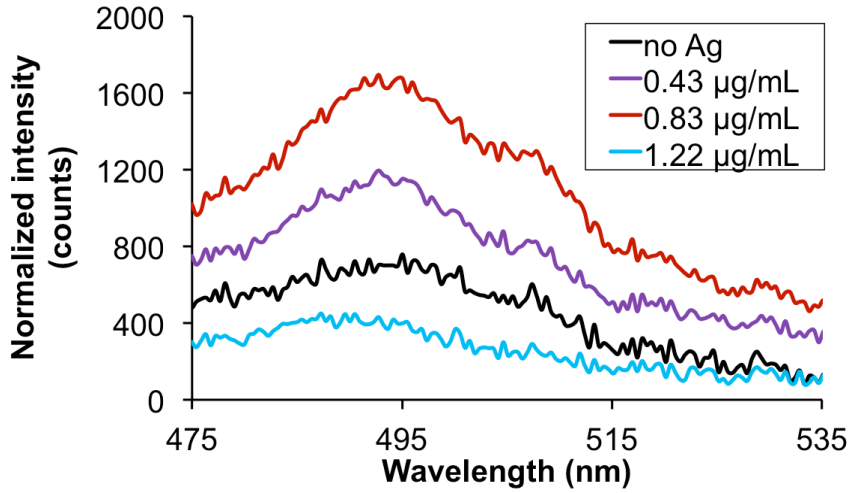

Figure 2.31. *Normalized fluorescence signal of dansyl-L-Phe tip (unwashed) with different amounts of Au or Ag NPs solution added in the MIP formulation: (A) Au, (B) Au2, (C) Ag NPs. Signal obtained after subtraction of the fluorescent background measured as 800 counts.*

The fluorescence enhancement effect by gold nanoparticles was also verified with the bifurcated fiber. The detection was performed again with the spectrometer of the Witec microscope, and a fluorescence amplification of about 5 times was observed in presence of gold nanoparticles, lowering the limit of detection to 1 µM (Figure 2.32).

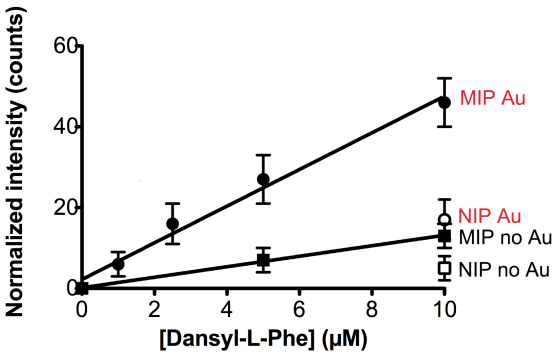

Figure 2.32. *Normalized fluorescence responses of the MIP and NIP tips without gold ("MIP no Au" and "NIP no Au", λ_{EM}= 495 nm) and of the gold composite tips ("MIP Au" and „NIP Au", λ_{EM}= 489 nm), incubated with increasing concentrations of dansyl-L-Phe in ACN. Experiments were performed in triplicate, errors bars represent standard deviations. The blank signal was recorded before each set of experiments.*

III.2.3. Conclusions

In this set-up, we explored another strategy for the fluorescence detection: the analyte was detected by measuring the fluorescence light emitted back into the fiber. We demonstrated that in this configuration, the MIP microtip also showed specific and selective binding towards the amino acid derivative dansyl-L-Phe. Moreover, the incorporation of gold nanoparticles into the MIP microtip also led to a signal enhancement. However, the sensitivity of the bifurcated fiber sensor still has to be refined: for example, it is impossible to use the core-shell format of the microtip, as the device is not

sensitive enough to collect any signal. To overcome this issue, using a multimode optical fiber with a larger core should considerably enhance the sensitivity of the sensor.

III.3. Sensing with a bifurcated multimode fiber and a fluorescent signaling MIP microtip

Until now, the experiments with the naphthalimide-based fluorescent MIP were performed only on the simple fiber set-up, as we were not able to measure a fluorescence signal with a core-shell microtip and the bifurcated fiber. Indeed the fluorescence signal was probably too low to be measured, as it has to go back through the poly(PETIA) core tip, and then through the optical fiber before reaching the detector. Loss of signal was high due to the small diameter of the telecom fiber (8 μm) and isotropic light diffusion. Furthermore the telecom fiber is optimized for the infrared range (typically 1200 nm), which means that loss of signal was unavoidable at 375 nm.

In order to improve the sensitivity of the sensor, we customized a bifurcated fiber using 400 μm core multimode optical fibers that are optimized for the range 300-1200 nm. Thereby, the larger core should result in a stronger signal. Just like the bifurcated telecom fiber, the MIP was located at the extremity of the common part of the Y fiber, while detection was performed on one arm of the Y fiber that was directly coupled to the Ocean Optics mini-spectrometer via a SMA connector (Figure 2.33; in fact, owing to the larger amount of collected light, the use of the ultra-sensitive WiTec spectrometric camera was not necessary anymore.). The MIP microtip was synthesized in the core-shell format: a poly(PETIA) core covered by a thin layer of MIP. The bifurcated fiber was applied for sensing of the herbicide 2,4-D, the mycotoxin citrinin and the sphingolipid D-*erythro*-sphingosine-1-phosphate. The new set-up combines now several advantages: possibilities of long-distance and real-time monitoring, faster detection with the Ocean Optics mini-spectrometer and more compact set-up.

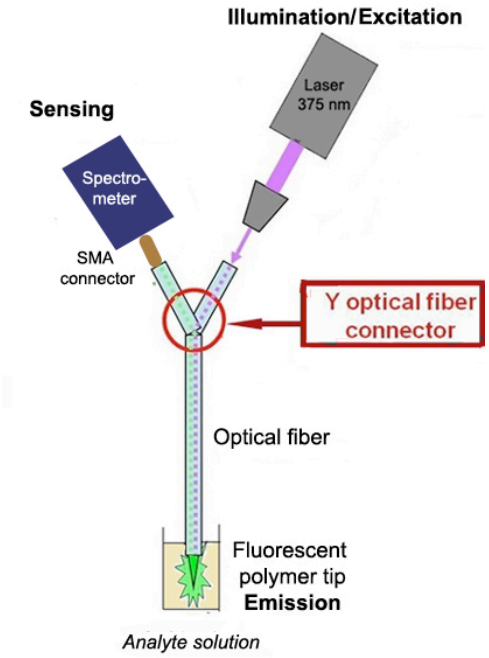

Figure 2.33. *Analysis by spectrofluorimetry of the polymer microtips with the bifurcated multimode fiber. A 375 nm diode laser is used both for microtip polymerization and for excitation of the fluorophore.*

III.3.1. Sensing of the mycotoxin citrinin

The citrinin-MIP **P4** (formulation in Table 2.4) was synthesized at the end of the bifurcated fiber. Due to the larger core diameter, the shape of the tip was different than the previous one, yielding a lense-like shape (Figure 2.34). The molecular recognition properties of the MIP were verified by incubating both MIP and NIP microtips with increasing concentrations of citrinin (Figure 2.35). The results obtained with the multimode Y fiber were quite consistent with the ones obtained with the simple fiber, even though the detection was different. Indeed with the multimode Y fiber, we measure the portion of emitted light that comes back through the fiber, until it reaches the arm of the fiber that is connected to the Ocean Optics spectrometer. With the simple fiber, the emitted light was collected at the tip level by the fiber of the spectrometer. The different modes of detection could explain the slight decrease in sensitivity observed with the multimode Y fiber.

This new set-up is very sensitive as the LOD and LOQ (limit of quantification) for citrinin are of only 5 ng/mL (in methanol). For comparisons, the MRL for citrinin set in China in dry functional kojic red rice is 50 ng/g, which is 10 times above our LOD. No MRL was set by the European Union, but the European Food Safety Authority estimated the maximal concentration of citrinin that would result in no concern for nephrotoxicity, that is between 19 and 100 ng/g in grains and grain-based products, for average consumers. Methanol can be used for the extraction of citrinin, often combined with water, for example methanol/water (70/30, v/v) (Sato et al., 2010).

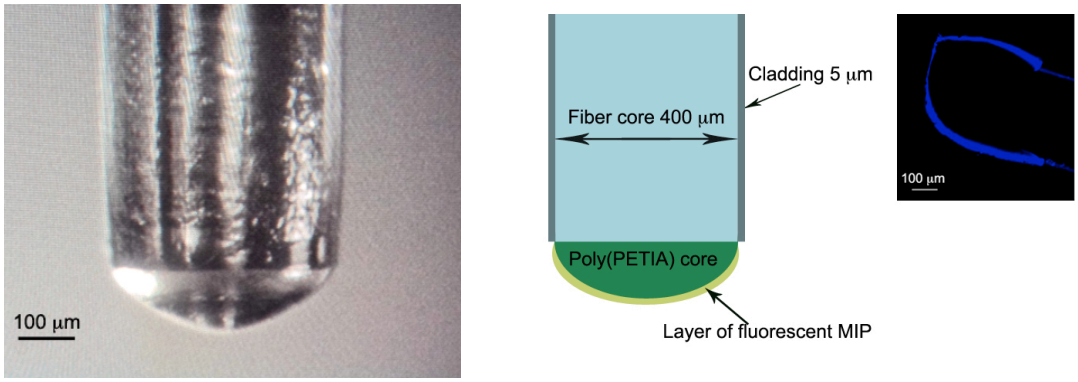

Figure 2.34. *(Left) Picture taken with a CCD camera and (right) schematic representation of the core-shell poly(PETIA)-MIP tip synthesized at the extremity of the multimode bifurcated fiber. Inset: confocal fluorescence microscope image of the core-shell microtip.*

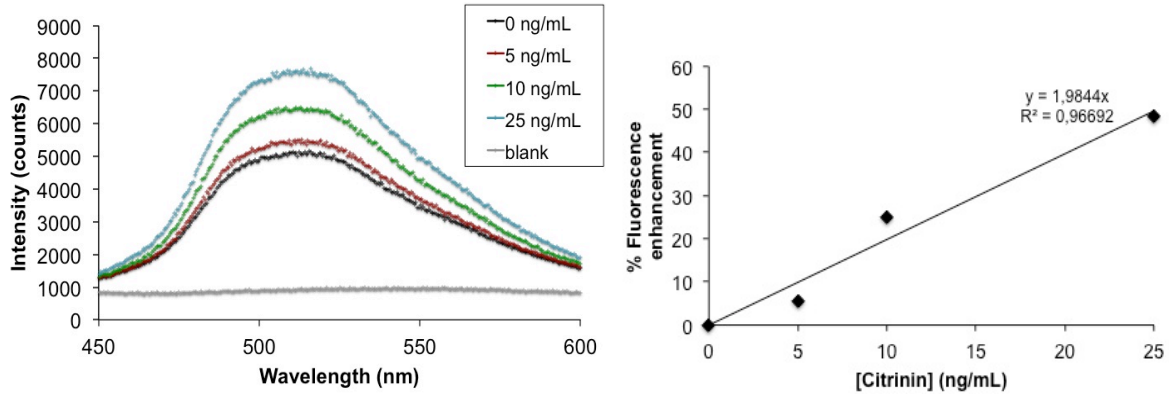

Figure 2.35*. (Left) Fluorescence spectra changes and (right) the corresponding calibration curve of the fluorescence response of the citrinin-MIP microtip* ***P4*** *on the multimode Y fiber, after incubation with 5 –*

10 – 25 ng/mL citrinin in MeOH (λ_{EX}=375 nm). Integration time: 5 ms. The blank signal corresponds to the signal recorded with no MIP microtip at the end of the fiber.

III.3.2. Sensing of the sphingolipid D-erythro-sphingosine-1-phosphate

Until now, we have applied our signaling monomer FIM for the detection of carboxylic acids. However, it would be interesting if FIM could also be applied to the detection of analytes carrying other oxo-anions such as, sulfate or phosphate. We have studied the interactions between FIM and a phosphate compound, the sphingolipid metabolite D-*erythro*-sphingosine-1-phosphate (S-1-P) (Figure 2.36). The function of sphingolipids is to protect the cell surface from harmful environments. Sphingolipid metabolites including sphingosine-1-phosphate have attracted attention because they could be used as bioactive signaling molecules as they are involved in cell functions, such as the regulation of cell growth, differentiation, senescence and apoptosis (Bartke and Hannun, 2009). Hence, monitoring of S-1-P, for example in blood plasma, is of great interest for biomedical applications.

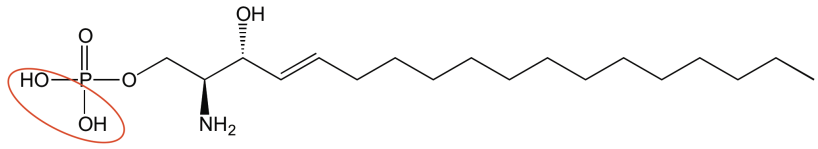

Interaction with FIM

Figure 2.36. *Chemical structure of S-1-P.*

Prior to the preparation of the fluorescent S-1-P imprinted polymer, the process of fluorescence enhancement of FIM was verified with spectrofluorimetric titrations of FIM (5 μM) with increasing concentrations of S-1-P (5-100 μg/mL in methanol, i.e. ≈ 13-260 μM). As a result (Figure 2.37), the fluorescence enhancement of FIM was observed to be concentration-dependent and increased with increasing concentrations of S-1-P, confirming that FIM could be used as a functional monomer to imprint S-1-P. We can also notice from the spectra that the maximum emission peak gets blue-shifted with high concentrations of S-1-P (from 515 nm to 506-507 nm). Indeed the medium is rendered more hydrophobic by the presence of S-1-P.

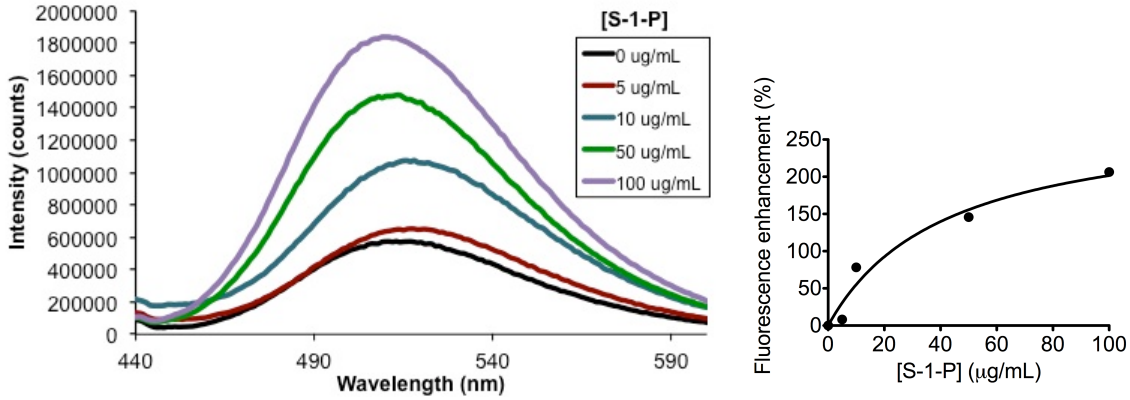

Figure 2.37. *Spectrofluorimetric titrations in methanol of FIM (5 μM) with increasing concentrations of S-1-P (5, 10, 50, 100 μg/mL) (λ_{EX} = 390 nm) (left) fluorescence spectra and (right) fluorescence responses of FIM as function of S-1-P concentration.*

Given the small quantity of S-1-P available, we chose to synthesize the MIP **P5** directly as an end-of-fiber microtip, on the multimode bifurcated fiber (Table 2.11). FIM was chosen as co-functional monomer with methyl methacrylate (MMA), because MMA is hydrophobic, such as S-1-P.

Table 2.11. *Formulation of the S-1-P imprinted polymer* ***P5***

Template	Functional monomers	Cross-linker	Initiator	Solvent
S-1-P	FIM/MMA	EDMA	Irgacure 819	Methanol (1 mL)
(1 mg; 2.6 μmol)	(5.3/5.3 μmol)	(52 μmol)	(1,1 μmol)	

The MIP microtip was immersed 15 minutes into different concentrations of solutions of S-1-P in methanol. As a result (Figure 2.38), the MIP showed fluorescence enhancement after incubation with S-1-P and the LOD was 0.5 μg/mL S-1-P (i.e. 1.3 μM). The fluorescence enhancement was specific as no or very little (<5%) signal change, was recorded with a non-imprinted control polymer microtip, after incubation with 0.5 and 1 μg/mL S-1-P (Figure 2.39).

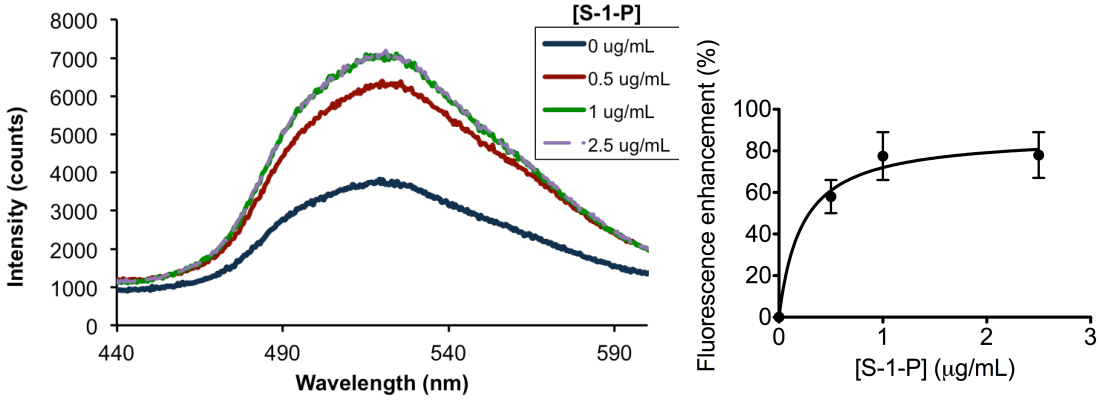

Figure 2.38. *(Left) fluorescence spectra and (right) fluorescence responses of the S-1-P MIP* ***P5*** *microtip as function of S-1-P concentration (λ_{EX} = 375 nm). Integration time: 5 ms.*

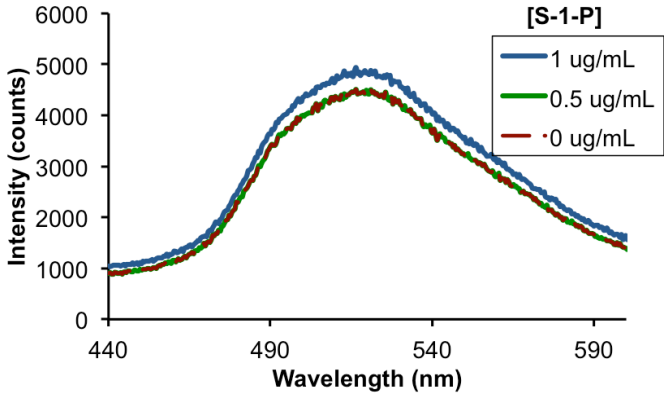

Figure 2.39. *Fluorescence spectra of the control NIP microtip as function of S-1-P concentration (λ_{EX} = 375 nm). Integration time : 5 ms.*

To assess the selectivity of our MIP, the MIP microtip was incubated with various concentrations of another phosphate compound, adenosine-5'-monophosphate (AMP) (structure in Table 2.1). As a result, the MIP showed no fluorescence enhancement after incubation with 1 and 2 μM AMP in methanol, but showed an enhancement of around 85% after incubation with 10 μM AMP,

such as with 10 μM S-1-P. Thus we can conclude that our MIP is selective, and that at least at low concentrations of other phosphate compounds do not interfere.

The LOD with the MIP **P5** was 0.5 μg/mL S-1-P (i.e. 1.3 μM). However, to be able to measure clinically relevant concentrations, we would need to lower the LOD by 100 times (i.e. 5 ng/mL S-1-P), which means that the S-1-P MIP formulation has to be optimized. We therefore took the same formulation as **P5** but added acrylamide (AAm) as a co-functional monomer, with FIM and MMA. We expect AAm to form hydrogen bonds with the hydroxyl and amine groups of S-1-P. The formulation of the MIP **P6** is described in Table 2.12.

Table 2.12. *Formulation of the S-1-P imprinted polymer* ***P6***

Template	Functional monomers	Cross-linker	Initiator	Solvent
S-1-P (1 mg; 2.6 μmol)	FIM/MMA/AAm (5.3/5.3/5.3 μmol)	EDMA (52 μmol)	Irgacure 819 (1,1 μmol)	Methanol (1 mL)

The MIP microtip was immersed 15 minutes into different concentrations of solutions of S-1-P in methanol. As a result (Figure 2.40), the MIP showed fluorescence enhancement after incubation with S-1-P and the LOD was 0.1 μg/mL S-1-P (i.e. 0.26 μM). However, even if the LOD was now 5 times lower, the relative signal enhancement measured was lower than that with MIP **P5** (after incubation with 1 μg/mL S-1-P, **P6** showed a maximal enhancement of 25% whereas with **P5**, a maximal enhancement of around 80% was obtained). This lower enhancement may be due to the presence of two other co-functional monomers (MMA and AAm) that also interact with S-1-P, resulting in a lower amount of S-1-P interacting with FIM, or in quenching due to AAm. We can notice that for both S-1-P MIPs, the maximal enhancement, which corresponds to the saturation of the binding, is rapidly reached.

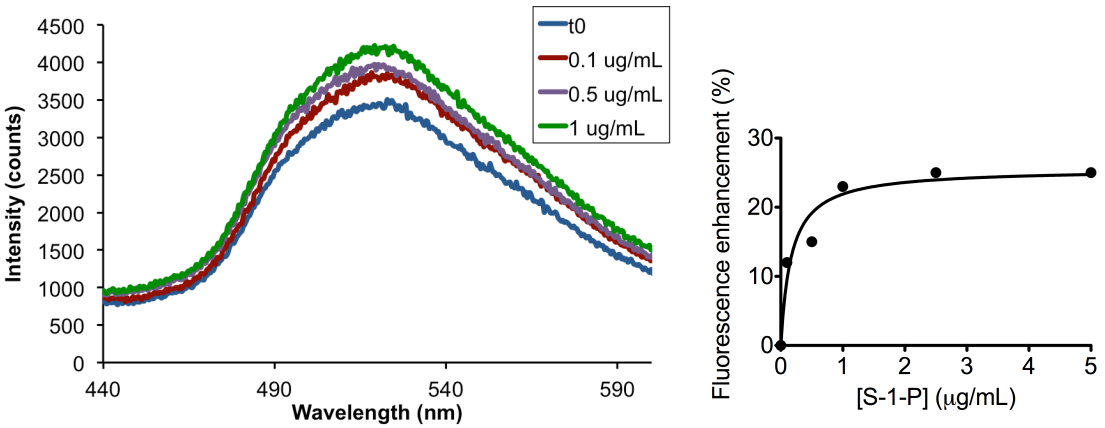

Figure 2.40. *(Left) fluorescence spectra and (right) fluorescence responses of the S-1-P MIP microtip* ***P6*** *as function of S-1-P concentration (λ_{EX} = 375 nm). Integration time: 5 ms.*

In order to increase the sensitivity of the S-1-P MIP, we used the bimetallic core-shell Au-Ag nanoparticles that were developed by Pande et al., 2007. In their work, Pande and co-workers have reported a method for the synthesis of Au and Ag nanoparticles, and their bimetallic conjugates, i.e. Au_{core}-Ag_{shell} and Ag_{core}-Au_{shell} NPs, using β-cyclodextrin as reducing and capping agent. The monometallic and bimetallic were applied for surface-enhanced raman scattering (SERS), and as a

result, the Au_{core}-Ag_{shell} NPs showed the best enhanced signal, especially compared to Au NPs. On the other hand, the Raman signal of the Ag_{core}-Au_{shell} NPs was a little bit lower than the signal of Ag NPs. We wanted to study the effect of these bimetallic Au_{core}-Ag_{shell} NPs on the fluorescence signal of our S-1-P MIP. Thus a new formulation of S-1-P MIP **P7-Au/Ag** was developed, and for comparison, a formulation of S-1-P MIP **P7** (same solvent but without the bimetallic NPs) was also synthesized (Table 2.13).

Both MIP microtips were incubated with different concentrations of solutions of S-1-P in methanol, ranging from 0.1 μg/mL to 1 μg/mL S-1-P, and no enhancement was observed. The addition of Au_{core}-Ag_{shell} NPs even resulted in a quenching of the fluorescence signal of the MIP, compared to the MIP **P7** (not illustrated). Therefore the use of Au_{core}-Ag_{shell} NPs was abandoned for the S-1-P MIP.

Table 2.13. *Formulation of the S-1-P imprinted polymers **P7** and **P7-Au/Ag***

Polymer	Template	Functional monomers	Cross-linker	Initiator	Solvent	Au_{core}-Ag_{shell} NPs
P7	**S-1-P (1 mg; 2.6 μmol)**	FIM/MMA/AAm (5.3/5.3/5.3 μmol)	EDMA (52 μmol)	Irgacure 819 (1,1 μmol)	Methanol/water (5/1) (1.2 mL)	-
P7 – Au/Ag	**S-1-P (1 mg; 2.6 μmol)**	FIM/MMA/AAm (5.3/5.3/5.3 μmol)	EDMA (52 μmol)	Irgacure 819 (1,1 μmol)	Methanol/water (5/1) (1.2 mL)	$2.5.10^8$ NPs

To conclude, our MIP-based fiber optic device can be used to detect S-1-P, and we have shown that FIM could be used to detect phosphate compounds. However, the limit of detection and the dynamic range can still be improved, by a further optimization of the MIP formulation, and also by incorporation of gold nanoparticles for metal-enhanced fluorescence.

IV. Conclusions and perspectives

We have developed a fluorescence-based optical fiber sensor using *in-situ* polymerized MIP microstructures as the recognition element. Photonic and physico-chemical parameters were optimized in order to tailor the photostructuring and molecular recognition properties of the MIP microtip. Two possibilities were evaluated for the detection of the fluorescence response of the analyte: either by external collection of the signal emitted by the tip, or by measuring the emitted signal passing in the other arm of a bifurcated fiber. We have first chosen the amino acid derivative Z-L-Phe as model template, and the imprinting effect was monitored with the fluorescent labeled dansyl-L-Phe. The MIP tip demonstrated specific binding towards dansyl-L-Phe, as well as selectivity between the L- and D- forms of dansyl-phenylalanine and *N*-carbobenzyloxy-phenylalanine. The concept of the MIP-based fiber-optic sensor with fluorescence detection was successfully demonstrated with the model analyte Z-L-Phe and by using a standard single-mode telecom fiber as the sensing device. The sensitivities of both sensors were improved by using gold nanoparticles embedded in the MIP, to enhance the fluorescence signal. In the case of the simple fiber sensor, the limit of detection was lowered from the μM to the nM range.

In order to be able to monitor non-fluorescent analytes, a naphthalimide-based fluorescent monomer was incorporated into the MIP, which shows fluorescence enhancement when analyte binding occurs. Using this system, a sensor containing a MIP specific for the herbicide 2,4-

dichlorophenoxyacetic acid could detect and quantify this analyte in methanol/water (4/1) at concentrations as low as 2.5 nM.

A more sensitive bifurcated fiber-based set-up was developed using 400 μm core multimode fibers. The naphthalimide-based fluorescent monomer was applied for a MIP for the mycotoxin citrinin, and the LOD was found to be 5 ng/mL of citrinin while the MRL set in China was 50 ng/g in rice. Besides carboxylate compounds, the signaling monomer was also applied for the imprinting of a phosphate compound, the sphingolipid D-*erythro*-sphingosine-1-phosphate (S-1-P). Monitoring of S-1-P is of high interest for biomedical applications as it is a bioactive molecule involved in many cell functions. At the moment, a LOD of 100 ng/mL was achieved. However we would like to lower the LOD to 5 ng/mL, so the performances of our S-1-P MIP can still be improved.

This concept, undoubtedly, could be generated to the detection of analytes in “real” samples. The MIP-based fiber optic sensing material we have developed will potentially make a powerful tool for the detection of biomolecules and environmental pollutants in complex matrices, as it offers several advantages such as portability, reusability, high specificity, accuracy, fast response and low cost.

V. References

Al-Kindy, S.; Badía, R.; Suárez-Rodríguez, J. L.; Díaz-García, M. E. Molecularly imprinted polymers and optical sensing applications. *Critical Reviews in Analytical Chemistry* **2000**, *30*, 291.

Bartke, N.; Hannun, Y. A. Bioactive sphingolipids: metabolism and function. *Journal of lipid research* **2009**, *50*, S91.

Dutta Choudhury, S.; Badugu, R.; Ray, K.; Lakowicz, J. R. Silver–Gold Nanocomposite Substrates for Metal-Enhanced Fluorescence: Ensemble and Single-Molecule Spectroscopic Studies. *The Journal of Physical Chemistry C* **2012**, *116*, 5042.

Epstein, J. R.; Walt, D. R. Fluorescence-based fibre optic arrays: a universal platform for sensing. *Chemical Society Reviews* **2003**, *32*, 203.

Ferguson, J. A.; Healey, B. G.; Bronk, K. S.; Barnard, S. M.; Walt, D. R. Simultaneous monitoring of pH, CO_2 and O_2 using an optical imaging fiber. *Analytica chimica acta* **1997**, *340*, 123.

Fuchs, Y.; Linares, A. V.; Mayes, A. G.; Haupt, K.; Soppera, O. Ultrathin Selective Molecularly Imprinted Polymer Microdots Obtained by Evanescent Wave Photopolymerization. *Chemistry of Materials* **2011**, *23*, 3645

Haupt, K.; Dzgoev, A.; Mosbach, K. Assay system for the herbicidee 2, 4-dichlorophenoxyacetic acid using a molecularly imprinted polymer as an artificial recognition element. *Analytical Chemistry* **1998**, *70*, 628.

Haupt, K.; Mosbach, K. Molecularly imprinted polymers and their use in biomimetic sensors. *Chem. Rev* **2000**, *100*, 2495.

Healey, B. G.; Walt, D. R. Fast temporal response fiber-optic chemical sensors based on the photodeposition of micrometer-scale polymer arrays. *Analytical Chemistry* **1997**, *69*, 2213.

Henry, O. Y. F.; Cullen, D. C.; Piletsky, S. A. Optical interrogation of molecularly imprinted polymers and development of MIP sensors: a review. *Analytical and Bioanalytical Chemistry* **2005**, *382*, 947.

Hill, R. R.; Richenburg, C. W.; Roberts, D. R. Relative fluorescence yields of dansyl amino acids: A sensitive probe for structures in solution. *Journal of Photochemistry and Photobiology A: Chemistry* **1996**, *97*, 109.

Jenkins, A. L.; Uy, O. M.; Murray, G. M. Polymer-based lanthanide luminescent sensor for detection of the hydrolysis product of the nerve agent soman in water. *Analytical Chemistry* **1999**, *71*, 373.

Jradi, S.; Soppera, O.; Lougnot, D. J.; Bachelot, R.; Royer, P. Tailoring the geometry of polymer tips on the end of optical fibers via control of physico-chemical parameters. *Optical Materials* **2009**, *31*, 640.

Kempe, H.; Kempe, M. Influence of salt ions on binding to molecularly imprinted polymers. *Analytical and Bioanalytical Chemistry* **2010**, *396*, 1599.

Kriz, D.; Ramstroem, O.; Svensson, A.; Mosbach, K. A biomimetic sensor based on a molecularly imprinted polymer as a recognition element combined with fiber-optic detection. *Analytical Chemistry* **1995**, *67*, 2142.

Kubo, H.; Nariai, H.; Takeuchi, T. Multiple hydrogen bonding-based fluorescent imprinted polymers for cyclobarbital prepared with 2, 6-bis (acrylamido) pyridine. *Chemical Communications* **2003**, 2792.

Lakowicz, J. R. Radiative decay engineering: biophysical and biomedical applications. *Analytical biochemistry* **2001**, *298*, 1.

Matsui, J.; Tachibana, Y.; Takeuchi, T. Molecularly imprinted receptor having metalloporphyrin-based signaling binding site. *Analytical Communications* **1998**, *35*, 225.

Medina-Castillo, A. L.; Mistlberger, G. n.; Fernandez-Sanchez, J. F.; Segura-Carretero, A.; Klimant, I.; Fernandez-Gutierrez, A. Novel strategy to design magnetic, molecular imprinted polymers with well-controlled structure for the application in optical sensors. *Macromolecules* **2010**, *43*, 55.

Munkholm, C.; Walt, D. R.; Milanovich, F. P.; Klainer, S. M. Polymer modification of fiber optic chemical sensors as a method of enhancing fluorescence signal for pH measurement. *Analytical Chemistry* **1986**, *58*, 1427.

Ng, S. M.; Narayanaswamy, R. Fluorescence sensor using a molecularly imprinted polymer as a recognition receptor for the detection of aluminium ions in aqueous media. *Analytical and Bioanalytical Chemistry* **2006**, *386*, 1235.

Nguyen, T. H.; Hardwick, S. A.; Sun, T.; Grattan, K. T. V. Intrinsic Fluorescence-Based Optical Fiber Sensor for Cocaine Using a Molecularly Imprinted Polymer as the Recognition Element. *IEEE Sensors Journal* **2012**, *12*, 255.

Niu, C. G.; Zeng, G. M.; Chen, L. X.; Shen, G. L.; Yu, R. Q. Proton “off-on” behaviour of methylpiperazinyl derivative of naphthalimide: a pH sensor based on fluorescence enhancement. *Analyst* **2004**, *129*, 20.

Pande, S.; Ghosh, S. K.; Praharaj, S.; Panigrahi, S.; Basu, S.; Jana, S.; Pal, A.; Tsukuda, T.; Pal, T. Synthesis of normal and inverted gold-silver core-shell architectures in β-Cyclodextrin and their applications in SERS. *The Journal of Physical Chemistry C* **2007**, *111*, 10806.

Piperno, S.; Tse Sum Bui, B.; Haupt, K.; Gheber, L. A. Immobilization of Molecularly Imprinted Polymer Nanoparticles in Electrospun Poly (vinyl alcohol) Nanofibers. *Langmuir* **2011**, *27*, 1547.

Queirós, R. B.; Silva, S.; Noronha, J.; Frazão, O.; Jorge, P.; Aguilar, G.; Marques, P.; Sales, M. Microcystin-LR detection in water by the Fabry–Pérot interferometer using an optical fibre coated with a sol–gel imprinted sensing membrane. *Biosensors and Bioelectronics* **2011**, *26*, 3932.

Ramstroem, O.; Andersson, L.; Mosbach, K. Recognition sites incorporating both pyridinyl and carboxy functionalities prepared by molecular imprinting. *The Journal of Organic Chemistry* **1993**, *58*, 7562.

Sato, T.; Higashihara, K.; Sasaki, A.; Toth, D.; Goto, T. Development and single laboratory validation of a method for citrinin. *World Mycotoxin Journal* **2010**, *3*, 129.

Soppera, O.; Jradi, S.; Lougnot, D. J. Photopolymerization with microscale resolution: Influence of the physico chemical and photonic parameters. *Journal of Polymer Science Part A: Polymer Chemistry* **2008**, *46*, 3783.

Stranik, O.; McEvoy, H.; McDonagh, C.; MacCraith, B. Plasmonic enhancement of fluorescence for sensor applications. *Sensors and Actuators B: Chemical* **2005**, *107*, 148.

Szablan, Z.; Junkers, T.; Koo, S.; Lovestead, T.; Davis, T.; Stenzel, M.; Barner-Kowollik, C. Mapping photolysis product radical reactivities via soft ionization mass spectrometry in acrylate, methacrylate, and itaconate systems. *Macromolecules* **2007**, *40*, 6820.

Takeuchi, T.; Mukawa, T.; Shinmori, H. Signaling molecularly imprinted polymers: molecular recognition-based sensing materials. *The Chemical Record* **2005**, *5*, 263.

Toma, K.; Dostalek, J.; Knoll, W. Long range surface plasmon-coupled fluorescence emission for biosensor applications. *Optics Express* **2011**, *19*, 11090.

Ton, X. A.; Tse Sum Bui, B.; Resmini, M.; Bonomi, P.; Dika, I.; Soppera, O.; Haupt, K. A Versatile Fiber-Optic Fluorescence Sensor Based on Molecularly Imprinted Microstructures Polymerized in Situ. *Angewandte Chemie International Edition* **2013**, *52*, 8317.

Verma, R.; Gupta, B. D. Fiber optic SPR sensor for the detection of 3-pyridinecarboxamide (vitamin B_3) using molecularly imprinted hydrogel. *Sensors and Actuators B: Chemical* **2013**, *177*, 279

Wagner, R.; Wan, W.; Biyikal, M.; Benito-Peña, E.; Moreno-Bondi, M. a. C.; Lazraq, I.; Rurack, K.; Sellergren, B. r. Synthesis, Spectroscopic, and Analyte-Responsive Behavior of a Polymerizable Naphthalimide-Based Carboxylate Probe and Molecularly Imprinted Polymers Prepared Thereof. *The Journal of Organic Chemistry* **2013**, *78*, 1377.

Walt, D. R.; Dickinson, T.; White, J.; Kauer, J.; Johnson, S.; Engelhardt, H.; Sutter, J.; Jurs, P. Optical sensor arrays for odor recognition. *Biosensors and Bioelectronics* **1998**, *13*, 697.

Wan, W.; Biyikal, M.; Wagner, R.; Sellergren, B.; Rurack, K. Fluorescent Sensory Microparticles that "Light-up" Consisting of a Silica Core and a Molecularly Imprinted Polymer (MIP) Shell. *Angewandte Chemie International Edition* **2013**, *52*, 7023.

Wang, X.-D.; Wolfbeis, O. S. Fiber-optic chemical sensors and biosensors (2008–2012). *Analytical Chemistry* **2012**, *85*, 487.

White, J.; Kauer, J. S.; Dickinson, T. A.; Walt, D. R. Rapid analyte recognition in a device based on optical sensors and the olfactory system. *Analytical Chemistry* **1996**, *68*, 2191.

Wulff, G. Molecular imprinting in cross linked materials with the aid of molecular templates - A way towards Artificial Antibodies. *Angewandte Chemie International Edition* **1995**, *34*, 1812.

Wulff, G. Enzyme-like catalysis by molecularly imprinted polymers. *Chemical Reviews* **2002**, *102*, 1.

Yong, K.-T.; Sahoo, Y.; Swihart, M. T.; Prasad, P. N. Synthesis and plasmonic properties of silver and gold nanoshells on polystyrene cores of different size and of gold–silver core–shell nanostructures. *Colloids and Surfaces A: Physicochemical and Engineering Aspects* **2006**, *290*, 89.

Yoshimatsu, K.; Reimhult, K.; Krozer, A.; Mosbach, K.; Sode, K.; Ye, L. Uniform molecularly imprinted microspheres and nanoparticles prepared by precipitation polymerization: The control of particle size suitable for different analytical applications. *Analytica chimica acta* **2007**, *584*, 112.

Zhou, Y.; Chen, J.; Dong, L.; Lu, L.; Chen, F.; Hu, D.; Wang, X. A study of fluorescence properties of citrinin in β-cyclodextrin aqueous solution and different solvents. *Journal of Luminescence* **2012**, *132*, 1437.

Chapter 3

Synthesis of molecularly imprinted polymer-coated sensing elements by evanescent wave photopolymerization and top-down deposition

Chapter 3: Synthesis of molecularly imprinted polymer-coated sensing elements by evanescent wave photopolymerization and top-down deposition

I. Introduction

I.1. Evanescent-wave fiber optic sensors

The previous chapter described the development of a highly selective and sensitive optical fiber sensor carrying *in-situ* polymerized molecularly imprinted microstructures, and based on fluorescence for detection, in particular by using a fluorescent signaling monomer. In this chapter, we use another sensing approach and we describe a new kind of MIP-based optical fiber sensors that could be used for fast, cheap and "single-use" detection of analytes. These sensors consist of polystyrene evanescent-wave fiber optic waveguides coated with MIPs. The principle of evanescent waves applied for fiber optic sensing is briefly explained below.

The formation of evanescent waves can be explained as follows: when a light beam travels from a higher refractive index medium (n_1) to a lower high refractive index medium (n_2), total reflection occurs if the incident light hits the interface n_1-n_2 at an angle higher than a critical angle θ_c, defined as: $\theta_c = \sin^{-1}(n_2/n_1)$. An evanescent wave is then generated at the interface n_1-n_2 and spreads into the n_2 medium, with an intensity that decays exponentially with distance from the surface (Figure 3.1), according to Equation (1):

$I(z) = I_0 \exp(-2\gamma z)$ (1)

Where I_0 is the intensity of the incident light and γ the decay rate defined by Equation (2) as:

$$\gamma = \frac{2\pi}{\lambda}\sqrt{(n_1 \sin\theta)^2 - n_2^2}$$

The penetration depth of the evanescent wave is given by $1/(2\gamma)$ and represents the theoretical distance from the interface at which the intensity of the evanescent field has dropped to 1/e (about 37%) of its original value. The penetration depth is typically of 100 nm (Rogers et al., 1992).

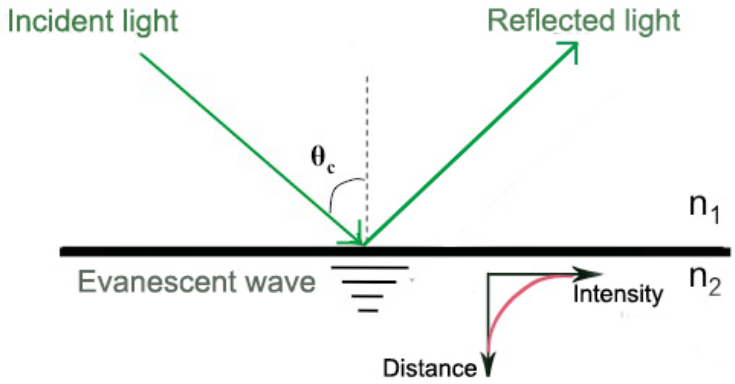

Figure 3.1. *Schematic representation of the formation of an evanescent wave created by the total reflection of the light at the interface n_1-n_2 (n_2<n_1).*

The principle of evanescent waves has been widely combined with fluorescence fiber optic biosensors (Wolfbeis, 2004; Taitt et al., 2005). Indeed if antigen (target) molecules are bound to immobilized antibodies on the surface of the fiber, only these bound antigens would interact with the light from the evanescent wave, and generate a signal. Interferences from the bulk sample matrix are thus limited, which makes possible measurements in complex samples. For example, evanescent-wave fiber optic biosensors have been used for the detection of *E.Coli* in food samples, mycotoxins in wheat, cocaine in urine, trinitrotoluene (TNT) in environmental waters, ricin in water and urine, hormones in plasma, and so on (Taitt et al., 2005).

The main targets of this part of this thesis are mycotoxins. We can cite as an example an evanescent-wave fiber optic immunosensor for the detection of the mycotoxin Fumonisin B_1 (FB_1) (Thompson and Maragos, 1996). Anti-FB_1 antibodies were covalently attached on the silanized surface of a 800 μm core fiber, and monitoring of FB_1 was performed by a displacement assay with fluorescently labeled FB_1-fluorescein isothiocyanate (FITC). As a result, the sensor showed a dynamic range of 10-1000 ng/mL FB_1 and a limit of detection of 10 ng/mL, which is far below the maximum residue limits of 200-4000 ng/mL (for the sum of Fumonisin B_1 and B_2, and depending on the food matrix), fixed by the EU Commission Regulation (EC) 1127/2007. The sensor showed cross-reactivity with Fumonisin B_2 but not with hydrolyzed FB_1 and other compounds. However, the time response of the sensor was rather long due to the several steps of the displacement assay. Moreover, the sensor set-up was complicated as the fiber was put into a flow cell, and the excitation and emission lights were conducted and collected through a set-up of several lenses and mirrors, and another optical fiber.

One particular fiber-optic sensing system was reported by Lim, 2003. They originally used a silica optical fiber, with several centimeters of the cladding removed. The surface of the fiber core was silanized and coated with streptavidin, and the capture antibodies were labeled with biotin and conjugated with streptavidin. Apart from these silica fibers, short polystyrene optical fibers were also used for sensing. These fibers cost only 3 US$ each (compared to 30 US$ for the silica fibers), and are to be used with an evanescent-wave fiber-optic biosensor. They are used in the sandwich fluoroimmunoassay format (Figure 3.2). Here, we use the same polystyrene fibers for fluorescence sensing with a MIP as the recognition element, containing a signaling functional monomer, for the monitoring of the herbicide 2,4-dichlorophenoxyacetic acid (2,4-D) and the mycotoxin citrinin (structures in Table 3.1). For signaling, we use the same naphtalimide-based monomer “FIM” as in Chapter 2, which shows fluorescence enhancement upon analyte binding.

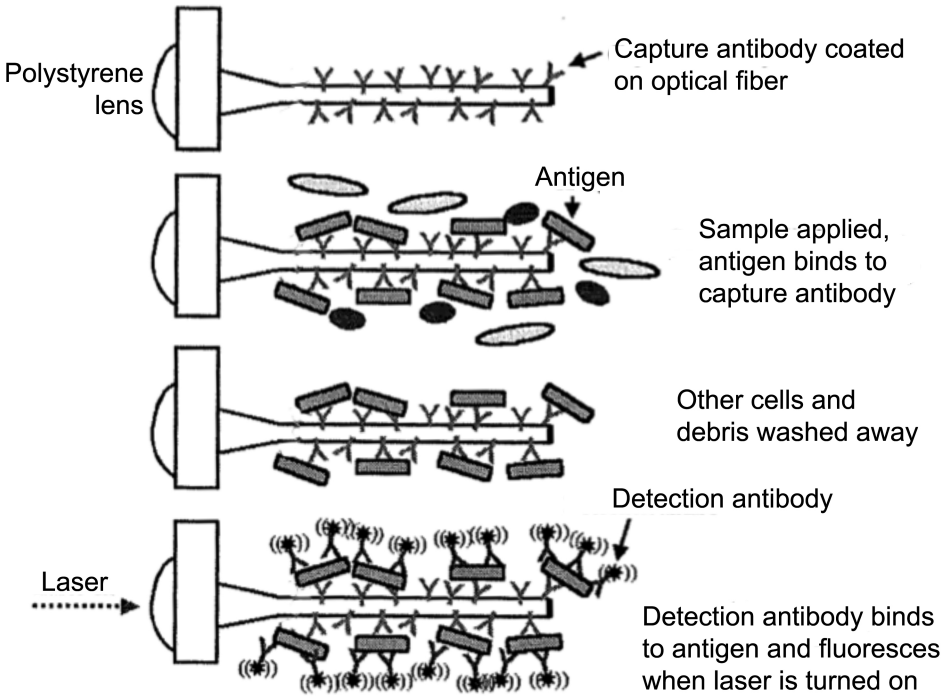

Figure 3.2. *A biosensor sandwich assay using the polystyrene optical fibers. The detection antibody is fluorescently labeled with the cyanine dye Cy5. Adapted from Lim, 2003.*

I.2. Photopolymerization by evanescent waves

Polymerization by evanescent waves is an interesting method for the synthesis of size-controlled, and in particular thickness-controlled, polymeric micro- or nanostructures, as the actinic light is confined in the penetration depth of the evanescent wave. Lougnot and co-workers showed that polymerization by evanescent waves was a good approach for the fabrication of ultra-thin polymeric objects (from few nm to 1 μm height) with nanometric resolution. They could control locally the thickness of their polymers as a function of the energy received, which is proportional to the laser power and the irradiation time (Ecoffet et al., 1998; Espanet et al., 1999).

Later, Soppera and co-workers reported the micro- and nanopatterning of a photosensitive polymer by evanescent waves (Soppera et al., 2007). The polymer consisted of poly(pentaerythritol triacrylate) with an amine as the co-initiator and Eosin Y as the sensitizer dye. The influence of the photonic conditions on the polymer thickness (from 50 to 700 nm) was evaluated. In addition, photostructuring by evanescent waves was studied using an interferometric optical set-up. As a result, 2D polymer graftings with tunable fringe spacing were obtained. Lines with sub-100 nm width could be fabricated. Considering the simplicity of the optical set-up and the wide choice of monomers, these nanopatterned polymers could potentially find many applications in optics, optical sensing, photonic crystals, biology, etc.

Whitcombe and co-workers reported the *in-situ* synthesis by evanescent waves of a sensing polymer layer on the surface of a SPR device (Chegel et al., 2009). The polymer formulation consisted of a photo-initiator couple of methylene blue as the sensitizer dye and sodium *p*-toluenesulfinate as the reducing agent, and a mixture of *N,N*-methylene-bis-acrylamide and methacrylic acid for the backbone of the polymer. Polymerization was performed at the focal point of the SPR. Parameters such as monomer concentration and exposure time were used to control the polymer thickness (20-200 nm). Protein G was then immobilized on the polymer layer through carbodiimide-mediated

activation with *N*-hydroxysuccinimide, and the SPR sensor was used to monitor IgG (immunoglobulin G).

Recently, our group demonstrated for the first time the fabrication of ultra-thin MIP microdots by polymerization by evanescent waves (Fuchs et al., 2011). The authors achieved the fabrication of MIP microdots of thickness < 100 nm on glass substrates in only ten seconds. The morphology of the MIP microdot (size and porosity) could be tuned by adjusting the photosensitive formulation. The MIP microdots were imprinted with *N*-carbobenzyloxy-L-phenylalanine (Z-L-Phe), used as a model template, and showed specific binding towards the fluorescent analyte dansyl-L-phenylalanine (dansyl-L-Phe), and enantioselecticity towards the L-enantiomer over the D-enantiomer.

In this chapter, we describe the work performed in order to use this approach for the fabrication of optical sensing elements. Initially, fluorescent polymer microdots, imprinted with a model analyte, the herbicide 2,4-D, were synthesized by evanescent wave photopolymerization on three different surfaces: normal glass, gold-coated glass, and glass coated with a microstructured gold film containing nanomicroholes for optical enhancement. The influence of the surfaces (presence of gold, nano/microholes) on the morphology and the binding properties of the MIP was investigated. This work could then be used as the basis for the further development of plasmonic MIP nanosensors.

Table 3.1. *Chemical structures of compounds used in this study.*

Reagents (abbreviation)	Role	Molecular structure
2,4-dichlorophenoxyacetic acid (2,4-D)	Template & target	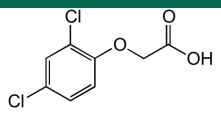
Citrinin	Template & target	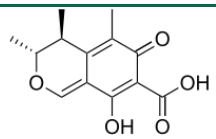
Adenosine monophosphate (AMP)	Target	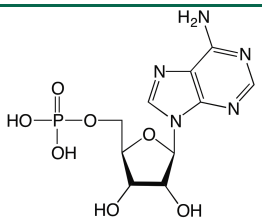
D-glucosamine-6-sulfate (GlcN-6S)	Target	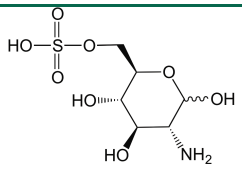
2,4-dichlorophenoxyacetic acid methyl ester (2,4-D-OMe)	Template analogue, competitor	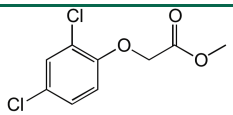
Phenoxyacetic acid (POAc)	Template analogue, competitor	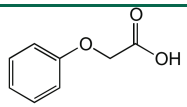
Fumonisin B_1 (FB_1)	Competitor	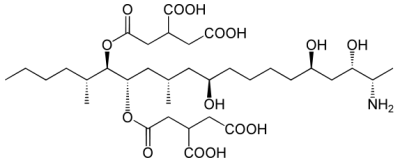

β-D-glucuronic acid (GlcA)	Competitor	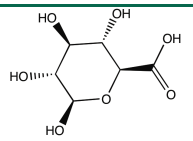
***N*-carbobenzyloxy-L-phenylalanine (Z-L-Phe)**	Competitor	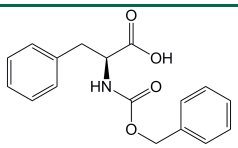
N-2-(6-(4-methylpiperazin-1-yl)-1,3-dioxo-1H-benzo[de]iso-quinolin- 2(3H)-yl-ethyl)acrylamide (FIM for "fluorescent monomer")	Functional monomer	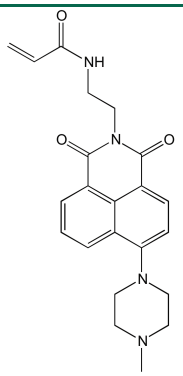
4-vinylpyridine (4-VPY)	Functional monomer	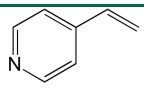
Ethylene glycol dimethacrylate (EDMA)	Cross-linker	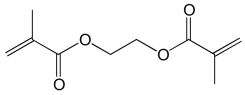
Bis(2,4,6-trimethylbenzoyl)phenyl phosphine oxide (Irgacure® 819)	Photoinitiator	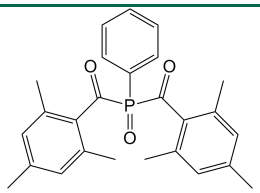
2,2'-azo-bis-(2,4-dimethylvaleronitrile) (ABDV, Vazo® 52)	Initiator	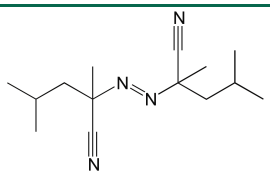

II. Materials and methods

II.1. Reagents and materials

All chemicals and solvents were of analytical grade and purchased from Sigma-Aldrich (St-Quentin Fallavier, France), unless otherwise stated. 2,2'-azobis(2,4-dimethylvaleronitrile) (ABDV) was obtained from DuPont Chemicals (Wilmington, USA). The initiator, bis(2,4,6-trimethylbenzoyl)-phenylphosphineoxide (Irgacure 819) was generously provided by Ciba Specialty Chemicals (Saint Fons, France). 4-vinylpyridine (4-VPY) was vacuum-distilled before use and all other reactants were employed before further purification. Water was purified using a Milli-Q system (Millipore, Molsheim, France).

The polystyrene optical waveguides were provided by Research International (Monroe, WA, USA) as part of the evanescent wave fiber optic biosensor Analyte 2000. The gold surfaces with nano/microholes were were generously provided by Dr. Jean-François Masson from the Université de Montréal (Canada). They were fabricated through the evaporation of gold on a glass substrate covered with a monolayer of silica nanoparticles that were then plasma-etched to reduce their size. The UV/visible multimode optical fiber SR300 used in this chapter was purchased from SEDI Fibres Optiques (Courcouronnes, France). The polystyrene optical fibers were from Research International (USA).

II.2. Synthesis and characterization of the fluorescent monomer "FIM" N-(2-(6-4-methylpiperazin-1-yl)-1,3-dioxo-1H-benzo[de]isoquinolin-2(3H)-yl-ethyl)acrylamide

The synthetic route for the preparation the fluorescent monomer FIM is described in the Materials and Methods part of Chapter 2.

II.3. Preparation of the molecularly imprinted polymers (MIPs) by precipitation polymerization

The formulations of the MIPs studied in this chapter are described in Table 3.2. For all MIPs, the template (2,4-D or citrinin), the functional monomers (FIM, 4-VPY), the cross-linker EDMA and the initiator ABDV were dissolved in the solvent, in a glass vial fitted with an airtight septum. The mixture was then sonicated at room temperature for 15 minutes and purged with nitrogen for 2 minutes on ice. Polymerization was done overnight at 40°C (50°C for **P3**) in a water-bath. The polymers were then washed with 3 rounds of methanol/acetic acid (7/3) and rinsed 3 times with methanol, followed by centrifugation. The particles were finally dried overnight under vacuum. The non-imprinted polymer (NIP) was prepared with the same protocol but in the absence of the template 2,4-D or citrinin.

Table 3.2. *Formulation of the MIP precursors solutions used in this study.*

Polymer	Template	Functional monomers	Cross-linker	Initiator	Solvent
P3	2,4-D (0.025 mmol)	FIM/4-VPY (0.05/0.05 mmol)	EDMA (0.5 mmol)	ABDV (0.016 mmol)	Methanol/water (4/1) (3 mL)
P-CIT1	Citrinin (0.02 mmol)	FIM (0.04 mmol)	EDMA (0.4 mmol)	ABDV (0.0084 mmol)	Methanol (1 mL)
P-CIT2	Citrinin (0.02 mmol)	FIM/4-VPY (0.04/0.04 mmol)	EDMA (0.4 mmol)	ABDV (0.0044 mmol)	Methanol/$CHCl_3$ (5/2) (700 μL)

II.4. Binding studies with the 2,4-D MIP P3

Fluorescence spectra were recorded using a Horiba Jobin-Yvon Fluorolog fluorescence spectrophotometer (Longjumeau, France). A stock solution of 500 nM of 2,4-D in methanol was prepared and stored in the dark at -20°C; and the polymer particles were suspended by sonication in methanol/water (4/1) at 0.5 mg/mL. From this stock suspension, a polymer concentration of 5 μg/mL was pipetted in 1.5 mL polypropylene microcentrifuge tubes and a volume ranging from 5 μL to 200 μL of 2,4-D solution was added so as to obtain final 2,4-D concentrations ranging from 2.5 nM to 100 nM. The final volume was adjusted to 1 mL with solvent. The tubes were incubated in the dark for 1 hour at ambient temperature on a tube rotator. The solutions were then transferred into a quartz cuvette to record their fluorescence emission spectra. Excitation was set at 390 nm. Fluorescence enhancement was calculated as follows: [(F-F0)/F0)*100, with F and F0 the emitted fluorescence intensity of MIP respectively in presence and in absence of the analyte. Experiments were performed in duplicate.

II.5. Binding studies of the citrinin MIPs P-CIT1 and P-CIT2

Fluorescence spectra were recorded using a Horiba Jobin-Yvon Fluorolog fluorescence spectrophotometer (Longjumeau, France). A stock solution of 10 μg/mL of citrinin in methanol was prepared and stored in the dark at -20°C. The polymer particles were suspended by sonication in methanol at 2 mg/mL. From this stock suspension, a polymer concentration of 0.04 mg/mL was pipetted in 1.5 mL polypropylene microcentrifuge tubes and a volume ranging from 50 μL to 250 μL of citrinin solution was added so as to obtain final citrinin concentrations ranging from 0.5 to 2.5 μg/mL. The final volume was adjusted to 1 mL with solvent. The tubes were incubated in the dark for 1 hour at ambient temperature on a tube rotator. The suspensions were then put into a quartz cuvette for recording of their fluorescence emission spectra. Excitation was set at 390 nm. Fluorescence enhancement was calculated as follows: [(F-F0)/F0)*100, with F and F0 the emitted fluorescence intensity of MIP respectively in presence and in absence of the analyte. Experiments were performed in duplicate.

II.6. Coating of the MIP particles P3 or P-CIT2 on the polystyrene optical waveguides and binding studies

The optical fiber was immersed into a four milliliter glass vial containing a suspension of 20 mg/mL of MIP **P3** or 5 mg/mL of MIP **P-CIT2** in water with 1.5% polyvinyl alcohol (PVA). The mixture was heated at 80°C in a water-bath under gentle magnetic agitation. After 30 minutes, the mixture with the optical fiber was let to cool down to room temperature under gentle agitation. The fiber was then removed from the vial, resulting in an immobilization of the MIP particles on the fiber surface, fixed by PVA.

For binding studies, the MIP-coated optical fibers were immersed into amber-colored four-milliliter glass vials containing solutions of

- 2,4-D (0, 1, 2.5, 5, 10, 25 and 50 nM) in methanol/water (4/1), for the MIP **P3** (10 minutes incubation)
- citrinin (1 and 2.5 μg/mL, i.e. 4 and 10 μM) in methanol, for the MIP **P-CIT2** (30 minutes incubation)

After incubation, the excitation (λ_{EX}=410 nm) was performed through the bifurcated fiber optic bundle of the spectrofluorimeter, through the lens of the fiber optic waveguide (Figure 3.3). λ_{EX}=410 nm was chosen in order to avoid UV-absorption of polystyrene, and measurements were performed in the

dark, with the fiber remaining immersed into the analyte solution. Fluorescence emission spectra were recorded through the same fiber optic bundle of the spectrofluorimeter. Experiments were performed in duplicate.

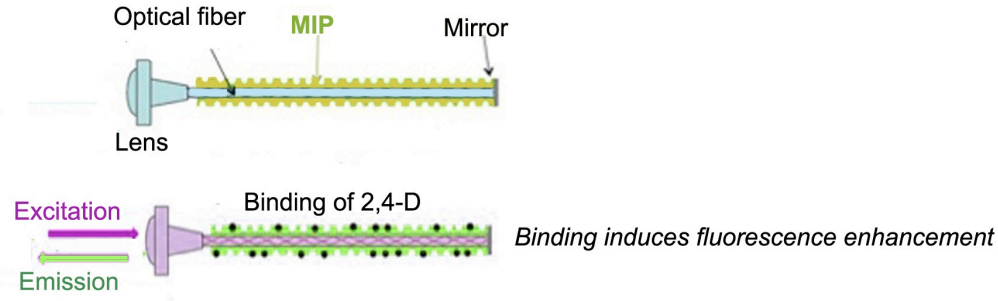

Figure 3.3. *Schematic principle of the polystyrene evanescent wave fiber optic waveguide coated with fluorescent MIP particles. Excitation (λ_{EX}) at 410 nm is performed with the fiber optic bundle of the Horiba Fluorolog spectrofluorimeter and fluorescence emission (λ_{EM}=515 nm) of the fluorescent MIP particles is collected via the same fiber optic bundle of the spectrofluorimeter.*

II.7. In-situ polymerization of the MIP on the fiber optic waveguides

The polystyrene fiber was immersed into a brown vial containing the pre-polymerization mixture of MIP **P3-b** (Table 3.3), and polymerization was performed by injecting the light (λ_{EX}= 410 nm, slit 5 nm) through the lens of the polystyrene fiber, with the fiber optic bundle of the Fluorolog, during 20 minutes, resulting in a MIP-coated fiber optic waveguide.

Table 3.3. *Formulation of the MIP* ***P3-b*** *polymerized in-situ on the fibers.*

Polymer	Template	Functional monomers	Cross-linker	Initiator	Solvent
P3-b	2,4-D (0.03 mmol)	FIM/4-VPY (0.06/0.06 mmol)	EDMA (0.6 mmol)	Irgacure 819 (0.026 mmol)	Methanol/water (4/1) (3.5 mL)

II.8. Fabrication of ultra-thin MIP microdots by evanescent-wave polymerization

The continuous gold films and the gold microholes arrays were fabricated and provided by Dr. Jean-François Masson (Université de Montréal, Canada).
The continuous gold films were prepared by coating directly a clean glass coverslip with a 2 nm Ti adhesion layer and a 50 nm Au film (Live et al., 2010). The gold nano/microholes arrays were fabricated by nanosphere lithography as described by Correia-Ledo et al., 2012.

A 375 nm diode laser was used as actinic light source, and light was carried by an UV/visible multimode optical fiber (reference SR300) with a silica core of diameter 300 μm. Three substrates were studied: normal glass, continuous gold film and gold microholes surface. To avoid any residual reflection between the prism and the substrate, 100 μL of an index match solution (n_1=1.52) was uniformly spread on the top of the prism before the substrate (glass or gold surface) was placed over it. Then 10 μL of the photosensitive MIP precursors solution **P2** (n_2=1.36) (Table 3.4) were deposited on the substrate (glass or gold) and covered with a microscope glass slide (Figure 3.4). The whole system was adjusted on a x-y table, and the polymerization performed with a laser power of 8 mW (spot size: around 3 mm x 5 mm). The irradiation time was set to 2 minutes, resulting in polymer

microdots of size around 3 mm x 5 mm. After polymerization, the substrate was carefully separated from the microscope slide, and unreacted monomers were removed from the substrate by rinsing with ethanol for a few seconds. The substrate was then dried under an air stream.

Table 3.4. *Formulation of the MIP* ***P2*** *used for the synthesis of microdots by evanescent-wave polymerization*

Polymer	Template	Functional monomers	Cross-linker	Initiator	Solvent
P2	2,4-D (0.02 mmol)	FIM/4-VPY (0.04/0.04 mmol)	EDMA (0.4 mmol)	Irgacure 819 (0.008 mmol)	Methanol/water (4/1) (1 mL)

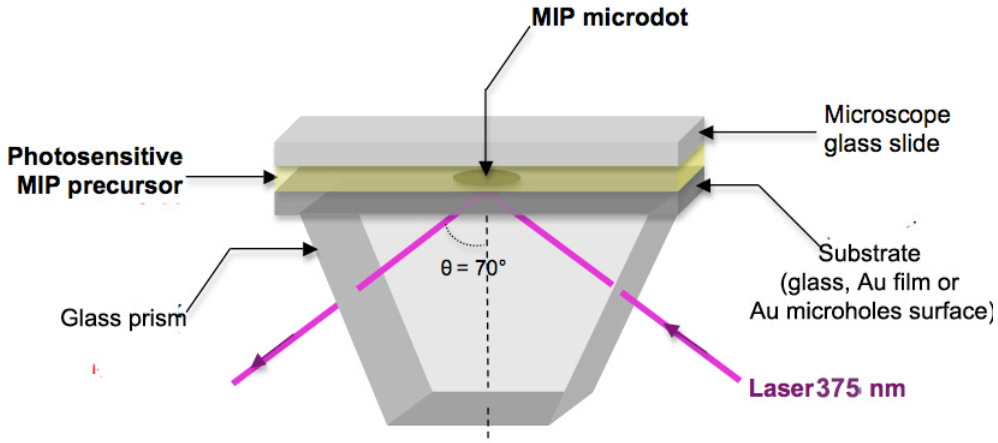

Figure 3.4. *Scheme showing the polymerization by evanescent waves of MIP microdots. Total internal reflection occurs. Note: index match solution deposited between the glass prism and the polymerization surface.*

II.9. Analysis of ultra-thin MIP microdots

II.9.1. Characterization

The surface morphology of the MIP microdots on the gold substrates (film and microholes) were analyzed by a Witec Alpha 300 atomic force microscope (AFM) (Ulm, Germany). The AFM was used in contact mode with Al-coated tips (force constant 0.2 N/m).

II.9.2. Analyte adsorption tests

The substrates bearing the MIP microdots were placed in a glass Petri dish and were incubated for 1 hour in 2 mL of a 0.5 μM 2,4-D solution in methanol/water (4/1), under gentle agitation and protected from light. After incubation, the microdots were briefly rinsed for 2 minutes with methanol and dried with nitrogen prior to fluorescence measurements. The fluorescence of the polymer microdots was measured using a Leica DMI6000 B fluorescence microscope, equipped with a 480 nm excitation / 520 nm emission filter cube (L5). The optical microscope parameters such as exposure time, gain and intensity were kept constant during the acquisition images of the MIP and NIP microdots. The fluorescence intensity values were then quantified using the software ImageJ (public domain, http://rsb.info.nih.gov/ij/), and were corrected from the fluorescent background of the support. Experiments were performed at least in duplicate.

III. Results and discussion

III.1. Sensing of biological and environmental analytes using an evanescent wave fiber optic waveguide coated with a signaling naphthalimide-based imprinted polymer

III.1.1. Sensing of 2,4-D

III.1.1.1 Synthesis and characterization of the 2,4-D imprinted polymer particles

In molecular imprinting, the formation of specific binding sites relies on the interactions taking place between the template and functional monomers. For this reason, prior to the preparation of the fluorescent 2,4-D imprinted polymer, the process of fluorescence enhancement of the signaling monomer FIM was verified with spectrofluorimetric titrations of FIM with increasing concentrations of 2,4-D (2.5 – 100 nM in methanol/water (4/1)), as described in Chapter 2, Figure 2.20. The signal enhancement of FIM was observed starting from 5.10^{-5} equivalent of 2,4-D. The concentration-dependence of the fluorescence enhancement of FIM was then used to determine the affinity of FIM for 2,4-D (Feng et al., 1998). The dissociation constants K_D of the binding sites were calculated as follows: the change in the MIP fluorescence intensity is attributed to the formation of the complex between FIM and 2,4-D described by the equilibrium (1):

FIM + *n* 2,4-D ↔ complex [FIM-2,4-D] (1)

The association constant of the complex is thus defined as:

$K_A = [complex] / ([FIM][2,4\text{-}D]^n)$ (2)

If $[FIM]_0$ is the overall amount (bound or unbound) of fluorescent monomer, then $[FIM]_0 = [complex] + [FIM]$, with [FIM] the unbound amount of fluorescent monomer. We also define F0 and F as the emitted fluorescence intensity of FIM respectively in the absence and in the presence of different concentrations of 2,4-D. If F is due to $[FIM]_0$, the change in fluorescence intensity (F-F0) is contributed by [complex]. This gives the relationship between the fluorescence intensity and concentrations of FIM that is $[complex]/[FIM] = (F-F0)/F0$, with the condition $[complex] << [FIM]_0$, so we can attribute F0 to [FIM]. Finally this leads to the following equation:

$\log((F-F0)/F0) = \log K_A + n \log[2,4\text{-}D]$ (3)

Thus, according to (3), the enhancement of the MIP fluorescence intensity of was used to estimate the binding constant K_A and the ratio 2,4-D:FIM in the complex. The inset in Figure 2.20 (Chapter 2) shows a linear plot for log ((F-F0)/F0) vs log[2,4-D]. The slope and the intercept gave us the following values: $K_A=1.83*10^8$ M^{-1}, and *n*=1.08. From this study, it was concluded that 2,4-D has a high affinity for the monomer FIM, as the dissociation constant K_D is estimated to be 5.5 nM, and that there is a single site for the interaction between 2,4-D and FIM, which is consistent with our theory of interaction between the piperazinyl nitrogen of FIM and the carboxylic acid moiety of 2,4-D.

The 2,4-D MIP **P3** (Table 3.5) was then synthesized by precipitation polymerization and nanoparticles of size ranging from around 150 nm to 500 nm were obtained (scanning electron microscopy (SEM), Figure 3.5).

Table 3.5. *Formulation of the 2,4-D MIP* ***P3*** *obtained by precipitation polymerization*

Polymer	Template	Functional monomers	Cross-linker	Initiator	Solvent
P3	2,4-D (0.025 mmol)	FIM/4-VPY (0.05/0.05 mmol)	EDMA (0.5 mmol)	ABDV (0.016 mmol)	Methanol/water (4/1) (3 mL)

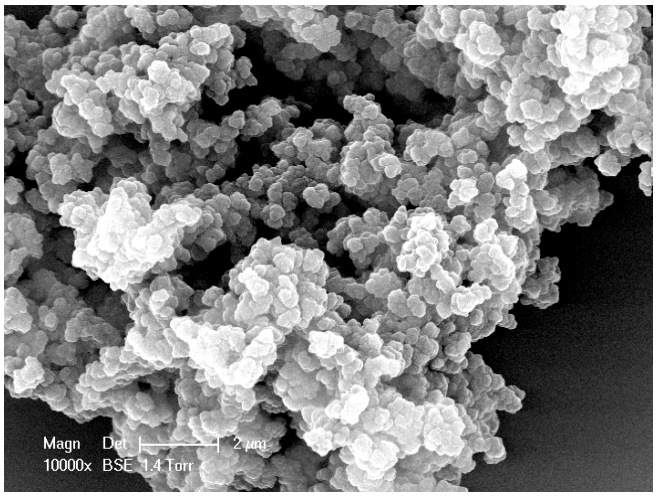

Figure 3.5. *Scanning electron micrograph of MIP* ***P3****. The scale bar corresponds to 2 μm.*

The binding properties of the MIP were evaluated by spectrofluorimetric titrations of the MIP with 2,4-D. For this study, suspensions of 5 μg/mL of MIP and NIP particles were incubated with 2.5 – 100 nM of 2,4-D in methanol/water (4/1). As shown in Figure 3.6A, the fluorescence response of the MIP increased with increasing concentrations of 2,4-D, with a limit of detection of 2.5 nM; and the MIP exhibited a higher fluorescence response than the NIP, allowing us to conclude about the specificity of the fluorescence enhancement.

Figure 3.6B shows the linear plots for log ((F-F0)/F0) vs log[2,4-D] for the MIP, with two distinct linear portions that indicate two types of binding sites: high-affinity sites and low-affinity sites. High-affinity sites are the specific imprinted sites while the low-affinity sites are source of non-specific binding. The respective values of K_A and *n* were calculated from the intercepts and the slopes. For high-affinity sites, the binding constant K_A was $8.5.10^6$ M^{-1}, giving a dissociation constant K_D=0.12 μM, and *n*=0.92, which means that there is a ratio FIM:2,4-D = 1:1. For low-affinity sites, the values were found to be K_A= 510 M^{-1}, giving K_D=2 mM, and *n*= 0.41, giving a ratio FIM:2,4-D = 2:1. For low concentrations of 2,4-D (< 25 nM), high-affinity sites are preferentially occupied. Then with increasing concentrations of 2,4-D (25-100 nM), the analyte also binds to low-affinity sites, which also explains the increasing non-specific binding for the NIP.

The LOD achieved was 2.5 nM, which is 50 times lower than the tolerated amount in drinking water of 30 μg/L, i.e. 135 nM, recommended by the World Health Organization (*Guidelines for drinking water quality*, 4th ed., 2011).

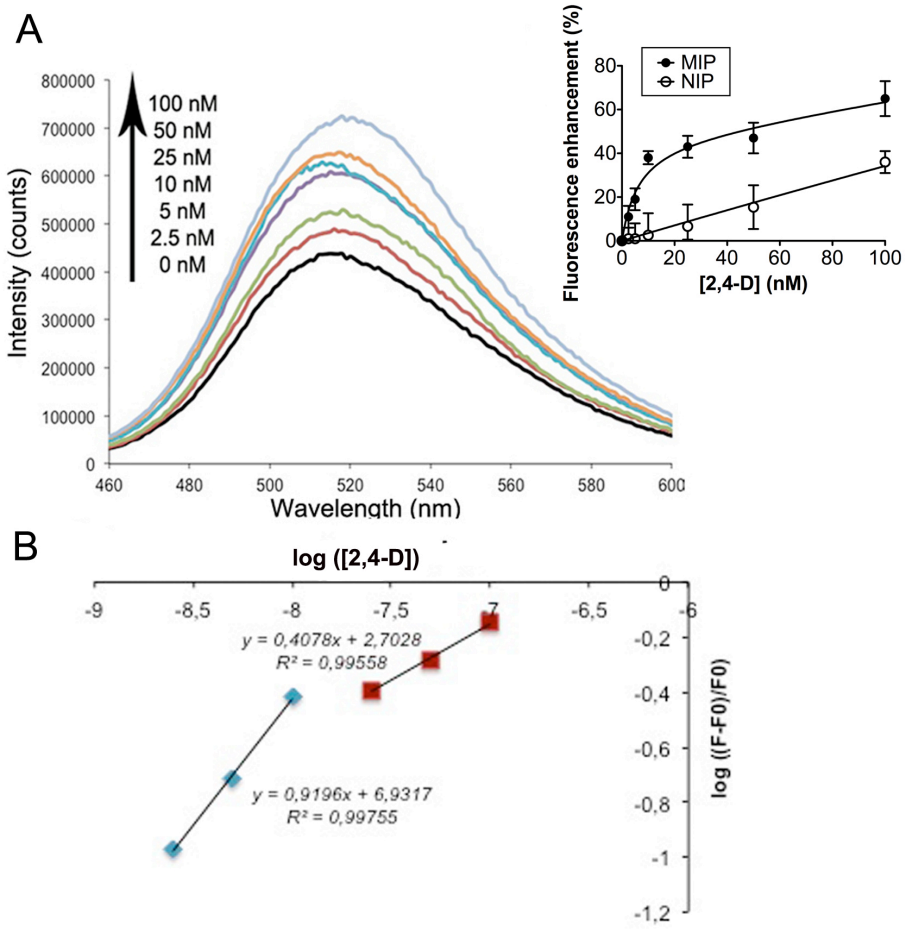

Figure 3.6. *(A) Fluorescence spectra of MIP (5 μg/mL) before and after incubation with 2,4-D (2.5, 5, 10, 25, 50, 100 nM) in methanol/water (4/1) (λ_{EX} = 390 nm). Inset: fluorescence response of MIP and NIP* ***P3*** *(5 μg/mL in methanol/water (4/1)) as function of 2,4-D concentration ($\lambda_{EX/EM}$ = 390/515 nm). (B) Linear plots of log (concentration of 2,4-D in M) vs log (fluorescence enhancement) with fluorescence enhancement defined as (F-F0)/F0 with F0 and F as the emitted fluorescence intensity of FIM respectively in the absence and in the presence of different concentrations of 2,4-D.*

To assess the selectivity of the MIP, similar fluorescence binding assays were performed with two structurally related compounds, 2,4-dichlorophenoxyacetic acid methyl ester (2,4-D-OMe), the carboxyl group of which is blocked, and phenoxyacetic acid (POAc), lacking the two ring chlorines; and with two non-related compounds, *N*-carbobenzyloxy-L-phenylalanine (Z-L-Phe) and β-D-glucuronic acid (GlcA), which also possess carboxylic acid moieties, but present very different structures from 2,4-D (Table 3.1). Hence 2,4-D-OMe, POAc, Z-L-Phe and GlcA should not be recognized by the MIP and thus cause no fluorescence enhancement. In the same way as described above, suspensions of 5 μg/mL of MIP particles were incubated in methanol/water (4/1) with 2.5 nM, 25 nM and 100 nM of each competitor. As shown in Figure 3.7, for all concentrations of the four competitors tested, no or little fluorescence enhancement (<20%) was observed, confirming the selectivity of the MIP for 2,4-D. Among the competitors, the analyte that showed the best enhancement was POAc (with 22% of fluorescence enhancement at 25 nM), which shows a very similar structure to 2,4-D, but is lacking the two ring chlorines and is thus less reactive. However, the enhancement was twice lower than the value obtained with 25 nM 2,4-D. Therefore, these results confirm the selectivity of our MIP for its imprinting template 2,4-D.

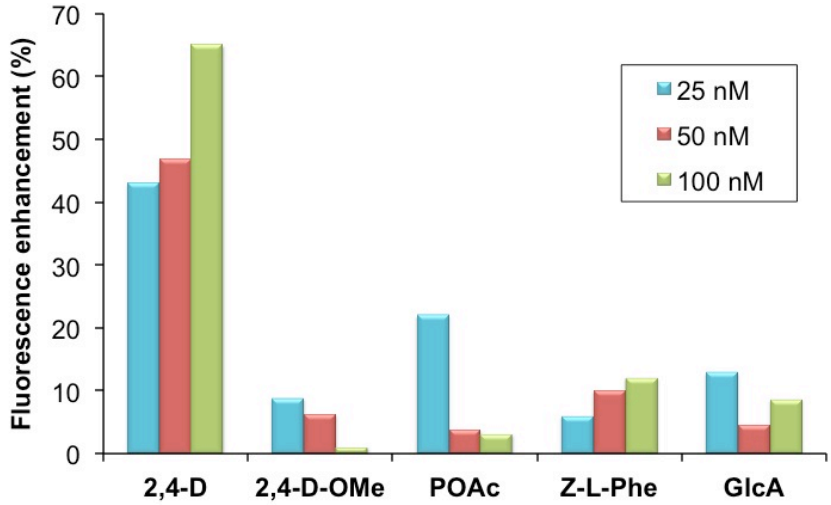

Figure 3.7. *Fluorescence enhancement response of the MIP particles* ***P3*** *(5 μg/mL) after incubation with 2,4-D, and the analogues 2,4-D-OMe and POAc, and the non-related compounds Z-L-Phe and GlcA, in methanol/water (4/1) (λ_{EX}=390 nm ; λ_{EM}=515 nm).*

III.1.1.2. Coating of 2,4-D MIP particles obtained by precipitation polymerization on the fiber optic waveguides

Our signaling MIP being successfully characterized, we aimed to apply it for optical sensing by integration of the MIP into a fiber optic device. For this application, we used 4-cm-long injection-molded tapered polystyrene optical fibers that possess a mirror at their end, enabling us to inject and collect the light signal through the same lens. These polystyrene waveguides are especially designed for an evanescent wave fiber optic biosensor manufactured by Research International (USA) and are normally coated with antibodies for fluoroimmunoassays (Lim, 2003). In our study, the MIP particles were coated on the fiber by using PVA as glue (Surugiu et al., 2001) (Figure 3.8). PVA was found to be suitable for this purpose as it dissolves in hot water for the preparation of the polymer suspension, but it is not soluble anymore under the conditions of the assay. SEM images (Figure 3.9) show a rather homogeneous coating of the MIP particles on the fiber, which is visible on the image to the right.

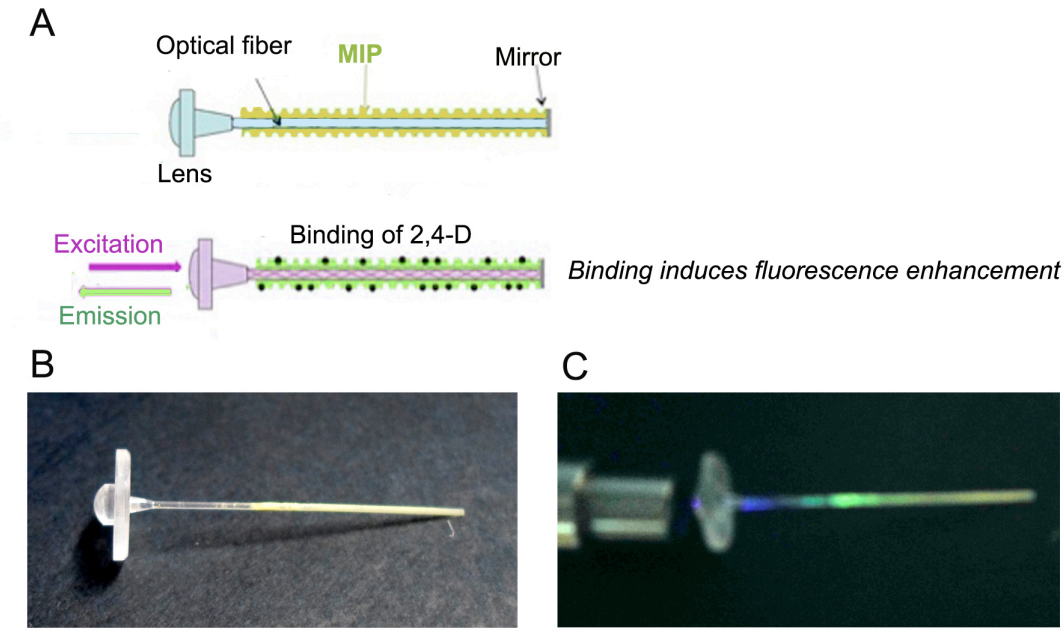

Figure 3.8. *(A) Schematic principle and (B) photograph of the polystyrene evanescent wave fiber optic waveguide coated with the fluorescent 2,4-D MIP particles. (C) Excitation (λ_{EX}) at 410 nm with the fiber optic probe of the Horiba Fluorolog spectrofluorimeter and fluorescence emission (λ_{EM}=515 nm) of the fluorescent MIP particles.*

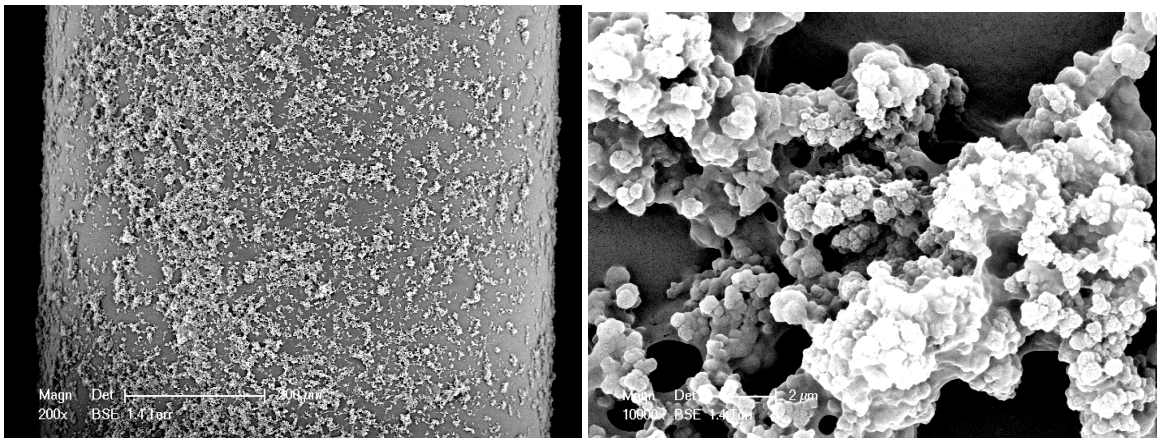

Figure 3.9. *Scanning electron micrographs of the surface of the 2,4-D-MIP-coated optical fiber. The scale bars correspond to (left) 200 μm and to (right) 2 μm.*

The MIP fluorescence response was measured after 10 minutes incubation with 2,4-D in methanol/water (4/1). Spectra are shown in Figure 3.10, and once again, the concentration-dependence of the MIP fluorescence response upon binding to 2,4-D was demonstrated, as well as the specificity of the MIP fluorescence enhancement compared to the NIP. The MIP-coated fiber optic device exhibited a limit of detection of 1 nM, and the limit of quantification was found to be 2.5 nM, indicating the very high sensitivity of our sensor. The results obtained with the fiber were congruent with those obtained with the MIP in batch.

Finally, to assess the selectivity of our device, the MIP-coated fiber was incubated 10 minutes with 5 nM 2,4-D-OMe, 5 nM POAc or a mixture of 5 nM of Z-L-Phe and 5 nM of GlcA in methanol/water (4/1). As a result (Figure 3.11), smaller fluorescence enhancement (<25%) was

measured, compared to the fluorescence enhancement of around 67% that occurred in response to incubation with 5 nM 2,4-D.

To summarize, this MIP-coated fiber optic device showed comparable sensing properties than the fiber optic sensor based on a MIP microtip described in Chapter 2, in terms of sensitivity, specificity and selectivity, even if with the previous set-up, we achieved a LOD of 250 pM with the incorporation of gold nanoparticles into the MIP.

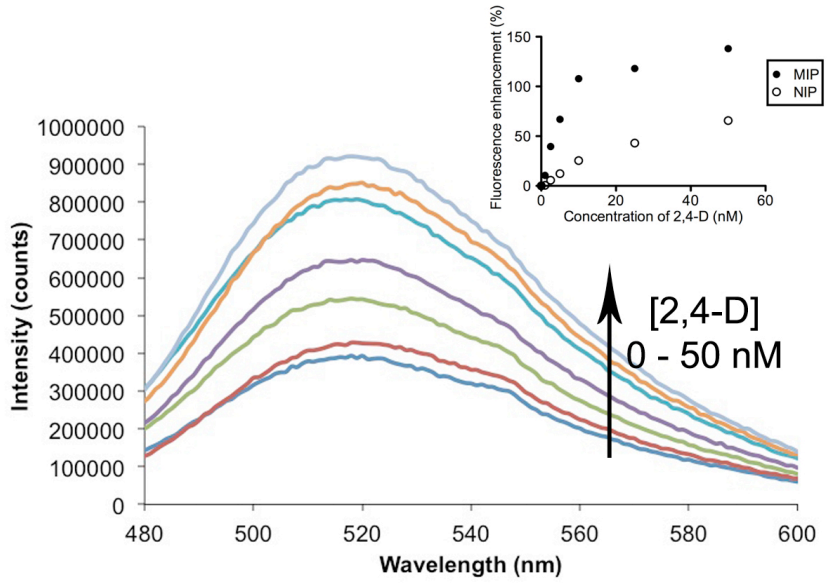

Figure 3.10. *Fluorescence spectra from the MIP-coated fiber optic waveguide before and after incubation with 2,4-D (1-50 nM) in methanol/water (4/1) (λ_{EX} = 410 nm). Inset: fluorescence response of MIP and NIP-coated fiber optic waveguides as a function of 2,4-D concentration in methanol/water (4/1).*

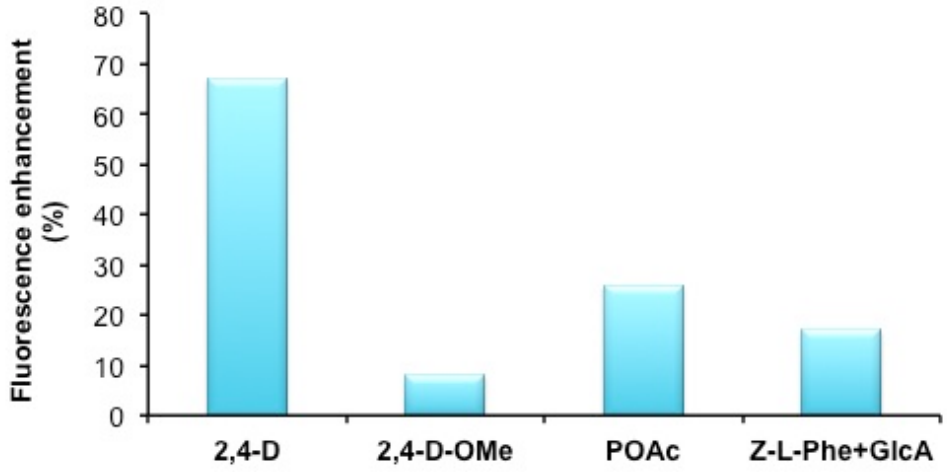

Figure 3.11. *Fluorescence enhancement response of the MIP-coated optical fiber after incubation with 5 nM 2,4-D, and 5 nM of the analogues 2,4-D-OMe and POAc, and a mixture of the non-related compounds Z-L-Phe and GlcA, in methanol/water (4/1) (λ_{EX}=390 nm ; λ_{EM}=515 nm).*

III.1.1.3. Fluorescence titrations studies of the 2,4-D MIP in other solvents

Sensing experiments with FIM were performed in methanol/water (4/1) that was the solvent of synthesis of our 2,4-D MIPs. However, it is interesting to check the behavior of the fluorescent monomer in other solvents, in particular in pure aqueous media.

Titration studies of the fluorescent monomer FIM and the batch of particles **P3** were performed with 2,4-D (2.5 – 100 nM) as well in distilled water (pH ≈ 6.6), water + 0.1% Tween 20 and in sodium phosphate buffer (pH=7, 20 mM), but no concentration-dependent fluorescent enhancement was obtained (not illustrated). This may be explained by the strong hydrogen bonding which may occur between FIM and the water molecules that probably interfere with the binding between 2,4-D and the monomer. Moreover, in aqueous media of pH < 8, the monomer FIM is already partly protonated by the water molecules, which means that high concentrations of 2,4-D are needed to interact with FIM and generate the process of fluorescence enhancement. However, we did not perform this experiment as very high concentrations of 2,4-D are not interesting for sensing purposes.

III.1.1.4. In-situ polymerization by evanescent waves of a fluorescent 2,4-D MIP on the fiber optic waveguides

Having established that MIP particles were synthesized beforehand by precipitation polymerization can be used for sensing in combination with these optical fibers, we now set out to synthesize this MIP *in-situ* by evanescent wave photopolymerization directly on the fibers. The actinic light source came from the optical fiber bundle of the Horiba Fluorolog spectrofluorimeter, and polymerization was carried out with an irradiation time of 20 minutes. The 2,4-D MIP formulation used is shown in Table 3.6.

Table 3.6. *Formulation of the MIP* ***P3-b*** *polymerized in-situ on the fibers.*

Polymer	Template	Functional monomers	Cross-linker	Initiator	Solvent
P3-b	2,4-D (0.03 mmol)	FIM/4-VPY (0.06/0.06 mmol)	EDMA (0.6 mmol)	Irgacure 819 (0.026 mmol)	Methanol/water (4/1) (3.5 mL)

After polymerization and template removal, the MIP-coated fiber was incubated for 15 minutes with 1 nM 2,4-D in methanol/water (4/1), but no enhancement was observed. However, incubation with 10 nM 2,4-D in methanol/water yielded a fluorescence enhancement of around **+ 13%**. The binding was specific, as no enhancement was observed for a NIP-coated fiber after incubation with 10 nM 2,4-D (Figure 3.12).

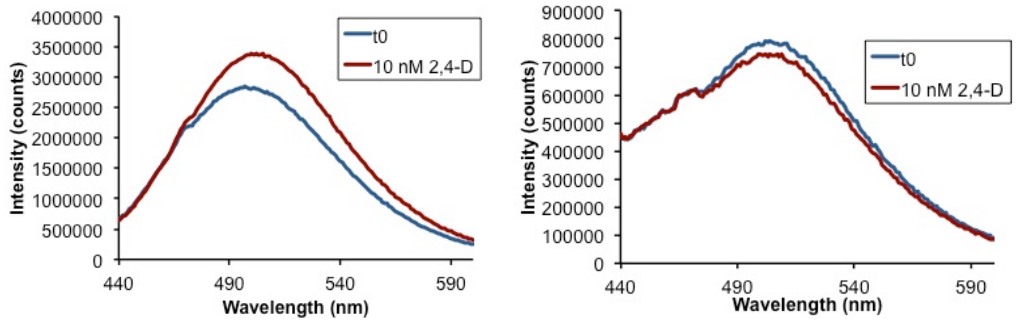

Figure 3.12. *Fluorescence spectra of the (left) MIP and (right) the NIP-coated fiber before (t0) and after incubation with 10 nM 2,4-D in methanol/water (4/1). (λ_{EX} = 410 nm).*

We can observe that the MIP-coated device obtained by *in-situ* polymerization is less sensitive than the previous one, with the MIP particles synthesized beforehand. This is probably due to the fact that less polymer is coated onto the fiber. Indeed, SEM images (Figure 3.13) show the *in-situ* polymerization did not lead to a homogeneous coating of the fiber. One can also notice that the morphology of the polymer film is different from the film consisting of preformed particles (Figure 9). Furthermore, an irradiation of 20 minutes may affect the properties of the fluorescent monomer FIM. For this reason, we finally used for further studies the device with the MIP particles synthesized beforehand. However, we have demonstrated that it was possible to synthesize *in-situ* the MIP particles on the fiber by evanescent-wave polymerization. The sensing properties of the device need now to be optimized, probably by an optimization of the protocol of *in-situ* polymerization, for example by using an actinic light source with a higher power.

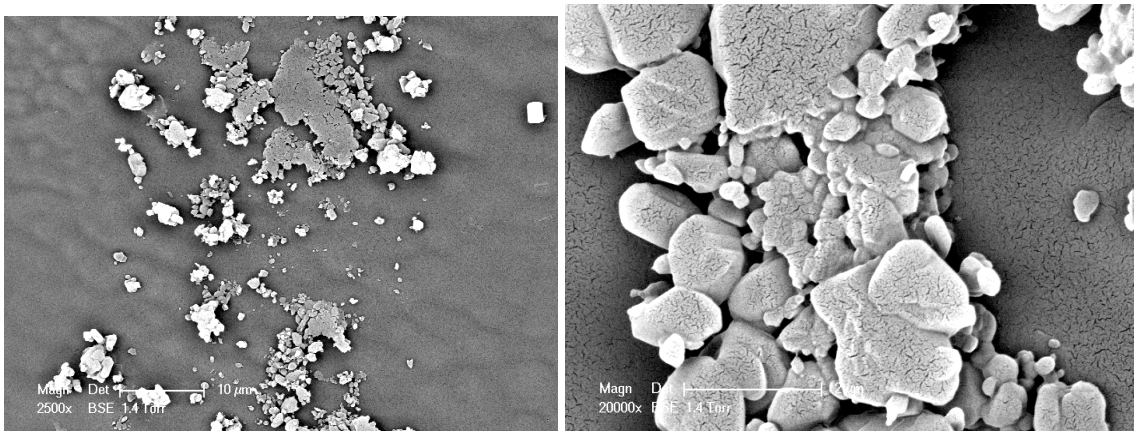

Figure 3.13. *Scanning electron micrographs of the surface of the 2,4-D-MIP-coated optical fiber by in-situ polymerization. The scale bars correspond to (left) 10 µm and to (right) 2 µm.*

III.1.2. Sensing of the mycotoxin citrinin

III.1.2.1. Synthesis and characterization of citrinin-imprinted polymer particles

The sensing properties of the MIP-coated evanescent-wave fiber optic waveguides have been demonstrated with the herbicide 2,4-D. We now wanted to apply this sensing device for the recognition of a mycotoxin, the main target of this thesis. We have chosen the mycotoxin citrinin, which possesses a carboxyl group that is likely to interact with the signaling monomer FIM (Table 1). Prior to the preparation of the fluorescent citrinin-imprinted polymer, the process of fluorescence enhancement of the signaling monomer FIM was verified with spectrofluorimetric titrations of FIM with increasing concentrations of citrinin in methanol. As a result (Figure 3.14), the fluorescence enhancement of FIM was observed to be concentration-dependent and increased with increasing concentrations of citrinin, confirming that FIM could be used as a functional monomer to imprint citrinin. The signal enhancement of FIM was observed starting from 0.02 equivalent of citrinin.

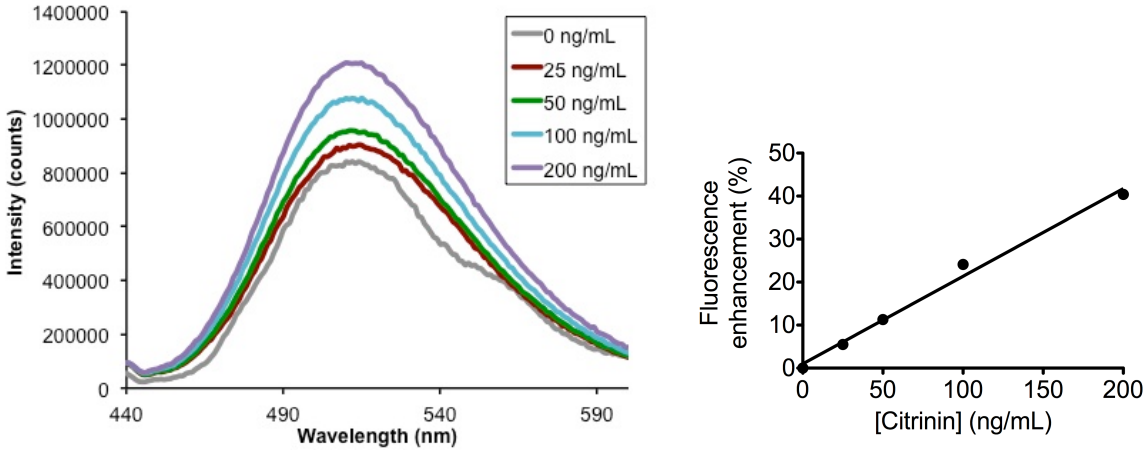

Figure 3.14. *Spectrofluorimetric titrations in methanol of FIM (5 μM) with increasing concentrations of citrinin (25, 50, 100, 200 ng/mL, i.e. 0.1 μM, 0.2 μM, 0.4 μM, 0.8 μM) (λ_{EX} = 390 nm) (left) fluorescence spectra and (right) fluorescence responses of FIM as function of citrinin concentration.*

In preliminary experiments, we synthesized by precipitation polymerization the MIP **P-CIT1** containing FIM as the functional monomer (Table 3.7). A ratio template:functional monomer of 1:2 was chosen, in order to ensure the formation of the pre-polymerization complex. In the previous chapter, a citrinin-imprinted polymer was fabricated under the format of an end-of-fiber microtip, and the MIP successfully showed specific binding towards citrinin. The MIP formulation contained FIM and 4-VPY as co-functional monomers. However, we also wanted see if in the case of citrinin, FIM could be used as the sole functional monomer. The binding properties of the MIP were evaluated with spectrofluorimetric titrations of the MIP with citrinin. For this study, suspensions of 0.04 mg/mL of MIP and NIP particles were incubated with solutions of citrinin in methanol, with concentrations ranging from 25 ng/mL (0.1 μM) to 2.5 μg/mL (10 μM). However, for both MIP and NIP and all concentrations of citrinin, no fluorescence enhancement was observed, suggesting that the imprinting process of citrinin did not take place in the polymer **P-CIT1.**

Thus we used another MIP formulation adapted from the successful formulation **P4** in Chapter 2, for the synthesis of particles by precipitation polymerization, including 4-VPY as co-functional monomer (MIP **P-CIT2**, Table 3.7). We also reduced the amount of solvent, as a too high dilution of monomers can affect the strength of the interactions between the template and the monomers. As a result, a batch of nanoparticles of size ranging from around 150 nm to 500 nm were obtained (Figure 3.15).

Table 3.7. *Formulation of the citrinin-imprinted polymers obtained by precipitation polymerization.*

Polymer	Template	Functional monomers	Cross-linker	Initiator	Solvent
P-CIT1	Citrinin (0.02 mmol)	FIM (0.04 mmol)	EDMA (0.4 mmol)	ABDV (0.0084 mmol)	Methanol (1 mL)
P-CIT2	Citrinin (0.02 mmol)	FIM/4-VPY (0.04/0.04 mmol)	EDMA (0.4 mmol)	ABDV (0.0044 mmol)	Methanol/$CHCl_3$ (5/2) (700 μL)

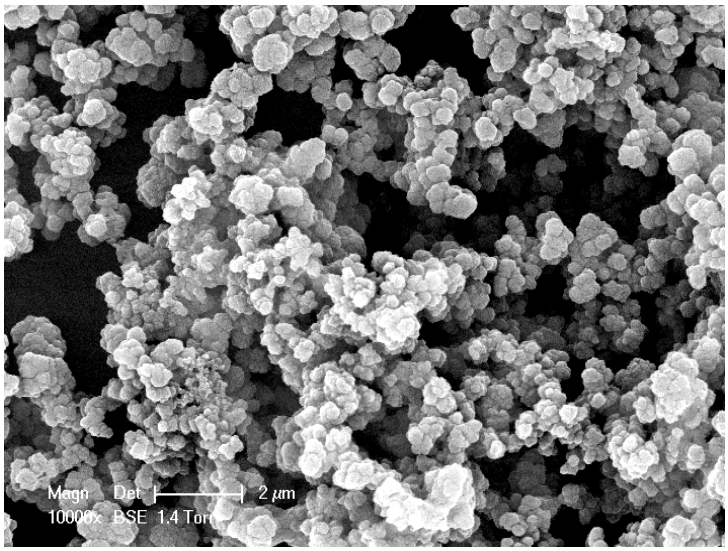

Figure 3.15. *Scanning electron micrograph of MIP* ***P-CIT2****. The scale bar corresponds to 2 μm.*

The binding properties of the MIP **P-CIT2** were evaluated with spectrofluorimetric titrations of the MIP with citrinin. Suspensions of 0.04 mg/mL of MIP and NIP particles were incubated with solutions of citrinin in methanol, with concentrations ranging from 50 ng/mL (0.2 μM) to 2.5 μg/mL (10 μM). As a result, a fluorescence enhancement of the MIP was observed for concentrations of citrinin starting from 0.5 μg/mL (2 μM) (Figure 3.16). The fluorescence enhancement was specific and concentration-dependent. To assess the selectivity of our MIP, the MIP particles were incubated with 4 μM and 10 μM of two other non-related compounds possessing carboxyl groups, namely 2,4-D and the mycotoxin Fumonisin B_1 (FB_1) that possesses four carboxyl groups. Figure 3.17 shows that compared to citrinin, a 3.5 to 4 times lower fluorescence enhancement observed for 2,4-D; and for FB_1, the fluorescence enhancement was 2.5 to 4 times lower. These results confirm the selectivity of MIP for citrinin.

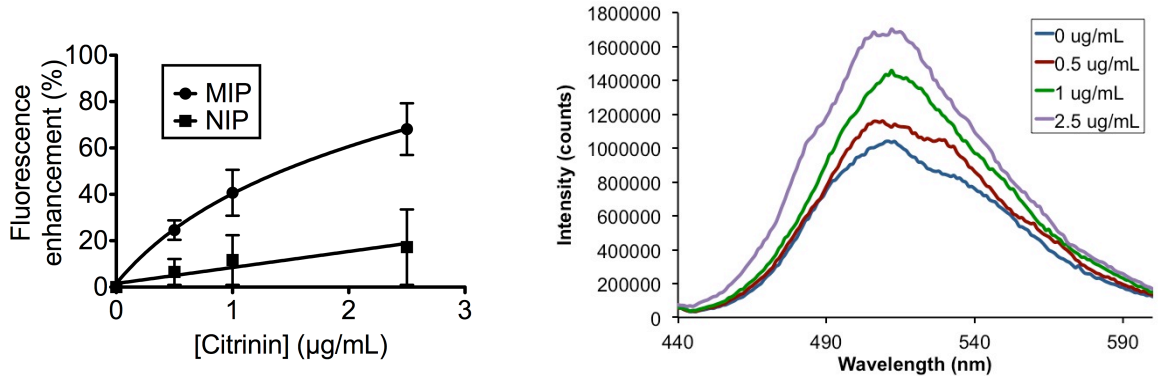

Figure 3.16. *(Left) Fluorescence enhancement responses of MIP and NIP particles* ***P-CIT2*** *(0.04 mg/mL) and (right) fluorescence spectra of MIP particles after incubation with increasing concentrations of citrinin in methanol. (λ_{EX} = 390 nm; λ_{EM} = 515 nm).*

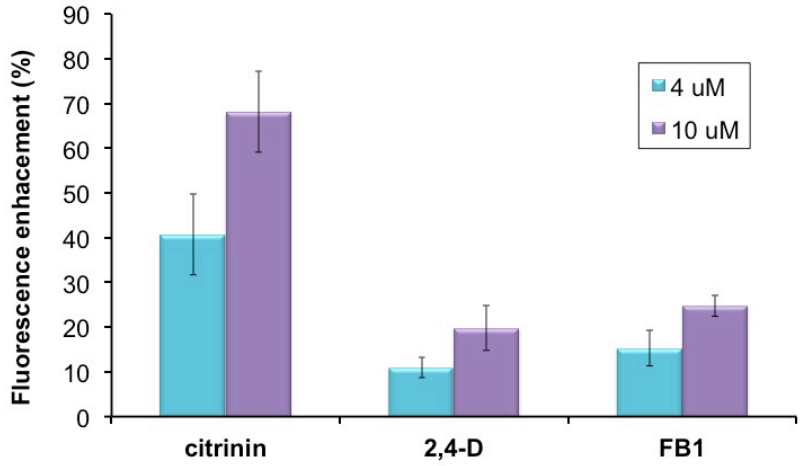

Figure 3.17. *Fluorescence signal of the MIP particles* ***P-CIT2*** *(0.04 mg/mL) after incubation with citrinin, and the non-related compounds 2,4-D and FB_1 in methanol. (λ_{EX}=390 nm ; λ_{EM}=515 nm).*

The LOD of 0.5 μg/mL (2 μM) is rather high, as the maximum residue limit (MRL) for citrinin set in China in dry functional kojic red rice is 50 ng/g, which is 10 times below our LOD. No MRL was set by the European Union, but the European Food Safety Authority estimated the maximal concentration of citrinin that would result in no concern for nephrotoxicity, that is between 19 and 100 ng/g in grains and grain-based products, for average consumers. However, given the good molecular recognition properties of the MIP **P-CIT2**, we decided to keep at the moment this formulation for the coating on the optical fibers.

III.1.2.2. Coating of the citrinin-imprinted polymer particles obtained by precipitation polymerization on the fiber optic waveguides

Now that the molecular recognition properties of the MIP **P-CIT2** have been successfully demonstrated, the MIP an NIP particles were coated on the fibers using PVA as glue, following the protocol described above (see Figure 3.18 for an SEM image of the coated fiber)). For sensing experiments, the fibers were incubated for 30 minutes with 1 μg/mL (i.e. 4 μM) and 2.5 μg/mL (i.e. 10 μM) of citrinin in methanol. As a result (Figure 3.19), the MIP-coated fiber showed a concentration-dependent fluorescence enhancement that was specific, as the NIP-coated fiber showed a smaller fluorescence enhancement (imprinting factors of 1.5 for 1 μg/mL citrinin and of 2.3 for 2.5 μg/mL citrinin). To assess the selectivity of our sensor, the MIP-coated fiber was incubated with 10 μM 2,4-D and 10 μM FB_1. As a result, the fluorescence response of the sensor was at least 3 times lower when put in presence of 2,4-D or FB_1, compared to citrinin.

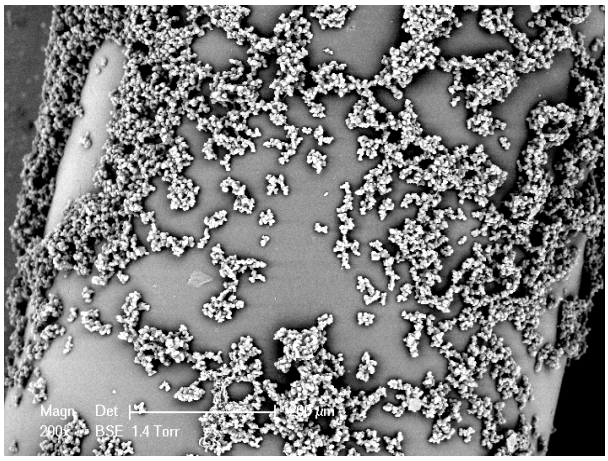

Figure 3.18. *Scanning electron micrographs of the surface of the citrinin-MIP-coated optical fiber. The scale bars correspond to 200 μm.*

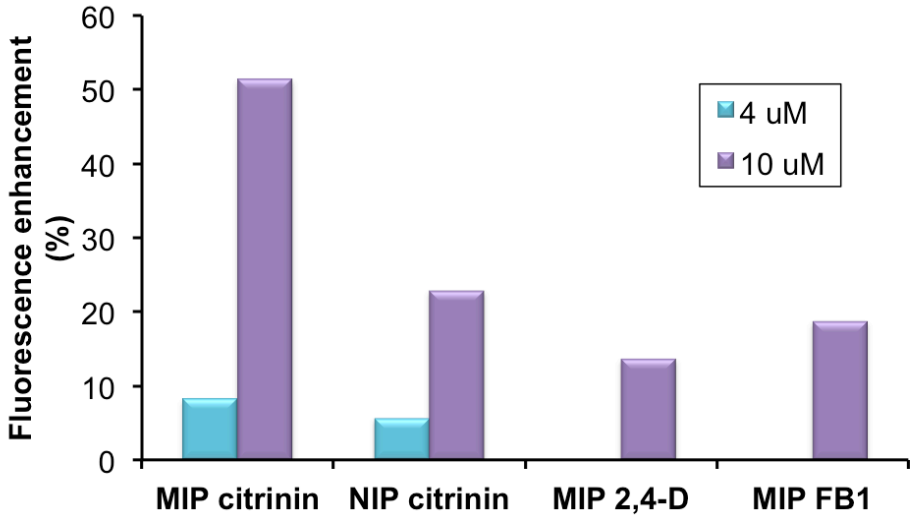

Figure 3.19. *Fluorescence signal of the citrinin-MIP and NIP-coated fibers after incubation with citrinin, and of the citrinin-MIP coated fiber after incubation with the non-related compounds 2,4-D and FB_1 in methanol. (λ_{EX}=410 nm ; λ_{EM}=515 nm).*

We successfully demonstrated the molecular recognition properties of our citrinin-MIP-coated fiber optic sensor. However, the sensing properties of our device (LOD, dynamic range, response time) still need to be optimized. Indeed the end-of-fiber citrinin-MIP microtip described in Chapter 2 demonstrated better sensing properties, as a low LOD of 5 ng/mL was achieved. The sensing properties of the device described here can probably be improved by an optimization of the MIP formulation and fiber coating processes.

III.1.3. Application of the fluorescent monomer FIM for the recognition of phosphate and sulfate analytes

The signaling monomer FIM was mostly applied for the detection of carboxylic acids. However, as already indicates in Chapter 2, FIM can potentially also be applied to templates containing other oxo-anions like sulfate or phosphate, which would considerably broaden the range of potential analytes.

In Chapter 2, FIM was applied for the detection of the phosphate sphingolipid D-*erythro*-sphingosine-1-phosphate (S-1-P). Fluorescence titrations of FIM (5 μM) were performed with increasing concentrations of S-1-P (5-100 μg/mL in methanol, i.e. ≈ 13-260 μM). As a result (Figure 2.37 in Chapter 2), the fluorescence enhancement of FIM was observed to be concentration-dependent and increased with increasing concentrations of S-1-P, confirming that FIM could be used as a functional monomer to imprint S-1-P. No fluorescence enhancement was observed for concentrations of S-1-P below 5 μg/mL (≈ 13 μM), which means that two equivalents of S-1-P are needed for the fluorescence enhancement process of FIM. A S-1-P MIP was then synthesized (see Chapter 2).

Besides S-1-P, we used FIM to imprint the nucleotide adenosine 5'-monophosphate (AMP) (Table 3.1). The interesting point is that fluorescence titrations were performed in pure aqueous medium (TRIS buffer, 0.01 M pH=7, contains 0.5 mM $MgCl_2$ and 0.1 mM $ZnCl_2$). As a result (Figure 3.20), concentration-dependent fluorescence enhancement was observed for concentrations of AMP starting from 2.5 μM, which means that 0.5 equivalent of AMP is needed to interact with FIM and generate the process of fluorescence enhancement. Given these results, we can conclude that FIM could potentially be used to imprint AMP, and the MIP be used in water.

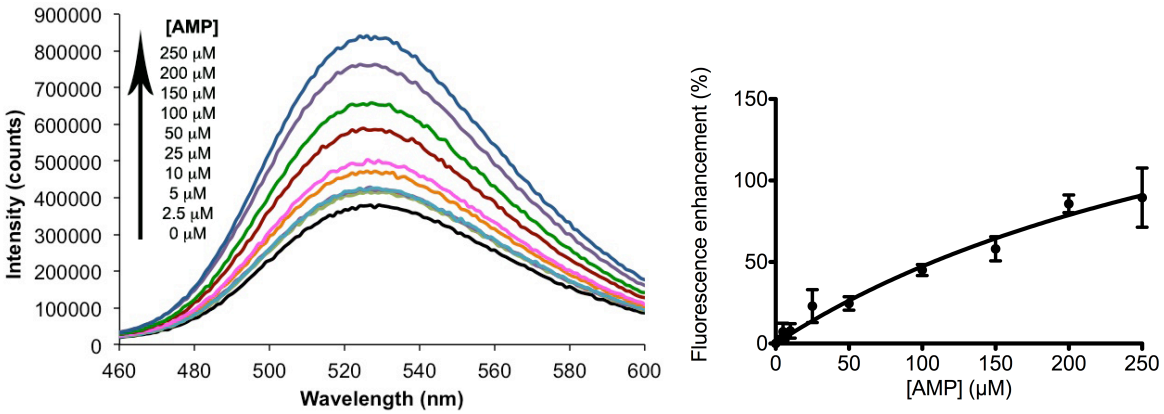

Figure 3.20. *Spectrofluorimetric titrations in TRIS buffer (0.01 M, pH 7) of FIM (5 μM) with increasing concentrations of AMP (2.5 - 250 μM) ($\lambda_{EX/EM}$ = 390 nm/515 nm) (left) fluorescence spectra and (right) fluorescence responses of FIM as function of AMP concentration.*

Besides phosphate analytes, we also tested the binding of the fluorescent monomer FIM with a sulfate analyte. We chose glucosamine-6-sulfate (GlcN-6S) as a model analyte. Similarly, fluorescence titrations of FIM (5 μM) were performed with increasing concentrations of GlcN-6S. For concentrations of GlcN-6S ranging from 10 nM to 2.5 μM, no fluorescence enhancement was observed. However, a concentration-dependent fluorescence enhancement was observed for concentrations of GlcN-6S starting from 5 μM (Figure 3.21), which means that one equivalent of the sulfate analyte GlcN-6S was needed to interact with FIM.

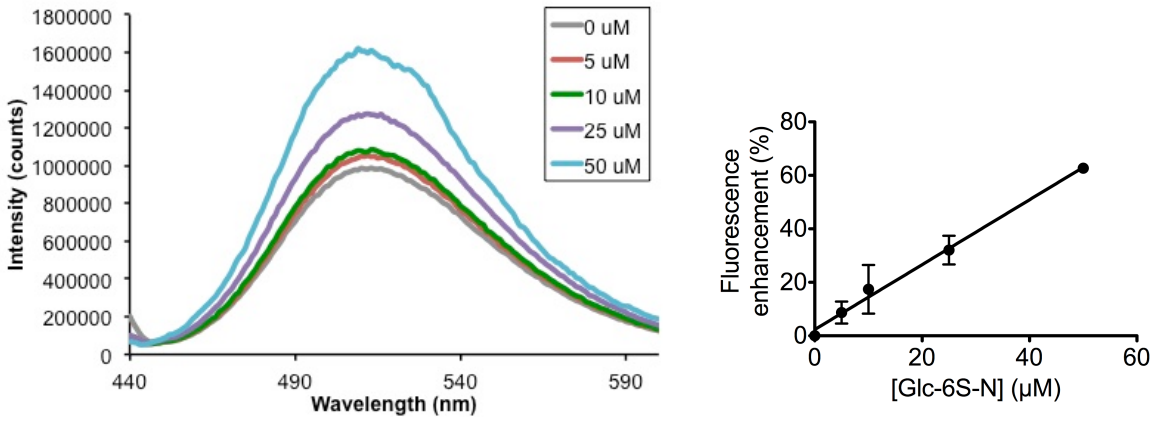

Figure 3.21. *Spectrofluorimetric titrations in methanol of FIM (5 µM) with increasing concentrations of GlcN-6S (5, 10, 25, 50 µM) ($\lambda_{EX/EM}$ = 390 nm/515 nm) (left) fluorescence spectra and (right) fluorescence responses of FIM as function of analyte concentration.*

In this section, we have shown that FIM is a versatile monomer that could potentially be used to imprint any oxyanion, and not only analytes bearing carboxyl groups. However, FIM seems to show less affinity for phosphate and sulfate analytes than for carboxylic acids, as during the fluorescence titrations, more equivalents of phosphate and sulfate analytes are required to interact with FIM and generate the enhancement. Nonetheless, these results are probably dependent on the solvent, and may be improved by changing the medium in which the assays are performed, or by adapting the MIP formulation in order to create more hydrophobic binding pockets that limit the influence of polar solvents.

III.1.4. Conclusions

In this study, a signaling MIP was prepared by precipitation polymerization with the fluorescent piperazinyl naphthalimide-based monomer FIM and imprinted with the herbicid 2,4-D. The fluorescent MIP demonstrated specific fluorescence enhancement upon binding to 2,4-D. A dissociation constant K_D=120 nM was calculated for the high-affinity specific binding sites, indicating the strong affinity of the MIP for 2,4-D. Then in order to use the MIP as a fluorescent probe, the polymer particles were coated on polystyrene evanescent wave fiber optic waveguides, by using PVA as glue. The MIP-coated optical waveguide could bind specifically and selectively 2,4-D with a limit of detection of 1 nM, indicating the extreme sensitivity of our sensor. Binding was monitored with the specific concentration-dependent fluorescence enhancement of the MIP. We have also developed a MIP-coated fiber optic device for the detection of the mycotoxin citrinin. The molecular recognition properties of the MIP could be demonstrated; however the performances of the sensor still need to be refined. Finally, we have shown by fluorescence titrations studies that the range of applications of the fluorescent monomer FIM could potentially be extended to phosphate and sulfate analytes, besides carboxylic acids.

III.2. Ultra-thin MIP microdots obtained by evanescent-wave polymerization – Synthesis on nanostructured gold surfaces.

III.2.1. Context

Evanescent wave photopolymerization is well adapted as a method to coat optical fibers with MIPs and other elements for use as sensors. The length of these fibers allow for a large number of internal reflections, which increases the sensitivity of the sensor. However, the same approach can be used to fabricate arrays of polymer dots on flat substrates, which can then potentially be used as biochips or for chip-based pseudo-immunoassays (Fuchs et al., 2011). In order to improve both the polymerization as well as the sensing with these dots, the use of a nanostructured metal surface can be envisaged. Indeed, gold nanostructure arrays have been widely applied for plasmonic chemical or biological sensing (Zhang et al., 2013). Masson and co-workers have developed gold nano/microhole arrays for surface plasmon resonance (SPR) and surface enhanced Raman scattering (SERS) biosensing (Live et al., 2010; Correia-Ledo et al., 2012). They showed that the nanoholes (and microholes) arrays exhibited improved SPR sensing properties, in terms of sensitivity (to refractive index and to monolayer formation) and binding events, compared to continuous Au films (Live et al., 2010). Moreover, the nanoholes arrays give large Raman enhancement factors, which is suitable for SERS measurements (Correia-Ledo et al., 2012). Their plasmonic properties were dependent on their structure, and the optimal microstructure was the one of diameter/periodicity = 0.5.

In this study, we intended to apply these plasmonic microstructures for fluorescence sensing using MIP microdots as recognition elements, and we present here the preliminary results of this work.

The fabrication of ultra-thin MIP microdots using polymerization by evanescent waves was for the first time demonstrated in our group (Fuchs et al., 2011). Following up on these early studies, we synthesized MIP microdots on gold films and microstructured gold surfaces used for plasmonic sensing. The MIP we used for this study is the fluorescent 2,4-D MIP **P2** (Table 3.8). To elucidate the potential effect of gold nanostructuring on the MIP binding properties and morphology (i.e., the polymerization process, the process of fluorescence enhancement, as well as the MIP recognition properties), polymer microdots were synthesized on three different surfaces: plain glass, continuous gold surface, and gold microholes arrays.

Table 3.8. *Formulation of the MIP* ***P2*** *used for the synthesis of microdots by evanescent-wave polymerization*

Polymer	Template	Functional monomers	Cross-linker	Initiator	Solvent
P2	2,4-D (0.02 mmol)	FIM/4-VPY (0.04/0.04 mmol)	EDMA (0.4 mmol)	Irgacure 819 (0.008 mmol)	Methanol/water (4/1) (1 mL)

II.2.2. Polymerization of the microdots by evanescent waves

Polymer microdots were synthesized by evanescent waves on the three surfaces: a microscope glass slide, a gold film and a microstructured gold surfaces consisting of microholes, under total internal reflection conditions.

The refractive index n_2 of the precursors mixture **P2** was measured with a refractometer to be 1.36. On the other hand, the refractive index n_1 of the index match solution, which corresponds to the refractive index of the gold substrates, was measured to be 1.52. At the same time, the glass microscope slide also exhibits a refractive index n_1=1.52. Owing to these values, the minimum angle

θ_c required for being in the conditions of total reflection was 63.5°. Experimentally, the angle θ was set at a slightly higher value of 70°.

For all substrates, the photonic conditions were kept constant: laser power = 8 mW and irradiation time = 2 minutes. As a result, on the three surfaces, polymer microdots of a size of around 3 mm x 5 mm were obtained.

The theoretical penetration depth of the evanescent field is defined as $1/(2\gamma)$, with γ that represents the decay rate and can be expressed by the equation:

$$\gamma = \frac{2\pi}{\lambda}\sqrt{(n_1.\sin(\theta))^2 - n_2^2}$$

The theoretical penetration depth was calculated to be 68 nm. This value gives the order of magnitude of the thickness of the polymer microdots synthesized by evanescent waves.

II.2.3. Morphology of the polymer microdots

The morphology of the polymer microdots was then visualized by fluorescence microscopy (as the MIP is fluorescent) and scanning electron microscopy (SEM) or atomic force microscopy (AFM).

II.2.3.1. Glass surfaces

In Figure 3.22 is shown the fluorescence microscope image of the polymer microdot formed on a glass surface with 2 minutes irradiation. As the microdot was too big to be imaged with the fluorescence microscope, smaller dots were synthesized just for the images (Figure 3.23, 20 seconds of irradiation). Figure 3.24 shows the SEM images of the MIP microdot (2 min irradiation). We can see from the SEM pictures that the polymer layer did not cover completely the glass surface, but consists of a regular structure with some zones without polymer.

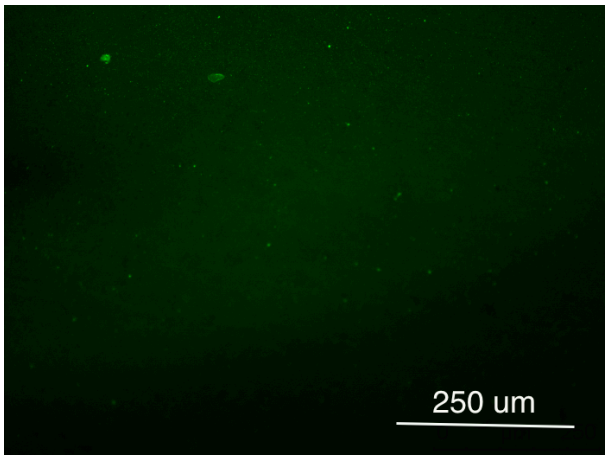

Figure 3.22. *Fluorescence microcope image (L5 filter) of the MIP microdot on the glass surface (2 min irradiation, partial view).*

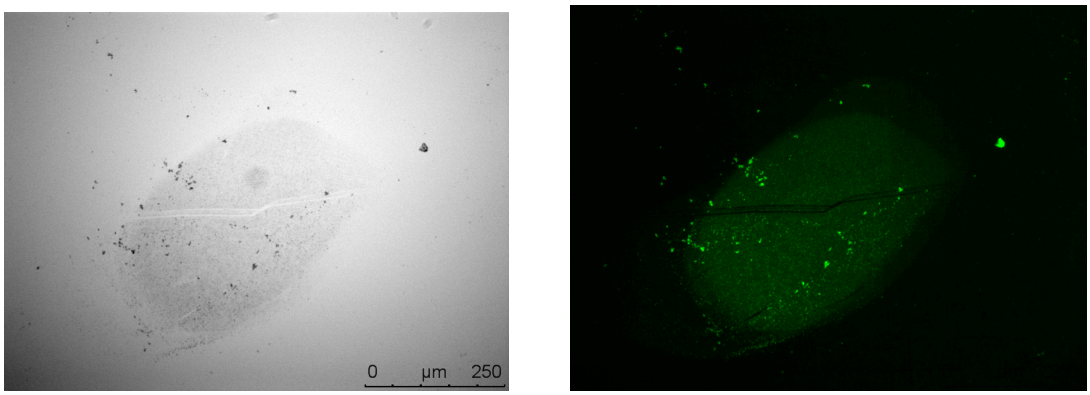

Figure 3.23. *(Left) Bright field image and (right) fluorescence microscope image (L5 filter) of the MIP microdot on the glass surface (20 seconds irradiation).*

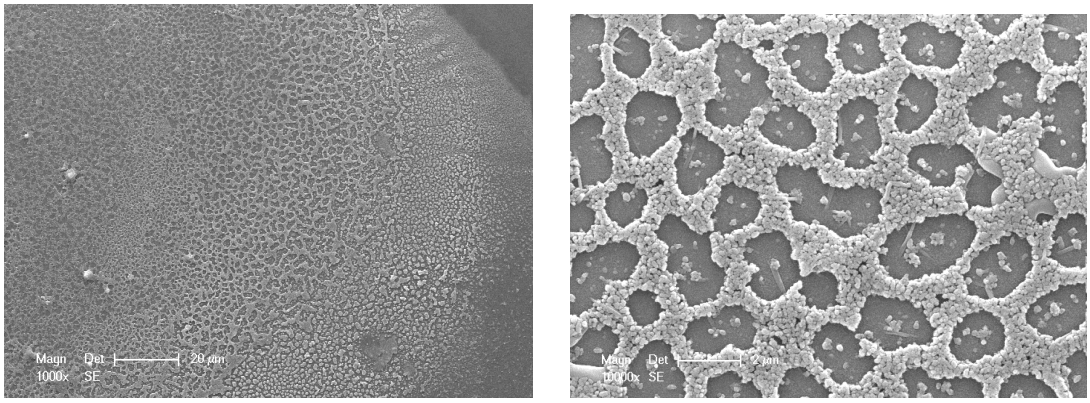

Figure 3.24. *SEM images of the MIP microdot formed on the glass surface. Scale bar: (left) 20 µm; (right) 2 µm.*

II.2.3.2. Gold film

The MIP microdot polymerized on the continuous gold film was visualized by fluorescence microscopy (Figure 3.25) and AFM (Figure 3.26). From the images, we can see that the microdot on the gold film presents a denser structure than the one polymerized on the glass surface whereas the same photonic conditions were used for polymerization. We assume that the polymerization is more efficient on the gold surface than on the glass surface, and that the light intensity is enhanced by the gold surface.

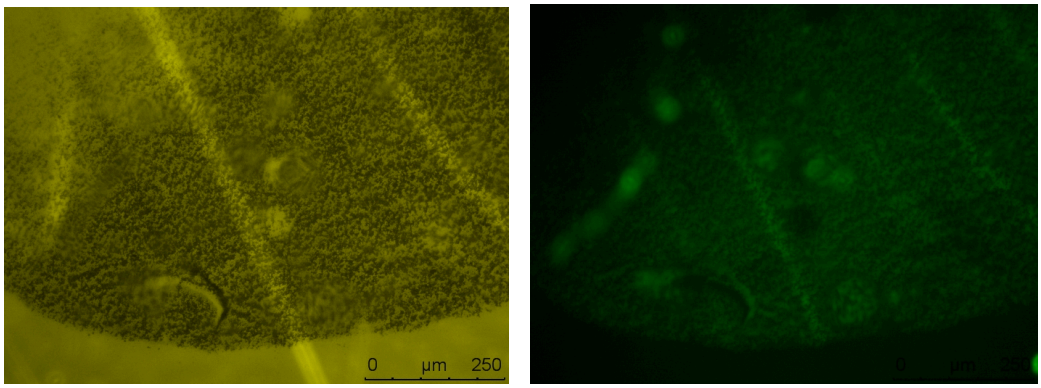

Figure 3.25. *(left) Bright field image and (right) fluorescence microcope image (L5 filter) of the MIP microdot on the Au film, before incubation (exposure time of fluorescence microscope: 200 ms)*

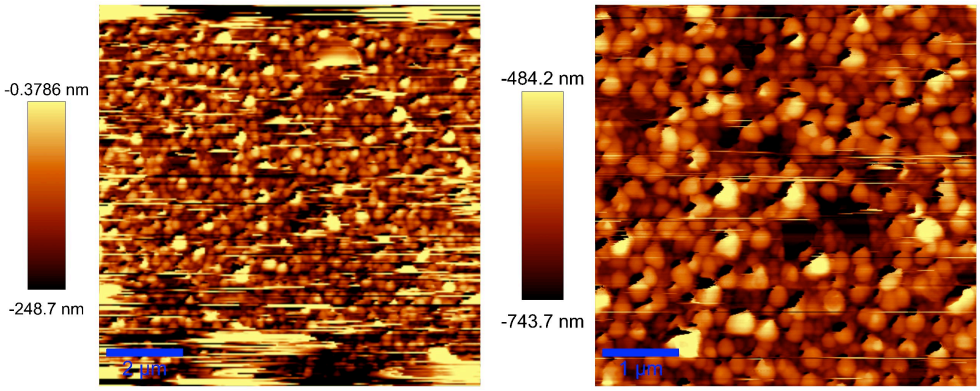

***Figure 3.26**. AFM topographical image of MIP microdot on Au film (contact mode). Scale bars: (left) 2 µm, (right) 1 µm.*

II.2.3.3. Gold microholes array

Figure 3.27 shows a SEM image of the surface of the gold microholes array. The array is constituted of holes of 1 µm diameter, separated by distances of around 2 µm. Indeed the optimal microstructure for plasmonic enhancement is the diameter/periodicity = 0.5 (Live et al., 2010).

The MIP microdot polymerized on the gold microholes surface was then visualized by fluorescence microscopy (Figure 3.28) and AFM (Figure 3.29). From the topographic AFM image, it can be seen that the MIP microdot exclusively polymerized on the microholes, which could be due to both the better transparency in this region (the hole diameter is larger than the wavelength of the light) or to the electromagnetic field being enhanced by the microholes. The latter hypothesis is the most likely to take place, as Masson and co-workers showed that for nanoholes of diameter/periodicity= 0.5, the surface plasmons were localized around the rim of the nanoholes (Correia-Ledo et al., 2012).

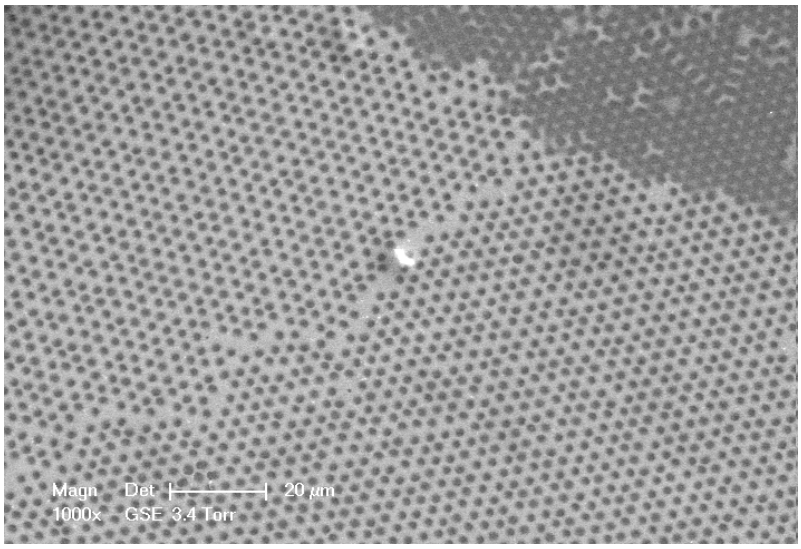

***Figure 3.27.** SEM image of the gold microholes surface (without polymer microdot). Scale bar: 20 µm.*

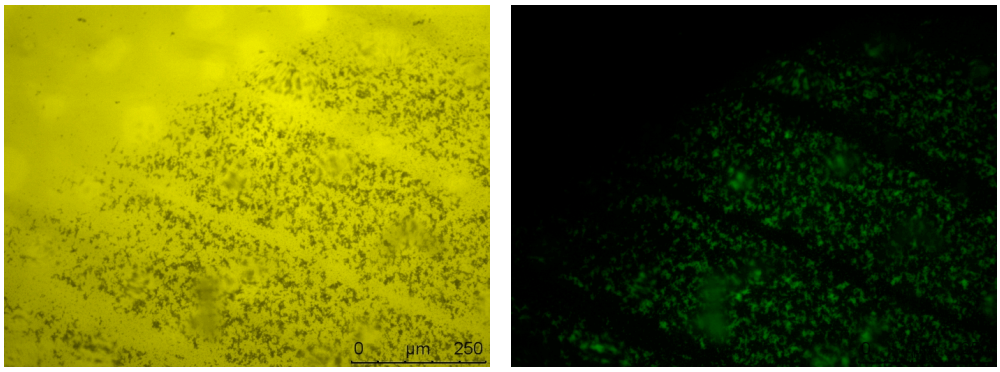

Figure 3.28. *(Left) Bright field image and (right) fluorescence microcope image (L5 filter) of the MIP microdot on the microholes, before incubation (exposure time of fluorescence microscope: 50 ms).*

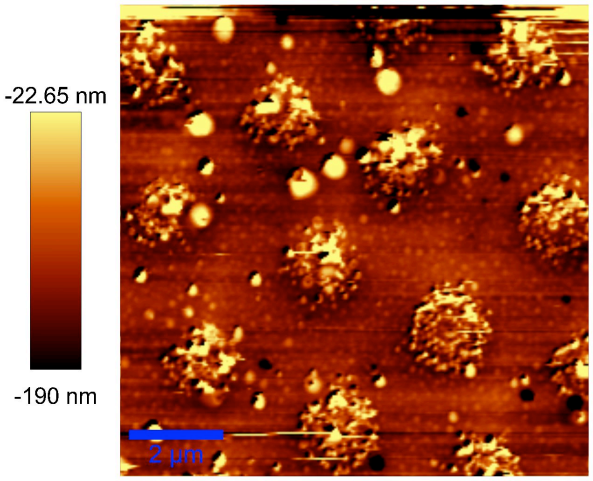

Figure 3.29. *AFM topographical image of MIP microdot on Au microholes surface (contact mode). Scale bar: 2 µm.*

II.2.4. Molecular recognition properties of the polymer microdots

The binding properties were studied by fluorescence microscopy. It should be noted first that different exposure times were used for the glass surface and the Au film (200 ms) and the Au microholes (50 ms). Indeed the initial fluorescence intensity of the microdots on the microholes surface was much stronger compared to the continuous Au film and the glass surface. So it seems that the microstructuring of the Au surface has an effect on the fluorescence signal and enhances it.

The binding properties of the microdots were verified by incubating the microdots for 1 hour in 0.5 µM 2,4-D in MeOH/water (4/1) (Figure 3.30). Binding was monitored by the fluorescence enhancement of the monomer FIM. The different binding properties of the microdots are summarized in Table 3.9.

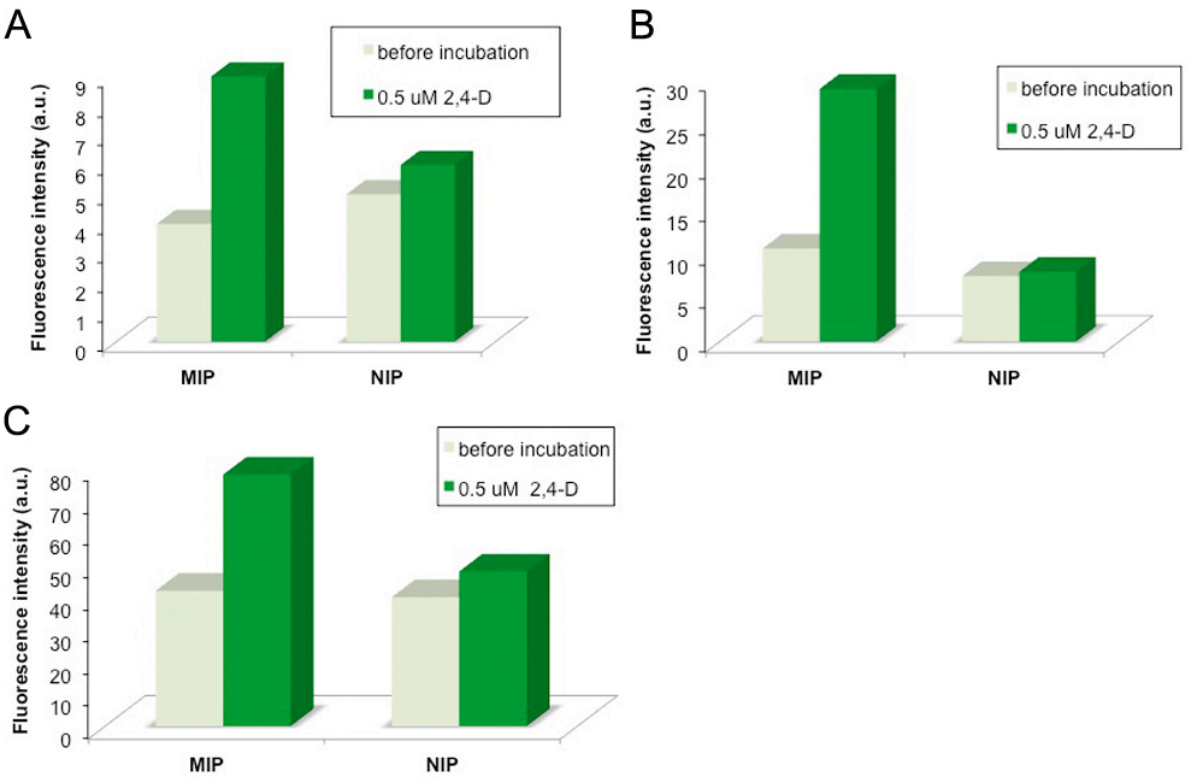

Figure 3.30. *Fluorescence signal ($\lambda_{EX/EM}$ = 480/520 nm) of polymer microdots measured by fluorescence microscopy before and after incubation in 0.5 μM 2,4-D in MeOH/water (4/1), synthesized on (A) a glass microscope slide, (B) a continuous gold film, and (C) a gold microholes array. The intensity and gain were kept constant, and the exposure time was set at 200 ms for (A) and (B) and 50 ms for (C).*

Table 3.9. *Binding properties of the polymer microdots synthesized on the different surfaces (glass, Au film and Au microholes array). The enhancement (%) is defined as [(F-F0)/F0]*100, with F and F0 respectively the fluorescence intensity of the polymer in presence and in absence of 2,4-D.*

	Glass	Au film	Au microholes
MIP enhancement	+ 125 %	+ 171%	+ 86%
NIP enhancement	+ 20%	+ 7%	+ 20%
Imprinting factor	6.25	24.4	4.3

If we compare the results obtained with the different microdots, we can observe that the MIP microdot synthesized on the Au film gave better results than the one synthesized on the glass surface, as the MIP initial signal and signal enhancement were higher. It seems then that the Au surface led to a signal enhancement. If we compare the results obtained with the Au film and the Au microholes array, the MIP signal enhancement upon analyte binding is higher in the case of the Au film. However, the initial fluorescence signal of the MIP microdot was much stronger on the Au microholes array than on the Au film, so detection should be more sensitive with the microholes array, even if the enhancement is less strong. This signal difference can be exclusively attributed to the microstructuring of the Au microholes array, as the MIP microdot was denser on the Au film than on the Au microholes array, which means that the stronger initial signal cannot be attributed to a higher amount of MIP. Thus, the Au microholes array constitutes the most interesting sensing platform in terms of sensitivity.

IV. Conclusions and perspectives

This chapter focused on the use of evanescent waves for the synthesis of MIPs on an optical fiber and on flat substrates, for use in sensing. The first part concerns the fabrication of evanescent-wave fiber optic waveguides coated with a signaling MIP. The detection was based on the fluorescence enhancement of the naphthalimide-based fluorescent monomer FIM incorporated into the MIP; signal enhancement that occurs upon analyte binding. The device was applied for the monitoring of the herbicide 2,4-D and a low LOD of 1 nM was obtained. Detection of the mycotoxin citrinin was also successfully performed, even if the performances of the sensor still have to be optimized. Then we showed through fluorescence titration studies that the naphthalimide-based monomer could interact with phosphate analytes (such as the nucleotide AMP and the sphingolipid S-1-P) and sulfate analytes (such as glucosamine-6-sulfate). Therefore, for further studies, MIPs for the recognition of phosphate and sulfate analytes can potentially be synthesized using FIM, and the MIP coated on the optical fibers either by *in-situ* photopolymerization or by top-down deposition, in order to constitute efficient tools for the rapid monitoring of various analytes in complex samples. If we compare the two types of fiber optic sensors we have described in Chapter 2 and in this Chapter, the intrinsic fiber optic sensor based on a MIP microtip (Chapter 2) was much faster to develop (the fabrication of the MIP microtip was achieved in only a few seconds), allows for long-distance measurements and thus can reach inaccessible sites, and a higher sensitivity was obtained, while the sensitivity of the MIP-coated fiber optic sensor was depending on the MIP that was coated on the fiber. However, the fiber optic sensor described in this Chapter is disposable and was much cheaper and easier to develop, as no optical set-up was required and only a MIP coating was performed. It is also much easier to carry this fiber on-site, so this sensor is suitable for a first fast and cheap screening of the media that need to be analyzed. Further analysis can be carried out by the intrinsic fiber optic sensor described in Chapter 2.

The second part describes the synthesis by evanescent waves of signaling MIP microdots on a gold film and a gold microholes array that are usually used as sensing platforms for SPR or SERS measurements. The MIP used here was the 2,4-D MIP synthesized with FIM as functional monomer. MIP microdots were synthesized on three different surfaces: glass, a continuous gold film and a gold microholes array. SEM and AFM imaging showed that the nature of the surface influenced the morphology of the polymer microdot, as the exact same photonic conditions were used for both surfaces. For example, the Au surface seemed to enhance the light intensity, as the polymer microdot was much denser on the Au film than on glass. Concerning the Au microholes surface, the energy seemed to be localized in the microholes, as the MIP exclusively polymerized on the microholes. The binding properties were then studied by fluorescence microscopy. As a result, the MIP on the Au film gave the best signal enhancement, which suggests that Au gives a better sensitivity compared to glass. The MIP on the Au microholes array gave a lower enhancement factor; however the signal intensities of the microdots on the microholes were much stronger than on the Au film and the glass. Therefore we can conclude that microstructuring induces signal enhancement and that the Au microholes array constitutes the best sensing platform in terms of sensitivity. For further studies, the sensing properties of the MIP microdots can be investigated more deeply, and the technique extended to all kinds of analyte.

V. References

Chegel, V.; Whitcombe, M. J.; Turner, N. W.; Piletsky, S. A. Deposition of functionalized polymer layers in surface plasmon resonance immunosensors by in-situ polymerization in the evanescent wave field. *Biosensors and Bioelectronics* **2009**, *24*, 1270.

Correia-Ledo, D.; Gibson, K. F.; Dhawan, A.; Couture, M.; Vo-Dinh, T.; Graham, D.; Masson, J.-F. Assessing the location of surface plasmons over nanotriangle and nanohole arrays of different size and periodicity. *The Journal of Physical Chemistry C* **2012**, *116*, 6884.

Ecoffet, C.; Espanet, A.; Lougnot, D. J. Photopolymerization by evanescent waves: a new method to obtain nanoparts. *Advanced Materials* **1998**, *10*, 411.

Espanet, A.; Dos Santos, G.; Ecoffet, C.; Lougnot, D. J. Photopolymerization by evanescent waves: characterization of photopolymerizable formulation for photolithography with nanometric resolution. *Applied Surface Science* **1999**, *138*, 87.

Feng, X. Z.; Lin, Z.; Yang, L. J.; Wang, C.; Bai, C. Investigation of the interaction between acridine orange and bovine serum albumin. *Talanta* **1998**, *47*, 1223.

Fuchs, Y.; Linares, A. V.; Mayes, A. G.; Haupt, K.; Soppera, O. Ultrathin Selective Molecularly Imprinted Polymer Microdots Obtained by Evanescent Wave Photopolymerization. *Chemistry of Materials* **2011**, *23*, 3645

Lim, D. V. Detection of microorganisms and toxins with evanescent wave fiber-optic biosensors. *Proceedings of the IEEE* **2003**, *91*, 902.

Live, L. S.; Bolduc, O. R.; Masson, J.-F. o. Propagating surface plasmon resonance on microhole arrays. *Analytical Chemistry* **2010**, *82*, 3780.

Rogers, K. R.; Anis, N. A.; Valdes, J. J.; Eldefrawi, M. E.: Fiber-optic biosensors based on total internal-reflection fluorescence. In *Biosensor Design and Application*; ACS Symposium Series (ACS Publications): Washington D.C., USA, 1992; Vol. 511; pp 165.

Soppera, O.; Jradi, S.; Ecoffet, C.; Lougnot, D. J.: Fabrication, Properties, Optics and Devices IV In *Proc. SPIE Nanoengineering*, 2007; Vol. 6647; pp 66470I.

Surugiu, I.; Danielsson, B.; Ye, L.; Mosbach, K.; Haupt, K. Chemiluminescence imaging ELISA using an imprinted polymer as the recognition element instead of an antibody. *Analytical Chemistry* **2001**, *73*, 487.

Taitt, C. R.; Anderson, G. P.; Ligler, F. S. Evanescent wave fluorescence biosensors. *Biosensors and Bioelectronics* **2005**, *20*, 2470.

Thompson, V. S.; Maragos, C. M. Fiber-optic immunosensor for the detection of fumonisin B1. *Journal of Agricultural and Food Chemistry* **1996**, *44*, 1041.

Wolfbeis, O. S. Fiber-optic chemical sensors and biosensors. *Analytical Chemistry* **2004**, *76*, 3269.

Zhang, N.; Su, X.; Free, P.; Zhou, X.; Neoh, K. G.; Teng, J.; Knoll, W. Plasmonic metal nanostructure array by glancing angle deposition for biosensing application. *Sensors and Actuators B: Chemical* **2013**, *183*, 310.

Commission Regulation (EC) no. 1127/2007 of 28 September 2007 of the European Union, setting maximum levels for certain contaminants in foodstuffs as regards Fusarium toxins in maize and maize products. http://eur-lex.europa.eu/LexUriServ/LexUriServ.do?uri=OJ:L:2007:255:0014:0017:EN:PDF

European Food Safety Authority (EFSA) Panel on Contaminants in the Food Chain (CONTAM). Scientific Opinion on the risks for public and animal health related to the presence of citrinin in food and feed. *EFSA Journal* **2012**,*10*, 2605.

Guidelines for drinking water quality, 4th edition, World Health Organization WHO, Geneva, **2011**, pp. 347.

Chapter 4

Direct fluorimetric sensing of UV-excited analytes in complex samples using molecularly imprinted polymer nanoparticles and fluorescence polarization

Chapter 4: Direct fluorimetric sensing of UV-excited analytes in complex samples using molecularly imprinted polymer nanoparticles and fluorescence polarization

I. Introduction

In the previous chapters, MIPs were used as recognition elements in optical sensors, in particular with optical fibers combined with fluorescence for detection. The aim of the work presented in this chapter was to develop another innovative sensing method based on the use of MIPs and fluorescence, in the form of pseudo-immunoassays, in order to allow the fast and direct quantification of analytes in food and environmental samples. We opted for the technique of fluorescence polarization assays, which are non-separation immunoassays that are rather insensitive to a number of influences by the sample components, and that can therefore be easily put into practice for routine analysis. We applied this technique to detect fluoroquinolone antibiotics in real samples, namely in tap water and milk.

I.1. Fluorescence polarization immunoassays (FPIA)

I.1.1. Principles of fluorescence polarization and introduction to FPIA

To define fluorescence polarization, it must be reminded that light is an electromagnetic wave, whose components are perpendicular to the direction of the light propagation. In our case, we are only interested in the electrical field. Polarizers are optical filters that let pass one direction of the electric vector. Fluorescence polarization is then defined by Equation (1) as:

$$p = \frac{I_{\parallel} - I_{\perp}}{I_{\parallel} + I_{\perp}} \qquad (1)$$

with p as the fluorescence polarization (without units) and $I_{||}$ and $I_{\perp}$, respectively the parallel and perpendicular intensity components of the emitted light of a fluorophore excited by a plane-polarized light.

According to the definition, the theoretical limit of p should be ± 1. However, in reality, this value is not reached because of the excitation photoselection of fluorophores. Briefly, if a fluorophore sample is excited with polarized light, the molecules with their transition dipoles aligned parallel with the electric vector of the excitation light have the highest probability to absorb the light. More precisely, this probability is proportional to the $\cos^2\theta$, where θ is the angle between the excitation polarized light and the transition dipole of the fluorophore. Hence, even if we excite a sample containing randomly oriented fluorophores with a plane-polarized light, at the end, only a population of specifically oriented fluorophores will be excited. This phenomenon is called *photoselection*. The limits of the fluorescence polarization values can be the calculated by considering two extreme situations. First, if the angle β between the excitation and emission transitions is 0° (which means that the excited fluorophore does not rotate during the excitation lifetime, for example in a frozen or very viscous medium), then we have p = + 1/2. Second, if we have β=90°, then p = - 1/3 (-0.33). The limits values for p are +1/2 and -1/3.

Details of the theoretical calculations can be found in the literature (Lakowicz, 2006). If these limit values are exceeded, this probably means that light scattering events occurred.

Another source of error is related to the instrument itself, because the varying polarization characteristics or efficiencies of monochromators at one given wavelength can affect the measurement of polarization. Thus the polarization value must be corrected using a "G-factor", expressed as:

$$G = I_{HV}/I_{HH} \qquad (2)$$

where I_{HV} is the intensity with the excitation and emission polarizers oriented horizontally and vertically respectively (based on the laboratory axes), and I_{HH} is the intensity with both excitation and emission polarizers oriented horizontally. Thus the corrected polarization value can be expressed as:

$$p = \frac{I_{\parallel} - GI_{\perp}}{I_{\parallel} + GI_{\perp}} \qquad (3)$$

In general, several parameters influence the values of p, such as the molecular size of the fluorophore, the fluorescence lifetime and the viscosity of the solvent. Briefly, concerning the molecular size, the bigger the fluorophore, the higher the polarization value, as the rotational rate decreases. This is the principle of fluorescence polarization immunoassays (FPIA). Second, the shorter the lifetime, the less the fluorophore will rotate and the higher the polarization value. Finally, the more viscous the solvent, the slower the rotation of the fluorophore and the higher the polarization value. Importantly, fluorescence polarization values do not depend on fluorescence intensities and fluorophore concentrations, but give the free to bound ratio. For this reason, fluorescence polarization is a very interesting technique for the study of antigen-antibody interactions in homogeneous solution and in real time.

Unlike batch binding assays where the fluorescence detection is based on intensity measurements of the free analyte in the supernatant after separation from the bound analyte, the fluorescence polarization method is a real-time method requiring no separation step of bound and free fluorophore. It involves the use of a plane-polarized light to excite the fluorophore. In the case of a small fluorophore, its tumbling rate is fast and thus the molecules become randomly oriented during the lifetime of the excited state, before emitting the fluorescence light, resulting in depolarized emission (typically, we will obtain a polarization value p=0.03 to 0.06). On the other hand, if the fluorophore is bound to the much larger receptor (an antibody or in our case, a MIP receptor), the rate of the tumbling motion of the complex will be comparable to the rate at which the fluorescence decays, resulting in polarized emission (typically about p=0.15 to 0.30). Consequently, the interaction of a small fluorophore with a receptor, such as a MIP, can be monitored through the increase in fluorescence polarization, which occurs with the change in fluorophore mobility upon complex formation. (Jameson and Ross, 2010; Smith and Eremin, 2008). In addition, interference by molecules present in the samples that influence the intensity of the excitation and/or fluorescence light are largely reduced in this method compared to simple intensity measurements. The principle of a fluorescence polarization immunoassay (FPIA) is described in Figure 4.1.

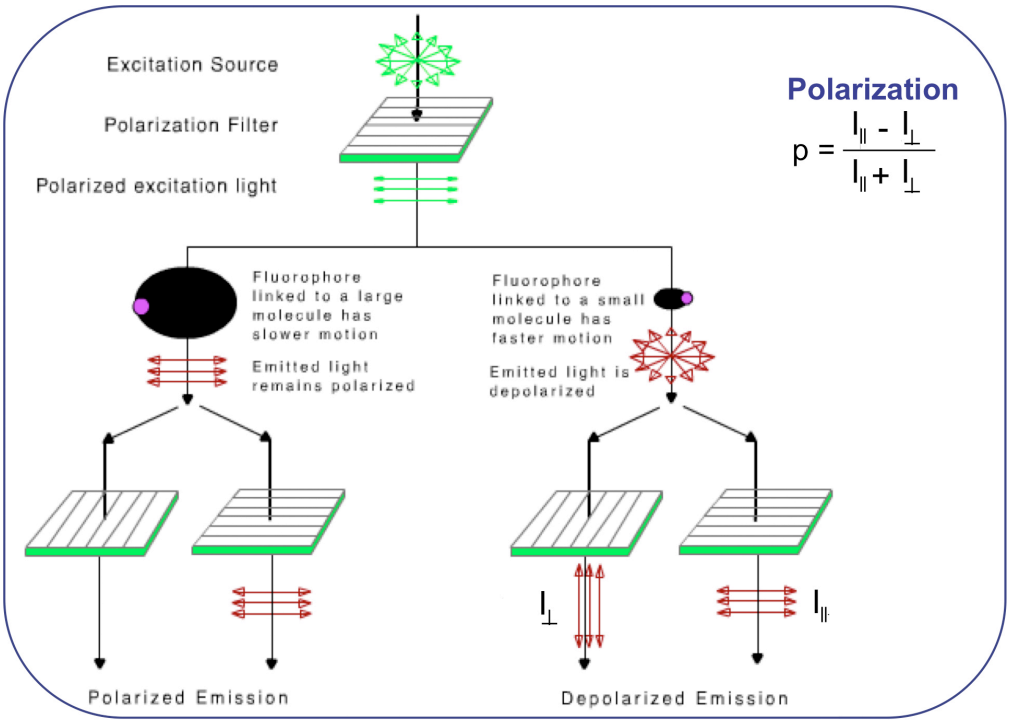

Figure 4.1. *Principle of a fluorescence polarization immunoassay (FPIA).*

I.1.2. Applications of FPIA

Dandliker and Feigen described the first FPIA in the early 1960s: they labeled the protein ovalbumin with fluorescein isothiocyanate (FITC) and used polarization and intensity measurements to study antibody-antigen binding (Dandliker and Feigen, 1961). Since then, FPIA have been widely used to monitor small molecules, including abused drugs (Perez-Bendito et al., 1994), therapeutic drugs (Tachi et al., 2011), hormones such as testosterone (Adamczyk et al., 1997), pesticides such as 2,4-dicholorophenoxyacetic acid (2,4-D) (Hatzidakis et al., 2002), environmental contaminants such as polycyclic aromatic hydrocarbons (Goryacheva et al., 2007), and food contaminants such as mycotoxins (Chun et al., 2009; Maragos, 2009; Shim et al., 2004).

FPIA have several advantages:

- rapidity : due to the very fast kinetics of immunoreaction, measurements usually take a few minutes or even seconds.
- high specificity and sensitivity : the working range is usually in the $ng.mL^{-1}$ to $\mu g.mL^{-1}$ interval, and the limit of detection was of 0.1 ng analyte detectable with the fluorescein label (Smith and Eremin, 2008).
- simplicity of procedure: only addition of the tracer to the analyte solution is required, and no separation or washing step is required.

Nonetheless, FPIA possess some limitations: the limit of detection is not always as low as that of ELISA technique, and FPIA is sensitive to light scattering and to the presence of other fluorophores in the sample. Furthermore, non-specific binding of the analyte to other components present in the sample matrix can occur.

However, FPIA has the advantage to be easily automated and thus is particularly suitable for simple and fast screening of small molecules for environmental control and food safety applications. Nowadays, FPIA is performed more than ELISA for therapeutic drug and abused drug monitoring

(Smith and Eremin, 2008), and has become a promising technique for determining the presence of small organic molecules in general.

More recently, molecularly imprinted polymers have been used as antibodies mimics in fluorescence polarization assays. Hunt *et al*. described the first pseudo-immunoassay using a molecularly imprinted polymer as an antibody mimic and a fluorescent probe 7-carboxymethoxy-4-methylcoumarin (CMMC), for the detection of the herbicide 2,4-D (Hunt et al., 2006). The assay was selective for 2,4-D among other structurally related analogues, and showed an IC_{50} (concentration of 2,4-D needed for 50% displacement of CMMC from the MIP) of about 10 μM. Fluorescence polarization was also used to measure the binding of S-propanolol to the corresponding MIP (Hunt and Ansell, 2006). Very recently, we have developed a fluorescence polarization-based assay for the monitoring of fluoroquinolone antibiotics in complex samples (Ton et al., 2012). In this study, we have chosen as a model analyte the fluoroquinolone antibiotic enrofloxacin (ENRO), and we showed that this technique can provide a rapid and sensitive tool for the direct measurement of piperazine-based fluoroquinolones below their maximum residue limits in water and milk samples, after simply adding a very low amount of MIP (5 μg in 1 mL sample).

I.2. Molecularly imprinted polymers for the detection of fluoroquinolones

Fluoroquinolones (FQs) (Figure 4.2), a class of broad-spectrum antibiotics, are widely used nowadays in human and veterinary medicine. Their extensive use has led to their persistence in foodstuffs of animal origin as well as in different environmental compartments. For instance, ENRO and its primary active metabolite, ciprofloxacin (CIPRO), can be found in the muscle, tissue and urine of animals (Caro et al., 2006), and also in milk (Christodoulou and Samanidou, 2007), water and soil (Golet et al., 2003). Concerns have emerged about the effect of these residues on human health because of the serious problems induced, such as the development of antibiotic-resistant bacteria or allergic reactions (Collignon et al., 2009). Therefore, for safety reasons, maximum residue limits (MRLs) have been established by the Commission Regulation (EU) no. 37/2010 of the European Union. The MRLs in milk have been fixed to 100 $\mu g.kg^{-1}$ for the sum of ENRO and CIPRO and 30 $\mu g.kg^{-1}$ for danofloxacin (DANO). No specific limits for antibiotics in environmental waters have been established but the threshold values for residues of veterinary drugs in ground waters has been set to 0.1 $\mu g.L^{-1}$ by the 1996-1997 guideline of the European Agency for the Evaluation of Medicinal products (EMEA) (Sturini et al., 2010). Due to the low concentration level of FQs to be analyzed, a sample pretreatment step involving a solid phase extraction (SPE) on anion-exchange resins or reversed-phased cartridges, or on more specific materials like molecularly imprinted polymers (MIPs) that afford cleaner extraction (Pichon and Haupt, 2006) is usually required.

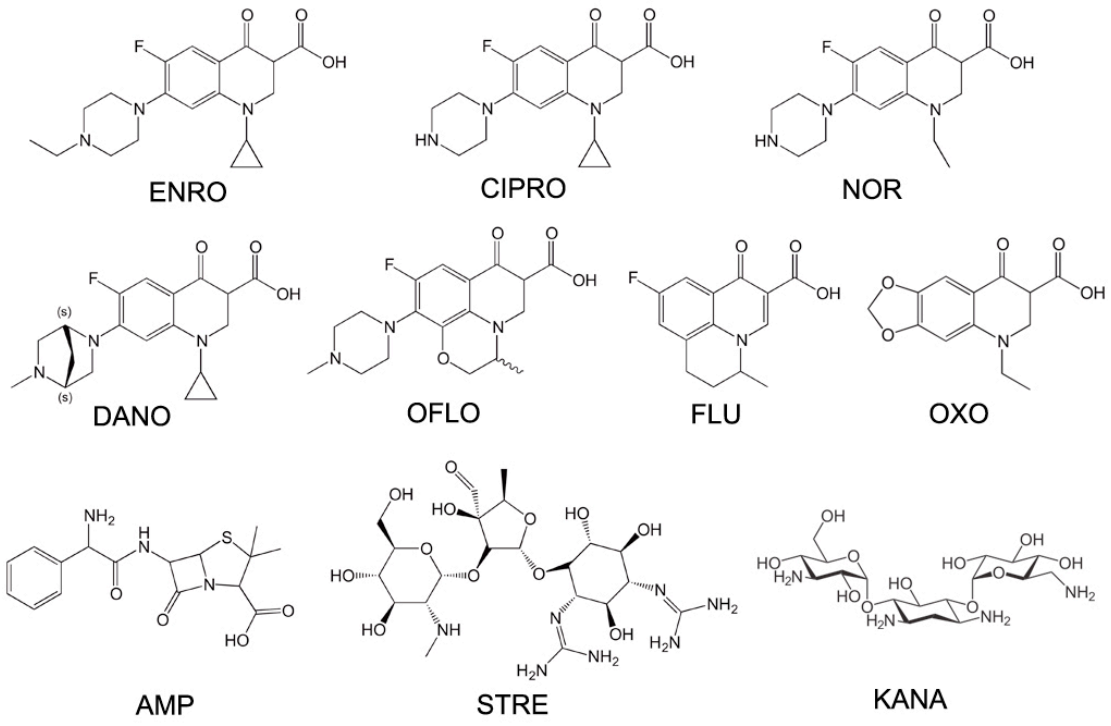

Figure 4.2. *Chemical structures of compounds used in this study. Fluoroquinolones: enrofloxacin (ENRO), ciprofloxacin (CIPRO), norfloxacin (NOR), danofloxacin (DANO), ofloxacin (OFLO), flumequine (FLU), the quinolone oxolinic acid (OXO) and other classes of antibiotics: ampicillin (AMP), streptomycin (STRE), kanamycin (KANA).*

A survey of the literature revealed the existence of several different protocols for the preparation of MIPs for FQs. MIPs were principally prepared by bulk polymerization (Benito-Peña et al., 2009; Qiao and Sun, 2010; Sun et al., 2008), and also by precipitation polymerization (Díaz-Alvarez et al., 2009; Prieto et al., 2011;Turiel et al., 2007); but other formats of MIPs were also developed, such as norfloxacin imprinted polymeric membranes that were synthesized on silica gel surfaces (Lv et al., 2012). The MIPs were exclusively applied as solid phase extraction or liquid chromatography sorbents for the clean-up and extraction of a mixture of FQs from several matrices, such as water (Prieto et al., 2011), baby food (Díaz-Alvarez et al., 2009), soils (Turiel et al., 2007), eggs and/or tissues (Blasco and Picó, 2012; Lv et al., 2012; Yan et al., 2007), serum (Sun et al., 2008), milk (Lombardo-Agüí et al., 2011; Lv et al., 2013) and urine (Benito-Peña et al., 2009). These MIPs show group specificity, since they not only bind the original imprinting template but also structurally related compounds. After extraction, the FQs were analyzed by HPLC with mass spectrometry (MS) (Prieto *et al.*, 2011), fluorescence (Benito-Peña *et al.*, 2009; Yan *et al.*, 2007) or UV-visible detection (Díaz-Alvarez *et al.*, 2009).

Alternative methods to the more laborious, time-consuming and solvent intensive chromatographic methods for measuring ENRO are enzyme-linked immunosorbent assays (ELISA) (Wang et al., 2007) and biosensors (Cao et al., 2007). Though ELISA is simple, sensitive and allows a high throughput procedure for the specific detection of the antigen, it is a heterogeneous immunoassay that involves separation of the bound and free analyte and multiple washing steps that lengthen the analysis. The same disadvantages arise for biosensors that require the regeneration of

the receptor surfaces between samples analysis. Since fluoroquinolones are intrinsically fluorescent, our objective was to synthesize a MIP that could be combined with a sensitive detection method, fluorescence polarization, for the direct detection and monitoring of FQ contamination in waters and milk. Fluorescence spectroscopy is a very sensitive method allowing for the detection of fluorescent analytes, for example certain antibiotics, mycotoxins, and other contaminants like polyaromatic hydrocarbons, in food and environmental samples. However, fluorescence methods are very sensitive to interferences present in the sample, therefore direct measurements are often impossible, more so if the fluorophore is excited in the UV range. Thus, a time-consuming sample preparation method normally has to be applied followed by separation before the detection of the fluorophore. In this study, we have investigated the possibility to directly determine such analytes in complex samples like milk, by providing selectivity through a molecularly imprinted polymer, and by using fluorescence polarization in order to specifically measure only the analyte bound to the polymer.

As we wished to synthesize a water-compatible MIP, we initially screened the literature for MIPs that could directly and selectively extract FQs in aqueous environments. Principally, methacrylic acid (MAA) but sometimes 2-hydroxyethyl methacrylate (HEMA), were employed as the functional monomer, with ethylene glycol dimethacrylate (EDMA) or trimethylolpropane trimethacrylate (TRIM) as cross-linker, and methanol (Díaz-Alvarez et al., 2009; Prieto et al., 2011; Turiel et al., 2007) or methanol/water (Qiao and Sun, 2010; Sun et al., 2008; Yan et al. 2007) as porogenic solvents. Additionally, a poly(MAA-co-HEMA-co-EDMA) polymer for ENRO was synthesized in Moreno-Bondi's group (Benito-Peña et al., 2009). In preliminary studies, we evaluated several polymer formulations, and in our hands, the poly(MAA-*co*-HEMA-*co*-EDMA) MIP showed the best recognition properties for ENRO in mixed ACN:100 mM HEPES buffer pH 7.5 (1:1), as revealed by batch equilibrium binding studies.

II. Materials and methods

II.1. Reagents and materials

All chemicals and solvents were of analytical grade and purchased from Sigma-Aldrich (St-Quentin Fallavier, France), unless otherwise stated. 2,2'-azobis(2,4-dimethylvaleronitrile) (ABDV) was obtained from DuPont Chemicals (Wilmington, USA). Water was purified using a Milli-Q system (Millipore, Molsheim, France). Purified water was pH ≈ 6.
Scanning electron microscopy (SEM) imaging was carried out on a Philips XL30 Field Emission Gun Scanning Electron Microscope (Amsterdam, Netherlands). Polymer particles were sputter coated with gold prior to the SEM measurement. The hydrodynamic size of the particles was determined by dynamic light scattering (DLS) using a Zeta-sizer Nano-ZS (Malvern Instruments Ltd., Worcestershire, UK).

II.2. Preparation of polymers

The polymers were prepared by precipitation polymerization. The monomers, methacrylic acid (MAA), 2-hydroxyethyl methacrylate (HEMA) and ethylene glycol dimethacrylate (EDMA) were used as purchased. 0.1 mmol ENRO, 0.4 mmol MAA, 0.4 mmol HEMA, 2 mmol EDMA and 0.02 mmol ABDV were dissolved in 3.5 mL (for fluorescence intensity studies) or 10 mL (for polarization studies) of anhydrous acetonitrile (ACN) in a glass tube fitted with an airtight septum. The mixture was then purged with nitrogen for 7 min on ice. Polymerization was done overnight at 40°C in a water-bath. The polymers were then transferred to 50 mL centrifuge tubes and washed on a tube rotator (SB2, Stuart Scientific) with 12 rounds of $CH_3OH/CH_3COOH/CF_3COOH$ (80:15:5) and 2 rounds of ACN/CH_3COOH (4:1). At this point, no fluorescence was detected in the supernatants. The polymer particles were then rinsed with ACN, water and CH_3OH, finally dried overnight under vacuum and stored at 4°C. The non-imprinted polymer (NIP) and the control polymer (CP) were synthesized using the same protocol, except for the omission of the template ENRO, or its replacement by flumequine, respectively. MAA-based polymers were synthesized in the same way except that no HEMA was present and the amount of MAA was 0.8 mmol.

II.3. Evaluation of the binding properties of the polymers

The binding properties of the polymers towards ENRO, in anhydrous ACN and in ACN:100 mM HEPES buffer pH 7.5 (1:1) were evaluated by equilibrium binding experiments, with fluorescence and fluorescence polarization measurements. The latter were done in 1.4 mL quartz cuvettes on a Varian Cary Eclipse fluorescence spectrophotometer equipped with polarization accessories (Agilent Technologies, Palo Alto, CA, USA), using the high PMT voltage setting. The excitation/emission wavelengths were set at 280/440 nm.

For fluorescence measurements, a stock solution of ENRO (2.5 mM) was prepared in anhydrous ACN and stored in the dark at -20°C. For the assays, an aliquot of the stock solution was freshly diluted to 100 μM in anhydrous ACN or to 5 μM in ACN:100 mM HEPES buffer pH 7.5 (1:1). The polymers were suspended in the incubation solvent and placed in a sonicating bath. From this stock suspension, polymer concentrations ranging from 0.2 to 4 $mg.mL^{-1}$ were pipetted in 1.5 mL polypropylene microcentrifuge tubes and 100 μL of ENRO solution was added. The final volume was

adjusted to 1 mL with solvent. The tubes were incubated in the dark overnight at ambient temperature on a tube rotator. They were then centrifuged at 19,000x*g* for 25 min and the amount of free ENRO in the supernatant was quantified by fluorescence measurements. The amount of ENRO bound to the polymers was calculated by subtracting the amount of free analyte from the initial amount of ENRO added to the mixture.

For the polarization measurements, the experimental set-up is the same as described above except that polymer concentrations ranging from 0.02 to 0.2 mg.mL^{-1} were used and the incubation time was only 15 min (identical results were observed after 15 min and overnight incubation, indicating that the binding equilibrium was rapidly reached). The fluorescence polarization was measured directly on the samples, without centrifugation.

Competitive binding assays were performed in a similar way to the binding studies described above. Stock solutions of flumequine, streptomycin, kanamycin and ampicillin (1 mM) were prepared in ACN. The antibiotics were added at concentrations ranging from 0.01 to 100 μM, in order to compete with 0.1 μM ENRO in the binding assays, with a constant amount of 0.1 mg of MIP per vial.

II.4. Screening of fluoroquinolones using fluorescence polarization

The excitation/emission wavelengths were set at: 280/440 nm for ENRO; 283/425 nm for CIPRO; 284/430 nm for NOR. Polymer stock suspensions of 2 mg.mL^{-1} were prepared in ACN:100 mM HEPES buffer pH 7.5 (1:1) and stored at 4°C. Working polymer suspensions were diluted fresh. Fixed amounts of polymers (0.1, 0.03, 0.01, 0.005 mg.mL^{-1}) were pipetted in 1.5 mL polypropylene microcentrifuge tubes and FQs, ranging from 10^{-3} to 10^{-9} M in 100 μL solvent was added. The final volume was adjusted to 1 mL with solvent. The tubes were incubated in the dark for 15 min at ambient temperature on a tube rotator, after which their polarization values were measured.

II.5. Water and milk samples analysis

Tap water samples were spiked with ENRO at concentrations levels from 2.10^{-10} M to 2.10^{-5} M, and then diluted 1:1 with ACN. The samples were additioned with 50 μL of a MIP suspension (0.1 mg.mL^{-1}), incubated 15 minutes on a tube rotator in the dark and analyzed by fluorescence polarization measurements.

Skimmed milk (0.2% (w/w) fat; Lactel, Laval, France) and full-cream milk (3.6% (w/w) fat; Lactel, Laval, France) were bought from a local supermarket. 0.2 mL aliquots of milk were spiked with ENRO at concentration levels from 1.10^{-10} M to 1.10^{-3} M, and 0.4 mL ACN was added. After vigorous vortexing, the samples were centrifuged at 30,000x*g* for 20 min to remove any precipitated proteins. 0.5 mL of the supernatant was added to 0.5 mL of 100 mM HEPES buffer. The samples were additioned with 30 μL of a MIP suspension (1 mg.mL^{-1}), incubated 15 minutes on a tube rotator in the dark and analyzed by fluorescence polarization measurements.

II.6. Fluorescence emission decay measurements

Fluorescence lifetime measurements were performed with a Horiba Jobin-Yvon Fluorolog fluorescence spectrophotometer (Kyoto, Japan), by right-angle illumination of the two samples: a solution of 0.5 μM ENRO in ACN:100 mM HEPES buffer pH=7.5 (1:1) and a suspension of MIP (0.5 mg.mL^{-1}) incubated 3 hours in the dark with 0.5 μM ENRO in ACN:100 mM HEPES buffer pH=7.5 (1:1). The excitation light source used was a pulse diode Horiba NanoLED (model N-280) with a peak

wavelength at 287 nm and a pulse duration of 1.1 ns. The fluorescence emission wavelength was set at 440 nm, and excitation and emission bandpass were set at 5 nm. The data were collected using DataStation as software, to 10 000 counts in the peak and the time calibration was 0.0549 ns per channel. The data were then analyzed using DAS6 software, and for both samples, a second-exponential fit was used as model. For free ENRO, the data were analyzed from channel 390 to channel 1100, and for the sample of the suspension of MIP incubated with ENRO, the data were analyzed from channel 410 to channel 1200.

III. Results and discussion

III.1. Synthesis and characterization of the polymers

In the search of the best water-compatible specific MIP for ENRO, at first, several polymer formulations for the synthesis of MIPs for fluoroquinolones were tested and their binding performances evaluated by equilibrium binding studies. Literature data showed that most of them were prepared with MAA or HEMA/EDMA or MAA/TRIM in methanol or methanol/water mixtures (Díaz-Alvarez *et al.*, 2009; Prieto *et al.*, 2011; Sun *et al.*, 2008; Turiel *et al.*, 2007; Yan *et al.*, 2007) or with MAA/HEMA/EDMA in acetonitrile (Benito-Peña et al., 2009). Since we wanted to obtain small particles, we opted for precipitation polymerization, instead of bulk synthesis. All the MIPs gave satisfactory specificities but those prepared in methanol and methanol/water yielded polydisperse particles > 1 μm which were not suitable for our studies (DLS measurements gave a polydisperse index of 1; data not shown). The protocol using MAA/HEMA/EDMA in acetonitrile led to homogeneous small particles and was therefore chosen for our work. The recognition properties of the polymers were evaluated by batch equilibrium binding assays both in anhydrous ACN, as MIPs often demonstrate the most specific recognition in the same solvent in which it is synthesized (Andersson, 1996) and in ACN:100 mM HEPES buffer pH 7.5 (1:1) (named later ACN:buffer (1:1)), where the highest specificity was observed, as determined by HPLC with a MIP stationary phase (Benito-Peña et al., 2009). The amount of ENRO that binds to the polymers was calculated by measuring the fluorescence of non-bound ENRO after separation of the polymers by centrifugation.

As the binding test of our ENRO-MIP will be performed in ACN and in ACN: buffer (1:1), the emission fluorescence signal of ENRO was recorded in these two solvents prior to the measurements with the MIP (Figure 4.3). As a result, the addition of water resulted in a shift of the maximum emission wavelength, from 425 nm in pure ACN, to 445 nm in ACN: buffer (1:1). Furthermore, the emission spectrum of a suspension of MIP in ACN: buffer (1:1) shows that more than 98% of the template was removed, based on a calibration curve with free ENRO. As expected, no fluorescence was observed in the suspensions of NIP and CP. It can be noticed that there is a shift of emission maxima between free ENRO in solution and trapped ENRO in the polymer (maximum emission wavelength of 425 nm for the bound form and 445 nm for the free form). So, in the presence of water (50%, v/v), bound ENRO displayed an emission spectrum comparable to that seen in ACN. This may be due to the fact that trapped ENRO molecules are not in contact with water molecules.

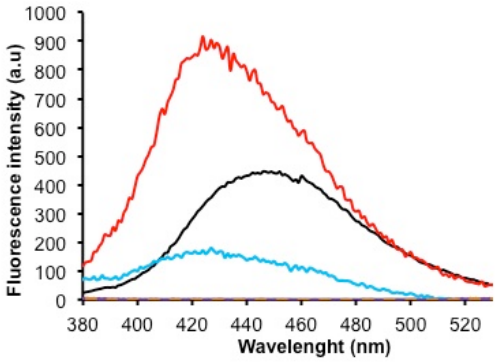

Figure 4.3. *Fluorescence emission spectrum in anhydrous ACN: 10 μM ENRO (red). Fluorescence emission spectra in ACN: buffer (1:1): 10 μM ENRO (black), 0.1 mg.mL^{-1} MIP (blue), 0.1 mg.mL^{-1} NIP*

(brown) 0.1 mg.mL^{-1} CP (violet). Excitation wavelength λ_{EM}=280 nm. The PMT voltage was set at high for all measurements except for the black curve, where medium PMT was used.

Equilibrium binding tests were performed with the MAA/HEMA-based polymers we have synthesized. The fluorescence of ENRO being highly influenced by the polarity of the solvent (Wu et al., 2007), 10 μM and 0.5 μM ENRO were employed for the assays in anhydrous ACN and ACN: buffer (1:1) respectively.

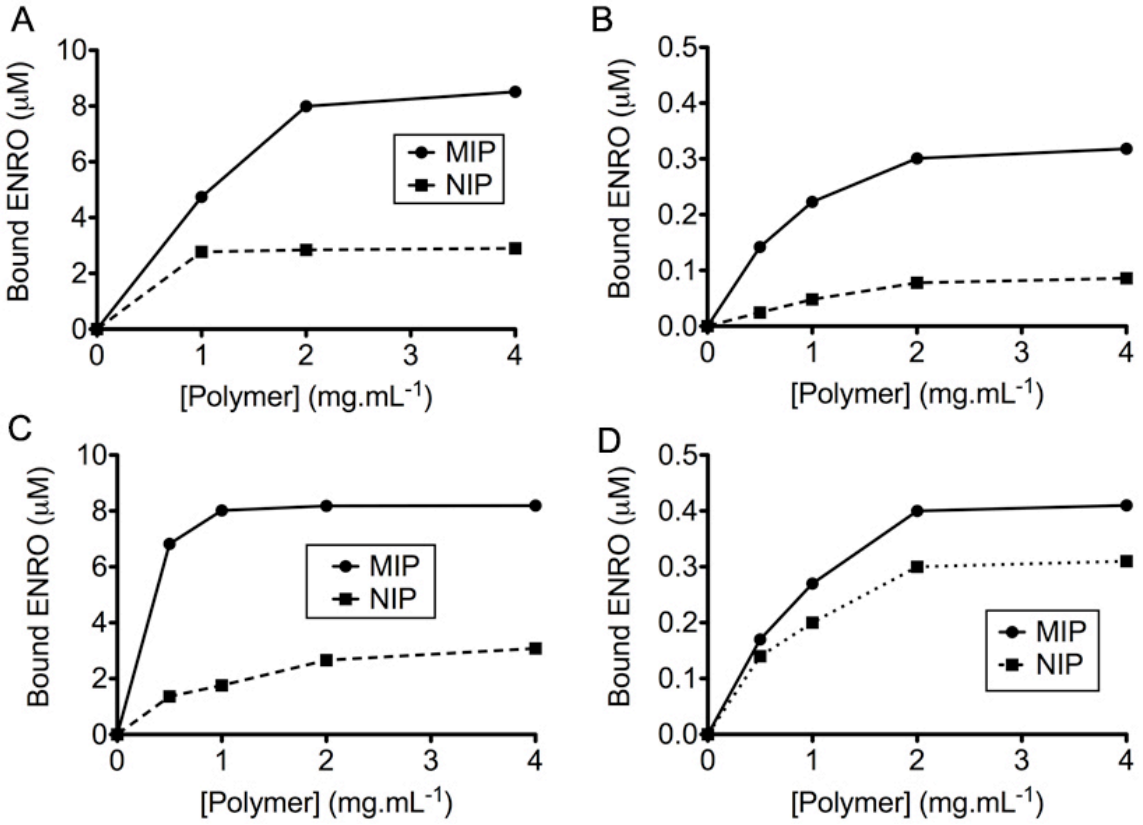

Figure 4.4. *Equilibrium binding isotherms for ENRO on MAA/HEMA MIP (circles) and NIP (squares) in (A) anhydrous ACN (B) ACN: buffer (1:1). Equilibrium binding isotherms for ENRO on MAA MIP (circles) and NIP (squares) in (C) anhydrous ACN (D) ACN: buffer (1:1). 10 μM and 0.5 μM ENRO were used in (A, C) and (B, D), respectively.*

Figure 4.4(A-B) show that in both media, there is some non-specific binding to the NIP but the MIP binds more ENRO than the NIP. Suspecting that the non-specific binding to the NIP could be due to the presence of HEMA in the polymerization protocol (in our group we have precedents of negligible non-specific binding with MAA-based polymers in acetonitrile (Tse Sum Bui et al., 2008, 2010)), we synthesized polymers without HEMA and investigated their binding characteristics. The low numbers of non-specific binding sites in MAA-based non-imprinted polymers has been attributed to the dimerization of methacrylic acid monomers that are not bound to template molecules. The aggregates are captured in the polymer matrix and are not available for non-specific binding, as the –COOH recognition groups are occupied by hydrogen bonds to adjacent monomers. At the same time, the formation of templated sites is also reduced but the overall effect is however an improvement in the ratio of templated binding sites to non-specific binding sites (Zhang et al., 2010).
Figure 4.4(A-C) shows that in anhydrous ACN, the MAA-based MIP has an approximately four times higher affinity for ENRO compared to the corresponding MAA-based NIP (i.e. the imprinting factor

defined as IF = binding(MIP)/binding(NIP) = 4), whereas for the MAA/HEMA-based polymer, the IF varies between 1.7 and 2.9. Thus the MAA-based MIP showed better specific binding to ENRO in ACN compared to the MAA/HEMA-based MIP. This can be explained by the fact that twice the amount of MAA per template molecule is available compared to the MAA/HEMA MIP, which shifts the equilibrium in the pre-polymerization solution towards complex formation between MAA and ENRO. The binding to the NIP is also slightly reduced at lower polymer concentrations in the case of the MAA MIP, the reason probably being dimerization of MAA molecules in the absence of HEMA and template prior to polymerization. In aqueous medium, non-specific binding to the NIP is higher in the case of the MAA polymer compared to the MAA/HEMA polymer, although the binding to the MIP is higher as well. This can be attributed to the MAA/HEMA polymers being less hydrophobic than the MAA polymers. Reduced binding to the non-imprinted polymer has also been observed for polymers of bupivacaine prepared with HEMA as co-monomer, which renders the material more hydrophilic (Dirion et al., 2003). It should be noted that no binding specificity was observed in pure water (≈ pH 6.6) and pure HEPES buffer (pH = 7.5), however, in ACN:HEPES buffer (1:9) the binding is specific at low polymer concentrations (Figure 4.5). While the MAA MIP performs better in ACN, our goal being direct measurements in aqueous samples, the MAA/HEMA-based polymers and ACN:buffer (1:1) assay conditions were kept for subsequent work.

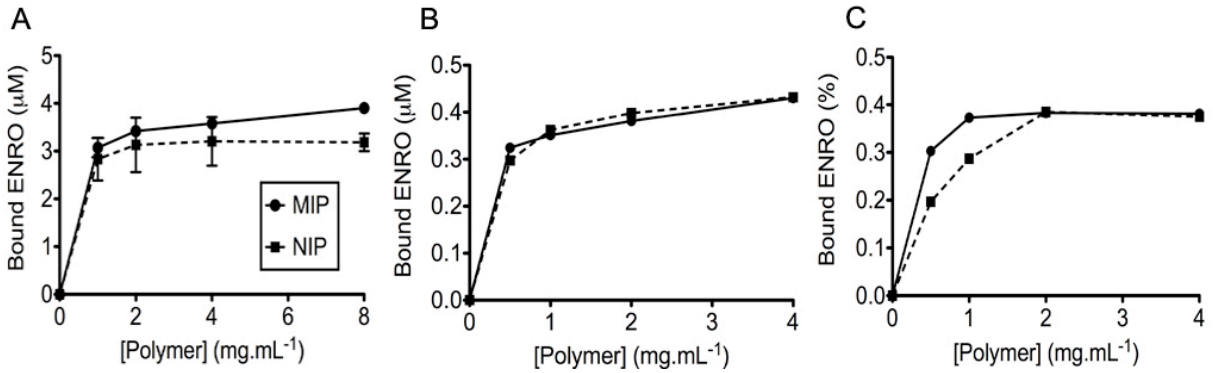

***Figure 4.5**. Equilibrium binding isotherms for ENRO on MIP (circles) and NIP (squares) in (A) pure water (≈ pH 6.6), (B) pure HEPES buffer (pH = 7.5) or (C) ACN:100 mM HEPES buffer pH 7.5 (1:9). 5 μM and 0.5 μM ENRO were used in (A) and (B, C), respectively. The error bars represent standard deviations for the experiments performed in triplicate. All experiments were performed at least in duplicate.*

To assess the MIP selectivity, equilibrium binding tests were performed in ACN:buffer (1:1) with four other piperazine-based FQs, CIPRO, norfloxacin (NOR), DANO and ofloxacin (OFLO), and two quinolones that do not possess the piperazine ring, flumequine (FLU) and oxolinic acid (OXO). As a result (Figure 4.6), the ENRO-imprinted polymer showed almost the same affinity for CIPRO and NOR who possess the most similar structures to ENRO, while very little binding (around 10%) was observed with the fluoroquinolones DANO and OFLO, which also possess the piperazine ring but present sterically hindered structures. Concerning the quinolones FLU and OXO, no binding (< 5%) was observed (not illustrated). These results suggest that the molecular recognition process is mostly based on the interactions taking place between the carboxylate group of the MAA monomer and the piperazine ring of the fluoroquinolone, and that the ENRO-imprinted polymer is group-selective.

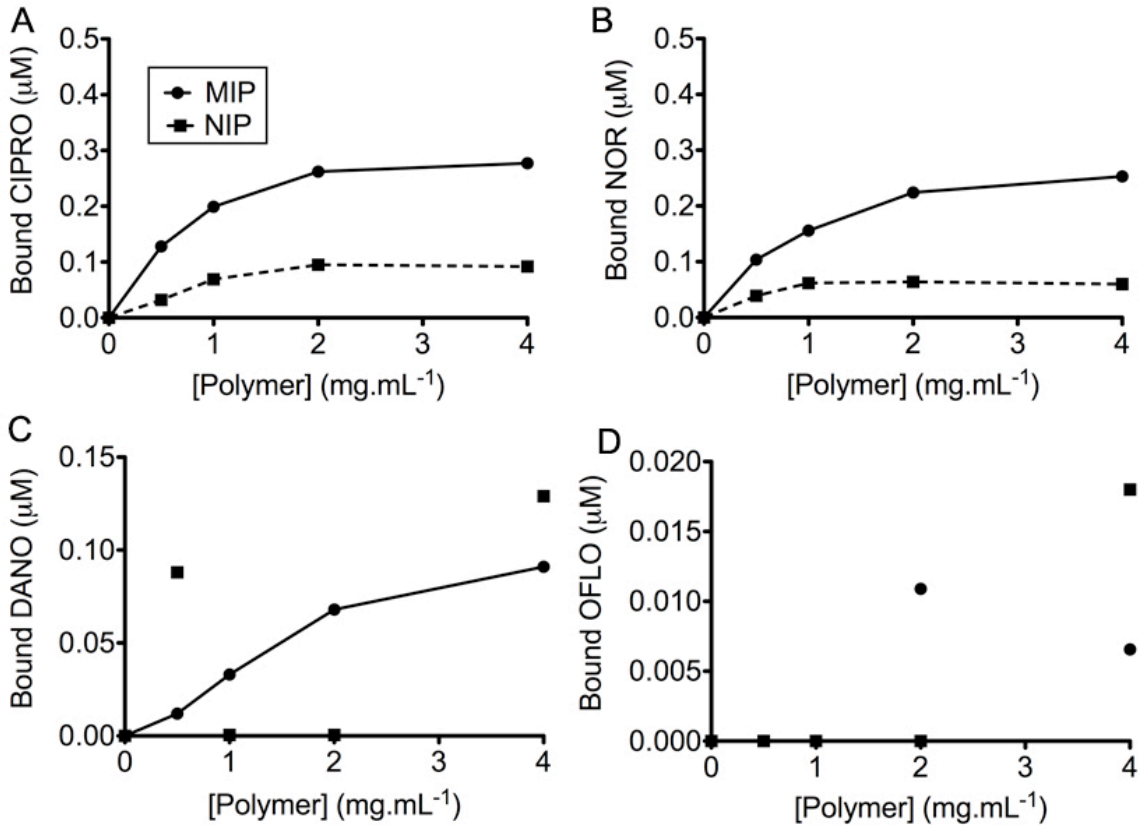

Figure 4.6. *Equilibrium binding isotherms on MIP (circles) and NIP (squares) for (A) CIPRO, (B) NOR, (C) DANO and (D) OFLO in ACN:100 mM HEPES buffer pH 7.5 (1:1). 0.5 μM and 0.1 μM ENRO were used in (A, B, C) and (D), respectively. All experiments were performed in duplicate and mean values are presented.*

III.2. Fluorescence polarization measurements

In order to perform fluorescence polarization measurements, it is important to avoid scattering of the excitation light by the polymer particles, which therefore should be small with diameters below the wavelength of the light. In addition, a good separation between the excitation and the emission peaks is preferred (Hunt et al., 2006) which is the case for ENRO, as the Stokes shift is high (Excitation wavelength λ_{EX} = 280 nm and emission wavelength λ_{EM} = 440 nm). The size of the MIP and NIP particles were 400 nm and 700 nm respectively, as measured by dynamic light scattering (DLS), which proved to be too big for the fluorescence polarization studies. Consequently, new polymers were synthesized using the same recipe but this time by adding three times more solvent to the MIP precursors solution. This resulted in smaller particles with a relatively narrow size distribution. SEM imaging (Figures 4.7(A-B)) showed that the MIP and the NIP particles have average diameters of d = 78 nm (± 13 nm) and d = 170 nm (± 32 nm), respectively. In order to study the hydrodynamic radius of the particles, the polymers were suspended in ACN, and analyzed by dynamic light scattering (DLS). MIP presented an average diameter of d = 120 nm and NIP, an average diameter d = 230 nm. The bigger size of the non-imprinted particles was still of a concern since they did not yield optically clear solutions, specially in the buffer medium. Moreover, a NIP is not an ideal control, as the presence of the template causes general changes in the morphology of the polymer (pore size and shape, surface area, etc). Alternatively, using a MIP for a different template as a control polymer is a better option (Kempe and Kempe, 2010). Thus, we additionally synthesized a control polymer (CP) using flumequine (FLU), a fluoroquinolone without the piperazine group, as the imprinting template. SEM

and dynamic light scattering measurements (see Figure 4.7C) showed that monodisperse beads of an average diameter d = 113 nm (± 38 nm) were obtained. The average hydrodynamic diameter of CP particles was 175 nm, which is closer to the values obtained with the ENRO MIP.

A. MIP

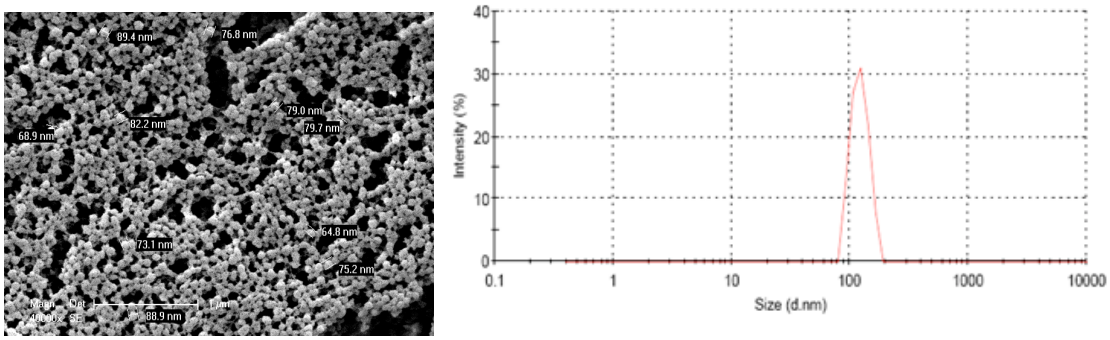

B. NIP

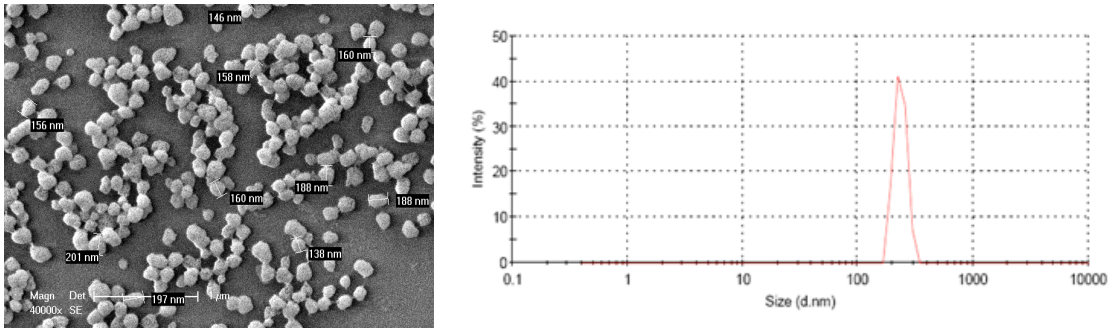

C. CP

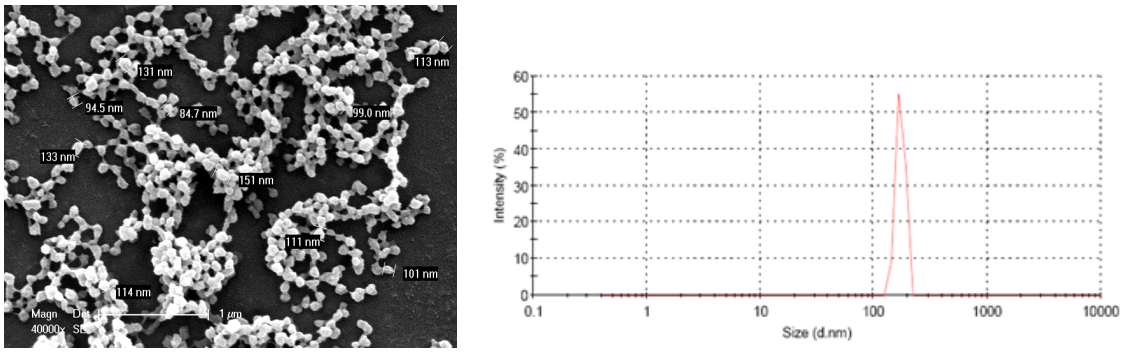

Figure 4.7. *Scanning electron micrographs and corresponding dynamic light scattering measurements in ACN of (A) MIP, (B) NIP, and (C) CP. The scale bar corresponds to 1 µm. Peak analyzes by intensity, volume and number all showed single, symmetrical peaks with a narrow distribution.*

Other qualitative considerations for fluorescence polarization are the fluorescence lifetime and the rotational relaxation time of the fluorophore, which have to be compared. Indeed, if the fluorescence lifetime is shorter than the rotational relaxation time, the fluorophore does not have the time to rotate during the relaxation time, and thus even the free ligand will give a high polarization value. On the contrary, if the lifetime is longer than the rotational relaxation time, the free fluorophore

can rotate and will give a low polarization value. In our case, we want to see the difference of polarization values between the free ligand and the ligand bound to the MIP, so it is important that the free ligand gives a low polarization value.

A rule exists in order to estimate the rotational relaxation time of a molecule in a low viscosity solvent: its molecular mass (in g/mol) must be divided by 1000 in order to give the value of the rotational relaxation time in nanoseconds (ns). It means that for ENRO, which has a molecular mass of 359.4 g/mol, its rotational relaxation time can be estimated to be 0.36 ns (Jameson et al., 2010).

The fluorescence lifetimes of free ENRO and of a suspension of MIP incubated with ENRO were measured in ACN:buffer (1:1). Figure 4.8 shows that the fluorescence decay kinetics for free ENRO and for a suspension of MIP incubated with ENRO, which were both fitted to a two-exponential function. Fluorescence lifetime values and respective amplitudes of both samples are summarized in Table 1.

Concerning the lifetimes of 2.22 ns and 3.27 ns found for free ENRO, we can conclude first that the lifetime values are higher than the estimated rotational relaxation time of ENRO (0.36 ns), which means that free ENRO in solution will give a low polarization value (low is typically p=0.03-0.06 (Smith and Eremin, 2008)). Second, as these lifetime values are short, it means that the ENRO bound to the MIP will probably give a high polarization value, as it will not have the time to rotate between the time of absorption and emission. We can note that two lifetimes were found for free ENRO in ACN/buffer. This can be explained by the presence of two solvents of different polarity (ACN and buffer), which means that the molecules of ENRO can be surrounded in majority by molecules of ACN or by molecules of water in their local environment, which will give different lifetime values. In a more polar environment, the lifetime tends to be shorter, because the large dipole moments of the surrounding molecules tend to increase the energy transfer (Lakowicz, 2006). In our sample of free ENRO in solution, the majority of ENRO molecules (73.56%) have a fluorescence lifetime of 2.22 ns (Table 4.1).

For the suspension of MIP incubated with ENRO, two fluorescence lifetimes (2.34 ns and 6.31 ns) were obtained. If we found again a first lifetime value of 2.34 ns similar to the one found for free ENRO, another longer lifetime of 6.31 ns was also found, which corresponds to the ENRO molecules that are bound to the MIP. The fact that the polymer is more hydrophobic and apolar results in the longer fluorescence lifetime of the bound ENRO. The relative amplitude reveals that 43.87% of the ENRO was bound to the MIP, which corresponds to 0.22 μM of ENRO. The fluorescence binding assay that was performed between 0.5 $mg.mL^{-1}$ MIP and 0.5 μM ENRO resulted in around 0.15 μM bound ENRO (Figure 4.4). With the fluorescence lifetime measurements, we found a slightly higher value, because the embedded ENRO in the MIP matrix (which corresponds to the ENRO molecules that were impossible to remove during the washing steps) are probably included in the population of ENRO that shows the longer lifetime of 6.31 ns.

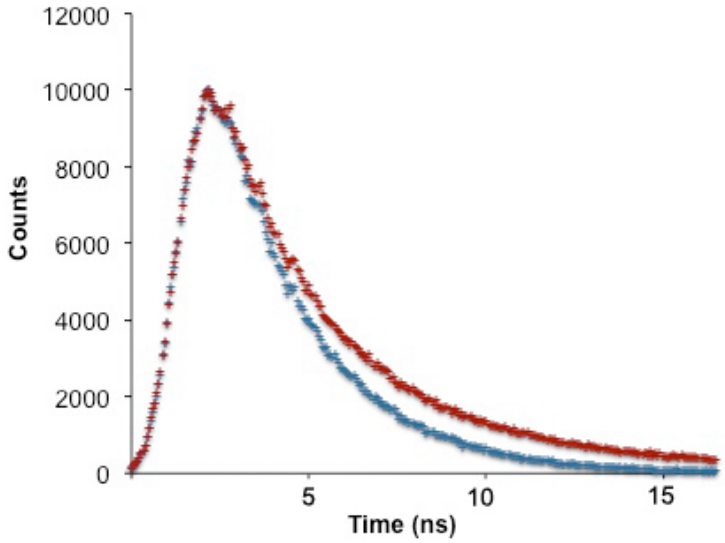

Figure 4.8. *Fluorescence decays kinetics of a solution of ENRO (0.5 μM in ACN:HEPES buffer (1:1)) (blue curve) and of a suspension of MIP (0.5 mg/mL) incubated 3 hours with 0.5 μM ENRO in ACN:HEPES buffer (1:1) (red curve).* $\lambda_{EX/EM}$*=280/440 nm.*

Table 4.1. *Fluorescence lifetimes and respective relative amplitudes obtained from least-square fitting of the fluorescence decays in Figure 4.8, using a second-exponential decay law.*

	τ_1 (ns)	A_1 (%)	τ_2 (ns)	A_2 (%)	χ^2
Free ENRO	2.22	73.56	3.27	26.44	1.27
MIP+ENRO	2.34	56.13	6.31	43.87	1.32

Figure 4.9 shows the binding of ENRO to increasing concentrations of MIP, NIP and CP in anhydrous ACN and in ACN: buffer (1:1), as measured by fluorescence polarization. NIP and CP gave the same polarization values in ACN but in the mixed buffer solution, CP gave lower polarization values than the NIP. CP was hence kept as the reference polymer for polarization experiments. The curves in Figure 9 can be interpreted as follows: the more rapid the motion of the fluorophore, the more the emitted fluorescence light is depolarized, which explains that in the absence of polymers, the p value is negligible. When ENRO binds to the MIP, its tumbling rate is reduced, resulting in an increase in polarization. In both media, the maximum p is reached at 0.1 mg of MIP that seems sufficient to bind completely the amount of ENRO present. The maximum polarization value reached is different in the two solvents as polarization is dependent on the viscosity (viscosity of ACN is 0.34 cP and pure water is 1 cP at 25 °C). When dealing with MIPs prepared with a fluorescent template, there could be interference from the fluorescence of some residual template trapped in the polymer. Therefore, polarization measurements were also made on the MIP alone. Whatever the concentration of MIP tested (0.02 to 0.2 $mg.mL^{-1}$), the same polarization value was obtained ($p \approx 0.34$ in ACN and $p \approx 0.23$ in ACN/buffer solution) (diamonds in Figure 4.9). This high polarization value indicates the presence of traces of trapped ENRO, which was impossible to remove during the washing steps following the polymerization process. However, this residual template does not seem to have any effect on the binding measurements. Indeed, a fluorescence scan of the MIP does indicate the presence of some residual ENRO (< 2%), emitting at a different wavelength from the ENRO added to the test. This shift in wavelength may be due to the fact that trapped ENRO is not in contact with the solution (Figure 4.3).

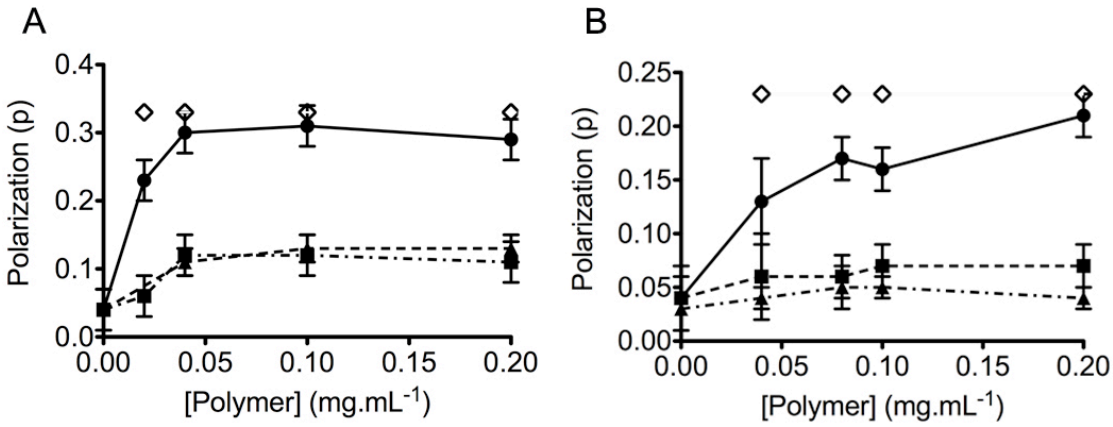

Figure 4.9. *Binding of ENRO to MIP (circles), CP (triangles) and NIP (squares) in (A) anhydrous ACN and (B) ACN:100 mM HEPES buffer pH 7.5 (1:1). 10 μM and 0.5 μM ENRO were used in (A) and (B), respectively. The 'diamonds' represent the polarization values of MIP alone (without addition of ENRO). Data are means of triplicate experiments. The error bars represent standard deviations.*

In order to check the influence of the solvent on the binding properties of the MIP, a fixed concentration of polymer (0.08 mg.mL^{-1}) was incubated with 0.5 μM ENRO in ACN:HEPES buffer, and the proportions of ACN and HEPES buffer were varied from 8:2 to 2:8 (v:v). As can be seen in Figure 4.10, both total and non-specific binding slightly increased with increasing proportion of HEPES buffer, but for all tested solvent, the binding was specific with an imprinting factor (IF) varying from 2.25 to 4.60 (Table 4.2). For reasons of convenience, we kept the ratio ACN:HEPES buffer at 1:1 for further studies, but we demonstrated that the binding remained specific in more aqueous media, such as ACN:HEPES buffer (2:8).

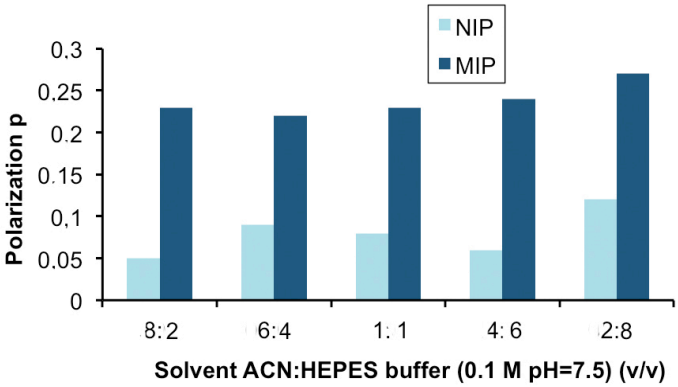

Figure 4.10. *Binding of 0.5 μM ENRO to 0.08 mg.mL^{-1} of MIP (dark blue bars) and NIP (squares) in the solvent ACN: 100 mM HEPES buffer pH 7.5, with the ratio varying from 8:2 to 2:8 (v:v).*

Table 4.2. *Imprinting factor (pMIP/pNIP) depending on the ratio ACN:HEPES buffer.*

Solvent ACN:HEPES buffer (ratio v:v)	Imprinting factor (p_{MIP}/p_{NIP})
8:2	4.6
6:4	2.4
1:1	2.9
4:6	4.0
2:8	2.3

III.3. Application of fluorescence polarization to measure ENRO in buffer media and in tap water

Our next objective was to use this MIP combined with the technique of fluorescence polarization to determine ENRO in aqueous media. Thus, all following experiments were done in ACN: buffer (1:1). A fixed amount of MIP (0.1 mg.mL^{-1}) was incubated with varying concentrations of ENRO, ranging from 10^{-9} M to 10^{-3} M. The polarization value of each sample was measured, generating a curve as shown in Fig. 4A. For low concentrations of ENRO (1-100 nM), the polarization value was high since all the ENRO is bound to the MIP. The polarization values decreased with increasing concentrations of ENRO, i.e. with increasing amounts of free ENRO. The recognition was specific as for all concentrations of ENRO incubated with CP (0.1 mg.mL^{-1}), the polarization value remains constant at p ≈ 0.04, which means that ENRO did not bind to the CP. Thus, it is possible to quantify the amount of ENRO present in solution for concentrations in the linear part of the graph, between 0.1 μM and 10 μM. The assay has a dynamic range, i.e. the difference between the highest and lowest standard, Δp of ≈ 200 mp.

FQs have been detected in surface, ground and tap waters at nanograms per litre level (Sturini et al., 2010) but sometimes at much higher concentrations, for instance 6.5 mg.L^{-1} for CIPRO, the most used clinical fluoroquinolone antibiotic in the world (the News magazine for Pharmacists, 2008), and up to 0.5 mg.L^{-1} for NOR, around industrial pharmaceutical production areas for world drug markets (Fick et al., 2009). We also performed fluorescence polarization assays with CIPRO and NOR. The MIP demonstrated identical recognition behaviors towards the three antibiotics, which is not surprising as the three FQs possess very similar structures and in particular the piperazinyl ring which plays an important role in the recognition mechanism (Benito-Peña et al., 2009 ; Turiel et al., 2007). No binding of these FQs to the CP was observed. The curves would allow the quantification of any of the three FQs present in the medium from 0.1 to 10 μM, i.e. 32 μg.L^{-1} – 3.6 mg.L^{-1} (Figure 4.10). Our method thus can provide a means for the initial on-site screening and monitoring of these FQs by just measuring the polarization values of a serial number of dilutions of the samples in ACN:buffer (1:1), a quicker and cheaper alternative to LC/MS-MS analysis (Fick et al., 2009).

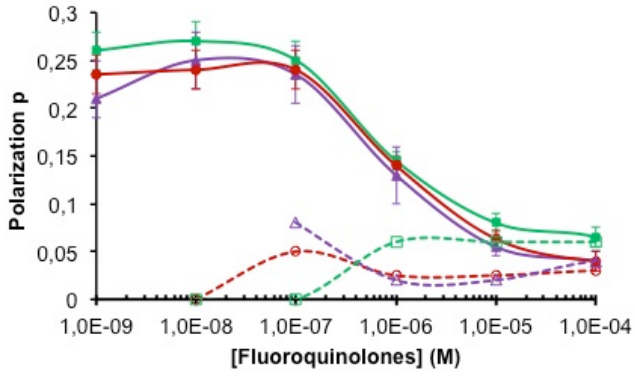

Figure 4.10. *Fluorescence polarization for varying concentrations of ENRO (red circles), CIPRO (green squares) and NOR (violet triangles), incubated with 0.1 mg.mL^{-1} MIP (solid curves, filled symbols) or CP (dashed curves, open triangles) in ACN:100 mM HEPES buffer pH 7.5 (1:1).*

However, the limit of detection of ENRO obtained with 0.1 mg.mL^{-1} of MIP in ACN: buffer (1:1) is 0.1 μM. In order to increase the sensitivity and to detect lower concentrations of ENRO (0.1, 1 and 10 nM), we tested lower concentrations of MIPs (0.03, 0.01 and 0.005 mg.mL^{-1}) in the assay. Indeed, a LOD of 0.1 nM ENRO can be reached with 5 μg.mL^{-1} MIP. This experiment shows that fluorescence polarization standard curves can be constructed by modulating the amount of MIP so as to match with the concentration of ENRO in the sample (Figure 4.11B). In fact, the measuring ranges of 0.1, 0.03, 0.01 and 0.005 mg.mL^{-1} MIP are (0.1-10 μM), (10 nM-10 μM), (1 nM-1 μM) and (0.1 nM-0.1 μM), respectively. These results suggest that in order to determine ENRO in an unknown sample, concentrations of 0.03 and 0.01 mg.mL^{-1} MIP, which offer the broadest linearity range, should be chosen as a starting point of the analysis.

To validate the procedure with real samples, tap water samples (pH 7.27), which showed no presence of ENRO, were spiked with the FQ at concentration levels from 2.10^{-10} M to 2.10^{-5} M, then diluted with an equal volume of ACN before incubation with 5 μg.mL^{-1} of MIP. The MIP showed the same binding behavior in ACN:tap water (1:1) as in ACN:buffer (1:1). So, an unknown concentration of ENRO in tap water can be determined by using a standard calibration curve of ENRO prepared in ACN:buffer (1:1). A LOD of 0.1 nM (36 ng.L^{-1}) ENRO was reached which is more sensitive than other immunoassay methods for instance based on a surface plasmon resonance immunosensor (LOD of 1 μg.L^{-1}) (Fernandez et al., 2011) or by ELISA (LOD of 9.3 nM) (Bras Gomes et al., 2010).

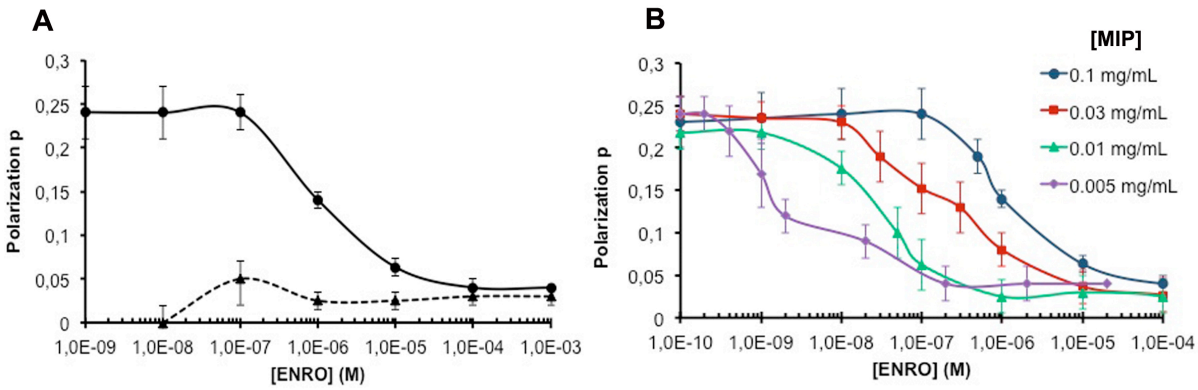

Figure 4.11. *Fluorescence polarization standard curves for ENRO incubated with (A) 0.1 mg.mL^{-1} MIP (circles) and CP (triangles) in ACN:100 mM HEPES buffer pH 7.5 (1:1); (B) 0.1 mg.mL^{-1} (blue circles), 0.03 mg.mL^{-1} (red squares), 0.01 mg.mL^{-1} (green triangles) in ACN:100 mM HEPES buffer pH 7.5 (1:1) and 0.005 mg.mL^{-1} (violet diamonds) in ACN: tap water (pH 7.27). Data are means of triplicate experiments. The error bars represent standard deviations.*

III.4. Application of fluorescence polarization to measure ENRO and FQs in milk

Milk is a complex medium and some of the components present, in particular proteins, sugars and fats are susceptible to interfere with the quantification of ENRO (Gasilova and Eremin, 2010). For sample preparation, 0.2 mL aliquots of skimmed milk samples were spiked with ENRO at nine concentrations levels from 1.10^{-10} M to 1.10^{-3} M and the proteins were precipitated with 0.4 mL of ACN (Rodriguez-Diaz et al., 2004). The mixture was centrifuged and the supernatant was diluted with an equal volume of 100 mM HEPES buffer pH 7.5. The solutions were incubated with 0.03 mg.mL^{-1} MIP and their fluorescence polarization measured. As it can be seen in Figure 4.12A, the useful measuring range for

ENRO in skimmed milk is 10 nM - 100 μM. European Legislation approves the administration of the following four FQs to animals from which milk is produced for human consumption: ENRO (and its metabolite CIPRO), DANO and marbofloxacin. Considering that the MRL for milk of the sum of ENRO and its metabolite CIPRO is 100 $\mu g.kg^{-1}$ (280 nM), the MIP would be able to detect the presence of these antibiotics residues present in milk. Since the calibration curve of Figure 4.12A has a similar profile to that observed with HEPES buffer (0.3 $mg.mL^{-1}$ in Figure 10B), this indicates that there is no matrix interference from the milk sample after modest dilutions. This implies that lower concentrations of ENRO in milk samples are accessible by using lower concentrations of MIPs.

Experiments were reproduced with full-cream milk, and as shown in Figure 4.12B, the fluorescence polarization curve for ENRO is similar than in skimmed milk, demonstrating that our assay is still valid in a more complex sample. The only difference is the higher polarization value for low concentrations of ENRO, which can be attributed to the higher quantity of fat present in the system.

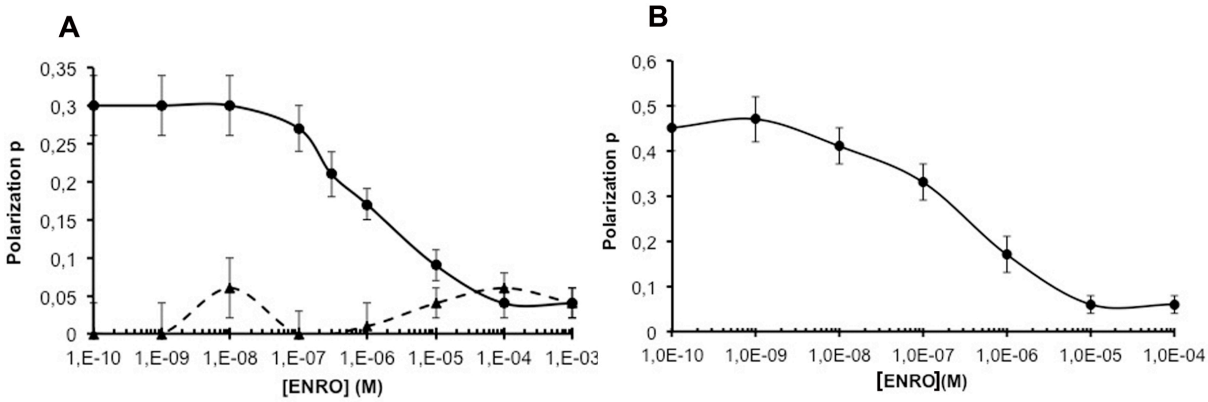

Figure 4.12. *Fluorescence polarization standard curves for ENRO with 0.03 $mg.mL^{-1}$ of MIP in (A) skimmed milk and (B) full-cream milk. Results from at least 3 different batches of milk.*

Antibiotics from other families that are allowed in milk-producing animals for human consumption are among others, kanamycin (KANA), streptomycin (STRE), ampicillin (AMP) and flumequine (FLU). According to the Commission Regulation (EU) no. 37/2010 of the European Union, the MRLs for FLU, KANA, STRE and AMP are respectively 50 $\mu g.kg^{-1}$ (190 nM), 150 $\mu g.kg^{-1}$ (310 nM), 200 $\mu g.kg^{-1}$ (340 nM) and 4 $\mu g.kg^{-1}$ (11 nM). To investigate whether the MIP can measure piperazine-based fluoroquinolones selectively even in the presence of these non-related antibiotics, milk samples were spiked with ENRO, DANO, FLU, KANA and STRE at their MRLs concentrations. After sample preparation and incubation with the MIP, the polarization was measured at λ_{EX} / λ_{EM} : 280 / 440 nm. The results are presented in Table 4.3 and show that the MIP is selective to FQs. Undoubtedly, this procedure can be applied to detect FQs in milk, even in the presence of high concentrations of other classes of antibiotics.

Competitive binding assays were additionally performed to confirm that the MIP has no affinity for FLU, KANA, STRE and AMP at higher concentrations than their MRLs values. Various concentrations of each competitive antibiotic, from 0.01 μM to 10 μM were added to compete with 0.1 μM ENRO in the binding assays. These antibiotics do not inhibit the binding of ENRO to the MIP (Figure 4.13) that means that they have no affinity for the MIP.

Table 4.3. *Polarization measurements (λ_{EX}=280 nm, λ_{EM}=440 nm) of spiked antibiotics at their MRLs concentrations in milk, with 0.03 mg.mL^{-1} of MIP. MRLs of ENRO, DANO, FLU, KANA and STRE are 0.28 μM, 0.08 μM, 0.19 μM, 0.31 μM, 0.34 μM respectively.*

Antibiotics	Polarization
ENRO	0.21 ± 0.03
ENRO + FLU	0.21 ± 0.03
ENRO + DANO	0.17 ± 0.03
ENRO + DANO + FLU	0.17 ± 0.03
ENRO + DANO + FLU + KANA + STRE	0.17 ± 0.03

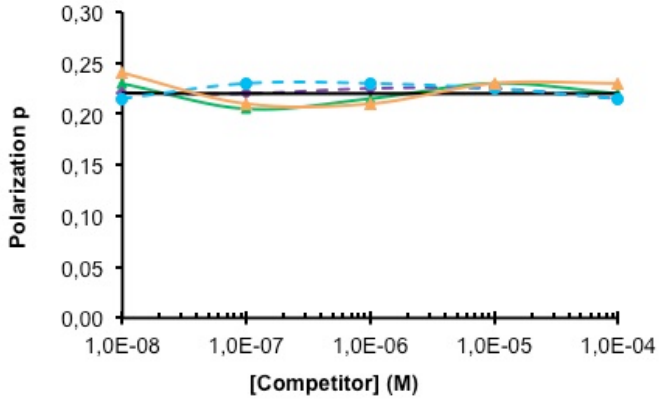

Figure 4.13. *Fluorescence polarization for ENRO (0.1 µM) and varying concentrations of competitors FLU (blue), STRE (green), KANA (violet) and AMP (orange) in the presence of 0.1 mg.mL^{-1} of MIP in ACN:100 mM HEPES buffer pH 7.5 (1:1). $\lambda_{EX}/\lambda_{EM}$=280/440 nm. There is no interference from the fluorescence of FLU ($\lambda_{EX}/\lambda_{EM}$: 235/360 nm).*

IV. Conclusions

A pseudo-immunoassay based on a molecularly imprinted polymer associated with fluorescence polarization measurements has been developed for the rapid on-site detection and screening of UV-excited analytes such as the piperazine-based fluoroquinolone antibiotics in water and milk samples. The MIP showed similar affinity for enrofloxacin, ciprofloxacin and norfloxacin, and none for flumequine and antibiotics from other families, which indicates its high selectivity for the three fluoroquinolones. The methodology was successfully applied to detect FQs in real samples, i.e. tap water and milk. A low LOD of 0.1 nM (36 $ng.L^{-1}$) could be achieved with 5 $\mu g.mL^{-1}$ of MIP, enabling the determination of 0.28 nM ENRO, the legal amount tolerated in water samples. ENRO and DANO, whose MRLs in milk have been fixed to 0.28 μM and 0.08 μM respectively could be easily detected. The procedure is very easy and practical as it consists of simply precipitating the milk proteins with acetonitrile, centrifuging and adding buffer and MIP to the supernatant before reading with a spectrofluorimeter. Remarkably, the fluorescence polarization measurements quantified only ENRO and DANO, among flumequine, kanamycin, streptomycin also present in the milk samples. Though this technique cannot distinguish individually the different fluoroquinolones, as compared to HPLC or LC/MS-MS, it can undoubtedly serve as an initial rapid, sensitive and cheap screening tool, to detect their presence in water and in milk, and probably in other matrices like meat extract for which the MRLs for the main antibiotics used in veterinary medicine are similar or higher than those in milk. Moreover, the stability of the MIP in organic solvents like acetonitrile and methanol, can be useful to analyze FQs under conditions in which natural antibodies are denatured. The assay mode presented in this study is a direct binding assay as the analyte is intrinsically fluorescent. The application of this method to the classic competition binding assay mode that requires a fluorescent tracer should be straightforward. In this case, the analyte in the sample will compete with the tracer for binding to the MIP and the polarization signal will decrease (Smith and Eremin, 2008). Our results are very promising as MIPs, which are more stable and robust than natural antibodies, and also more quickly obtainable, could replace the latter in the application of fluorescence polarization to high throughput screening.

V. References

Adamczyk, M.; Chen, Y.-Y.; Johnson, D. D.; Reddy, R. E. A stereoselective synthesis of 1α-(3′-Carboxypropyl)-4-androsten-17 β-ol-3-one: Preparation of immunoreagents for quantification of testosterone by fluorescence polarization immunoassay. *Tetrahedron* **1997**, *53*, 12855.

Benito-Peña, E.; Martins, S.; Orellana, G.; Moreno-Bondi, M. C. Water-compatible molecularly imprinted polymer for the selective recognition of fluoroquinolone antibiotics in biological samples. *Analytical and Bioanalytical Chemistry* **2009**, *393*, 235.

Blasco, C.; Picó, Y. Development of an Improved Method for Trace Analysis of Quinolones in Eggs of Laying Hens and Wildlife Species Using Molecularly Imprinted Polymers. *Journal of Agricultural and Food Chemistry* **2012**, *60*, 11005.

Cao, L.; Lin, H.; Mirsky, V. M. Surface plasmon resonance biosensor for enrofloxacin based on deoxyribonucleic acid. *Analytica chimica acta* **2007**, *589*, 1.

Caro, E.; Marce, R. M.; Cormack, P. A.; Sherrington, D. C.; Borrull, F. Novel enrofloxacin imprinted polymer applied to the solid-phase extraction of fluorinated quinolones from urine and tissue samples. *Analytica chimica acta* **2006**, *562*, 145.

Christodoulou, E. A.; Samanidou, V. F. Multiresidue HPLC analysis of ten quinolones in milk after solid phase extraction: Validation according to the European Union Decision 2002/657/EC. *Journal of separation science* **2007**, *30*, 2421.

Chun, H. S.; Choi, E. H.; Chang, H.-J.; Choi, S.-W.; Eremin, S. A. A fluorescence polarization immunoassay for the detection of zearalenone in corn. *Analytica chimica acta* **2009**, *639*, 83.

Collignon, P.; Powers, J. H.; Chiller, T. M.; Aidara-Kane, A.; Aarestrup, F. M. World Health Organization ranking of antimicrobials according to their importance in human medicine: a critical step for developing risk management strategies for the use of antimicrobials in food production animals. *Clinical Infectious Diseases* **2009**, *49*, 132.

Dandliker, W.; Feigen, G. Quantification of the antigen-antibody reaction by the polarization of fluorescence. *Biochemical and biophysical research communications* **1961**, *5*, 299.

Díaz-Alvarez, M.; Turiel, E.; Martín-Esteban, A. Selective sample preparation for the analysis of (fluoro) quinolones in baby food: molecularly imprinted polymers versus anion-exchange resins. *Analytical and Bioanalytical Chemistry* **2009**, *393*, 899.

Golet, E. M.; Xifra, I.; Siegrist, H.; Alder, A. C.; Giger, W. Environmental exposure assessment of fluoroquinolone antibacterial agents from sewage to soil. *Environmental Science & Technology* **2003**, *37*, 3243.

Goryacheva, I. Y.; Eremin, S. A.; Shutaleva, E. A.; Suchanek, M.; Niessner, R.; Knopp, D. Development of A fluorescence polarization immunoassay for polycyclic aromatic hydrocarbons. *Analytical Letters* **2007**, *40*, 1445.

Hatzidakis, G. I.; Tsatsakis, A. M.; Krambovitis, E. K.; Spyros, A.; Eremin, S. A. Use of L-lysine fluorescence derivatives as tracers to enhance the performance of polarization fluoroimmunoassays. A study using two herbicides as model antigens. *Analytical Chemistry* **2002**, *74*, 2513.

Hunt, C. E.; Ansell, R. J. Use of fluorescence shift and fluorescence anisotropy to evaluate the re-binding of template to (S)-propranolol imprinted polymers. *Analyst* **2006**, *131*, 678.

Hunt, C. E.; Pasetto, P.; Ansell, R. J.; Haupt, K. A fluorescence polarisation molecular imprint sorbent assay for 2, 4-D: a non-separation pseudo-immunoassay. *Chemical Communications* **2006**, 1754.

Jameson, D. M.; Ross, J. A. Fluorescence polarization/anisotropy in diagnostics and imaging. *Chemical Reviews* **2010**, *110*, 2685.

Lakowicz, J. R.: *Principles of fluorescence spectroscopy - Third Edition*; Springer, 2006; Vol. 1.

Lombardo-Agüí, M.; Gámiz-Gracia, L.; Cruces-Blanco, C.; García-Campaña, A. M. Comparison of different sample treatments for the analysis of quinolones in milk by capillary-liquid chromatography with laser induced fluorescence detection. *Journal of Chromatography A* **2011**, *1218*, 4966.

Lv, Y.-K.; Ma, Y.; Zhao, X.-B.; Jia, C.-L.; Sun, H.-W. Grafting of norfloxacin imprinted polymeric membranes on silica surface for the selective solid-phase extraction of fluoroquinolones in fish samples. *Talanta* **2012**, *89*, 270.

Lv, Y.-K.; Yang, L.; Liu, X.-H.; Guo, Z.-Y.; Sun, H.-W. Preparation and evaluation of a novel molecularly imprinted hybrid composite monolithic column for on-line solid-phase extraction coupled with HPLC to detect trace fluoroquinolones residues in milk. *Analytical Methods* **2013**, *5*, 1848

Maragos, C. Fluorescence polarization immunoassay of mycotoxins: a review. *Toxins* **2009**, *1*, 196.

Perez-Bendito, D.; Gomez-Hens, A.; Gaikwad, A. Direct stopped-flow fluorescence polarization immunoassay of abused drugs and their metabolites in urine. *Clinical chemistry* **1994**, *40*, 1489.

Pichon, V.; Haupt, K. Affinity Separations on Molecularly Imprinted Polymers with Special Emphasis on Solid‐Phase Extraction. *Journal of Liquid Chromatography and Related Technologies* **2006**, *29*, 989.

Prieto, A.; Schrader, S.; Bauer, C.; Möder, M. Synthesis of a molecularly imprinted polymer and its application for microextraction by packed sorbent for the determination of fluoroquinolone related compounds in water. *Analytica chimica acta* **2011**, *685*, 146.

Qiao, F.; Sun, H. Simultaneous extraction of enrofloxacin and ciprofloxacin from chicken tissue by molecularly imprinted matrix solid-phase dispersion. *Journal of pharmaceutical and biomedical analysis* **2010**, *53*, 795.

Shim, W. B.; Kolosova, A. Y.; Kim, Y. J.; Yang, Z. Y.; Park, S. J.; Eremin, S. A.; Lee, I. S.; Chung, D. H. Fluorescence polarization immunoassay based on a monoclonal antibody for the detection of ochratoxin A. *International journal of food science & technology* **2004**, *39*, 829.

Smith, D. S.; Eremin, S. A. Fluorescence polarization immunoassays and related methods for simple, high-throughput screening of small molecules. *Analytical and Bioanalytical Chemistry* **2008**, *391*, 1499.

Sturini, M.; Speltini, A.; Maraschi, F.; Profumo, A.; Pretali, L.; Fasani, E.; Albini, A. Photochemical degradation of marbofloxacin and enrofloxacin in natural waters. *Environmental science & technology* **2010**, *44*, 4564.

Sun, H.; Qiao, F.; Liu, G.; Liang, S. Simultaneous isolation of six fluoroquinolones in serum samples by selective molecularly imprinted matrix solid-phase dispersion. *Analytica chimica acta* **2008**, *625*, 154.

Tachi, T.; Hase, T.; Okamoto, Y.; Kaji, N.; Arima, T.; Matsumoto, H.; Kondo, M.; Tokeshi, M.; Hasegawa, Y.; Baba, Y. A clinical trial for therapeutic drug monitoring using microchip-based fluorescence polarization immunoassay. *Analytical and Bioanalytical Chemistry* **2011**, *401*, 2301.

Ton, X.-A.; Acha, V.; Haupt, K.; Tse Sum Bui, B. Direct fluorimetric sensing of UV-excited analytes in biological and environmental samples using molecularly imprinted polymer nanoparticles and fluorescence polarization. *Biosensors and Bioelectronics* **2012**, *36*, 22.

Turiel, E.; Martín-Esteban, A.; Tadeo, J. L. Molecular imprinting-based separation methods for selective analysis of fluoroquinolones in soils. *Journal of Chromatography A* **2007**, *1172*, 97.

Wang, Z.; Zhu, Y.; Ding, S.; He, F.; Beier, R. C.; Li, J.; Jiang, H.; Feng, C.; Wan, Y.; Zhang, S. Development of a monoclonal antibody-based broad-specificity ELISA for fluoroquinolone antibiotics in foods and molecular modeling studies of cross-reactive compounds. *Analytical Chemistry* **2007**, *79*, 4471.

Yan, H.; Qiao, F.; Row, K. H. Molecularly imprinted-matrix solid-phase dispersion for selective extraction of five fluoroquinolones in eggs and tissue. *Analytical Chemistry* **2007**, *79*, 8242.

Commission Regulation (EU) N° 37/2010 of 22 November 2009 of the European Union, on pharmacologically active substances and their classification regarding their maximum residue limits in foodstuffs of animal origin. http://ec.europa.eu/health/veterinary-use/maximum-residue-limits/developments_en.htm

General Conclusions and Perspectives

In this Ph.D. thesis, several innovative optical sensing platforms and methods based on molecularly imprinted polymers as synthetic recognition elements combined with fluorescence for detection, have been developed. Focus was given to the use of fiber optic detection platforms, which offer the potential of being simple and cheap and hence are of particular interest for practical applications.

The first part describes the development of a versatile fluorimetric fiber optic sensor that employs *in situ* polymerized MIP microstructures, generated in a few seconds, by laser photopolymerization. Initially, the proof-of-concept was demonstrated with a MIP templated with N-carbobenzyloxy-L-phenylalanine (Z-L-Phe) and a fluorescent amino acid derivative dansyl-L-phenylalanine as analyte. The fluorescent analyte was detected in the low nM concentrations. We then showed that the sensitivity of the sensor could be improved by exploiting the signal enhancement induced by gold nanoparticles embedded in the polymer. In order to render the sensor versatile and hence detect non-fluorescent analytes, a naphthalimide-based signalling monomer was synthesized and incorporated into the MIP, which showed fluorescence enhancement upon analyte binding. A detection limit as low as 250 pM for the herbicide 2,4-dichlorophenoxyacetic acid (2,4-D), comparable to that of LC/MS techniques, was achieved. The mycotoxin citrinin could also be monitored with a limit of detection (LOD) of 5 ng/mL, which is below the recommendations of the European Food Safety Authority that are in the range 19-100 ng citrinin/g in grains and grain-based products, for average consumers. This method is applicable to analytes carrying carboxylate but also phosphate groups. Indeed the sphingolipid D-*erythro*-sphingosine-1-phosphate, which is of high interest for biomedical applications, was also monitored. The sensitivity of the MIP (LOD: 500 ng/mL) still needs to be improved by at least 100-fold, but the proof of concept was successfully demonstrated. Moreover, we showed through fluorescence titrations studies that the naphthalimide-based signaling monomer interacted with another phosphate analyte adenosine-5'-monophosphate and a sulfate compound glucosamine-6-sulfate, thus demonstrating the versatility of our method.

To conclude, we developed a sensing system that combined versatility, fast synthesis and high sensitivity. Hence our sensor can be applied for routine monitoring, long-distance monitoring (the fiber can reach inaccessible sites) and can be easily multiplexed with other transduction platforms if needed. Further work should be dedicated to the synthesis of different signaling monomers in order to apply our sensing method to a wider range of analytes. The MIP formulations could also be optimized to make sensing possible in aqueous environments, in order to extend our method to "real" sensing in media such as environmental waters or biological fluids (blood plasma, urine, tears…). Possibly, the sensitivity of our sensor can be enhanced by performing an in-depth study and optimization of the plasmonic signal enhancement induced by noble metal nanoparticles.

In the second part of the thesis, a complementary approach, based on the use of a disposable, cheap and versatile evanescent wave fiber optic sensor, developed by coating a signaling fluorescent MIP on a 4-cm long polystyrene optical waveguide, was considered. The MIP was composed of the naphthalimide-based fluorescent monomer described above, which showed fluorescence enhancement upon binding with 2,4-D and citrinin. The coating of the MIP was either performed *ex-situ*, by dip-coating the fiber in a suspension of MIP particles synthesized beforehand, or *in-situ* by evanescent-wave photopolymerization directly on the fiber.

The sensor detected 2,4-D, with a limit of detection of 1 nM and citrinin, with a limit of detection of 1 μg/mL (4 μM), which still needs to be improved. However, the concept of the sensing method was successfully demonstrated. This type of technology could possibly be extended to detect other carboxyl-containing analytes as well as phosphate and sulfate moieties and would be useful for on-site screening of environmental and biological analytes. Future work should be dedicated to the optimization of the procedure of the *in-situ* polymerization by evanescent waves of the MIP on the fiber, so as to increase its sensitivity.

Besides the development of fiber optic sensors that were the main purpose of this thesis, we extended our study to the development of other optical transduction techniques. Evanescent waves were used for the polymerization of ultra-thin MIP microdots on flat substrates such as gold films and gold microhole arrays. This approach was developed for the first time in our group, and is particularly interesting for SPR chips or other sensing applications that require the deposition of very thin MIP layers. In this work, we intended to make use of the plasmonic properties of the gold microholes arrays for the signal enhancement of MIP microdots. The signaling 2,4-D MIP was used for this study. The binding assays revealed that the MIP on the Au film gave the best signal enhancement, compared to glass and the Au microholes array. The MIP on the Au microholes array gave a lower enhancement factor but the signal intensities of the microdots on the microholes were much stronger than on the Au film and the glass. Hence the Au microholes array seems to be the most interesting for developing a sensitive sensing platform. As perspectives, the properties of the micro- and nanostructured gold surfaces and their influence on the MIP binding properties need to be further investigated, notably by studying several types of micro- or nanostructured gold surfaces with different morphologies: microholes, nanoholes, nanotriangles.

In the last part of this thesis, we developed a new sensing system based on the use of fluorescence polarization and MIP nanoparticles as antibody mimics. Instead of integrating MIPs with transduction platforms in order to develop a sensor, we used directly the MIP nanoparticles as sensory materials in a pseudo-immunoassay. Our MIP was imprinted with the fluoroquinolone antibiotic enrofloxacin and showed selective binding towards the other piperazine-based fluoroquinolones. Our methodology was successfully applied to detect the fluoroquinolones antibiotics in tap water and milk. A low limit of detection of 0.1 nM (36 ng/L) could be achieved in water, enabling the determination of 0.28 nM enrofloxacin, the legal amount tolerated in water samples. Enrofloxacin and danofloxacin, whose MRLs in milk have been fixed to 0.28 μM and 0.08 μM respectively, could be easily detected. Thus our sensing method constitutes a cheap, fast and sensitive tool for the initial screening of the presence of analytes of interest in food or environmental samples. In the future, the format of the binding assays could be improved, to move from the format of the cuvette in the spectrofluorimeter to microtiters plates for high throughput screening.

Annex: Achievements

Publications

- **X.A. Ton**, V. Acha, K. Haupt, B. Tse Sum Bui, "Direct fluorimetric sensing of UV-excited analytes in biological and environmental samples using molecularly imprinted polymer nanoparticles and fluorescence polarization", *Biosensors and Bioelectronics* (**2012**), 36 (1), 22-28.

- Y. Fuchs, **X.A. Ton**, I. Dika, K. Haupt, A.G. Mayes, O. Soppera, "Photopolymerization and photostructuring of molecularly imprinted polymers for sensor applications", *IEEE Sensors 2012 Conference Proceedings* (**2012**), 2235-2238.

- **X.A. Ton**, B. Tse Sum Bui, M. Resmini, P. Bonomi, I. Dika, O. Soppera, K. Haupt, "A versatile fiber-optic fluorescence sensor based on molecularly imprinted microstructures polymerized in-situ", *Angewandte Chemie International Edition* (**2013**), 52 (32), 8317-8321.

Manuscripts in preparation

- **X.A. Ton**, B. Tse Sum Bui, I. Dika, O. Soppera, K. Haupt, "Photodriven 'multi-scale' structuring of molecularly imprinted polymers for fiber optic sensors".
- **X.A. Ton**, V. Acha, P. Bonomi, B. Tse Sum Bui, K. Haupt**,** "A disposable evanescent wave fiber optic sensor coated with a molecularly imprinted polymer as a selective fluorescence probe".
- **X.A. Ton**, B. Tse Sum Bui, P. Bonomi, Z. Kaya, J.F. Masson, K. Haupt, "Synthesis of molecularly imprinted polymer-coated sensing elements by evanescent-wave photopolymerization on gold microstructured surfaces for signal enhancement"

Oral communications

- **X.A. Ton**, V. Acha, B. Tse Sum Bui, K. Haupt

"Molecularly imprinted polymer-based fiber optic sensors for the detection of mycotoxins"
Intelligent Recognition Materials for Extraction and Detection (IRMED project) - 1st Summer School, Ile d'Oléron, France, 16th -21st May 2011.

- **X.A. Ton**, B. Tse Sum Bui, I. Dika, O. Soppera, K. Haupt

"Molecularly imprinted polymer-based fiber optic sensors for the fluorimetric detection of environmental and biological analytes"
7th International Conference on Molecularly Imprinted Polymers "MIP 2012", Paris, France, 27th-30th August 2012.

- **X.A. Ton**, B. Tse Sum Bui, M. Resmini, P. Bonomi, I. Dika, O. Soppera, K. Haupt

"A fluorescence fiber optic sensor based on photostructured molecularly imprinted polymers"
2nd EOS conference on Optofluidics "EOSOF 2013", Munich, Germany, 13th-15th May 2013.

- **X.A. Ton**, B. Tse Sum Bui, M. Resmini, P. Bonomi, I. Dika, O. Soppera, K. Haupt

"A versatile fluorescence fiber optic sensor based on molecularly imprinted microstructures polymerized in-situ"
E-MRS 2013 Fall Meeting, Warsaw, Poland, 16th- 20th September 2013

- K. Haupt, **X.A. Ton**, B. Tse Sum Bui, M. Resmini, P. Bonomi, I. Dika, O. Soppera

"In-situ polymerisation of molecularly imprinted polymer nanostructures for chemical sensing with holographic and fiber-optical transducers"

The 6th International Workshop on Surface Modification for Chemical and Biochemical Sensing " SMCBS 2013 " , Lochow, Poland, 8th-12th November 2013

Poster presentations at conferences

- **X.A. Ton**, K. Haupt, B. Tse Sum Bui

"Development of a fluorescence polarization assay for the determination of fluoroquinolones in water using molecularly imprinted polymers"

10th Workshop on Biosensors and Bioanalytical microtechniques in environmental and clinical analysis "bbmec 2011", Weimar, Germany, 19th-22nd June 2011.

- **X.A. Ton**, B. Tse Sum Bui, I. Dika, O. Soppera, K. Haupt

"Molecularly imprinted polymer-based fiber optic sensors for the detection of fluoroquinolones"

XI conference on optical chemical sensors and biosensors "Europtrode XI", Barcelona, Spain, 1st-4th April 2012.

- **X.A. Ton**, B. Tse Sum Bui, I. Dika, O. Soppera, K. Haupt

"Molecularly imprinted polymer-based fiber optic sensors for the detection of fluoroquinolones"

Biosensors 2012, Cancun, Mexico, 15th-18th May 2012.

- **X.A. Ton**, K. Haupt, B. Tse Sum Bui

"Development of a fluorescence polarization assay for the determination of fluoroquinolones in water and in milk using molecularly imprinted polymers"

7th International Conference on Molecularly Imprinted Polymers "MIP 2012", Paris, France, 27th-30th August 2012.

- **X.A. Ton**, B. Tse Sum Bui, I. Dika, O. Soppera, K. Haupt

"Molecularly imprinted polymer-based fiber optic sensors for the fluorimetric detection of environmental and biological analytes"

7th International Conference on Molecularly Imprinted Polymers "MIP 2012", Paris, France, 27th-30th August 2012.

Prizes

- 7th June, 2012: "Collegium Price of Innovation" (UTC – CNRS INSIS), 5000 euros.

Other activities

- **Teaching**: *2010-2011*: 64 hours of laboratory work: 40h biochemistry (TP BL10) and 24h cellular biology (TP BL20).
- **Supervision:**
  - *2012 (5 months)*: Two Master students from Agricultural University of Athens (Greece)
  - *2013 (5 months)*: One Master student from Shanghai University (China)